Proceedings of the

5th NATIONAL CONFERENCE

on Research and Development in Science, Engineering and Technology

Organized by

St. Anne's College of Engineering and Technology

NCRDSET '19

Volume 2

Proceedings of

ISTE sponsored

5th National Conference on Research and Development in Science, Engineering and Technology.

NCRDSET '19

(Volume II)

28th February, 2019

Organised by

St. Anne's College of Engineering and Technology

Anguchettypalayam, Panruti – 607106.

Preface

St. Anne's College of Engineering and Technology feels proud in its consistent progress to organize the **Fifth National Conference on Research and Development in Science, Engineering and Technology (NCRDSET '19)** on 28th February, 2019.

In the recent days Technology has witnessed the enormous development in many fields. To import the development and the Technological advancements in the fields of Science, Engineering and Technology, this conference provides a platform to track the quality Research and Development updates from researchers, engineers, scientists, industrialist, academicians and students. It also provides them to express their talents and innovative ideas that will contribute to all fields of Engineering and Science in the upcoming years.

This conference is jointly organized by the Departments of Mechanical Engineering, Electrical and Electronics Engineering, Electronics and Communication Engineering, Computer Science and Engineering and Science & Humanities in association with Indian Society for Technical Education (ISTE) and its aims to exchange and stimulate research in the various areas of Science, Engineering and Technology.

It is believed that the research papers included in these proceedings will create a solid background for useful discussions during the conference and for further research. It is also hoped that these proceedings will provide valuable reference material and a source of information on academic achievements and current debate in Engineering and Technology education.

After peer review, the editorial board selected 110 papers from the 189 papers submitted. The selected papers covered a wide range of topics: Advance Trends in Engineering Design, Recent Methods in Manufacturing, AI and Deep Learning, IoT and Networking, VLSI Design/ Embedded Systems, Recent Trends in Communication, Smart Grid and Microgrid Systems, Special Electrical Machines, Smart Materials and Crystalline Materials and Recent Advancements in Applied Mathematics.

All the presentations were much impressive with high level of professionalism, and in many cases original ideas and activities have been accomplished or proposed. The organizing committee would like to congratulate all the authors for their interests and efforts. Also, thank all the participants for their support in making the conference a great success.

Organizing Chair

Dr. R. Arokiadass, M.E., Ph.D.
Principal
St. Anne's College of Engineering and Technology

ORGANIZING COMMITTEE

PATRON

Rev. Dr. Sr. Y. Yesu Thangam, SAT
Secretary
St. Anne's College of Engineering and Technology

ORGANIZING CHAIR

Dr. R. Arokiadass
Principal
St. Anne's College of Engineering and Technology

ORGANIZING SECRETARY

Sr. S. Anita, SAT
Vice Principal
St. Anne's College of Engineering and Technology

CO - ORDINATORS

Mr. S. Bala Baskar
Associate Professor
Department of Electronics and Communication Engineering

Mr. K. Sriram
Assistant Professor
Department of Electrical and Electronics Engineering

STEERING COMMITTEE

Dr. D. Ommurugadasan
Professor & Head
Department of Mechanical Engineering

Dr. A. John Peter
Professor & Head
Department of Science and Humanities

Mr. A. Richard Pravin
Associate Professor & Head
Department of Electrical and Electronics Engineering

Sr. A. Punitha Jilt
Assistant Professor & Head
Department of Computer Science and Engineering

MESSAGE FROM CHIEF GUEST

21st February, 2019

I am happy to note that St. Anne's College of Engineering and Technology, Panruti, is organizing the **5th National Conference on Research and Development in Science, Engineering and Technology** on 28th February, 2019. There is a pressing need for strong and sustained efforts in development and application of Science and Technology for socio-economic development. It is necessary to mobilize the scientists, engineers and technologists to evolve new strategies and device new technologies to ensure that these technologies reach the end-users. It is also pertinent to note that any research or development will serve its purpose only if it demonstrates a tangible improvement in the quality of life of the society at large. There is also a necessity to expose students to recent advances and trends in science, engineering and technology as they play an important role in disseminating the advances in Science and Technology.

In this context, this conference is a welcome effort in the right direction. I wish the conference all success.

Dr. S. Manickam
Professor
Department Of Manufacturing Engineering
Annamalai University

MESSAGE FROM CHIEF GUEST

24th February, 2019

In a world increasingly propelled by technology, Institutional research is the foundation of any nation's economic growth. This is because Science and Engineering research conducted in academic institutions plays a critical role in raising our standard of living, creating jobs, improving health, and providing for national security. Interestingly, India is among the top most countries in the world in the field of scientific research.

This premier institute, St. Anne's College of Engineering and Technology has put forth concerted efforts to align in focus with the national goal of achieving technological self-reliance through conducting this **5th National Conference on Research and Development in Science, Engineering and Technology** in the thrust areas of Engineering like Computer science, Electrical, Electronics and Communication, Mechanical along with Engineering Sciences.

It's a great privilege and profound honor bestowed on me to share my thoughts through my keynote address and through this message column with the maverick and creative minds of this reputed Institute committed to scholastic excellence.

At the outset, I wish to express my heartiest congratulations to the organizers of this wonderful conference. I also genuinely look forward for the active involvement of the conference Participants and make the best out of this wonderful opportunity.
My best wishes to all.

Dr. K. Jayanthi
Professor
Dept. of ECE
Pondicherry Engineering College

MESSAGE FROM SECRETARY'S DESK

In this globalised and technological scenario, knowledge as power, quality education, super fast communication systems, and higher level jobs have been some of the concepts which direct the world. In this context, St. Anne's College of Engineering and Technology, a distinguished centre for modern learning, aims at character formation, excellence in teaching, learning, research and placement, empowerment of rural youth, and has grown in all directions with its **Motto: To Build a Holistic Society**. The commitment and continuous hard work of our Faculty instill originality and creativity in teaching, learning and research and one such fruit of their effort results in conducting a **National Conference on Research and Development in Science, Engineering and Technology (NCRDSET)** every year. I deem it a great joy to congratulate the Principal, organizers, committee members and all the Faculty and Non-teaching staff for their involvement and cooperation to conduct this 5th NCRDSET.

This National Conference, NCRDSET '19, provides ample opportunity to the Faculty, Industrialists and Students to exhibit their research articles, share and exchange their views and aspirations and learn novel methods and approach in their respective field.

I congratulate all the eminent Faculty and erudite Scholars as well as the young Engineering Students from various Institutions who contributed for the Proceedings of the 5th NCRDSET which comprises the articles with novel themes like Cloud, Soft and Green Computing, IoT and Networking, Smart Grid, Microgrid and Renewal Energy Systems, Emerging trends in Power System, Power Electronics Controllers, Energy Storage System, Advanced Trends in Engineering Design and Manufacturing, Computational Field Dynamics, Designing Tool and Cutting Materials, Composite Materials, Alternative Fuels, VLSI Design / Embedded Systems, Audio / Medical Signal Processing, Advanced Antennas, Green / Lifi Communication, Environment Science, Crystalline Materials, Nano Materials and Nano Structures, Material Science and Chemistry, Mathematical Analysis, Advancement, and Applied Mathematics and English Language Teaching Methodology.

I wish and pray for the fruitful deliberation of this Conference. May the Lord Almighty inspire and enrich every participant to acquire more wisdom, insight and knowledge through this Conference!

Rev. Dr. Sr. Yesu Thangam
Secretary
St. Anne's College of Engineering and Technology

MESSAGE FROM VICE-PRINCIPAL

Dear Participants,

On behalf of the organizing committee, I take great pleasure to welcome you all for the 5th National Conference on Research and Development in Science, Engineering and Technology (NCRDSET '19).

Conference is the platform that gives access to academicians, researchers, industry professionals, and students to come together to discuss and interact on an issue or a topic from different perspectives. In this regard, the purpose of this conference is to bring together the fresh and innovative developments in Engineering and Science, and to explore academic research results. The conference received more than 189 papers from 5 tracks. The higher number of submissions has provided an excellent opportunity for a high-quality program, and also calls for a greater demanding and laborious evaluation process. I am indeed thankful to the national experts who have agreed and come forward to enrich the conference with their valuable suggestions. At the outset of this Conference, I extend a heartfelt gratitude to the Editors of the Scopus and UGC approved Journals for their magnanimity hearts to make known the society the contributions of this conference.

I welcome wholeheartedly all the participants working in different areas of Science and Technology and request to make this event a grand success.

Rev. Sr. S. Anita
Vice Principal
St. Anne's College of Engineering and Technology

TABLE OF CONTENT

11	NCRDSET 1099	To Improve Performance Response of Economic Load Dispatch by using Grey Wolf Optimization Technique	Mr. K. Sriram Mr. R. Rajkumar Mr. P. Pasupathi Mr. R. Elumalai Mr. Y. Magimai Xavi Thomas	71
12	NCRDSET 1101	PV Battery Charger Using an L3C Resonant Converter for Electric Applications	Mr. A. Sundara pandiyan Mr. R. Manikandan	79
13	NCRDSET 1106	IoT Based Induction Motor Controlling and Monitoring by Using Raspberry-Pi	Mr. J. Ramesh Mr. A. Prakashraj Mr. M. Sindhan Mr. P. Jayavel Mr. P. Sivapushnam	88
14	NCRDSET 1110	Dragon Fly Algorithm Based Forecasting of Substation Demands	Ms. J. Arul Martinal Ms. D. Dhatchayani Ms. R. Keerthana Ms. Y. Monica Ms. P. Banupriya	92
15	NCRDSET 1114	Solar Optiverter – A Novel Hybrid Approach to the Photovoltaic Module Level Power Electronics	Ms. R. Janani Ms. D. Akalya	100
16	NCRDSET 1119	21 Level Staircase Sine Wave Inverter with Reduced Switches and THD	Sr. A. Annai Theresa Mr. Sinu Cleetus Mr. A. Abinesh Mr. C. Thamizharasan Mr. S.Shanmuganatham	106
17	NCRDSET 1121	Smart Prepaid Energy Meter using GSM and Arduino	Sr. A. Annai Theresa Ms. M. Nirmala Ms. J. Santhini Ms. V. Dhivya Ms. M. Suvedha	113
18	NCRDSET 1145	Control strategy of Permanent Magnet Brushless DC Motor with Snubber circuit using Fuzzy Logic Control	Mr. V. C. Eugin Martin Raj Mr. P. Harish Mr. M. Praveen Kumar Mr. S. Anbumathi Mr. S. Selvaraj	120
19	NCRDSET 1156	Carrier level shifted based control method for the PWM 3L-T-type qZS with capacitor imbalance compensation	Mr. V. Balaji Mr. C. Vignesh Mr. M. Vignesh Mr. G. Ragul Mr. Mohamed Shaffiullah	131

Live Health Care Monitoring System using Arduino

Mr. B.Sarathkumar[1]
PG Scholar,
Department of Electrical and electronics Engineering,
Krishnasamy college of Engineering and Technology,
S.Kumarapuram,Cuddalore-607 109.

Dr. D.Periyaazhagar[2]
Assistant Professor,
Department of Electrical and electronics Engineering,
Krishnasamy college of Engineering and Technology,
S.Kumarapuram,Cuddalore-607 109.

Abstract –Innovative technology approaches have been increasingly investigated for the last two decades aiming at human-being long-term monitoring.The main aim of this paper is to supervise the patients affected from chronic diseases, blood pressure and the elderly people at their home itself with an android application. By doing this, unwanted visit to the hospital can be avoided. The system was developed to supervise the vital signs such as temperature, blood pressure, heart rate, gas sensor and fall detection. The system design consists of an Arduino controller andGSM900A module. The monitored values can be sent through the mobile phones and if it detects abnormal state then it enables the buzzer and the information is passed to the concerned members through the mobile application. In case of regular check up there is no need for the patient to go and meet the doctor or physician with the proposed system. The patient can send an SMS as CHECK to test the body condition to detect the health condition of the patient from the ECG signal. The system will also transmit thedata of healthcare information to the concerned doctor's mobile phone through app.

Keywords: Healthcare Monitoring, GSM/Global Positioning System, ECG signal and Fall detection.

I. INTRODUCTION

This is a fact that the global population is both growing and ageing. As a consequence of this demographic change, there has also been a corresponding increase in chronic age related diseases, such as congestive heart failure, dementia, sleep apnea, cancer, diabetes, and chronic obstructive pulmonary diseases. Furthermore, the total number of people suffering from some type of disability (either life-long, or injury related, or more commonly related to chronic conditions) will continue to rise.

Nowadays, the requirement for healthcare system development is rigorously increasing. In the past, consumer used to see doctor whenever they found problems of their health status. However, prevention is much more efficient than curing. Advanced technology can help to check their health Status as well as providing location services wherever instant health problems happened. In recent years, there has been a tremendous change in the healthcare system considering the both convenience and efficiency which allows consumer to instantly locate the position of patient who has instant problem health problem.

It is important for patients that healthcare practitioners cooperate closely and efficiently in the chain. This is especially critical when caring for and treating the chronically ill. The complexity of healthcare lies in making the correct diagnosis and avoiding duplicate

analysis. The right tests and examinations should be carried out, and information should be shared among all the relevant healthcare practitioners. This means both professional information and information about the patient, his or her illness, past and future treatment and medication. It has often been said that we need coordinators in healthcare to link all the parties to one another and organize things from the patient's perspective. Of course, general practitioners do not monitor patients every single day.

II. RELATED WORKS

This section present the most related research approach and techniques based on healthcare monitoring devices for elderly.

Nikolaos G. Bourbakis et al [1] This paper attempts to comprehensively review the current research and development on wearable biosensor systems for health monitoring. A variety of system implementations arecompared in an approach to identify the technological shortcomings of the current state-of-the-art in wearable biosensor solutions. Y.Ravi Sekhar Maradugu Anil Kumar [2]The health care scheme is focus on the measurement and Monitoring various biological parameters of patient's body like heart rate, oxygen saturation level in blood and temperature using a web server and android application, where doctor can continuously monitor the patient's condition on his smart phone using an Android application .The functioning of the intelligent system developed by Wang et al. [4] is mainly based on the collected blood pressure and pulse signals from the patients for the functioning of the heart automatically. The authors tested and experimented this with a simulation model. An emergency healthcare system is developed by Kang et al. [5] which is a ubiquitous integrated biotelemetry system. Because, all the primary data's like blood pressure, pulse rate etc., are all prerecorded and sent to the hospital prior to the patient's arrival through a wearable device.

The system proposed by Vaidehi et al. [6] utilized a camera to monitor the patient's activity inside the room. The main drawback with this is that it can estimate if the patient stays in that room for a long period of time. Hsieh et al. [7] come up with a wrist-worn motion-sensing device to detect falling events; the sensing device consists of a tri-axis accelerometer and a three-axis gyroscope. The disadvantage with this is that it does not detect the location of falling objects. Wang et al. [8] proposed an enhanced fall detection system based on a smart sensor worn on the body for elderly people to monitor and operate monthly once by sitting at home. Bai et al. [9] utilized the accelerometer of a smart phone to design and implement a GPS based monitoring system for the user. The system concentrated on analyzing the six typical actions of humans in addition to the change of acceleration.

Torkestani et al (2012) [10] concentrated on Wireless Personal Area Networks (WPAN) from small and low-power digital radios. The low power consumption features of ZigBee network have not become one of its limitations in data transmissions. This network usually enables devices to achieve the data transmission over almost 100 meters despite its low-powered characteristics.

Zhen et al. (2007) [03] concluded that it is very critical to predict the Clear Channel Assessment (CCA) between ZigBee and Wi-Fi. The author identified the Wi-Fi is insensitive towards ZigBee. However ZigBee is oversensitive to Wi-Fi. Thus CCA range for coexistence behavior was 25 m with free space path loss model.

III. PROPOSED METHODOLOGY

This paper proposed a methodology based on health monitoring that overcomes the above mention disadvantages. This project is designed to reduce the work of visiting the hospital for usual checkup for the patients. To protect the ill patients & aged persons by embedded system based real time patient distance monitoring system using GSM/GPS

technologies. Sensors such as temperature, gas, fall detection, heart rate and blood pressure rate adopted in this work to effectively maintain the proposed health monitoring system. A monitoring system, specifically designed for cardiac care with electrocardiogram (ECG) signal analysis as the core diagnostic technique, could play a vital role in early detection of a wide range of cardiac ailments, from a simple arrhythmia to life threatening conditions such as myocardial infarction. The system that have developed consists of three major components, namely, (a) mobile gateway, deployed on patient's mobile device, that receives 12-lead ECG signals from any ECG sensor, (b) remote server component that hosts algorithms for accurate annotation and analysis of the ECG signal and (c) point of care device of the doctor to receive a diagnostic report from the server based on the analysis of ECG signals. The focus has been toward developing a system capable of detecting critical cardiac events well in advance using an advanced remote monitoring system. A system of this kind is expected to have applications ranging from tracking wellness/fitness to detection of symptoms leading to fatal cardiac events

Vital signs are measurements of the body's most basic functions. The main vital signs routinely measured by health care unit and doctors are:

- Body temperature
- Pulse rate
- Respiration rate (rate of breathing)
- Blood pressure

(The Blood pressure is not considered a vital sign, but is often measured along with the vital signs.)

Vital signs are used to detect and monitor medical problems. In this system temperature, pulse rate, ECG is considered. The body temperature of a person normally varies depending on gender, recent activity, food and fluid consumption, time of day, and, in women, the stage of the menstrual cycle. For a healthy adult the normal body temperature can range from 97.8 degrees Fahrenheit (36.5 degrees Celsius) to 99 degrees Fahrenheit (37.2 degrees Celsius).

The pulse rate is a measure of number of times the heart beats per minute and the heart rate. The arteries expand and contract when heart pushes blood through arteries. The pulse measured only measures the heart rate, but also can represent the Heart rhythm and Pulse strength.

The normal pulse value for the healthy adults ranges from 60 to 100 beats per minute. During exercise, illness, injury, and emotions the pulse rate may fluctuate and increase. Than males, 12 age and older females tend to have faster heart rates. Athletes, such as runners, may have heart rates near 40 beats per minute due to cardiovascular conditioning and experience no problems. According to the National Heart, Lung, and Blood Institute (NHLBI) the high blood pressure for adults is given as

- 140 mm Hg or greater systolic pressure
- 90 mm Hg or greater diastolic pressure

In an update of NHLBI guidelines in 2003 for hypertension, a category of new blood pressure called pre hypertension

- 120 mm Hg – 139 mm Hg systolic pressure
- 80 mm Hg – 89 mm Hg diastolic pressure

The NHLBI guidelines define normal blood pressure as follows

- Below 120 mm Hg systolic pressure
- Below 80 mm Hg diastolic pressure

3.1 Block Diagram Description

The following diagram shown in Figure 3.1 is the block diagram of the proposed system.

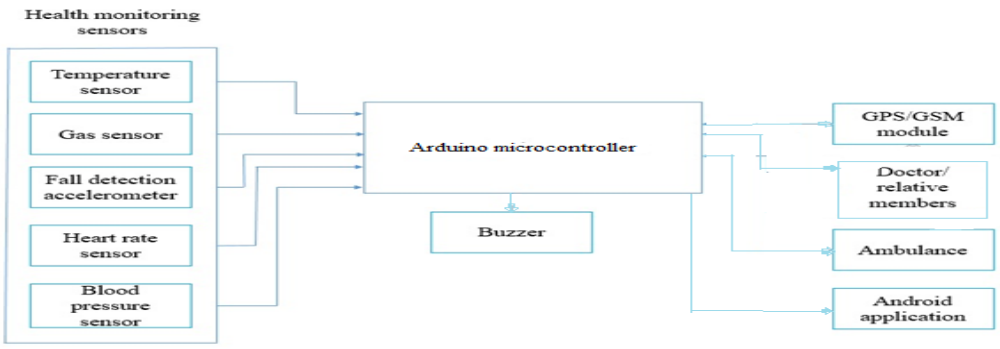

Figure 3.1 Block Diagram of the Proposed System

3.2 Temperature Sensor

The body temperature is measured by using the temperature sensor LM35. It is a three terminal device. Pin number one is 5 volt voltage supply and three are for ground. Pin two is analog voltage output with respect to temperature. There is no need of extra circuitry to operate it. Arduino UNO microcontroller is used to read temperature value. The Relation between the temperature and analog output voltage is:

1ogC = 10m volt (1)

The LM35 series are precision integrated circuit temperature sensors, with an output voltage linearly proportional to the temperature (centigrade) which is advantageous over the sensors that measures the temperature in Kelvin. By using this, the user need not have to go for temperature conversion.

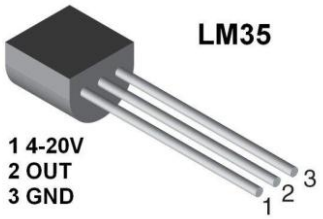

Figure 3.2. LM35

One more advantage with this sensor is it does not need any external calibration or trimming to provide typical accuracies of ± ¼ °C at room temperature and ± ¾ °C over a full −55°C to 150°C temperature range. Due to the trimming and calibration at the wafer level, it costs very less. With the features of low output impedance, linear output, and precise inherent calibration of the device, the interfacing with readout or control circuitry becomes easy.

3.3 Heart Beat Sensor

The new version uses the **TCRT1000** reflective optical sensor for photo plethysmography. The use of TCRT100 simplifies the build process of the sensor part of the project as both the infrared light emitter diode and the radar are arranged side by side in a leaded package, thus blocking the surrounding ambient light, which could otherwise affect the sensor performanceThe output pulse can be fed to either an ADC channel or a digital input pin of a microcontroller for another processing and retrieving the heart rate in beats per minute (BPM).The project is based on the principle of photoplethysmography (PPG) which is a non-invasive method of leveling the variation in blood body in tissues using a light source and a detector. Since the change in blood volume is synchronous to the heart beat, this capacity can be used to calculate the heart rate. Transmittance and reflectance are two basic types of photo plethysmography

Figure 3.3 Heart Beat Sensor

3.4 Arduino Uno

An Arduino board consists of an Atmel 8, 16 or 32 bit with an AVR microcontroller which can be programmed and incorporated into other circuits. It consists of standard connectors, which connect the CPU board to a variety of interchangeable add-on program shields. The communication between the shields and the Arduino board can be done directly over various pins or the shields are individually addressable via an I²C serial bus. It is possible to use it in parallel by stacking many shields.

3.5 Blood Pressure Sensor

The BMP180 is the next-generation of sensors from Bosch, and replaces the BMP085. The good news is that it is completely identical to the BMP085 in terms of firmware/software - you can use our BMP085 tutorial and any example code/libraries as a bit-in replacement. The XCLR pin is not physically present on the BMP180 so if you need to know that data is ready you will need to query the I^2C bus. This board is 5V compliant - a 3.3V regulator and a I2C level shifter circuit S included so you can use this sensor safely with 5V logic and power.

- Vin: 3 to 5VDC
- Logic: 3 to 5V compliant
- load sensing range: 300-1100 hPa (9000m to -500m above sea level)
- Up to 0.03hPa / 0.25m resolution
- 40 to +85°C operational range, +-2°C temperature accuracy
- This board/chip uses I2C 7-bit address 0x77.

3.6 Gas Sensor

Sensitive material of MQ-6 gas sensor is SnO2, which has lower conductivity in clean air. As the concentration of the gas is rising, sensor's conductivity is also becoming high. It is very sensitive to Propane, Butane and LPG, also it responds to Natural gas. Mostly, the gas sensor is widely used to find different combustible gas, particularly Methane. It is mainly used because of its low cost and suitability to different application. This sensor composed of micro AL2O3 ceramic tube, Tin Dioxide (SnO2) sensitive layer, measuring electrode and heater are fixed into a layer made by plastic and stainless steel net. The main function of the heater is to provide a suitable state for the working of sensitive components.

3.7 ADXL345

The ADXL345 is a small, thin, low power, 3-axis accelerometer with high resolution (13-bit) measurement at up to + or - 16 *g*. Digital output data is formatted as 16-bit twos complement and is accessible through either a SPI (3- or 4-wire) or I2C digital interface. The ADXL345 is well suited for mobile material applications. The static acceleration of gravity in tilt-sensing applications, and the dynamic acceleration resulting from motion or shock can be measured with this. Its high resolution (4 m*g*/LSB) enables measurement of inclination changes less than 1.0°.

3.8 GSM

GSM/GPRS engine SIM900A, works on frequencies 900/ 1800 MHz. The Modem is coming with RS232 interface, which allows you connect PC along with microcontroller among RS232 Chip (MAX232). The baud rate is configurable from 9600-115200 through AT command.

IV. SIMULATION RESULTS

The Arduino Uno is the heart of the whole system that program is loaded and compiled to run. The output is verified using the virtual terminal window. Virtual Terminal is a tool in Proteus, which is used to view data coming from Serial Port (DB9) and also used to send the data to Serial Port. The following Figure 4.1 shows the simulated results of the proposed system using Proteus 8.1.

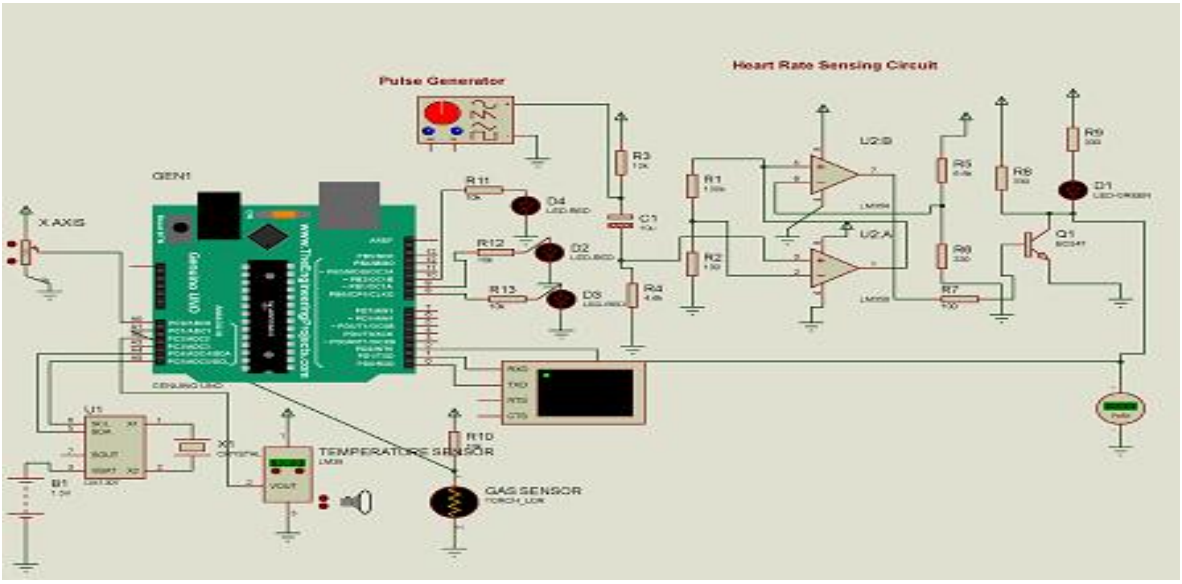

Figure 4.1 Simulation results

The Figure 4.1 shows the patient normal values of vital sign.

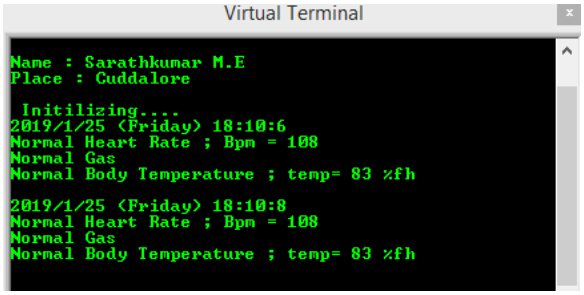

Figure 4.2 Normal values of vital sign

The patient abnormal values of vital sign are shown in the Figure 4.2.

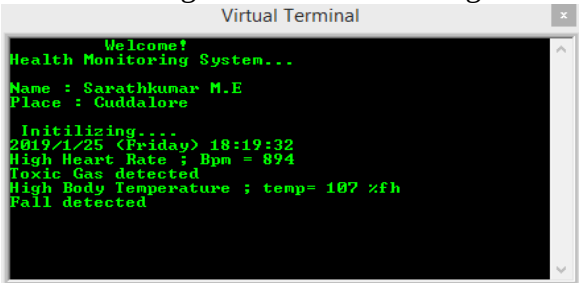

Figure 4.3 Abnormal values of vital sign

V. CONCLUSION

The outdoor health monitoring system which is effectively used in real time medical applications is developed here. This system monitors the vital signs of the patient in the home and there is no need to visit hospital often. It uses the ARDUNIO UNO controller to receive input and transmit to external devices. It uses the GSM 900A modem which transmits the messages and when it receives the text as check it automatically monitors the respective parameters to transfer. This system is designed to reduce the work and it can be implemented with the low cost and for the daily usage to save life in emergency condition. The simulation for the whole model is designed and tested using Proteus 8.1.

REFERENCES

1. Alexandros Pantelopoulos and Nikolaos G. Bourbakis, *Fellow*. "A Survey on Wearable Sensor-Based Systems for Health Monitoring and Prognosis", *ieee* vu university amsterdam applications and reviews, vol. 40, no. 1, january (2010).
2. Maradugu Anil Kumar, Y.Ravi Sekhar. "Android Based Health Care Monitoring System" *IEEE* Sponsored 2nd International Conference on Innovations in Information, Embedded and Communication systems (ICIIECS) 2015.
3. Zhen, H.-B. Li, S. Hara, and R. Kohno, "Clear channel assessment in integrated medical environments," EURASIP Journal on Wireless Communications and Networking, vol. 2008, pp. 1–8, 2007.
4. C. H. Wang, M. F. Horng, J. W. Lee, Y. C. Liu, R. S. Tsai, W. T. Wang, L. Chang, Y. H. Kuo, P. C. Chung, and K. F. Ssu, "Development of Intelligent Home Health-Care Box Connecting Medical Equipment and Its Service Platform," in Proc. The 9th Int. Conference on Advanced Communication Technology, pp. 311-315, Feb. 2007.
5. J. Kang, I. H. Shin, Y. Koo, M. Y. Jung, G. J. Suh, and H. C. Kim, "HSDPA (3.5G)-Based Ubiquitous Integrated Biotelemetry System for Emergency Care," in Proc. 2007 29th Annual Int. Conference of the IEEE Engineering in Medicine and Biology Society, pp. 3665-3668, Aug. 2007.
6. V. Vaidehi., K. Ganapathy, K. Mohan, A. Aldrin, and K. Nirmal, " Video based automatic fall detection in indoor environment," in Proc. 2011 Int. Conference on Recent Trends in Information Technology (ICRTIT), pp. 1016-1020, Jun. 2011.
7. S. L. Hsieh, C. C. Chen, S. H. Wu, and T. W. Yue, "A wrist -worn fall detection system using accelerometers and gyroscopes," in Proc. 2014 IEEE 11th Int. Conference on Networking, Sensing and Control (ICNSC), pp. 518-523, Apr. 2014.
8. J. Wang, Z. Zhang, B. Li, S. Lee, and R. Sherratt "An enhanced fall detection system for elderly person monitoring using consumer home networks," IEEE Trans. Consumer Electronics, vol. 60, no. 1, pp. 23-29,Feb. 2014.
9. Y. W. Bai, S. C. Wu, and C. L. Tsai, "Design and implementation of a fall monitor system by using a 3- axis accelerometer in a smart phone," in Proc. IEEE 16th Int. Symp. Consumer Electronics (ISCE), pp. 1-6, Jun. 2012
10. S.S. Torkestani, S. Sahuguede, A. Julien-Vergonjanne, J.P. Cances, "Indoor optical wireless system dedicated to healthcare application in a hospital," in Communications, IET , vol.6, pp.541-547, March 27 2012.

Embedded Modelling and Control of Asymmetric Cascaded Multilevel Inverter

Mr. V. Bharathiraja[1]
PG Scholar,
Department of Electrical and Electronics Engineering,
Krishnasamy college of Engineering and Technology,Cuddalore, Tamil Nadu,India
bharathiraja.v10@gmail.com

Mr. S. Siva Sakthi[2]
Associate Professor and Head Of the Department,
Department of Electrical and Electronics Engineering ,
Krishnasamy college of Engineering and Technology,Cuddalore, Tamil Nadu,India
Sivasakthi_gayu@yahoo.co.in

Abstract— The multilevel inverter is one of the power electronic converters which are used for medium voltage and high power applications with the additional remuneration of lesser total harmonic distortion and lower switching stress, hence reducing the size of the filter and bypassing the usage of the bulk input transformer. It produces the staircase AC output voltage from the input DC sources. Multilevel inverters can be divided into two classes such as Asymmetric multilevel inverter and Symmetric multilevel inverter. The proposed multilevel inverter is an asymmetrical type. Advanced pulse width modulation design is appropriated. In this paper, a new asymmetrical three-phase multilevel inverter is proposed using trinary DC source cascaded H Bridge. This trinary DC source cascaded H Bridge can provide nine level output voltage and it has experimented with both R and RL load. The simulation of a suggested three-phase multilevel inverter is tested using MATLAB-SIMULINK. This method is predictable to be helpful for higher power and higher voltage applications.

Key words: **Multilevel inverter, pulse width modulation, total harmonic distortion, cascaded h-bridge multilevel inverter, trinary DC source.**

I. INTRODUCTION

The need for a high power converter in the application has developed in modern years. Multilevel inverters have installed as easy replacements of a low power converter in many applications. The multilevel inverter includes a group of power semiconductor devices and a collection of source voltage equipment like capacitors or independent sources. The basic concept of certain inverters depends on the connection of series/parallel of power semiconductor devices and input DC sources to produce a stepped or staircase output voltage waveform. The multilevel inverter performs an extraordinary role in improving the perfection of high power and medium voltage distribution networks, high power conditioning systems, flexible speed drive systems etc [1]. The included system was suggested for eliminating the harmonics of asymmetrical cascade H-bridge multilevel inverter has explained. The suggested included system was combined with two intelligence methods that were fuzzy logic and PSO algorithm. The harmonic elimination concert of the approved system was reviewed with the seventh level asymmetrical cascade multilevel inverter (ACMLI). An automated controller has analyzed for two and a three-level

inverter which has modified to work on an asymmetrical nine level active power filter. The controller has now excellent to make all required assignments for the perfect operation of the active power filter, such as current harmonic elimination and removal of larger frequency noise. The below-switching frequency response of nine level inverters was a fundamental benefit in the performance of the automated controller.

The matrix converter is an AC to AC power switching topologies that have installed extensive research concentration as another to conventional AC to DC to AC converter. A matrix converter is able to convert energy from an AC source (Alternating) to an AC load without the necessity of an enormous and short lifetime energy storage system [4]. Shunt interleaved electrical drive arrangements including of various parallel medium voltage back-to-back converters provide power grades of tens of MVA, lesser current distortions, and an accurate smooth air gap torque. To chance unrelenting reliability and approachability goals despite the heavy parts count, the modularity of the drive arrangement essentials to be employed and a meet fault approach design that permits the exclusion and separation of faulted threads is compulsory [5, 6]. The control of four quadrant converters of electric traction vehicles agreed by an AC railway grid has to chance specific conditional limitations with concern to harmonics content and strength. The operation is increased by constantly changing the location dependent grid impedance and voltage harmonics contents earlier limited in the grid voltage. Fault tolerance capacity of the hexagram inverter motor drive modes, due to its single interconnecting nature, the hexagram inverter can permit single leg failure stripped of balancing the power circuit topologies [7, 8]. The trinary DC Source multicarrier based PWM technology is applied to create a nine-level ac output voltage with several PWM scheme. In [9], Phase shift pulse width modulation system is favored as the excellent modulation scheme for a 20MW voltage source converter HVDC with a concern of the total harmonic distortion of the system output voltage. In [10], the study of the switching status of an individual unit division of a cascaded multilevel inverter detects that the operating state of the switching of a chopper arm makes avoidable switching beneath the existing USPWM. Single phase 5level inverter designed by two separate PWM switching schemes and this predicted PWM switching is planned based on the least switching power loss and smallest harmonic distortion [11].

II. PROPOSED TRINARY DC SOURCE MULTILEVEL INVERTER.

The suggested three-phase trinary DC source cascaded asymmetrical multilevel inverter consists of three single phases multilevel inverter. Every single-phase unit carries two full bridges with irregular DC source. The first full bridge operates the input DC source of 1Vdc and the second full bridge operates the input DC source 3Vdc as exhibited in Fig. 2.1. Every input DC source is connected in series to construct a suggested three-phase MLI. Every inverter generates a three different (unequal) output voltage levels, such as positive (+Ve), zero (0) and negative (-Ve) levels by separate groupings of the four power semiconductor switches S1, S2, S3, and S4.

Whenever switches, S1 and S4 is switched ON, then the inverter output voltage is positive level (+Ve); whenever the switches S2 and S3 is switched ON, then the inverter output voltage is negative level (-Ve); whenever either pair of switches (S1 and S2) or (S3 and S4) is switched ON, then the output voltage will be at zero levels (0).

Then the output voltage of the first bridge can be made equal to the −1Vdc, 0, or 1Vdc, correspondingly the output voltage of the second bridge can be made similar to the −3Vdc, 0, or 3Vdc by switching ON and switching OFF its power semiconductor switches suitably. Consequently, the output voltage of the inverter values for −4Vdc, −3Vdc, −2Vdc, −1Vdc, 0, 4Vdc, 3Vdc, 2Vdc, 1Vdc, can be produced. Table 1 describes the switching sequence of a suggested multilevel inverter.

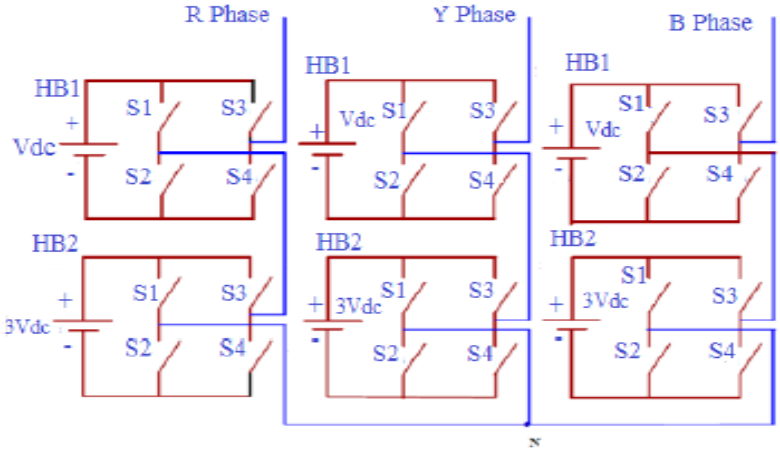

Fig. 2.1. Proposed trinary DC source multilevel inverter

The lower inverter (HB2) provides a fundamental output voltage with three levels, and then the upper inverter (HB1) adding or subtracting one level from the fundamental output voltage wave to create stepped waves. Here, then the final output voltage levels enhance the summing of every terminal voltage of cascaded Half Bridge, and then the output voltage of the load is given in (1).

$$V_{out}=V_{HB1}+V_{HB2}\ (\text{Or})\ V_{out}=V_{dc}+3V_{dc} \qquad (1)$$

The output voltage of the first bridge is registered by Vdc and the second full bridge is registered by 3Vdc. In the suggested inverter circuit topologies, if m number of cascaded H bridge section has unbalanced DC sources in order of the power of 3, an expected output voltage levels are provided as,

$$V_m=3^m\ ,m=1,2,3..... \qquad (2)$$

III. OPERATION OF PROPOSED MULTILEVEL INVERTER.

The lower inverter (HB2) provides a necessary output voltage with three levels, and then the upper inverter (HB1) adding or subtracting one level from the fundamental output voltage wave to produce stepped waves. Following represents the switching sequence of three-phase nine level inverter with R Phase and other two-phase (Y and B Phase) are similar to R Phase. To produce a staircase/ stepped output voltage, the following steps should be observed.

Step 1: For an output voltage level, *Vout* =0Vdc, the power semiconductor switches S2 and S4 are tuned on at both full bridge inverter.

Step2: For an output voltage level, *Vout* = 1Vdc, the power semiconductor switches S1 and S4 are turned on at upper full bridge, S2 and S4 are turned on at lower full bridge inverter.

Step 3: For an output voltage level, *Vout* = 2Vdc, the power semiconductors switches S2 and S3 are turned on at upper full bridge, S1 and S4 are turned on at lower full bridge inverter.

Step 4: For an output voltage level *Vout*=3Vdc, the power semiconductor switches S2 and S4 are turned on at upper full bridge, S1 and S4 are turned on at lower full bridge inverter.

Step 5: For an output voltage level *Vout*= 4Vdc, the power semiconductor switches S1 and S4 are turned on at upper full bridge, S1 and S4 are turned on at lower full bridge inverter.

Step 6: For an output voltage level *Vout* = -1Vdc, the power semiconductor switches S2 and S3 are turned on at upper full bridge, S2 and S4 are turned on at lower full bridge inverter.

Step 7: For an output voltage level *Vout*= -2 Vdc, the power semiconductor switches S1 and S4 are turned on at upper full bridge, S2 and S3 are turned on at lower full bridge inverter.

Step 8: For an output voltage level *Vout*= -3Vdc, the power semiconductor switches S2 and S4 are turned on at upper full bridge,S2 and S3 are turned on at lower full bridge inverter.

Step 9: For an output voltage level *Vout* = -4Vdc, the power semiconductor switches S2 and S3 are turned on at upper full bridge, S2 and S3 are turned on at lower full bridge inverter.

IV. ADVANCED PULSE WIDTH MODULATION TECHNIQUE.

The sinusoidal PWM technique is most widely used PWM technique but it has the drawback of producing the low fundamental RMS output voltage. Due to overcome the drawback, advanced pulse width modulation has been developed. In this work, advanced PWM with multicarrier arrangement is used for generating the triggering pulse for proposed trinary sequence based CHBMLI. For an 'm' level inverters in bipolar multi-carrier techniques, 'm-1' carriers with same frequency fc and same peak to peak amplitude Ac are required [12, 13].

The triggering signals are generated by comparing a triangular wave carrier signals with a modulating trapezoidal reference wave. This type of modulation techniques increases the peak fundamental RMS output voltage. The trapezoidal reference wave signal can be achieved from a triangular wave carrier signal by restrictive its magnitude to A_m which is interrelated to the peak value of $A_{r(max)}$ is given by

$$A_r = \alpha\, A_{r(max)} \tag{3}$$

Where α is called as the triangular wave factor.

Because the waveform becomes a triangular wave signal when α=1.Then the modulation indices Ma is given by

$$M_a = \frac{A}{A_c} = \frac{\alpha A_{r(max)}}{A_c} \tag{4}$$

The angle of the flat portion the trapezoidal reference wave is given by

$$2\phi = (1-\alpha)\pi \tag{5}$$

For stable values of *Ar(max)* and A_c, the magnitude and level of output voltage changes with respect to the modulation index. *H*ere, *Ar(max)* is called as peak amplitude value of trapezoidal reference wave. A_c is called as peak amplitude of carrier triangular signals. Here,

trapezoidal wave signal is used as a reference signal and triangular wave is used as carrier signal. There are many control techniques are possible, some of those techniques are discussed in this paper which is given below:

4.1. Phase disposition pulse width modulation technique (PD).
4.2. Phase opposition disposition pulse width modulation system (POD).
4.3 Alternate phase opposition disposition pulse width modulation system (APOD).
4.4 Carrier overlapping pulse width modulation system (COP).
4.5 Variable frequency pulse width modulation system (VF).

The formula of Amplitude modulation indices (M_a) for phase disposition PWM, Phase Opposition Disposition PWM, Alternate Phase Opposition Disposition PWM and Variable Frequency PWM is given below

$$M_a = \frac{4A_m}{(m-1)\ A_c)} \quad (6)$$

For the carrier overlapping PWM

$$M_a = \frac{A_m}{(2.5)^* A_c)} \quad (7)$$

Here, A_m- Amplitude of a Modulating signal (Reference Signal), A_c -Amplitude of a carrier signal, m – output level, M_a - Modulation index.

4.1 In Phase Disposition Pulse Width Modulation Technique

For an m-level inverter, (m-1) carriers with the same carrier frequency of (f_c) and the same amplitude of carrier signal is (A_c) are required. In phase disposition pulse width modulation technique (PD), all carriers are in phase with each other and it has same amplitude. The carrier wave arrangement of three-phase multilevel inverter with trapezoidal reference is shown in Fig. 4.1(a).

4.2 Phase Opposition Disposition Pulse Width Modulation Technique

For an m-level inverter, (m-1) carriers with the same carrier frequency of (fc) and the same amplitude of carrier signal is (Ac) are required. Phase opposition disposition pulse width modulation technique (POD), all carriers are in phase with above and below the modulating signals in zero values. These carriers which below the zero values are 180 degrees out of phase width. The carriers' wave arrangement of three-phase multilevel inverter with trapezoidal reference is shown in Fig. 4.1 (b).

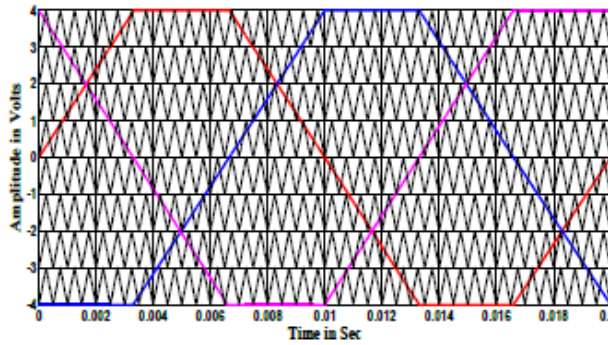

Fig.4.1. (a) Triangular Carrier and Trapezoidal reference wave arrangement: PD PWM system;

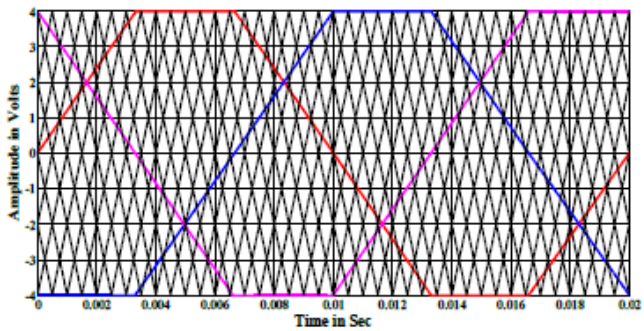

Fig.4.1. (b) Triangular Carrier and Trapezoidal reference wave arrangement: POD PWM System;

4.3 Alternate Phase Opposition Disposition Pulse Width Modulation Technique

For an m-level inverter, (m-1) carriers with the same carrier frequency of (f_c) and the same amplitude of carrier signal is (A_c) are required. Alternate phase opposition disposition pulse width modulation technique (APOD), the carriers are 180 degree phase displaced with its neighbor carrier. The carrier wave arrangement of a three phase multilevel inverter with trapezoidal references is shown in Fig. 4.1 (c).

4.4 Carrier Overlapping Pulse Width Modulation Technique

All carriers have the same frequency fc and same amplitude Ac is disposed such that their bands occupy overlapping with each other carriers. The overlapping vertical distances between each carrier are Ac/2 which is shown in Fig. 4.1 (d).Amplitude of the reference waveform is A0 and frequency is f0 and it is centered in the middle of the carrier signals.

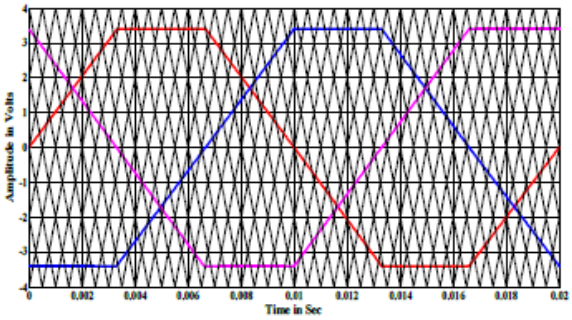

Fig.4.1. (c) Triangular Carrier and Trapezoidal reference wave arrangement: APOD PWM system;

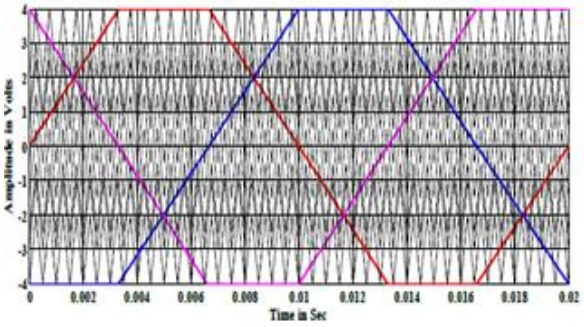

Fig..4.1. (d) Triangular Carrier and Trapezoidal reference wave arrangement: Carrier arrangement of VF PWM System;

V. SIMULATION RESULTS AND DISCUSSION.

A trinary DC source cascaded asymmetrical three phase multilevel level inverter for generating the nine level output voltage is modeled in MATLABSIMULINK using power systems block set. The proposed multilevel inverter simulation circuit is shown in Fig. 4.1. Simulations result of %THD is carried out for different values of ma ranges from 0.8 to 1using the FFT plot. Table 1 shows the values of %THD for R and RL load in different carrier arrangement. Table 2 shows the fundamental RMS output voltage of Vrms of proposed MLI in both R and RL load for various carrier arrangements during the modulation indices range of 0.8 to 1.

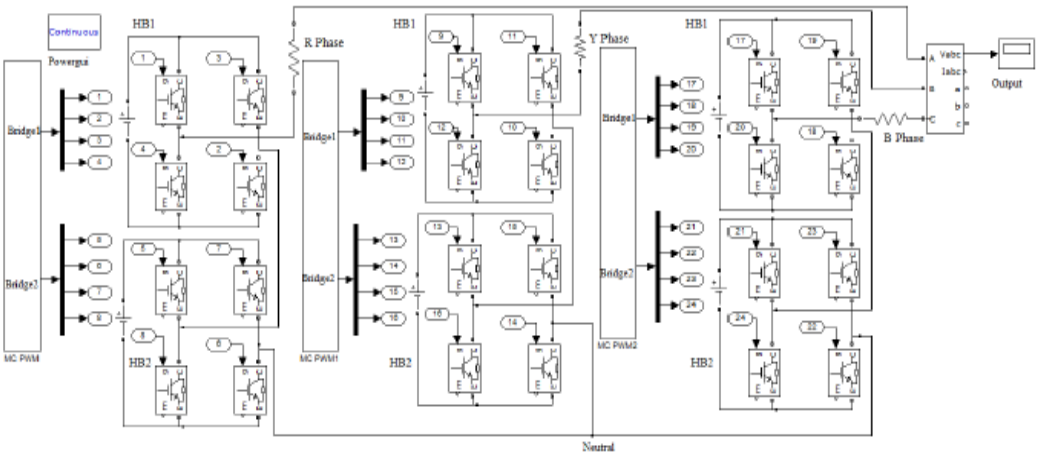

Fig.4.1. Simulink model of Trinary DC source asymmetrical three phase cascaded multilevel inverter

5.1 R Load

Fig. 4 represents the output voltage created by carrier based PWM control with trapezoidal reference for R Load. For a modulation indices (ma=0.85), it is observed from the Fig. {5 (a), 5(b), 5(c), 5 (d) and 5(e)} the harmonic energy level is governing in: Fig. 5(a) characterizes the harmonic energy level in PD PWM techniques shows 5thth, 20th, and 40th order of harmonic. Fig. 5(b) characterizes the harmonic energy level in POD PWM techniques shows 5th, 19th, 20th, 29th, 31st and 40th order of harmonic. Fig. 5(c) represents the harmonic energy level in APOD PWM techniques shows 5th, 7th, 29th, 31st, 35th, 37th and 39th order of harmonic. Fig. 5(d) characterizes the harmonic energy level in COP PWM techniques shows 5th and 40th order of harmonic.

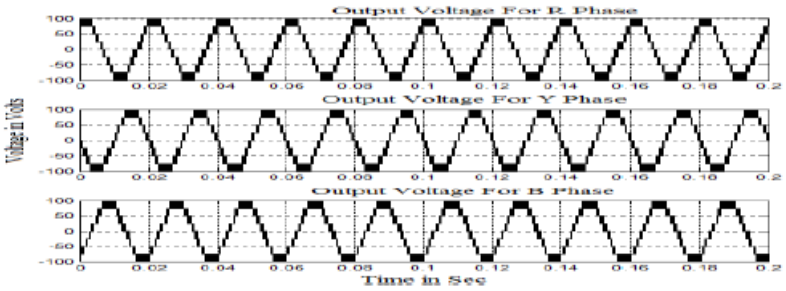

Fig. 4. Output voltages created by All Carrier based PWM control with Trapezoidal reference for R load

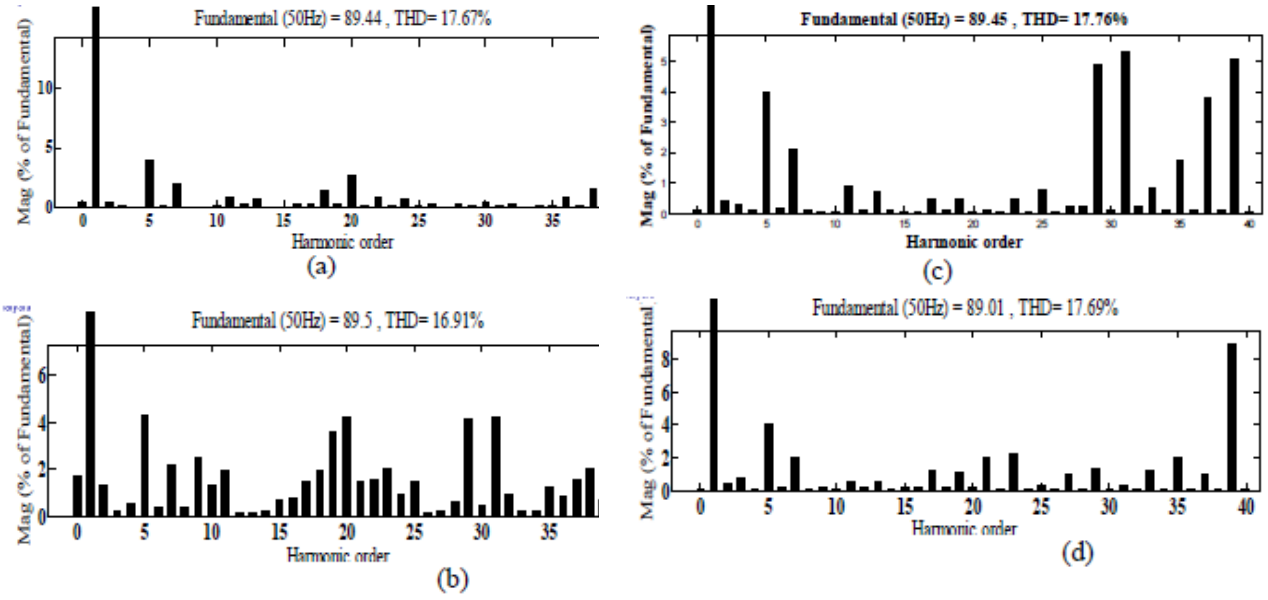

Fig. 5. FFT plot for output voltage of PWM control with Trapezoidal reference with R Load: (a) PD PWM system; (b) POD PWM system; (c) APOD PWM system; (d) COP PWM System;

5.2 RL Load

Fig. 6 represents the output voltage created by carrier based PWM control with trapezoidal reference for RL Load. For a modulation indices (ma=0.85), it is observed from the Fig. 7(a), 7(b), 7(c), and 7(d)} the harmonic energy level is governing in: Fig. 7(a) characterizes the harmonic energy level in PD PWM techniques shows 5thth and 39thorder of harmonic. Fig. 7(b) characterizes the harmonic energy level in POD PWM techniques shows 5th, 20thand 40th order of harmonic. Fig. 7(c) represents the harmonic energy level in APOD PWM techniques shows 5th, 7th, 29th, 31st, 35th, 37th and 39th order of harmonic. Fig. 7(c) characterizes the harmonic energy level in COP PWM techniques shows 5th and 40th order of harmonic. Fig. 7(d) characterizes the harmonic energy level in VF PWM techniques shows 5th, 11th, 19th, 27th, 29th, 39th and 40th order of harmonics.

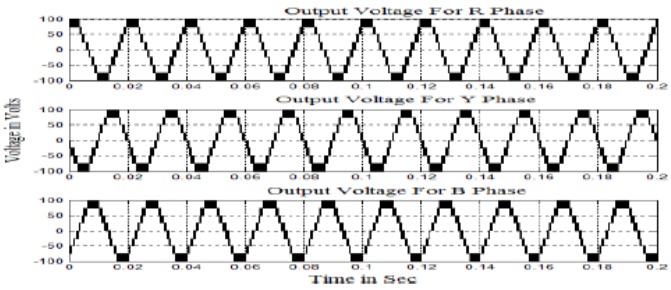

Fig. 6. Output voltages created by All Carrier based PWM control with Trapezoidal reference for RL Load

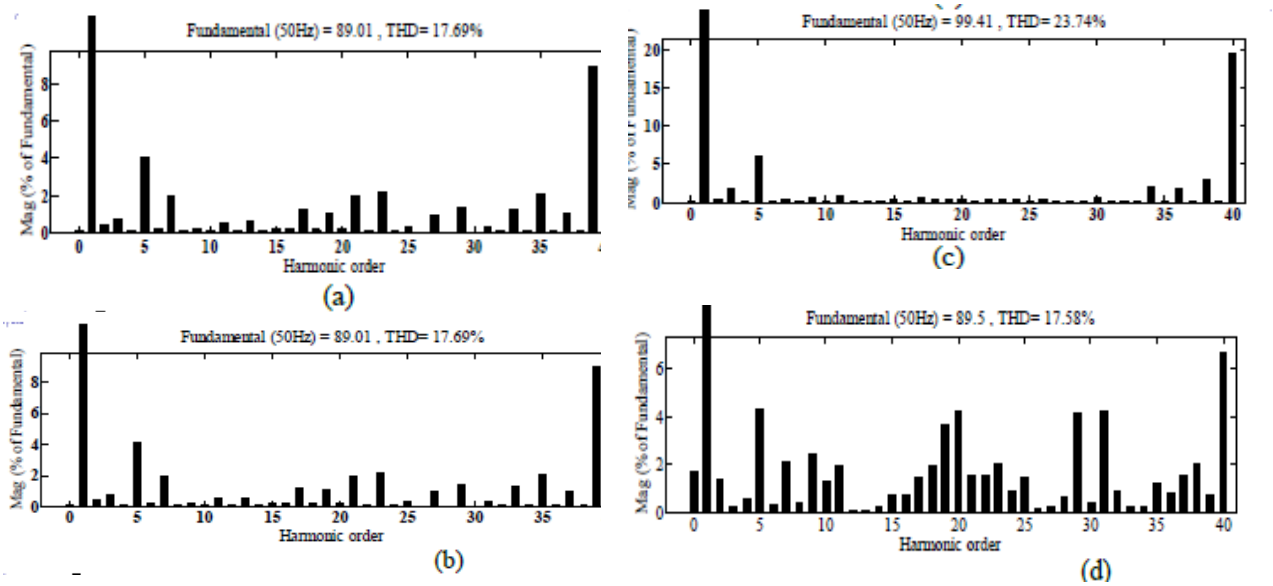

Fig. 7. FFT plot for output voltage of PWM control with Trapezoidal reference with RL Load :(i) IPD PWM system; (ii) POD PWM system; (iii) COP PWM System; (iv) APOD PWM system; (v) VF PWM System.

Table 1: % THD for Different Modulation Indices

Ma	R Load					R L Load				
	PD	POD	APOD	COP	VF	PD	POD	APOD	COP	VF
1	12.56	11.87	12.40	19.79	12.92	12.08	11.42	12.21	19.31	12.39
0.95	15.25	15.39	15.24	20.98	15.64	15.16	15.02	15.27	20.95	15.46
0.9	17.99	16.81	17.04	22.43	17.01	17.02	16.12	19.78	22.79	17.16
0.85	17.67	16.91	17.76	23.74	17.69	17.69	16.13	17.77	23.74	17.58
0.8	17.48	17.23	17.53	25.31	17.11	17.45	17.03	17.48	25.31	17.19

Table2: Fundamental RMS Voltage for Different Modulation Indices

Ma	R Load					R L Load				
	PD	POD	APOD	COP	VF	PD	POD	APOD	COP	VF
1	74.34	74.29	74.49	77.55	74.51	74.33	70.29	74.34	77.47	74.49
0.95	70.68	70.18	70.65	75.21	70.51	70.67	70.79	70.62	75.13	70.09
0.9	66.97	67.11	66.95	72.08	67.18	66.94	67.05	66.96	72.01	67.18
0.85	63.25	62.94	63.25	70.29	63.29	63.22	62.89	63.26	70.20	67.18
0.8	59.45	59.41	59.53	67.61	59.49	59.49	59.44	59.55	67.01	59.41

Table 1and represent the THD contrast of IPD, POD, APOD, COP and VF pulse width modulation techniques with R and RL load no more than one pulse modulation techniques such as POD in R load (Phase Opposition Disposition) it hold minimum quantity of harmonic distortion. Table 2 represent the VRMS contrast of IPD, POD, APOD, COP and VF pulse width modulation techniques with R and RL load no more than one pulse modulation techniques such as COP in R load (Carrier Overlapping) it hold maximum quantity of fundamental RMS output voltage.

VI. CONCLUSION.

A trinary based asymmetric three phases cascaded H Bridge multilevel inverter with R and RL load has been presented in this paper. It is mentioned that the phase opposition disposition PWM system (RL Load) with trapezoidal reference delivers excellent output waveform with comparatively low total harmonic distortion and carrier overlapping PWM system (RLoad) with trapezoidal reference delivers comparatively greater fundamental RMS output voltage (VRMS). The execution parameters like Total Harmonic Distortion (THD) and Fundamental RMS output voltage (VRMS) are determined and tabulated. The simulation circuit is performed to show the strong point of the suggested new asymmetrical three phase multilevel inverter with trinary DC source cascaded H Bridge. This topology could be analyzed with renewable energy sources like photovoltaic panel or wind energy in future. Also, it could be tested with other pulse width modulation techniques like space vector pulse width modulation or soft computing algorithms.

REFERENCES

1. Prabaharan, N, Palanisamy, K.: A comprehensive review on reduced switch multilevel inverter topologies, modulation techniques and applications. In: Renewable and Sustainable Energy Reviews, Vol.: 76C, 2017, pp.1248-1282.
2. Malarvizhi, M., Gnanambal, I.: An Integrated Technique for Eliminating Harmonics of Multilevel Inverter with Unequal DC Sources. In: International Journal of Electronics, Vol.102, No.2, 2015, 2015, pp. 293–311.
3. Varschavsky, A., Dixo, J., Rotella, M., Morán, L: Cascaded Nine-Level Inverter for Hybrid-Series Active Power Filter, Using Industrial Controller. In: IEEE Transactions on Industrial Electronics, Vol.57, No.8, 2010, pp. 2761-2767.
4. Lee, M.Y., Wheeler, P., Klumpner, C.: Space-Vector Modulated Multilevel Matrix Converter. In: IEEE Transactions On Industrial Electronics, Vol.57, No.10, 2010, pp. 3385-3394.
5. Geyer, T., Schroder, S.: Reliability Considerations and Fault-Handling Strategies for Multi-MW Modular Drive Systems. In: IEEE Transactions On Industrial Electronics, Vol.46, No.6, 2010, pp. 2442-2451.
6. Oettmeier, M., Heising, C., Staudt, V., Steimel, A.: Dead- Beat Control Algorithm for Single-Phase50-kW AC Railway Grid Representation. In: IEEE Transactions on Power Electronics, Vol.25, No.5, 2010, pp. 1184-1192.
7. Zhou, L., Smedley, K.M.: Post fault Control Strategy for the Hexagram Inverter Motor Drive. In: IEEE Transactions on Industrial Electronics, Vol.57, No.8, 2010, pp. 2719-2729.
8. Mariusz Malinowski, K. Gopakumar, Jose Rodriguezand Marcelo A. Pérez, "A Survey on Cascaded Multilevel Inverters" IEEE Transactions on Industrial Electronics, vol. 57, n. 7, July 2010, pp 2197 – 2206.

9. Choi, J.Y., Han, B.M.: An Improved Phase-Shifted Carrier PWM for Modular Multilevel Converters with Redundancy Sub-Modules. In: Journal of Power Electronics, Vol.16, No.2, 2016, pp. 473-479.
10. Dong, X., Yu, X., Yuan, Z., Xia, Y., Li, Y. An Improved SPWM Strategy to Reduce Switching in Cascaded Multilevel Inverters. In: Journal of Power Electronics, Vol.16, No.2, 2016, pp. 490-497.
11. Sayed, M.A., Ahmed, M., Elsheikh, M.G., Orabi, M.:PWM Control Techniques for Single-Phase Multilevel Inverter Based Controlled DC Cells. In: Journal of Power Electronics, Vol.16, No.2, 2016, pp. 498-511.
12. Prabaharan, N, Palanisamy, K.: Investigation of single phase reduced switch count asymmetric multilevel inverter using advanced pulse width modulation Technique. In: International Journal of Renewable Energy Research, Vol.: 5, No.:3, 2015, pp.879-890
13. Prabaharan, N, Palanisamy, K.: A Comparative analysisof symmetric and asymmetric reduced switch MLI topologies using unipolar pulse width modulation strategies. In: IET Power Electronics, Vol.: 9, No.: 15, 2016, pp.2808-2823.

Automatic Winder to Prevent Excess Coil Loss

Mr. K. Thangaraj[1]
Assistant Professor, Department of Electerical and Electronics Engineering
Sri Manakula Vinayagar Engineeing College, Puducherry
thangaraj.electres@gmail.com

Mr. M. Haridoss[2], Mr. V. Balakrishnan[3], Mr. V. Gowtham [4]
UG scholars, Department of Electerical and Electronics Engineering
Sri Manakula Vinayagar Engineeing College, Puducherry

Abstract - The proposed model is brief summary of an industrial project in REIL Industries Pvt Ltd. In that Industry they are manufacturing starters, generators etc. In the starter there is a solenoid part, which constitutes of copper winding. For winding process they are using a Single Spindle Winder (Present Working Model) which is too costly and complex. Some of the problems they are facing in the existing model are, at the time of power cut, winding operation gets stopped and the same process has to be start from the beginning. This mainly causes wastage of copper coil and time consumption in the Industry.

To overcome the above mentioned problem we introduce Arduino, IR sensor and LCD display to control and monitor the overall operation. IR sensor is used to count the rotation in a motor. And the counted values are instantly displayed in the LCD. Arduino controller conquers the overall operation that has been carried out in the project. To maintain the Arduino in on state throughout we are providing an external battery source. So that the same operation can be resumed after power failure. The main advantage of the project is developing the model at low cost, to prevent the excess coil usage.

***Keywords*—Gear motor,lcd,Arduino**

I. INTRODUCTION

REIL Electricals India Limited formerly known as Remy Electricals India, earlier known as Sahney Paris Rhone Ltd, was setup in 1977 with French Technology to manufacture electrical products for automotive original equipment manufacturers. Our products include Starter Motors and Alternator/Generators.

REIL Electricals India Limited has manufacturing facilities at Pondicherry for heavy duty, medium & light duty applications.

Presently, the specialized equipment's called single spindle winder which is used to wind the solenoid coil by the company is not economical. As a adverse effect of it, there are only two to three winding sections are there in the company, If the cost of the winder is made economical then the winding sections in the company may be escalated further in future. Normally a single spindle winder costs around 70,000– 80,000.

So in this project we have planned to design a prototype to overcome this problems faced by the company. First thing is to design a automatic winder at a cheap cost, Secondly to display the number of turns wounded in the workpiece at the time of wounding process.

In the existing model they are facing a problem due to power failure. During winding process, Eg.(Note: Each workpiece has to complete a rotation of 260 turns)If the power failure occurs at the time of 100th turn, then the workpiece is wasted because retrieval methodology is not available in the existing model. the process has to be reiterated at the time of power supply.

We have planned to design a winder to resume the process which is caused at times of power failure. To continue the overall process from where it stops, and to display the no of

turns wounded in the workpiece. Main motto is to do all this at a very cheap cost.

II. PRPOPOSED SYSTEM

The Block diagram consists of a DC motor which is used to hold the workpiece and two IR sensors. One is used to detect the workpiece to be placed in the shaft of the motor, second one is used to count the no of turns in the shaft so that number of turns can be measured and displayed in the LCD. Overall process is done with the help of an Arduino Board.controlling the pulse width, the speed of motor can be controlled.

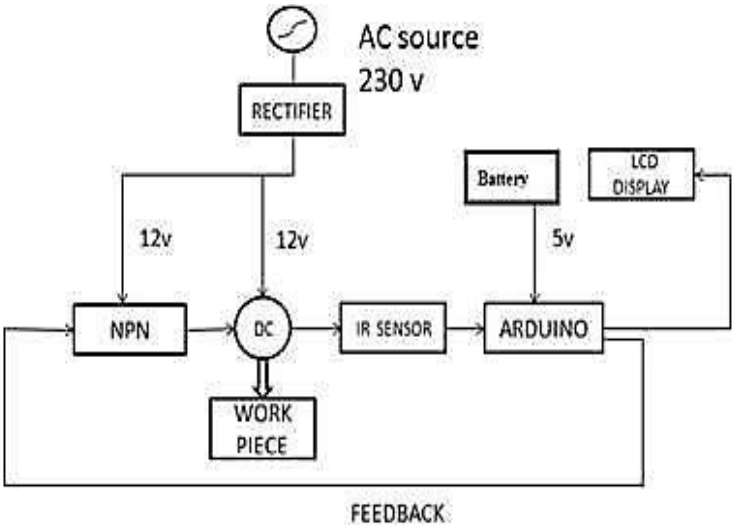

Figure 2.1 Block diagram

A 12V, 2A, DC Gear motor (TG 47E), 500 rpm is used to hold the workpiece. It deals with the triggering which is done by the arduino using npn transistor. The motor has a high torque to drive the workpiece. There is no need of erecting the motors at outdoors, so we don't need any protective measures against atmospheric influences.

ON and OFF time of the motor is decided by the Arduino. During any fault in the motor, the arduino will trip the motor. Even at the time of back emf flown through the arduino board.

Based on a simple basic Idea, this IR obstacle sensor, is easy to build, easy to calibrate and still, it provides a detection range of 10- 30 cm. This sensor can be used for most indoor applications where no important ambient light is present. It is the same principle in all Infra-Red proximity sensors. The basic idea is to send and receive a signal. The detection range of an IR obstacle sensor can be adjusted using a potentio meter which is available at the top of it.

Using this IR obstacle sensor we are going to carry out the two operations,

1. To detect the workpiece.
2. To measure the number of turns.

A proximity sensoris a sensor able to detect the presence of nearby objects without any physical contact. A proximity sensor often emits an electromagnetic field or a beam of electromagnetic radiation (infrared, for instance), and looks for changes in the field or return signal. The object being sensed is often referred to as the proximity sensor's target. Different proximity sensor targets demand different sensors. For example, a capacitive proximity sensor or photoelectric sensor might be suitable for a plastic target; an inductive proximity sensor always requires a metal target.

The maximum distance that this sensor can detect is defined nominal range. Some sensors have adjustments of the nominal range or means to report a graduated detection distance. Some know these processes as "thermosensation".

Proximity sensors can have a high reliability and long functional life because of the absence of mechanical parts and lack of physical contact between sensor and the sensed object.

Proximity sensors are commonly used on mobile devices. When the target is within nominal range, the device lock screen UI will appear, thus emerging from what is known as sleep mode. Once the device has awoken from sleep mode, if the proximity sensor's target is still for an extended period of time, the sensor will then ignore it, and the device will eventually revert into sleep mode. For example, during a telephone call, proximity sensors play a role in detecting (and skipping) accidental touchscreen taps when mobiles are held to the ear.Proximity sensors are also used in machine vibration monitoring to measure the variation in distance between a shaft and its support bearing. This is common in large steam turbines, compressors, and motors that use sleeve- type bearings.

In the ir proximity sensor it consists of two led lights. One is IR transmitter and the other is IR receiver .The transmitter transmits the infrared rays to an object, if the object surface is made up of white colour the reflected ray varies with the speed when compared to the black surface. For eg. Reflection from a white surface is with high intensity whereas for a black surface it is partial.

BLACK SURFACE	WHITE SURFACE
0	1.5
0	1.3
0	1.2
0	1.2
0	1.2

Table 2.1 Number of count detection based on sensor

- 5VDC operating voltage.
- I/O pins are 5V and 3.3V compliant.
- Range: Up to 20cm.
- Adjustable Sensing range.
- Built-in Ambient Light Sensor.
- 20mA supply current.
- Mounting
- Size: 50 x 20 x 10 mm (L x B x H)
- Parking sensors, systems mounted on car bumpers that sense distance to nearby cars for parking
- Ground proximity warning system for aviation safety
- Vibration measurements of rotating shafts in machinery
- Top dead centre (TDC)/camshaft sensor in reciprocating engines.
- Sheet break sensing in paper machine.
- Anti-aircraft warfare
- Roller coasters
- Conveyor systems
- Beverage and food can making lines.

The model diagrammatic representation of "Semi Automatic Winder to Prevent excess coil usage" in the industry and to display the total number of turns in the solenoid. It also tabulates various advantages over the other logic controller which is used at the past.

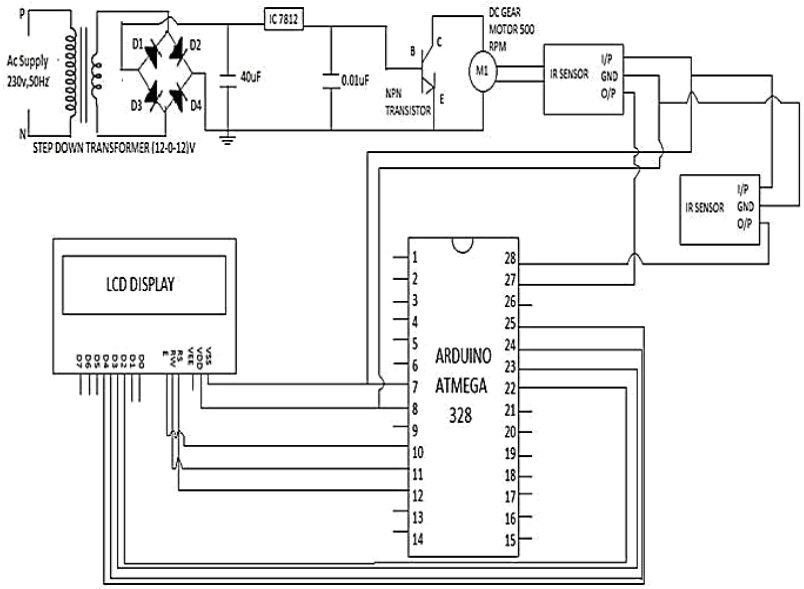

Figure 2.2. Overall circuit diagram

Above figure shows that the overall connection and circuit of the project. This diagram explains about the connection between ir sensors, motor and arduino and some other external devices. Overall circuit diagram of this project helps us to know easily about ir sensors, aurdino and LCD display interface with any device for controlling and monitoring purpose.

III. CONCLUSIONS

This proposed method to wind the coil using an Arduino uno which is used to count and display the turns in a winding section to prevent many faults which is existing already. The logical program was developed and feeded into the Arduino which meets the objective of our project. In Arduino Software, the coding part is done and fed to the Arduino board and all the above prescribed things are done using a PC. By implementing Arduino, the advantage is meeting the requirements at ease of cost.

Arduino reduces the use of external hardwares and complex wiring and also overcoming the limitations. LCD screen shows the entire operations such as 1. Whether the coil is placed or not. 2. Counting the turns and displaying each count. 3. And also notifying to remove the coil. Life span of the developed prototype is high, except the motor all other components are static device which eliminates wear and tear operations. By this project, we have fulfilled our desires, in design and development to the fullest satisfaction by adopting the latest technology

REFERENCES

1. V J Sivanagappa " Speed control of DC Motor via arduino interfacing" describes about the history of arduino and its evolution from time and various components used to increase the efficiency of the output.
2. " Speed Control Systems" describes aboutthe use of industrial computers in industrial sectors and its advantages over other controllers.
3. The paper " Infrared Sensor in Detecting Various Object Shapes" describes how to identify an object and also it is taken as a interrupt signal to the arduino controller.
4. Tharun Agarwal " Interfacing LCD display using an arduino" describes the communication between the human world and machines world.

Dual Axis Solar Tracking System using LDR Sensors

Mr. S. Sivabalan[1], Mr. K. Sharan[2], Mr. S. Sudhakar[3]
PG Student, Department of Electrical and Electronics Engineering,
Krishnasamy College of Engineering and Technology,
S. Kumarapuram, Cuddalore-607 109.

Mr. S. Sivasakthi[4]
Associate Professor, Department of Electrical and Electronics Engineering,
Krishnasamy College of Engineering and Technology,
Cuddalore-607 109.

Abstract— The main goal of increasing the efficiency is to get the maximum power from the solar panel. The project is to design and implementation simple and cheap price solar tracker system with two axes (azimuth angle as well as altitude angle) using Light Dependent Resistor (LDR) with real dimensions the project composed of solar panel, two-motor satellite dish and ball-joint, LDR sensor module and an electronic circuit. This project is compared with fixed solar panel and the results showed that solar tracker more output power than fixed solar panel. The project is divided into two parts; hardware and electronic. Hardware part generally composed of solar panel, two-DC motors with gearbox and LDR sensor module. Second part is electronic circuit. In this work sensing of the sun position carried out in two stages, first stage or direct sensing performed via set of LDR sensors as output tuning to trims the azimuth and altitude angles. second stage, when the weather is cloudy, dusty or rain, the tracking system will stop so the system stays in the position of the sun without move but according to Kelly cosine relation the power will decrease. The energy extracted from photovoltaic (PV) or any solar collector depends on solar irradiance. For maximum extraction of energy from the sun, the solar collector panel should always be normal to the incident radiation Solar trackers moves the solar collector to follow the sun path and keeps the orientation of the solar collector at an optimal tilt angle. Solar tracking system improves substantially the energy efficiency of photovoltaic (PV) panel. In this paper, an automatic dual axis solar tracking system is designed and developed using Light Dependent Resistor (LDR) and DC motors on a mechanical structure with gear arrangement. The results indicated that the automatic solar tracking system is more reliable and efficient than fixed one.

I. INTRODUCTION

Solar energy is the most inexhaustible, renewable source of energy known to humanity. In order to increase the efficiency of solar energy systems, solar tracker is added at the expense of system's complexity and cost. The two basic categories of trackers are single axis and dual axis. Single axis tracker has one axis of freedom, vertical or horizontal. Dual axis tracker has both a vertical and a horizontal axis of freedom, so it able to track the position of the sun precisely. A prototype of the automatic two-axis solar tracking system with a new design of sun-position tracker mechanism. Two angle sensors are used to measure the physical angles on both outlet shafts of azimuth and elevation to make sure the desired angles are reached. Set of four LDR light sensor are used to trim the errors of altitude and azimuth angles, as shown in the figure 1.1. As a result of experiments the power generated by the proposed tracking system is increased in the overall of about 10% ~ 40% more than fixed angle system in general. The increase of the output power from solar panel increases the

efficiency of the system and increase this output power whenever the solar radiation fell on the solar panel perpendicularly, but the earth revolves around the sun throughout the year, so the position of the sun changes constantly in the sky, the angle of solar radiation falling on the ground also changes, as the various solar applications need to fall solar radiation vertically on its surface.

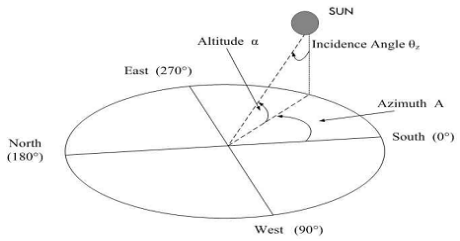

Fig.1.1Azimuth and Altitude angles

The theoretical value of altitude and azimuth angles are translated into digital commands for driving DC motors to the corresponding position. Then, the system automatically trims the altitude and azimuth angle of the PV panel according to feedback signal of the proposed LDR sensor module. The sunlight sensor module consists of four LDR- sensors. Two angle sensors are placed on outlet shafts of altitude and azimuth angles for measuring the final value of altitude and azimuth angles and transmitting these values to the supervisory computer user interface [1-3]. The Kelly cosine value relationship between relative current generated from solar panel and sun incidence angle in degree as shown in the figure 1.2.

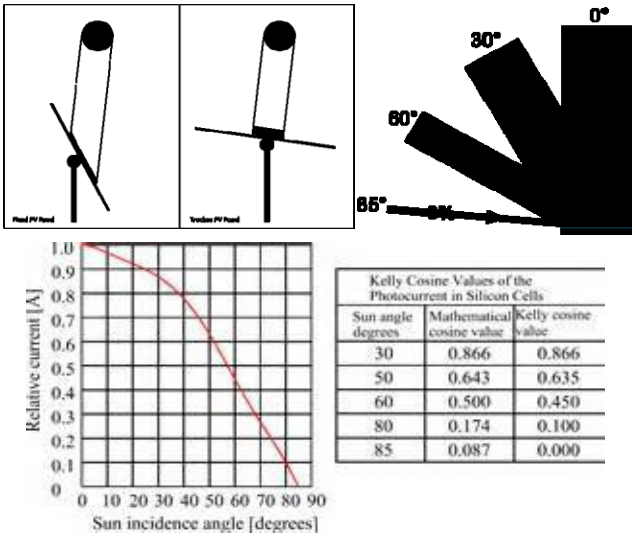

Kelly Cosine Values of the Photocurrent in Silicon Cells

Sun angle degrees	Mathematical cosine value	Kelly cosine value
30	0.866	0.866
50	0.643	0.635
60	0.500	0.450
80	0.174	0.100
85	0.087	0.000

Fig.1.2 solar panel and sun incidence angle

So we need a specific mechanism that moves the solar system and makes it follow the solar radiation falling from the sun on the surface of the earth, This mechanism is a solar tracker, a device that makes the payloads (photovoltaic panel, parabolic troughs, Fresnel reflectors, lenses or the mirrors of a heliostat) oriented toward the sunbeam to get most of the radiation energy that falls on the surface of the panel or collector to increase the converted energy. The majority of the solar panels that are done in our nation are fixed, however fixed systems can collect the maximum power for a few hours through days but the solar tracker can follow the sun from sunrise to sunset all day through a year the solar trackers have several types that depend on their mechanism for tracking the Sun trajectory on one or two axes Single axis tracking and Dual axis tracking

II. SOLAR TRACTING SYSTEM DESCRIPTION

The main task is the design and implementation of solar tracking system in outdoor. To achieve maximum output power that produced by solar panels as the sun moving across the sky and keeps the panel perpendicular to the radiation sun. We used two-axis solar tracking system with active tracking cause it the effective way to track the sun in elevation and azimuth angles. some electronic part for tracking electronic circuit: Component of project Two solar panels 80 watt has length 120 cm and width 54 cm, Silicon polycrystalline type. Two electrical motors satellite dish actuator Four LDR (Light Dependent Resistor) charge controller two IC LM324

Fig. 2.1. The complete system

The mechanical part: The mechanical structure of the solar tracking system consists of fixed parts and movable parts to allow the system to track the movement of the sun throughout the day during the year. The structure is designed to be portable to carry the system as well as be resistant to natural elements such as heat and wind, as the system is stay outdoor.

The first part of the design of the structure is the strong base that can be carried the solar panel with motors, and also can be moved to change the place of the system, at the centre of the base is placed a column.

Fig. 2.2. Show the part of mechanical structure

At the other end of the column set shaft with 60˚angle and in the end of shaft placed ball joint that connected with the solar penal Which allows the system to move to track the movement of the sun. Two arms are connected to the column that used to carry the motors and the other side of motors connected to solar panel by ball joint.

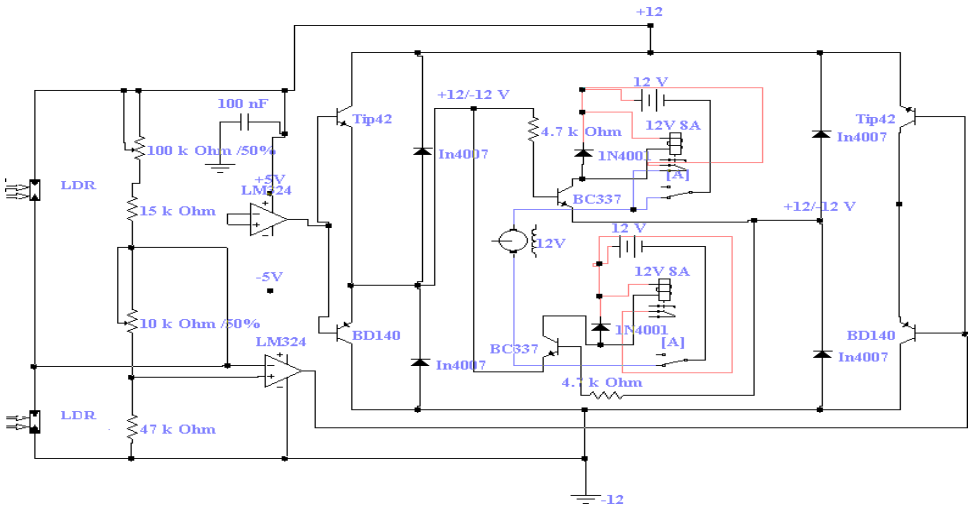

Fig. 2.3 Electronic circuit of tracking system

The electronic part: Solar cells work to give more energy and better efficiency when they are at the right angle with the sun means solar radiation falling vertically on the solar cell, that happens by using a solar tracking system that uses sensors that are detected the sunlight. The sensors are connected with an electronic circuit that receives and interprets the desired action which in turn commands the motor to move in clockwise or anticlockwise to track the sun potion and keep the solar panel in directly with the sun. In our project we needed four sensors that were designed in the vertical way. A LDR sensor was placed in the end side and installed on the edge of the solar panel. To Knowing the error ratio in tracking system of the sun we design and drew 10 circles with colours and put metal bar in the medal, each circle represents one degree.

III. SOLAR TRACTING SYSTEM DESCRIPTION

3.1 Schematic arranging

The main goal of this project is to design a very precise solar tracker. The project is divided into two parts; hardware and software. The main constituents of the tracking system are shown in Figure2. Hardware part generally composed of solar panel, two-DC motors with gearbox, LDR sensor module and electronic circuit. Software part represents the thinking behaviour of the system, that is how the system acting under several weather conditions.

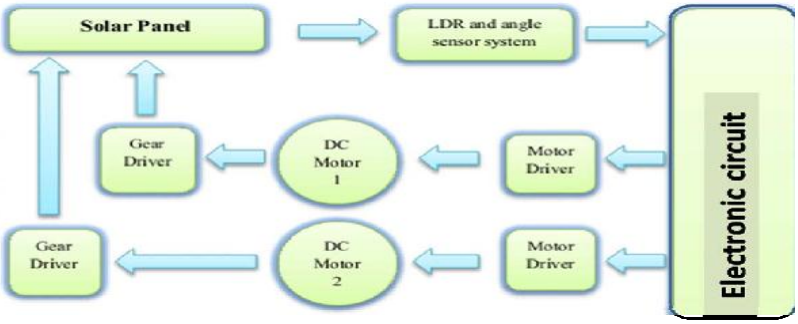

Fig. 3.1. System design block diagram

3.2 Sun position sensing method used in the control circuit

To track the sun it is vital to locate the position of the sun accurately. In this work sensing of the sun position carried out in two stages primary and secondary. Primary stage or

indirect sensing performed via sun-earth relationship as a coarse adjustment and second stage or direct sensing performed via set of LDR sensors as output tuning to trims the azimuth and altitude angles. If the weather is cloudy or dusty, the tracking system uses primary stage or sun-earth geometrical relationships only to identify the location of the sun; so the system tracks the position of the sun regardless the weather condition.

3.3 Mechanical structure depiction

The whole mechanical structure of the proposed dual axis solar tracking system is shown in Figure 4.LDR sensor module is attached in a plane parallel with solar collector. A plastic box covered with tin foil is used for covering the electronic control circuit. Two DC motors with gearbox arrangement are used to obtain the required movements. Also, aluminium structure is used to hold the solar panel.

IV. RESULTS AND DISSCUSSION

Two solar panels were tested. One of them fixed and the other placed on the solar tracking system that was executed. In the test, the current and voltage from the solar panel were calculated that occur by placing a load (Two lamps 12 volts 70w, 21w),To calculate the current and voltage used by the load of the solar panel and showed the results.

Fig. 4.1.

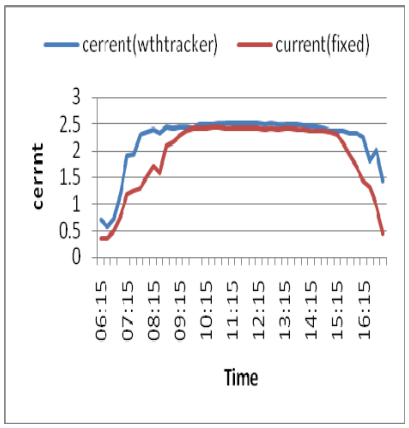

Fig. 4.2.

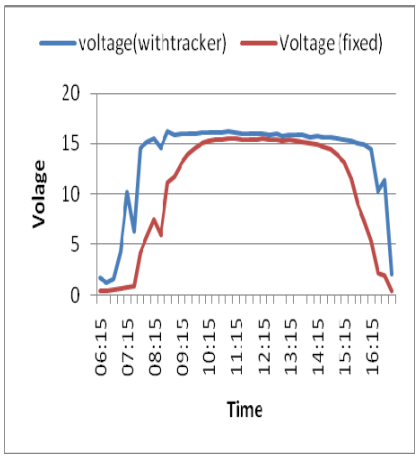

Fig. 4.3.

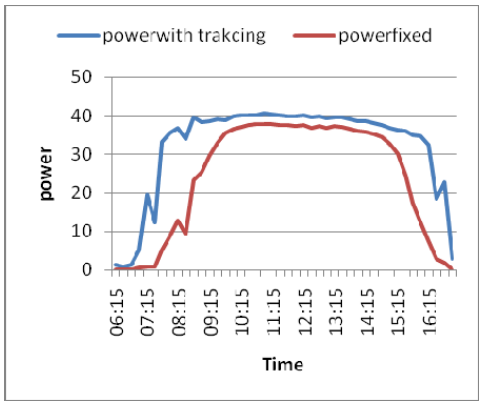

Fig. 4.4

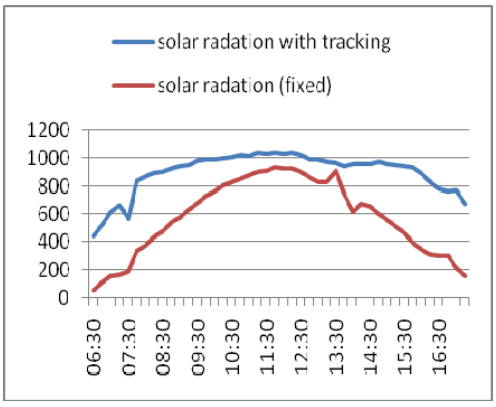

Fig 4.5.

We also calculated the solar radiation value on the solar panels that results of the solar tracking system was 56% increase than in solar panel. And also the error rate in the system does not exceed 5%. We calculate the efficiency of PV Panel in both systems with tracking

and without by Comparison between the resulting powers generated of both systems. The power efficiency is 35% increase in solar tracking system than in solar fixed system.

V. CONCLUSION

As solar energy is considered one of the main sources of energy in the near future, In this paper, we give a simple and concise overview of the solar tracking mechanism to improve the solar gain energy, also the costs of the solar tracker operation and cost maintenance is relatively low. In this paper, Design and implementation of solar tracker with two axes that Use in motor satellite dish to track the sun accurately and use LDR sensor to determine the intensity of falling sunlight. We found that the solar tracking system is more effective than the fixed solar panel. The energy gained from the solar panel with the dual tracker exceeds 35% of the energy gained from the fixed solar panel, In analysing the data, the energy gained from the solar tracker is mostly in the morning and in the evening because at noon time there is little difference and this proves that the fixed solar panel is efficient during noon time only. The dual-axle solar tracking system is efficient as it can be placed anywhere and ensure a high energy gain.

REFERENCES

1. Power from the sun. (n.d.). Retrieved from http://www. powerfromthesun.net/Book/
2. The Sun's Position. (2013, March 28). In Photovoltaic Education Network, from http://pveducation.org/pvcdrom/properties-of- sunlight/suns-position
3. Zhan, T., Lin, W., Tsai, M. and Wang, G. Design and Implementation of the Dual-axis Solar Tracking System IEEE. 37th Annual Computer Software and Applications Conference.pp.276–277, 2011
4. Zolkapli, M., AI-Junid S. A., Othman Z., Manut, A., and MohdZulkifli, IEEE .International Conference on Technology, Informatics,Management, Engineering & Environment.pp.43-47, 2013
5. Nader Barsoum, Intelligent Control and Automation, 2, 57-68, 2011
6. Nabeel Abid Al-Sahib, Falah. I. Mustafa , Ayad M. Kwad, The Fourth International Renewable Energy Congress December 20-22, 2012 – Sousse, Tunisia.
7. Falah Mustafa, Abd Salam Al-Ammri, Farouk Ahmad: The eighth International Renewable Energy Congress (IREC 2017). on March 21 – 23, 2017 in Amman, Jordan.
8. Soumen Ghosh, Nilotpal Haldar, International Journal of Emerging Technology and Advanced Engineering, Volume 4, Issue 12, December, 2014
9. Hussain S. Akbar1,*, Abulrahman I.Siddiq2, Marwa W. Aziz, American Journal of Energy Research, Vol. 5, No. 1, 23-27, 2017
10. Deekshith K , Dhruva Aravind , Nagaraju H , Bhaskar Reddy International Journal of Scientific & Engineering Research, Volume 6, Issue 9, September 2015

Radial Movement Optimization (RMO) Technique for Solving Unit Commitment Problem in Power Systems

Mrs. S. Lese[1]
Associate Professor,
Department of Electrical and Electronics Engineering,
St. Anne's College of Engineering and Technology,
Anguchettypalayam, Panruti – 607106.

Ms. K. Kalpana[2], Ms. B. Subishya[3]
UG Student,
Department of Electrical and Electronics Engineering,
St. Anne's College of Engineering and Technology,
Anguchettypalayam, Panruti – 607106.

Abstract - Unit commitment (UC) is one of the nonlinear optimization problems with linear and nonlinear constraints. In this work, radial movement optimization (RMO) is employed to solve the optimal thermal unit commitment problem. Radial movement optimization is a novel global optimization technique used to solve the complex optimization problems. In this work, 10, 20, 40, 60, 80 and 100 unit systems are considered for implementing the RMO technique in the cost estimation of thermal unit commitment problems. The simulation test results show economic results and good convergence, while satisfying the constraints of the objective function. The results also show that the RMO algorithm outperforms the other algorithms like GA, PSO, DE etc. with minimum cost.

Keywords: **Radial movement optimization; Optimization; Unit commitment; Thermal**

I. INTRODUCTION

In electrical power systems, unit commitment (UC) problem is considered as a complex problem because of its nonlinearity and it is a mixed-integer optimization problem. Unit commitment is a blend of generator scheduling problem and the generation allocation problem. It deals with the optimum amount of time for which a generating unit must be operated at a per hour basis in order to meet the load requirements effectively. With the help of this optimization, it is possible to supply power with least possible losses and minimum fuel consumption, in order to maximize the profit. Besides achieving minimum total production cost, a generation schedule needs to satisfy a number of operating constraints. These constraints reduce freedom in the choice of starting-up and shutting-down of generating units. The constraints to be satisfied are usually the status restriction of individual generating units, minimum up time, minimum down time, capacity limits, generation limit for the first and last hour, limited ramp rate, group constraint, power balance constraint, spinning reserve constraint etc., (Saravanan et al., 2013).

Regarding the power demand variations, the UC problem is to commit adequate units at appropriate time and with enough generated power, economically. In addition, most of the unit types in the electric power systems are the thermal units which cannot instantly turn on and produce power.

In this paper, a simple and efficient stochastic optimization algorithm is employed to solve the unit commitment problem in power systems. Radial movement optimization is applied to solve the unit commitment problem and the results obtained are compared with various methods.

II. UNIT COMMITMENT PROBLEM

2.1. Objective function

The objective of the unit commitment problem is the minimization of thermal cost for committed units over a scheduling period T. It can be written as

$$\text{Minimize } F = \sum_{i=1}^{T} i \sum_{I=1}^{Ng} \{\text{uit Ft (i, t)} + \text{SC (i, t)}\}$$

Where

u_{it}—Operating status of the i^{th} thermal unit at a time t

Ng—Number of generating units in the system

F_t—Total fuel cost and

SC—Start-up cost

The production cost can be expressed in a general quadratic form using cost coefficients of the thermal plant.

2.2. System constraints

2.2.1. Load balance constraint

The load balance is written as

$$\sum_{i=1}^{Ng} uitPit = PDt$$

Where P_{Dt}—total system demand at time t.

2.3. Spinning reserve constraint

During the operation of a power system, the spinning reserve must be available to minimize the probability of load interruption. It is considered to be a pre-specified amount or a given percentage of the forecasted peak demand (Jeong et al., 2009). It is given by

$$\sum_{i=1}^{Ng} uitP\text{max}i - PDt \geq Rt \quad (3)$$

where Rt—reserve requirement at time t.

The reserve requirement was 10% of the hourly load and the start-up cost was calculated as

$$SC(i, t) = \begin{cases} HSC(i), \text{ if } md(i) \leq X^{off}i \leq md(i) + CST(i) \\ CSC(i), \text{ if } X^{off} > md(i) + CST(i) \end{cases} \quad (4)$$

where CST is the cold starting hour.

2.4. Unit constraints

The generator capacity constraints are expressed as

$$u_{it}P^{\min} \leq P_{it} \leq u_{it}P^{\max}i \quad (5)$$

where min and max represent the minimum and maximum values.

The minimum uptime (*mu*) defined as the minimum number of hours for which a committed unit should be turned on. It is represented as

$$mu_i \leq X^{on}{}_{\text{i}}$$

Minimum down time limit (*md*): It is defined as the minimum number of hours for which a de-committed unit should be turned off. It is given as

$$md_i \leq \quad X^{off}i \tag{7}$$

where X^{on} and X^{off} represent the duration for which the unit is continuously on and off respectively.

III. RMO ALGORITHM

3.1. Radial movement optimization for unit commitment problem

The RMO algorithm is used for solving the unit commitment problem. UC is a mixed integer non-linear optimization problem which includes continuous variables (X) representing the generation schedules and discrete variables (Y) representing the operating status of the thermal units. The RMO algorithm is modified to handle both these variables.

Therefore unit commitment problem is well suited for the application of mixed integer RMO algorithm. The different steps involved in the RMO algorithm for solving the unit commitment problem are detailed below:

3.1.1. Step—1: initialization

The initial particles in the search space are randomly generated within their limits. The initial population is represented as

$$X^0i,i \quad = (X_{\min}, Y_{\min}) + +P_i\,(X_{\max} - X_{\min}) + round\,[P_i\,(Y_{\max} - Y_{\min}) \tag{8}$$

where round represents the nearest integer to the real number.
The population vector consists of both integer and discrete variables.

3.1.2. Step—2: generate the initial velocity vector

The velocity vector v_{ij} is randomly generated using the following equation For integer variables representing on/off states of generator:

$$V_{ij} = \text{round}\,(rand\,(0, 1) \times V_{\max(j)}) \tag{9}$$

For real variables representing the power generation:

$$V_{ij} = rand(0, 1) \times V_{\max(j)} \quad \text{for real variables} \tag{10}$$

where i = 1, 2, 3 .....m and j = 1, 2, 3 s, for integer; s + 1 .
n for real

$$V_{\max}\,(j) = round^{(}X_{\max(j)} - X_{\min(j)}$$

K for integer variables

$$V_{\max}\,(j) = X_{\max(j)} - X_{\min(j)}$$

K for real variable
K is an integer number which is choosen judiciously. X_{max} (j) and X_{min} (j) are the minimum and maximum limits of j^{th} control variable respectively.

3.1.3. Step—3: locate the center point

The fitness of each particle in the population vector is estimated using the following equation

$$\Psi = \sum_{t=1}^{T} \quad \sum_{i=1}^{Ns}\{\text{u (i, t)FC (i, t)} + \text{SC (i, t)}\} + \sum_{z=1}^{Nc} \emptyset |VIOLz|$$

where $Ø_z$ is the penalty factor.
The population vector which gives the minimum fitness value is chosen as the initial center point (C_p) and it is the gbest vector in the initial population.

3.1.4. Step—4: to find the radial movement

The radial movement of the particles from the center point Cp is given by

$$U_{ij} = round(W \times V_{ij} + center\ (j))$$

$$U_{ij} = W \times V_{ij} + center\ (j)$$

W is the inertial weight which is calculated in each iteration using

$$W = W_{\max} - \left(\frac{W\max - W\min}{Generation\ \max} \right) \times Generation$$

W_{max} is fixed as 1 and W_{min} is fixed as 0.

Here the particles are sprinkled. If any control variable in the population in the population vector V_{ij} violates their maximum or minimum limits then that variable is fixed at their violated limit.

Hour	1	2	3	4	5	6	7	8	9	10	11	12
Demand	700	750	850	950	1000	1100	1150	1200	1300	1400	1450	1500
Hour	13	14	15	16	17	18	19	20	21	22	23	24
Demand	1400	1300	1200	1050	1000	1100	1200	1400	1300	1100	900	800

Table 2: Daily load demand (10 unit system).

3.1.5. Step—5: evaluate the fitness of the particle and determine the new centre location

The fitness of each vector in the population U_{ij} is evaluated. The particle which gives the minimum error is selected as radial best (Rbest) vector. The new center location (center 1) is updated using the following equation

$$Center^{K+1} = round(Center^{K} + (\ C_1\ [G_{best} - Center^{K}\ ]) + (\ C_2\ [R_{best} - Center^{K}\ ]\ ))$$

where K is the iteration number.

j=1,2, ... s

j=1,2, ... s+1

The fitness of radial best vector is compared with the fitness of global best (Gbest) vector. If R best is better than Gbest, Gbest is replaced by Rbest.

The convergence of radial movement optimization is improved by generating number of trial vectors around the Gbest is

$$V_{ij} = round\ (G_{best} + unifrnd\ (0,1) * U_{r1j} - U_{r2j}$$

i = 1,2,...m; j = 1,2,...n

where r_1 and r_2 are randomly selected vector which are mutually different from each other. The fitness of each vector in V_{ij} is evaluated and are compared with Gbest. If the fitness of trial vector is better than Gbest, trial vector replaced the Gbest vector. This step is repeated for Nt times for each vector in every iteration.

The iteration is incremented by 1. The steps 1-4 is repeated for predefined iterations.

IV. RESULTS AND DISCUSSION

In this study, unit commitment test systems comprising of 10-100 thermal units are considered as case studies. For small-scale UC problem 10 unit test system is considered and for large-scale UC problem 20, 40, 60, 80 and 100 unit test systems are considered. The data for unit commitment problem are collected from the literature (Kazarlis et al., 1996) and are

tabulated in Tables 1 and 2. The unit commitment problems with 20, 40, 60, 80 and 100 generating units are duplicated by the amounts of ten units system, considering a time horizon of 24 h. The total number of decision variables is 480 (i.e. 10 × 24 + 10 × 24) for 10 unit system, representing the generations of units and their operating status (Lakshminarasimman and Subramanian, 2008). In this work, the duplicated test problems have 960, 1920, 2880, 3840 and 4800 binary variables for 20, 40, 60, 80 and 100 unit system respectively.

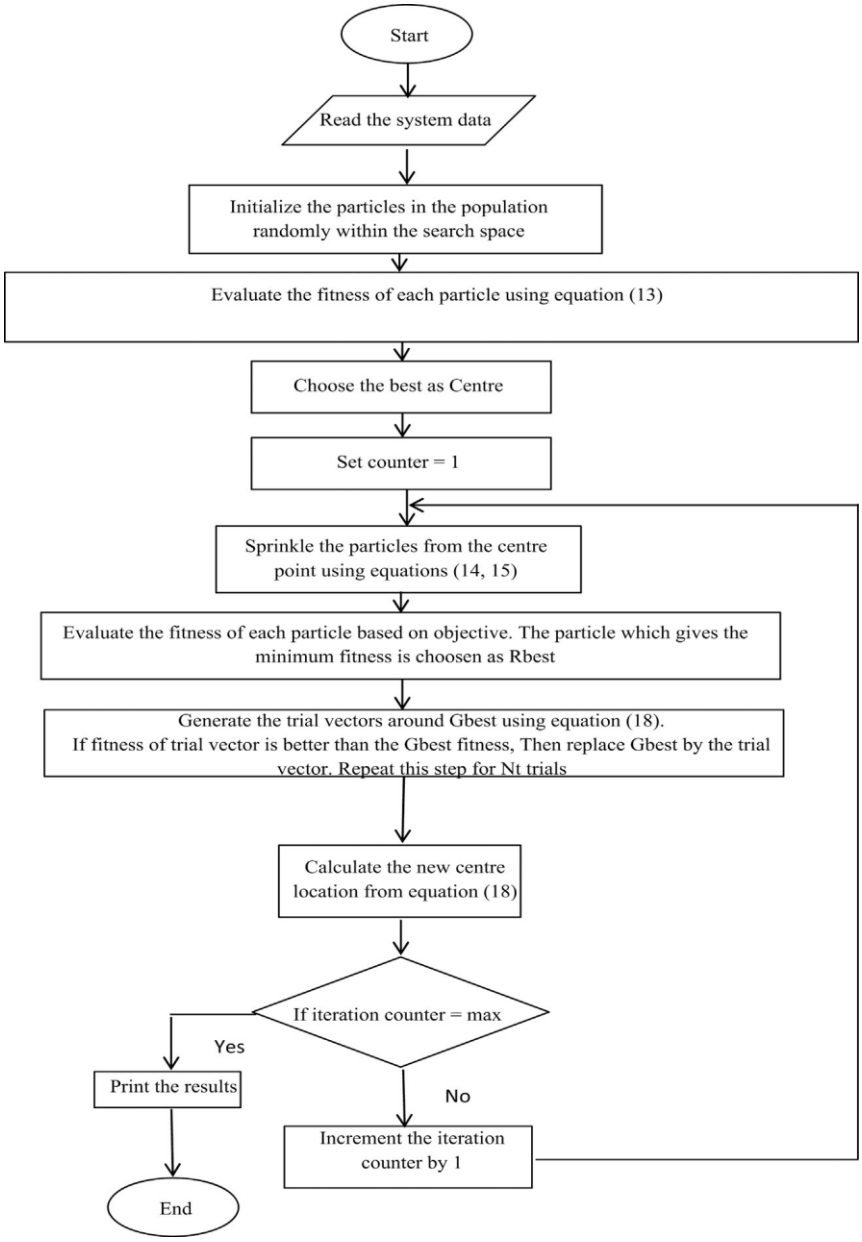

Fig. 4.1. Flowchart for solving unit commitment problem using RMO.

RMO technique is employed to solve 10, 20, 40, 60, 80 and 100 generating units test system and the results are analyzed. In order to establish the effectiveness of the RMO algorithm, the numerical results of the RMO technique is compared with various metaheuristics

techniques. The algorithm (Fig. 4.1) is applied in MATLAB (2011) and the simulation results are presented in Tables 3 and 4. Simulation is performed in an Intel core i3 PU with 2 GB RAM.The on/off status for the 10 unit system by RMO technique is shown in Table 3. The optimal power generation outputs for 10 unit system are shown in Table 4. It is also found from Table 4 that the optimal results satisfy all constraints. Hence, the RMO is successfully developed to solve the UC problem with 10 units. The power load demandshared for 24 h by the units 1-10 is shown in Fig. 4.2. From the figure it was observed that the unit 1 shares most of the load and unit 10 shares no load. A maximum power of 10,920 MW is generated by Unit 1. In order to identify the effectiveness of the RMO technique for large-scale power systems, the 10 units system is duplicated to 20, 40, 60, 80 and 100 units test systems. The duplicated system is composed of X copies of original generators and the duplicated load which can be provided by generation in all copies. In this duplicated approach, different copies are not isolated but are able to influence each other. The simulation results obtained for these duplicated systems are compared with the results obtained by other methods and given in Table 5. The operating (ON/OFF) result of RMO with a total operating cost of $558,578, 1,122,535, 2,240,054, 3,354,166, 4,471,835 and 5,600,028 for the 10, 20, 40, 60, 80 and 100-unit test system respectively. It is also found from Table 5, that the RMO gives the best optimal results on nearly all test systems.

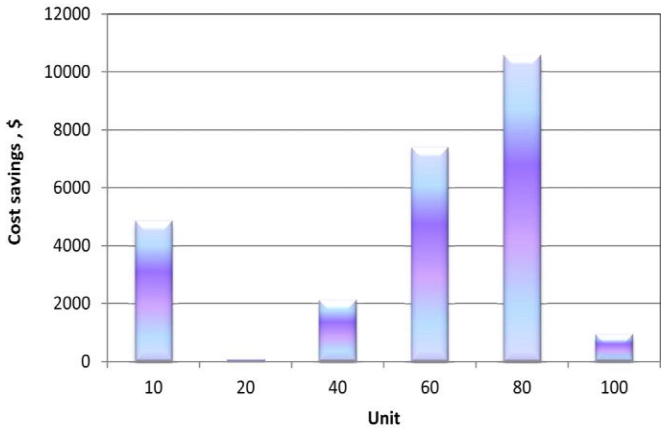

Fig.4.2. Convergence characteristics of RMO for UC problem (10 unit system).

A comparison is made between the cost savings ($) obtained by the best solution of RMO and the best solution obtained by the various algorithms given . A maximum savings of $ 10,582 is attained by RMO for 80 unit system when compared to the best solution of ATHS (Anup Shukla and Singh, 2016). respectively. It shows that the implementation of RMO can reduce a huge amount in the Unit commitment problem.The optimal convergence characteristic of RMO for 10 unit systems is shown in From the figure it was found that the results are converged at faster rate. It shows the effectiveness of RMO in solving the UC problem. The average execution times for the different unit systems were given. It is found that the average execution time is found to be low. Even though it may not be directly comparable due to variation of system configuration or programming languages, but some observation can be attained.

V. CONCLUSIONS

In this paper, the RMO is effectively implemented to solve the unit commitment problem. The simulation result reveals that the RMO is effective in searching global or near global optimal solution to the UC problem. The RMO methodology is simple, easy and applicable for

large-scale systems. From the results, it is observed that the RMO gives economical solution for large scale UC problem compared to all other methods reported in the literature, within a reasonable computational time. Also the results show a faster convergence to the solution. Hence RMO based optimization is a promising technique for solving complicated optimization problems in power systems.

REFERENCES

1. Amiri, M., Khanmohammadi, S., 2013. A primary unit commitment approach with a modification process. Appl. Soft Comput. 13, 1007–1015.
2. Barati, M., Farsangi, M.M., 2014. Solving unit commitment problem by a binary shuffled frog leaping algorithm. IEEE Gener. Transm. Distrib. 8, 1050–1060.
3. Benhamida, F., Abdelbar, B., 2010. Enhanced Lagrangian relaxation solution to the generation scheduling problem. Int. J. Electr. Power Energy Syst. 32, 1099–1105.
4. Bukhari, S.B.A., Ahmad, A., Raza, S.A., Siddique, M.N., 2016. A ring crossover genetic algorithm for the unit commitment problem. Turk. J. Electr. Eng. Comput. Sci. 24, 3862 3876.
5. Chakraborty, S., Ito, T., Senjya, T., Saber, A.Y., 2012. Unit commitment strategy of thermal generators by using advanced fuzzy controlled binary particle swarm optimization algorithm. Int. J. Electr. Power Energy Syst. 43, 1072–1078.
6. Chandrasekaran, K., Hemamalini, S., Simon, S.P., Padhy, N.P., 2012. Thermal unit commitment using binary/real coded artificial bee colony algorithm. Electr. Power Syst. Res. 84, 109–119.
7. Chandrasekaran, K., Simon, S.P., Padhy, N.P., 2013. Binary real coded firefly algorithm for solving unit commitment problem. Inf. Sci. 249, 67–84.
8. Chen, P.H., 2012. Two level hierarchical approach to unit commitment using expert system and elite PSO. IEEE Trans. Power Syst. 27, 780–789.
9. Chung, C., Yu, H., Wong, K.P., 2011. An advanced quantum-inspired evolutionary algorithm for unit commitment. IEEE Trans. Power Syst. 26, 847–854.
10. Cohen, A.I., Yoshimura, M.A., 1983. A branch and bound algorithm for unit commitment. IEEE Trans. Power Appar. Syst. 2, 444–451.
11. Damousis, I.G., Bakirtzis, A.G., Dokopoulos, P.S., 2002. A solution to the unit commitment problem using integer coded genetic algorithm. IEEE Trans. Power Syst. 19, 1165–1172.

Dynamic Power Management System Employing Single Stage Power Converter for Standalone Solar PV Applications

Mr. A. Richard Pravin[1]
Assistant Professor,
Department of Electrical and Electronics Engineering,
St. Anne's College of Engineering and Technology,
Anguchettypalayam, Panruti – 607106.

Mr. J. Albert Wilson[2], Mr. M. Anastraj[3], Mr. V. Arulraj[4], Mr. K. Mark Vilfar Kennady[5]
UG Student,
Department of Electrical and Electronics Engineering
St. Anne's College of Engineering and Technology,
Anguchettypalayam, Panruti – 607106.

Abstract - This paper presents a dynamic power flow management system for a solar PV system employing a single stage single inductor based dual input/output DC-DC converter feeding standalone DC loads backed up by a rechargeable battery. A time sharing voltage mode control scheme has been proposed for power flow management between solar PV, battery and standalone DC load and also it maintains a constant DC load voltage and performs MPPT operation of solar PV. The implementation of the control scheme has been described in detail. The steady state performance of the single stage converter has been explained with the relevant analytical expressions derived along with the characteristics. A state space average model was developed for simulating the transient behavior and validating the working of the system for step changes in the input solar PV power and the DC loads. A hardware prototype of the proposed system has been fabricated and the proposed controller has been implemented using dSPACE DS1103 Real Time interface (RTI) board. The working of the proposed scheme for the different levels of input solar insolation and DC Load power demand has been satisfactorily demonstrated and the corresponding results are also provided.

***Index Terms*—DC-DC power conversion, Batteries, Solar power generation, Power converter, Multiport circuits and Photovoltaic power systems.**

I. INTRODUCTION

Harnessing renewable energy sources such as wind energy, solar energy, tidal, etc. is critical for overcoming problems due to global warming and environmental degradation caused by the use of fossil fuels. Among all renewable energy sources, solar PV is abundant, has high power density, is modular and scalable. Solar PV is used both in grid connected applications and standalone applications. It can be used in a wide range of applications from a microwatt internet of things (IoT) system to a megawatt scale solar PV plant [1], [2]. Solar PV operates in a wide range of DC voltages, while electrical and electronic systems also have different levels of DC voltage requirements [3]. Hence, it is necessary to use power electronic interfaces for solar PV applications. Since the energy from solar PV is intermittent in nature, it is necessary to combine energy storage systems and other renewable energy sources to maintain reliable operation for standalone PV systems. This can be achieved by many single

input/output (dual port) DC-DC converters in parallel or multiport DC-DC converters. The centralized architecture of multiport converters uses fewer switches, has compact structure, lower cost, higher efficiency and avoids the need to use communication systems as compared to multiple single input/output DC-DC converters [4], [5].

Sun et al. [4] have proposed a three port converter incorporating solar PV, battery as power sources feeding DC loads with galvanic isolation. The control structure involved a complex hybrid modulation technique (PWM + PFM) with soft switching. Ray et al. proposed an integrated dual output DC-DC converter which had both buck and boost outputs using PWM to regulate output voltages]. Various possible topologies for multiport converters have been discussed in]. However, using multiple inductors results in large converter size and cost. In order to overcome these problems, single inductor multiple input/output topologies have been proposed. Single inductor multiple ouput DC-DC converters based on buck, buck-boost and boost topologies have been proposed in various literature. This reduces the cost, circuit complexity and results in greater efficiency. Nami et al. have proposed single input multi output boost converters based on diode clamped topology for multiple series and multiple parallel outputs using cascaded voltage and current control loops. Khaligh et al have proposed a single inductor based multi input bidirectional DC-DC converter which operates in buck, boost and buck-boost mode. Various non-isolated single inductor multi input/output topologies have been reviewed. Isolated converters are used when there is a requirement for high step up ratio and galvanic isolation. But the drawbacks are larger size and complexity compared to non-isolated converter topologies. Single inductor multi input multi output topologies, which are a hybrid of multi input and multi output converters utilizes multiple power sources to supply power to multiple applications.

Bandyopadhyay and Chandrakasan present a multi input multi output DC-DC converter utilizing three different power sources namely piezoelectrics, solar PV and thermoelectric for low voltage applications. Huang and Chen presented a multi input multi output DC-DC converter with buck and boost outputs for low power portable applications using hysteresis and PWM control. Shao et al. presented a dual input/output DC-DC converter for low power applications using solar PV as power source and battery as energy storage device. Two modes of operation of the converter – dual input mode during deficit solar PV power and dual output mode during surplus solar PV power is presented. Babaei and Abbasi proposed a switched capacitor based boost converter topology which is used for multiple outputs in series. A detailed analysis of the converter topology was carried out. Keyhani and Toliyat proposed a zero voltage switching single inductor multi input multi output converter with buck-boost mode of operation.

This paper proposes a novel and simple time sharing closed loop control technique for solar PV system with a single inductor power converter stage, wherein the controller maintains a constant DC load voltage and a power flow management system to balance the power flow between solar PV, battery and stand-alone DC loads. The power converter is capable of operating in dual input/output mode controlled by an effective energy storage/energy management system for providing uninterrupted power supply to the standalone DC load from a battery to take care of both excess and deficit PV power availability situations. Steady state analysis is performed by deriving analytical expressions and the transient analysis by developing a state space average model of the proposed system. Starting with the description of the proposed system, steady state analysis, the simulated and experimental waveforms of various electrical quantities are presented in the succeeding sections.

II. PROPOSED SOLAR PV POWER FLOW MANAGEMENT SYSTEM AND OPERATION

The proposed system consists of a solar PV module as power source, battery as energy storage element to supply during absence of solar PV, a single inductor based dual input/output DC-DC converter feeding a standalone DC load and a controller which modulates power flow between a solar PV module, a battery and a standalone DC load and performs voltage regulation at the standalone DC load terminals. The various functional blocks of the proposed system is as follows:

2.1 Solar PV Module:

The solar PV module is the primary source of power for the standalone DC load. The power generated by the solar PV module for a given temperature and level of irradiation depends on PV voltage and current drawn by the load. Hence, in order to do load matching, a maximum power point tracking (MPPT) control is used to set the converter at maximum power point (MPP) by varying the duty ratio of the appropriate switch and hence the current drawn by the converter from the solar PV module. There are many algorithms used to track the MPP like constant voltage, perturb and observe, incremental conductance and beta method. Among them, a simple perturb and observe (P&O) algorithm is selected for the proposed system. A 24 V 60 W solar PV module is selected for the proposed system and the same is modelled using the five parameter model. The output current of the solar PV module used in modelling is,

$$I_{pv} = I_L - I_o \left(e^{\frac{q(V + IR_s)}{nKT}} - 1 \right)$$

2.2 Energy Storage:

Since the power from the solar PV module is intermittent, a rechargeable battery has to be used as an energy buffer to maintain continuous operation of the system. During times of surplus PV power, it stores excess energy and during times of deficit or absence of PV power, it complements or replaces the solar PV module as the power source. There are primarily two types of rechargeable batteries used for stationary power applications - the lead acid battery and the lithium ion battery. Since lead acid batteries are inexpensive and have less safety issues, it is used for the proposed system. Jongerden and Haverkort have discussed various battery models. For modelling of the system, Kinetic Battery Model, an intuitive battery model based on electrical elements is selected. Lead acid batteries' Ampere hour capacity is rated for particular duration of discharge – typically 10 hour and 20 hour rates of discharge. If the battery is discharged faster than rated discharge, lesser amount of capacity is available and the battery has to be rested to recover the remaining charge. Kinetic battery takes this into account by modelling the lead acid battery into two charge wells – available charge with charge Q1 and non-available charge Q2. The dynamic equations for the two charge wells are,

$$\frac{dq_1}{dt} = -I + k^{'} (h_2 - h_1)$$
$$\frac{dq_2}{dt} = -k^{'} (h_2 - h_1)$$

The sum of the charges in the two charge wells gives the total remaining charge in the battery.

2.3 Single Inductor Based Dual Input/Output DC-DC converter:

The boost derived single inductor based dual input/output DC-DC converter (SI-DIO) used in the proposed power flow management system. It consists of diode Din which interfaces the solar PV module to the converter and also prevents reverse power flow to the solar PV module. The capacitor Cin is connected in parallel to the solar PV module to reduce the solar PV voltage ripples. The switches 2 and diode D2 is used to set the battery as an output to store excess solar PV power. The switch S3 is used to set the battery as an input to supply power to the standalone DC load. The capacitor Co is connected across the output to reduce the output voltage ripples. The converter has two modes of operation namely dual output boost mode (DOBM) when the power from solar PV module exceeds DC load demand and dual input boost mode (DIBM) when there is a deficit.

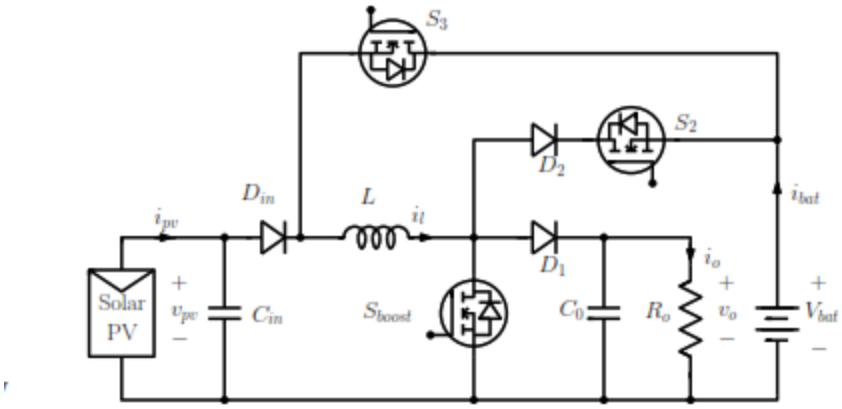

Fig. 2.1 Single inductor based dual DC DC converter

During DOBM, the solar PV module acts as a power source feeding the battery through the switch S2 and the DC load through the diode D. The single inductor based dual input/output DC-DC converter has three states. In the first state, the inductor is charged by power from the solar PV module through switch Sboost. In the second state, switch Sboost is turned off and the inductor discharges to the DC load through the diode D1. In the third state, the surplus power is discharged to the battery by turning on the switch S2. Since, the required voltage of the standalone DC load is higher than that of the battery, the diode D1 is reverse biased and the standalone DC load is cut off. Typical waveforms for the inductor current il, the inductor voltage vl, the battery current ibat and the output DC load voltage vo for this mode. By volt second principle, the output DC load voltage of the converter in DOBM is obtained as,

$$V_o = \frac{V_{pv} - V_{bat} D_{S2}}{D_{D1}}$$

The equation is similar to the conventional boost converter equation, in which the effective input voltage is the difference between the solar PV module voltage vpv and the pulse modulated fraction of the battery voltage, VbatdS2. The variation of standalone DC load voltage with respect to variation of duty cycles dD1 and dS 2 for an input voltage of 24 V DC is observed. It is seen that the standalone DC load voltage increases with either decrease in dD1 or by increasing dS 2.

III. PROPOSED TIME SHARING CONTROL STRATEGY

The overall time sharing control consists of a proportional integral controller based voltage regulator to regulate the standalone DC load voltage of 48 V. The reference voltage (V_o) and the actual standalone DC load voltage (vo) are given to an error amplifier, which gives the absolute standalone DC load error voltage (voe) and it is then converted to a per unit error voltage (voepu) by using the reference standalone DC load voltage as the base voltage. This per unit error voltage is the input for the PI controller. The output of the voltage regulator (dV olt) modulates the power flow for DC load to address excess and deficit power based on the PV power availability by setting the appropriate mode of operation such as dual input boost mode (DIBM) and dual output boost mode (DOBM). A simple perturb and observe method is used for extracting the maximum power from the solar PV module by control signal dMP P T

The mode change control decides the mode of operation of the converter by generating mode signal msel based on the standalone DC load power demand and the power extracted from the solar PV module. The rise in the standalone DC load voltage more than the standalone DC load reference voltage(V_o) shows the power extracted from the solar PV is more than the load power demand and vice versa, which confirms the operation of dual output/input

IV. RESULTS AND DISCUSSION

The proposed power flow management system is simulated by implementing the state space model derived in the MATLAB/Simulink environment. The values of the passive elements used are 100 H for boost inductor L, 1000 F for input capacitor Cin and output capacitor Co. A 60 W solar PV module with a MPP voltage of 24.5 V DC and MPP current of 2.44 A and a battery with 36 V DC are used as power sources. The reference voltage of the standalone DC load is set at 48 V DC. The PI controller had values of kp = 5 and ki = 15 for per unit error input.

Increase in solar insolation from 300 W/m2 to 600 W/m2: The power flow management system is initially operating in DIBM with a solar PV insolation of 300 W/m2, capable of supplying 18 W. The standalone DC load power demand is 50 W. The MPPT control maintains a dMP P T of 0.3 to extract 18 W from the solar PV module. The battery makes up for the power deficit of 32 W. At the time instant tspv1 shown in Fig. 10, the solar insolation level is increased to 600 W/m2, making the solar PV module capable of supplying a power of 36 W. The MPPT algorithm increases the duty ratio dMP P T to 0.4 to extract maximum power. Since the effective input voltage VpvDDin + Vbat (DSboost DDin) shown in eqn.7 decreases, the voltage controller increases the duty ratio dV olt to maintain constant standalone DC load. Due to higher increase in dMP P T compared to dV olt, dS 3 decreases in accordance with eqn. 14 and 13 and hence the share of the battery power to the DC load power demand reduces to 14 W.

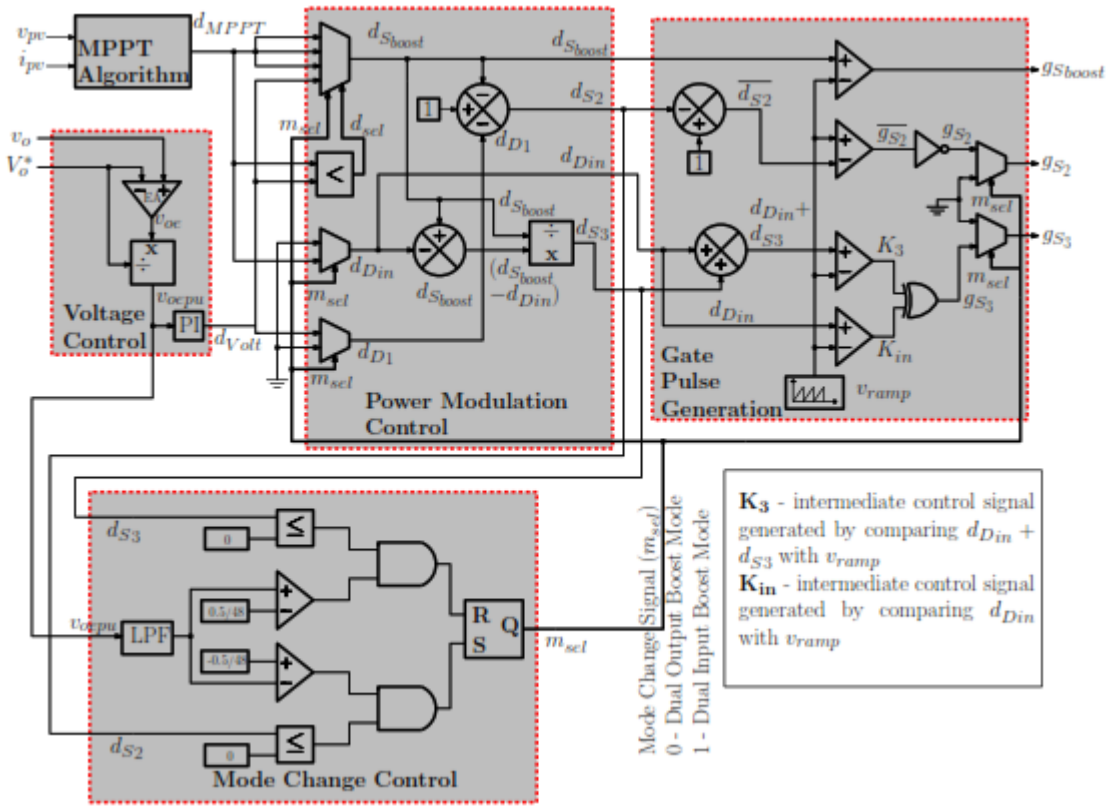

Fig. 4.1 Time sharing control scheme

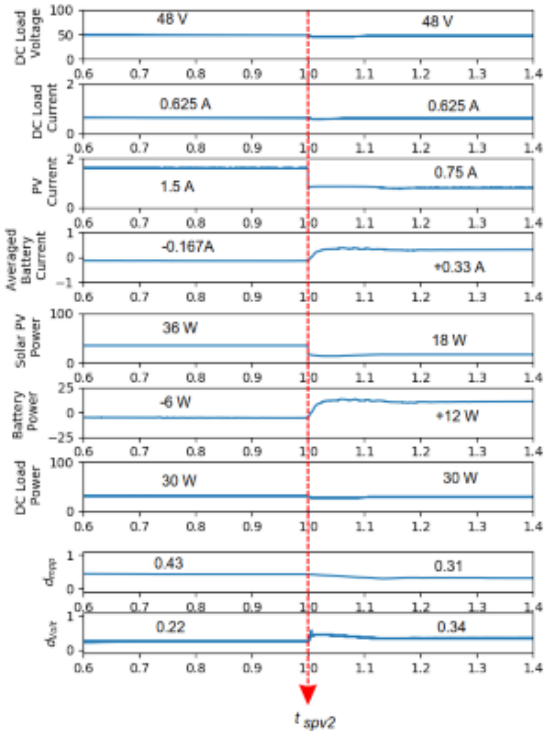

Fig. 4.2 Dynamic response of the control scheme

V. CONCLUSION

A power flow management system for battery backed standalone solar PV systems employing single stage single inductor dual input/output DC-DC converter has been presented. A novel time sharing voltage mode control scheme has been proposed for power flow management between solar PV, battery and DC loads to maintain constant DC load voltage and also extract maximum power from solar PV. The converter is capable of operating both in surplus and deficit PV power. A hardware prototype of the proposed system consisting of solar PV, the single inductor based dual input/output DC-DC converter and a battery bank has been fabricated and the control circuits has been implemented on a dSPACE DS1103 Real Time Interface(RTI) board. The steady state operation of both the dual output boost mode and dual input boost mode has been simulated and validated using the MATLAB programming language and the characteristics are presented. A state space average model of the proposed system was developed to perform transient analysis of the system. Simulated waveforms of the PV current, the standalone DC load voltage, the standalone DC load current, the averaged battery current, the solar PV power, the battery power and the standalone DC load power were obtained using this model are shown for changes in levels of incident solar insolation and DC load on the system. These dynamic changes were also carried out in the experimental setup and the waveforms of the corresponding electrical quantities were captured in the DSO and are presented. The simulation and and experimental performance presented confirms the satisfactory working of the controller in maintaining the desired DC load voltage, under the varying operating conditions of solar PV insolation and consumer load.

REFERENCES

1. X. Liu and E. S´anchez-Sinencio, "A highly efficient ultralow photovoltaic power harvesting system with mppt for internet of things smart nodes," IEEE Transactions on Very Large Scale Integration (VLSI) Systems, vol. 23, no. 12, pp. 3065–3075, Dec. 2015.
2. M. Ito, K. Kato, H. Sugihara, T. Kichimi, J. Song, and K. Kurokawa, "A preliminary study on potential for very large-scale photovoltaic power generation (vls-pv) system in the gobi desert from economic and environmental viewpoints," Solar Energy Materials and Solar Cells, vol. 75, no. 3-4, pp. 507–517, 2003
3. C. D. Xu and K. W. E. Cheng, "A survey of distributed power system - ac versus dc distributed power system," in 2011 4th International Conference on Power Electronics Systems and Applications, Jun. 2011, pp. 1–12.
4. X. Sun, Y. Shen, W. Li, and H. Wu, "A pwm and pfm hybrid modulated three-port converter for a standalone pv/battery power system," IEEE Journal of Emerging and Selected Topics in Power Electronics, vol. 3, no. 4, pp. 984–1000, Dec. 2015.
5. Y. C. Liu and Y. M. Chen, "A systematic approach to synthesizing multi-input dc-dc converters," IEEE Transactions on Power Electronics, vol. 24, no. 1, pp. 116–127, Jan. 2009.

High Step-Up DC–DC Converter with Active Soft-Switching and Voltage-Clamping for Renewable Energy Systems

Mr. A. Richard Pravin[1]
Assistant Professor,
Department of Electrical and Electronics Engineering,
St. Anne's College of Engineering and Technology,
Anguchettypalayam, Panruti – 607106.

Mr. S. Dinesh[2], Mr. S. Praveen Kumar[3], Mr. U. Prakash[4]
UG Student,
Department of Electrical and Electronics Engineering
St. Anne's College of Engineering and Technology,
Anguchettypalayam, Panruti – 607106.

Abstract - ***A novel high step-up DC-DC converter with coupled-inductor and switched-capacitor is proposed in the paper, which is widely used in the renewable energy system as the front-end stage for low voltage source. The combinational employment of switched-capacitor and coupled-inductor makes high voltage gain achievable without extreme duty cycle, resulting in reduced voltage stress on power switches. Hence, MOSFETs with low resistance RDS(ON) could be utilized as the main switch to reduce conduction loss. Meanwhile, due to the leakage inductance of coupled inductor, the current falling rate becomes controllable and reverse-recovery problem of output diode is alleviated. Importantly, by incorporating active clamped-circuit, not only voltage spike caused by leakage inductance is restrained, but also zero-voltage switching (ZVS) could be obtained for the main and auxiliary switches. Specially, the clamped-circuit plays a role of energy transfer to boost the gain as well. Finally, a prototype with power rating of 500W is implemented to verify the performance of the proposed converter.***

***Index Terms*—high gain, switched-capacitor, zero-voltage switching (ZVS), active clamp.**

I. INTRODUCTION

In renewable energy systems with photovoltaic (PV) and fuel cells, high step-up DC-DC converters are in pressing demand because the low voltage generated by the PV and fuel cells should be boosted to a relatively high-standard dc bus voltage for the grid-connection. For instance, the output voltage of the most fuel cell stacks or individual PV cells should be less than 40 V in consideration of cost and reliability issues for household applications, which means that a front-end DC-DC converter with over ten times voltage gain is essential to converse low output voltage of the fuel-cell stack or PV to a standard high bus voltage before a 220-V ac output grid-connected. How to extend voltage gain, reduce the voltage stress on the switches and improve the conversion efficiency constitutes the main concerning issues [1][2][3].

There are several approaches to attain high gain. Beyond all doubt, the conventional boost converter could not be qualified to provide a high voltage gain. High voltage stress on

switches and extreme duty cycle, which results in huge conduction and switching loss and slow transient response, makes it weakly competitive in high step-up applications. Although some improved boost topologies have been reported, the mentioned issues have never been solved well due to inherent defect of this kind of converters [4][5].

Some isolated converters such as fly-back, forward, push-pull, half-bridge, and full-bridge by changing the turn ratio of a transformer are another approach to achieve a high step-up voltage gain[6][7]. However, the main switches of these converters will suffer from high voltage spikes and high power dissipation due to the leakage inductor of the transformer. What's more, the power transformer volume blocks the development of a compact converter. Furthermore, the loss will increase because all the energy should be transferred through the transformer to the load in the isolated converters. To solve these drawbacks, a non-dissipative snub circuit and an active clamp circuit have to be utilized. And it is ineluctable to bring about addition cost. To achieve a high step-up voltage gain with improved conversion efficiency, various single power stage topologies have been developed as well in recent years. The switched-capacitor converter (SCC) is one of such hot classes of converters[8][9]. Unfortunately, the main disadvantage of the SCC topology captures their poor regulation, resulting in pulsating input current and fixed voltage conversion ratio. Even that some researches have made much effort to improve the regulation ability for SCCs [10]-[14], the regulation margin is still limited. Also, there is no report about regulation methods for high gain if the voltage levels of SCCs have been extended. Coupled-inductor-based technology is another solution for gain extension[15][16]. However, the leakage inductance of the coupled inductor and the parasitic capacitor of the output diode maybe resonate together, and a proper snub circuit is required to absorb the voltage ringing on the output diode, and the using of additional protection circuit increases both the cost and complexity of the circuit. Meanwhile, the pulsating input current and high peak current flowing through the clamp capacitor kills system efficiency further.

II. PROPOSED CONVERTER AND OPERATION PRINCIPLE

The coupled-inductor is represented by its equivalent transformer model, which includes an ideal transformer, magnetizing inductance Lm and leakage inductance Lk referred to the primary. The voltage multiplier consists of two switched-capacitorsCf1 and Cf2 and feed-forward diodes Df1 and Df2. Switched-capacitors Cf1 and Cf2 are charged in parallel and discharged in series by the secondary side of coupled-inductor when the main switch S is turned on and turned off, respectively. The active clamped-circuit is composed of auxiliary switch Sau and clamped-capacitor Cc. Thus, leakage inductance energy of the coupled-inductor is recycled to the capacitor Cc, and voltage stress of the main switch Swill be clamped. Besides, the recycled energy in capacitor Cc can be transferred to switched-capacitors Cf1, which extends the voltage gain further. And the output diode Do and output capacitor Co play the similar roles as them in a normal boost converter.

Before the operation analysis, the following conditions are assumed:
1) The magnetizing current is operated in continuous mode.
2) The switches and other components are considered to be ideal device without parasitic parameters except the leakage inductance for the coupled-inductor and parasitic capacitor Cr for the main switch.
There are eight operation modes in one switching period. and the simplified equivalent circuit for each mode is sketched. The operation modes are described as follows.
In the mode, main switch S is turned on and voltage across Cr maintains zero during the whole mode, while auxiliary switch Sau keeps off-state. The current of magnetizing

inductance Lm and leakage inductance Lk increases linearly. Switched-capacitor Cf1 is charged through clamped-capacitor Cc, feed-forward diode Df1 and the secondary winding of coupled-inductor. At same instant, switched-capacitor Cf2 is charged through feed-forward diode Df2 and the secondary winding of coupled-inductor, Output diode Do is reverse-biased, and output capacitor Co transfers its energy to load. The current of magnetizing inductance Lm and leakage inductance Lk are given by V

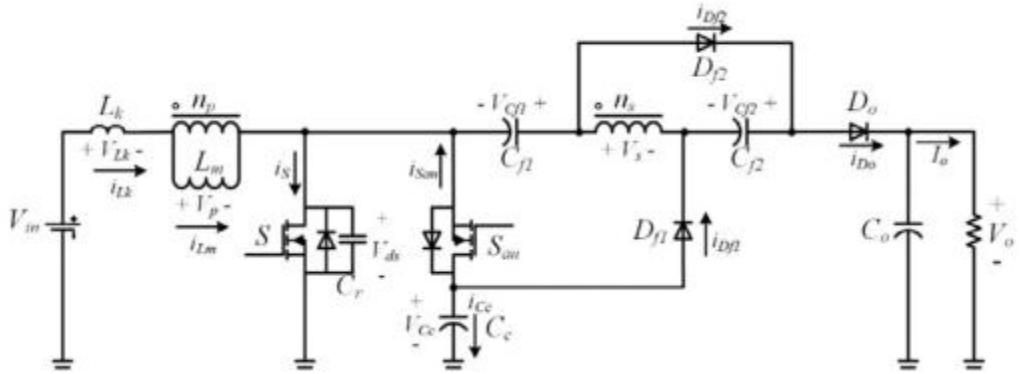

Fig. 2.1 Soft switching high step up DC DC converter

III. ZVS OPERATION ANALYSIS

When the switch S is turned off under ZVS condition due to the parasitic capacitor, the energy stored in leakage inductance will be transferred to the clamped capacitor through the anti-parallel body diode of auxiliary switch Sau, which creates ZVS turn-on condition for auxiliary switch Sau. Voltage across parasitic capacitor of main switch S equals to voltage across clamped-capacitor when Sau is turned on. Therefore, Sau can be turned off under ZVS condition. At this instant, when Sau has been turned off, a new resonant loop composed of input power source, leakage inductance and parasitic capacitor Cr will form. Then, when the parasitic capacitor is discharged by leakage inductance completely, the ZVS turn-on condition will be produced for main switch S because it's anti-parallel body diode has conducted.

Based on above analysis, in order to realize soft-switching, there is some constraint condition to be considered. Firstly, the auxiliary switch Sau need to be turned on after its anti-parallel body diode conducts, Secondly, Sau should be turned off timely to make sure that the interval of modes 6 and 7 is shorter than the half of resonant period, which is determined by leakage inductance and parasitic capacitor. The responding equations are given by

$$t_l = t_7 - t_5 \le \frac{\pi}{\omega_3}$$

Where, tl is interval time between falling edge of gate signal for Sau and rising edge of gate signal for S. Finally, the parasitic capacitor should be discharged completely by leakage inductance to guarantee conduction for anti-parallel body diode of main switch S, And the current of leakage inductance at t5 can be obtain as

$$i_{Lk}(t_5) = \left(M - \frac{2N}{1-D} \right) I_o$$

$$I_{o\min\_ZVS} = \sqrt{\frac{C_r}{L_k}} \frac{1-D}{(2-ND)(2N+2-ND)} V_o$$

it is obvious that the ZVS turn-on condition for main switch S in the proposed converter is dependent on Lk rather than load. The boundary cure between ZVS and non-ZVS range against Lk. Considering the parameters used in the experiment, the ZVS load boundary

IOmin_ZVS is 0.4777 A, as the red point shown in the curve. It means that the ZVS turn-on condition can be guaranteed from a 38.2% load to a full load. On the other hand, the ZVS will be lost below a 38.2% load condition. Thus, it seems that a large leakage inductance is preferable to a wide ZVS range. However, large leakage inductance will make voltage gain decay, so that the duty ratio D should be increased for compensation, unfortunately, which will cause the increase in the peak and RMS values of the primary leakage current. Therefore, Lk should be designed reasonably.

IV. EXPERIMENTAL RESULTS

The conversion efficiency against output power between the proposed converter and its own hard-switching counterpart is shown in Fig. 4.1, the maximum efficiency of proposed converter reaches up to 96.2% and the full-load efficiency is approximately 94.4%. An average improvement of approximately 3% in the conversion efficiency is provided by the proposed converter compared with its own hard-switching counterpart. Importantly, the converter could work under high efficiency in wide load range.

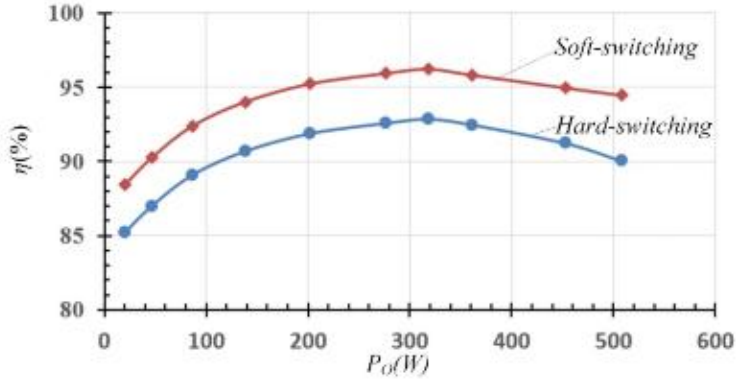

Fig. 4.1 Efficiency of the proposed converter

V. CONCLUSION

The paper has developed a compact high step-up DC-DC converter with relative small components and simply controls strategy to achieve extreme gain with soft operation and active clamping. The feature of the proposed converter can be summed up as follows:

1) Wide input operation range and high voltage gain without an extreme duty cycle can be achieved;

2) Voltage stress on power devices are reduced greatly and low ON-resistance MOSFET can be employed for conduction loss reducing;

3) The reverse recovery problem of output diode is alleviated due to leakage inductance;

4) Voltage spike on main switch is effectively clamped by active clamp circuit;

5) Active clamped-circuit takes the role of resonance as well, achieving soft-switching for main switch and auxiliary switch in wide load range, reaching high efficiency in wide load range;

6) Active clamped-circuit participates in gain enhancement; Therefore, the proposed converter can obtain high gain with high efficiency, which can be effectively used in renewable energy systems as the front-end converters.

REFERENCES

1. L. Zhang, D. Xu, G. Shen, M. Chen, A. Ioinovici and X. Wu, "A High Step-Up DC to DC Converter Under Alternating Phase Shift Control for Fuel Cell Power System," IEEE Trans. Power Electron., vol. 30, no. 3, pp. 1694-1703, Mar.2015.
2. K. C. Tseng, J. T. Lin and C. C. Huang, "High Step-Up Converter with Three-Winding Coupled Inductor for Fuel Cell Energy Source Applications," IEEE Trans. Power Electron., vol. 30, no. 2, pp. 574-581, Feb. 2015.
3. Y. Hu, W. Xiao, W. Cao, B. Ji and D. J. Morrow, "Three-Port DC-DC Converter for Stand-Alone Photovoltaic Systems," IEEE Trans. Power Electron., vol. 30, no. 6, pp. 3068-3076, Jun. 2015.
4. H. Wu, Y. Lu, T. Mu, and Y. Xing, "A family of soft-switching DC-DC converters based on a phase-shift-controlled active boost rectifier," IEEE Trans. Power Electron., vol. 30, no. 2, pp. 657-667, Feb. 2015.
5. Y.Gu, D. Zhang, and Z.Zhao, "Input/output current ripple cancellation and RHP zero elimination in a boost converter using an integrated magnetic technique," IEEE Trans. Power Electron., vol. 30, no. 2, pp. 747-756, Feb. 2015.
6. K. C. Tseng, J. Z. Chen, J. T. Lin, C. C. Huang and T. H. Yen, "High Step-Up Interleaved Forward-Flyback Boost Converter with Three-Winding Coupled Inductors," IEEE Trans. Power Electron., vol. 30, no. 9, pp. 4696-4703, Sept. 2015.
7. X. Pan and A. K. Rathore, "Naturally clamped zero-current commutated soft-switching current-fed push-pull DC/DC converter: Analysis, design, and experimental results," IEEE Trans. Power Electron., vol. 30, no. 3, pp. 1318-1327, Mar. 2015.
8. L. He. "High-Performance Bridge Modular Switched-Capacitor Converter with Small Component Requirement Based on Output Impedance Analysis for Low Loss," IEEE Trans. Power Electron., vol.28, no.10, pp: 4668-4680, Oct. 2013.
9. L. He. "A Novel Quasi-resonant Bridge Modular Switched-Capacitor Converter with enhanced efficiency and reduced output voltage ripple," IEEE Trans. Power Electron., Vol.29, No.4,pp. 1881- 1893, Apr.2014.
10. Y. Lee, Y. Ko, M. Cheng, and L. Liu," Multiphase Zero-Current Switching Bidirectional Converters and Battery Energy Storage Application," IEEE Trans. Power Electron., vol. 28, no.8, pp. 3806-3815, Agu.2013.
11. Y. Ye, K. W. E. Cheng, J. Liu, and C. Xu, "A Family of Dual-Phase-Combined Zero-Current Switching Switched-Capacitor Converters ", IEEE Trans. Power Electron., vol. 29, no. 8, pp. 4209-4218, Aug. 2014.

Speed Control of Single Phase Induction Motor Using Firefly Algorithm

Mrs. S. Lese[1]
Associate Professor,
Department of Electrical and Electronics Engineering,
St. Anne's College of Engineering and Technology,
Anguchettypalayam, Panruti– 607106.

Mr. A. Arivazhagan[2], Mr. R. Ramkumar[3], Mr. K. Selvam[4], Mr. R. Yuvaraj[5]
UG Student,
Department of Electrical and Electronics Engineering
St. Anne's College of Engineering and Technology,
Anguchettypalayam, Panruti– 607106.

Abstract - This paper is concerned with real time speed control of single phase induction motor and implementation of voltage/frequency (V/F) speed control method with the help of variable frequency drive (VFD), Firefly algorithm. Because of its simplicity, the V/F control also called as the scalar control, is the most widely used speed control method in the industrial applications. The proposed technique gives better performance for single phase induction motor than the conventional technique. The main advantage of the proposed system is quick settling time, intelligent technique. The speed control is obtained by firefly control, because PI has difficulty in dealing with dynamic speed. The proposed control is done by using MATLAB/SIMULINK and also implemented in hardware.

***IndexTerms*— Firefly algorithm, Induction motor, Microcontroller, MATLAB/SIMULINK, Variable Frequency Drive (VFD).**

I. INTRODUCTION

Electrical Energy has the contribution more than 40 % of all energy sources usage on Earth. In the upcoming years the percentage contribution of Electrical Energy will be increase. More utilization of Electrical Energy is to convert the Electrical Energy into Mechanical Energy via different kinds of electric motors like DC Motors, Induction Motors and Synchronous Motors. From the economic point of view Induction Motor are cheap compared to DC and Synchronous Motors. Induction Motors are most popular and widely used drives in industries as well as for domestic applications. It is very important to control the speed of induction motors in industrial and domestic applications. Induction motors can be broadly classified into two types based on their speed control techniques – scalar control and vector control. By using scalar control method we can control the magnitude of voltage or frequency of the induction motor [10].In the present time, in the most of the applications, AC machines are preferable over DC machines suitable to their simple and most robust construction without any mechanical commutators. Induction motors are the most widely used motors for appliances like Industrial control, and automation; hence, they are often called the workhorse of the motion industry [1]. Control of voltage, frequency and current is required in variable speed applications for ac machines drives. Speed of induction motor can be determined with the help of frequency of supply system.

II. V\F SPEED CONTROL METHOD OF SINGLE PHASE INDUCTION MOTOR

The torque developed by the induction motor is directly proportional to the magnetic field, which is produced by the stator. The stator voltage is directly proportional to the product of stator flux and angular velocity. This makes the flux produced by the stator proportional to the ratio of applied frequency and voltage of supply. The voltage and frequency varied by the same ratio, the torque can be kept constant throughout the speed range. This makes constant ratio of voltage and frequency is the most common speed control of an induction motor. The torque developed by the induction motor is directly proportional to the ratio of voltage and frequency. By varying the voltage and frequency, keeping their ratio constant, then the torque produced by induction motor will remain constant for all the speed range.Fig.1 shows the torque-speed characteristics of the induction motor with V/F control. The voltage and frequency reaches the maximum value at the base speed .We can drive the induction motor beyond the base speed. The torque developed by the induction motor is directly proportional to the V/F ratio will not remain constant throughout the speed [1].

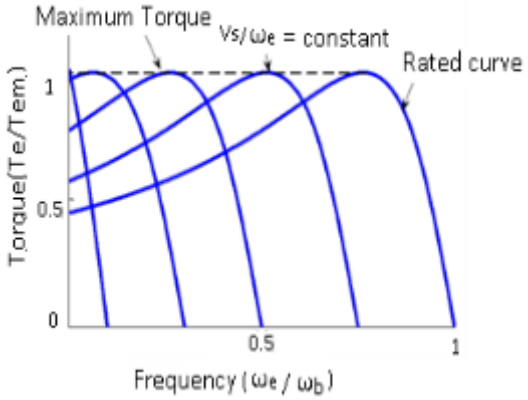

Fig. 4.1 Torque-frequency characteristics

Other than the variation in speed, the to the torque-speed characteristic of the V/F control is the following:

The starting current is low.

The constant operating region of the motor is increased. Instead of simply running at its base/ rated speed (NB), the motor can be run normally from 5% of the synchronous speed (N_S) up to the base speed. The torque created by the motor can be kept constant throughout this region.

Then almost constant rated torque is available over the entire operating range, the speed range of the motor becomes wider. User can set the speed as per the load requirement, thereby achieving the higher efficiency.

III. FIREFLY ALGORITHM

In a mathematical optimization, the firefly algorithm is a metaheuristic proposed by Xin-She Yang by the flashing behaviour of fireflies.

- All fireflies are unisexual, so that any single firefly will be attracted to all other fireflies.
- Attraction is proportional to their brightness, and for any two fireflies, the fewer bright one will be attracted by (and thus move towards) the brighter one. Though, the intensity (apparent brightness) decrease as their mutual distance increases.
- If there are no fireflies brighter than a given firefly, it will be travel randomly.
- The intensity should be associated with the objective function.

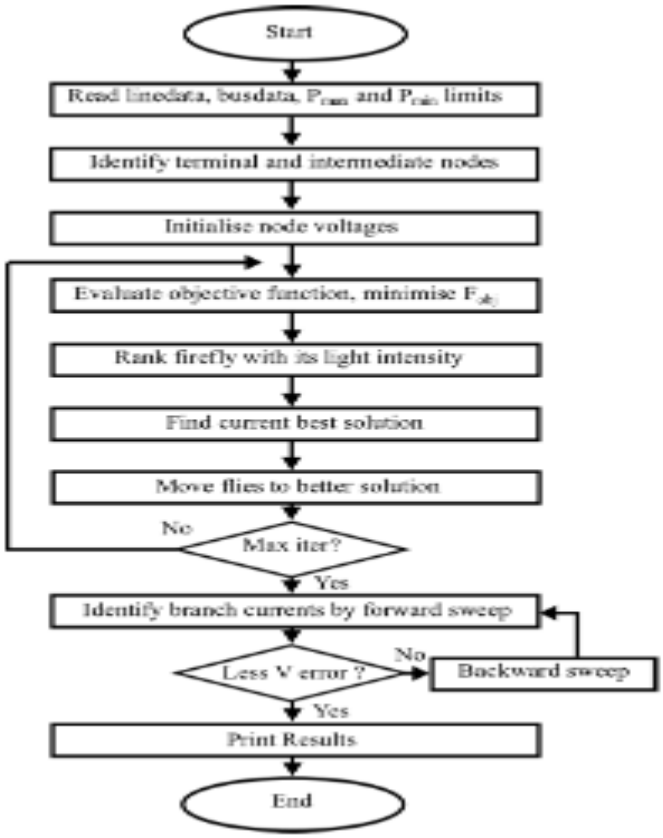

Fig. 4.2 Flowchart for Firefly Algorithm

Firefly algorithm is specified based on the steps shown in below pseudo code.

Objective function $f(\boldsymbol{x})$, $\boldsymbol{x} = (x_1, ..., x_d)^T$.
Generate an initial population of n fireflies $\boldsymbol{x}_i$ $(i = 1, 2, ..., n)$.
Light intensity I_i at $\boldsymbol{x}_i$ is determined by $f(\boldsymbol{x}_i)$.
Define light absorption coefficient γ.
while (t <MaxGeneration),
for $i = 1 : n$ all n fireflies
  for$j = 1 : n$ all n fireflies (inner loop)
  if ($I_i < I_j$)
    Move firefly i towards j.
    end if
    Vary attractiveness with distance r via $\exp[-\gamma r^2]$.
    Evaluate new solutions and update light intensity.
  end for j
end for i
Rank the fireflies and find the current global best $\boldsymbol{g}_*$.
end while
Post-process results and visualization.

IV. PIC18F452 MICROCONTROLLER

The 18F452 has 153GB of RAM and 16k of program memory. It has four port namely as port a, port b, port c and port d. Each port has eight pins. As shown in figure the pin number RA belongs to port a and same as for RB, RC and RD.

These are the power supply pins. VSS is ground and VDD is the positive supply pin. The range of supply is 5V to 3V. The maximum supply is 5V and minimum is 3V. Since

microcontroller has some kind of timing, so we connect an external clock with these pins. In normal mode this pin connects to the positive (5V) supply. Specially, this pin is used to erase the memory location. These are the bidirectional ports. That can be configured as an input and output. The number following RA0, RA1 is the bit number. There is another clock, which operate as an internal timer. There are two ways for programming, the easy and DIY way. The easy way is to buy a PIC burner, which will connect to your PC and you can program it by using software. The DIY is to build your own burner and use free software to program it. In these tutorial, first we will learn the programming of PIC and will see the simulation by using Proteus. Then we will proceed to the hardware**.**

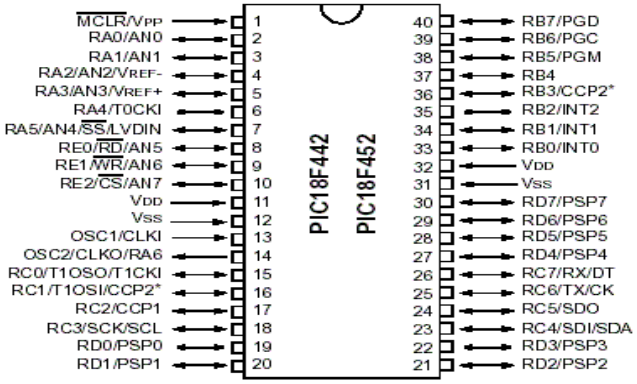

Fig. 4.3 Pin Diagram of PIC18F452

V. VARIABLE FREQUENCY DRIVE (VFD)

AC60E is a mini general purpose frequency inverter, is our independently developed electrical equipment. As a new generation of high performance v/f control drive, it is included to have modular design, small size, small temperature rise, low noise, and reliable performance**.**

• 220V (single-phase power) 0.4 - 2.2 kW
• 380V (three-phase power) 0.75 - 3.7 kW

A Variable Frequency Drive (VFD) is a device that control the voltage and frequency. That is being supplied to a motor and controls the speed of the motor. To meeting the required process demands, the system efficiency is improved. A VFD is capable of the speed and torque of an induction motor. VFD's are made in a number of different low and medium voltage AC-DC and DC-AC topologies.

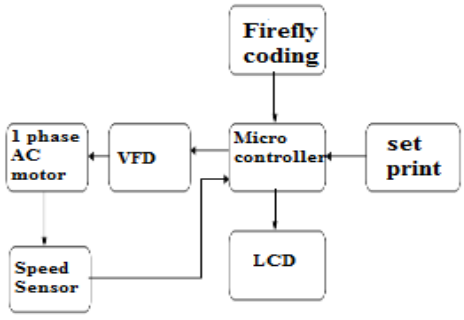

Fig. 4.4 Block Diagram of Proposed System

In this proposed system, we used to control the speed of the three phase induction motor, by using v/f method. The speed of the induction motor is, set by the set pointer, and then the set speed is displayed LCD display. The microcontroller is employed with the Firefly coding.

The VFD (Variable Frequency Drive) receive the signal from microcontroller is used to drive the 3 phase induction motor .The purpose of this VFD (Variable Frequency Drive) is used to convert the fixed voltage and frequency into variable voltage and frequency. The variable voltage is used to drive the AC motor frequently. The sensor is used to sense the speed of induction motor into microcontroller. While using the PI controller we have some disadvantages. In order to overcome that, we use firefly algorithm.

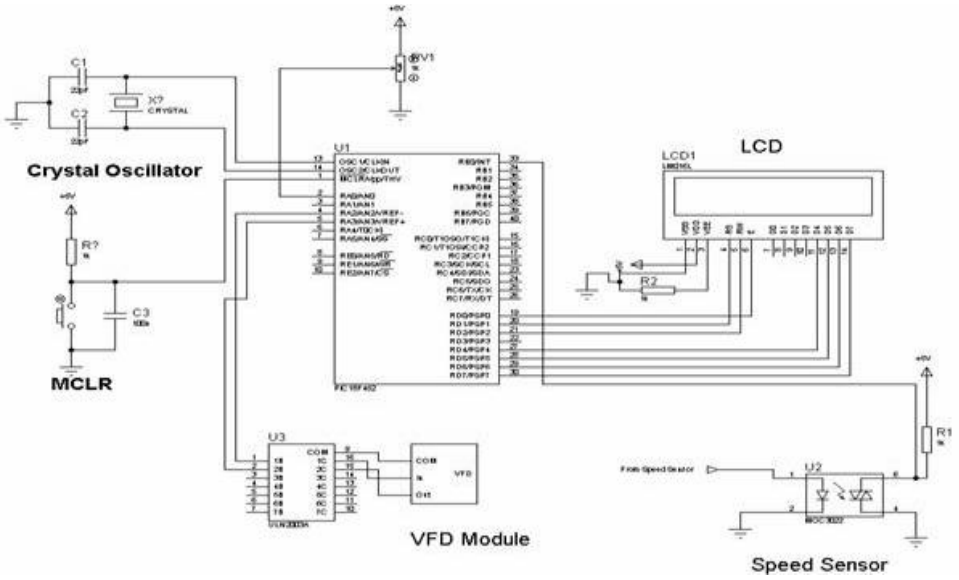

Fig. 4.5. Circuit Diagram of the Proposed System

The above circuit diagram is denotes the hardware implementation of speed control of three phase induction motor using variable frequency drive.

VI. SIMULATION RESULT

The figure.4.6 shows speed and torque characteristics of three phase induction motor. In this waveform denotes 1000 rpm and 0.5 torque.

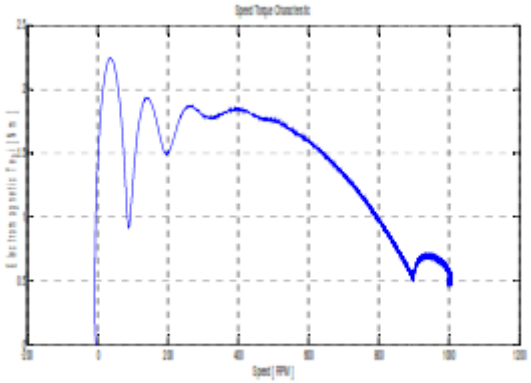

Fig. 4.6 Torque Speed Characteristics

VII. CONCLUSION

Induction motor drives are most widely used in the industrial applications. Various speed controlled methods have been developed. Out of which the V/F is the most common and easy to implement. The experimental result presented v/f controlled voltage source inverter fed induction motor. In this project we controlled single phase Induction Motor speed in real time, by using variable frequency drive and firefly algorithm. Simulation result shows the performance of VSI control and firefly control. Hence we concluded that VFD's provide

the most energy efficient means of capacity control. This drive comes in a lead role for energy saving products for all the Industries using electrical motors. To adding a variable frequency drive (VFD), in a motor driven system can offer potential energy savings in a system in which the loads vary with time. The operating speed of a motor connected with VFD, is varied by changing, the frequency of the motor supply voltage. The VFD becomes, very reliable and economically beneficial. The hardware Implementation is verified successfully and the simulation was done by using MATLAB\SIMULINK.

REFERENCES

1. M.s.Aspalli., Asha.r, P.V. Hunagund "Three phase induction motor drive Using IGBTs and constant v/f Method", International Journal of Advanced Research in Electrical, Electronics and Instrumentation Engineering Vol. 1, Issue 5, November 2012.
2. Ashutosh Mishra, Prashant Choudhary "Speed Control Of An Induction Motor By Using Indirect Vector Control Method", International Journal of Emerging Technology and Advanced Engineering Certified Journal, Volume 2, Issue 12, December 2012.
3. C. Saravanan, A. Mohamed Azarudeen & S. Selvakumar "Performance of Three Phase Induction Motor Using Modified Stator Winding", Global Journal of Researches in Engineering Electrical and Electronics Engineering Volume 12 issue 5 Version 1.0 April 2012.
4. Shilpa V. Kailaswar,Prof.R.A.Keswani "Speed Control of Three Phase induction Motor by V/F method for Batching Motion System", International Journal of Engineering Research and Application (IJERA) Vol.3,Issue2,March-April 2013.
5. Pabitra kumar Behera, Manoj Kumar Behera, Amit Kumar Sahoo "Speed Control of Induction Motor using Scalar Control Technique", International Journal of Computer Applications (0975-8887) International Conference on Emergent Trends in Computing and Communication (ETCC-2014).
6. P.M. Palpankar, ShraddhaWaghmare, B.Shikkewal "Speed Control of an Intrenational Motor using Rasberry PI", International Journal of Innovative Research in Science, Engineering and Technology vol. 4, Issue 8,August2015.
7. Aswathy MS, M. Waheeeda Beevi "High Performance Induction Motor Drive in field Weakening region", International Conference on Control, Communication & Computing India (ICCC) 19-21November 2015.
8. Jongkwang kim, Yongkeun lee, Janghyeon lee "A Sensorless Speed Estimation for Indirect Vector Control of Three-Phase Induction Motor Using Extended Kalman filter", on this Work was Supported by the National Research Foundation of Korea(NRF) Grant funded by the Korea Government(MEST) 2016.
9. C. Nandhini, M. Jagadeeswari "FPGA Implementation for Speed Monitoring and Speed Control of AC Motor using V/F Control", International Journal of Innovative Research in Science, Engineering and Technology Vol. 5, Issue 5, May 2016.
10. K. Rajput "Speed Control of Induction Motor by using V/F Control Method in Matlab Simulink", National Conference on Innovative Trends in Science and Engineering (NC-ITSE'16) Volume: 4 Issue: 7.
11. Dr.K.Kannan Kaliappan1, S.Anusiya, K.Kavipriya, R.Logeswari, V.Suganya "DSPIC Based Speed Control of Three Phase Induction Motor Using V/F Method", International Journal of Advanced Research in Electrical, Electronics and Instrumentation Engineering Vol. 6, Issue 2, February 2017.

Effect of DC Ripple and Commutation on the Line Harmonics of Current-Controlled AC-DC Converters

Mr. V. Balaji[1]
Assistant Professor,
Department of Electrical and Electronics Engineering,
St. Anne's College of Engineering and Technology,
Anguchettypalayam, Panruti – 607106.

Abstract - Line harmonics are usually predetermined under the simplified assumption that the dc current is sufficiently smoothed. However, in practical operation of controlled converters, e.g., feeding medium-size dc drives, it frequently happens that the dc ripple cannot be neglected. For the predetermination of l i e harmonics, this means that the operating point is specified by the emf and the mean value of the dc current, i.e., the associated control and commutation angles, are unknown. The consideration of the basic effects of commutation and dc ripple leads to line current harmonics that are separated into positive and negative sequence systems. Selected results of systematic evaluations show the amplitude and phase as a function of dc reactance as well as of the emf and mean dc current in the range of usual low-and medium-voltage supply networks. In comparison with the conventional pre calculation assuming sutllcient dc smoothing, significant deviations occur in the case of higher dc ripple.

Index Terms— **AC – DC Converters and Line Harmonics.**

I. INTRODUCTION

Since the share of converter loads in electrical power supplies is increasing, the disturbances they cause must also be increasingly taken into account. In the case of current-controlled ac/dc converters, these disturbances include not only the variable reactive power consumption but, in particular, the harmonics of the line current that generate corresponding voltage harmonics at the internal impedance of the supply net-work. In the interest of other loads, these voltage disturbances may not exceed certain limits (compare, e.g., [1] and [2] and should therefore be known at the planning stage. The line current harmonics are usually predetermined under the assumption that the dc current is sufficiently smoothed.

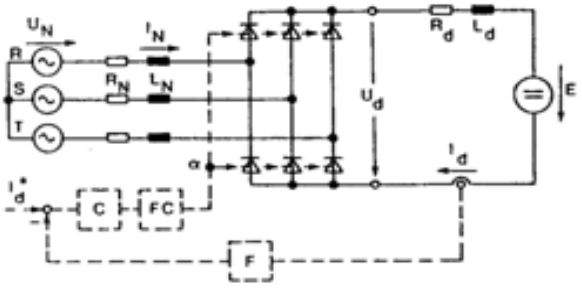

Fig. 1.1 Basic circuit of a current-controlled six-pulse bridge converter

the calculation, this means a decoupling between the three-phase and the dc side, and therefore, a correspondingly simple predetermination is feasible. However, in practical operation of controlled AC/DC converters, it frequently happens that the dc current shows a ripple that cannot be neglected. This appears in cases such as medium-size dc drives in which an additional dc inductance is omitted for cost reasons.

Starting from a simplified time behavior of the line cur-rent, [3] specifies the basic effect of the dc ripple on the harmonics, [4] takes the influence of commutation into account approximately, and calculations are carried out in [5] and *[6]* for given control angles. For controlled converters, however, the mean dc current determines the operating point, i.e., the associated control and overlap angles are unknown and must therefore be determined. This is usually performed by means of digital simulation in the time domain or directly with the aid of Newton's method [7], [8]. Starting from these preliminary works, the influence of dc ripple and commutation will be investigated systematically. Fig. 1.1 shows the basic circuit of a controlled six-pulse bridge converter considered here, where C: current controller, *FC:* firing control, *F :* filter, and *Id:* current set point given by supervised control system, e.g., for dc drives usually by the speed controller.

Fig. 2.1 Normalized amplitudes of the line current harmonics *I h c / I h z* **according to** *(2)* **shown in negative (above) and positive (below) sequence systems.**

II. BASIC EFFECT OF COMMUTATION AND RIPPLE

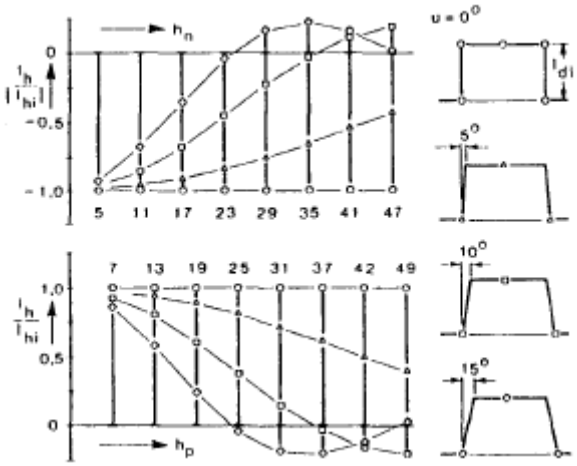

In this introduction, the basic effect of commutation and dc ripple on the harmonics of the line current will be derived from the literature and presented in line with our further objectives. For the idealized square-wave shape of the line current of a six-pulse bridge circuit, i.e,. neglecting commutation and dc riple, the well-known Fourier series applies, if the zero point *wt* = 0 is chosen at the midpoint of a positive square wave. From the ideally smoothed dc current *I&,* the amplitude ofthe fundamental is *11i = 2&'Idi/7r = 1.10'Idi.* The harmonics of order *h = 6k* f *1* are determined by *Ihi = f I l ; / h ,* where *h, =* ***6k*** *+ 1 = 7, 13,* 19, ... represent positive and *h, =* ***6k*** *- 1 =* 5, *11, 17,. . .* negative sequence systems [9].

The effect of the *commutation* can be described approx-imately in the usual firing-angle range of controlled ac/dc converters by a trapezoidal line current waveform, and then applies for the harmonics, where *U* is the overlap angle [lo]. It should be noted that the curve *Ihc = f (h)* for *hu/2 =* ***R*** contains a zero crossover, *7r < hu/2 < 27r* means a sign change with respect to the idealized value *Ihi.* Fig. ***2*** shows line current waveforms and the corresponding harmonics split into negative sequence systems *Ihc/(lhi(=* ***f(hn)*** and positive sequence systems *Ihc/Ihi =* ***f(h,).*** The special case *U* = 0 corresponds to the idealized square-wave shape according to **(l),** which is further used **as** the reference value for the harmonic amplitudes.

To explain the basic effect of the ***dc ripple,*** it is initially useful to consider the operation at the pulsation limit with emf *E* = 0. Neglecting the ohmic resistances, the mean value of the dc current is

where

U N	phase voltage of the network
Xd = WLd	dc reactance
X N = W L N	network reactance
w = 2.f~	with ***f~*** network frequency.

In this boundary case, the amplitude of the fundamental of the line current *I1 = 1.12 . Idm* is

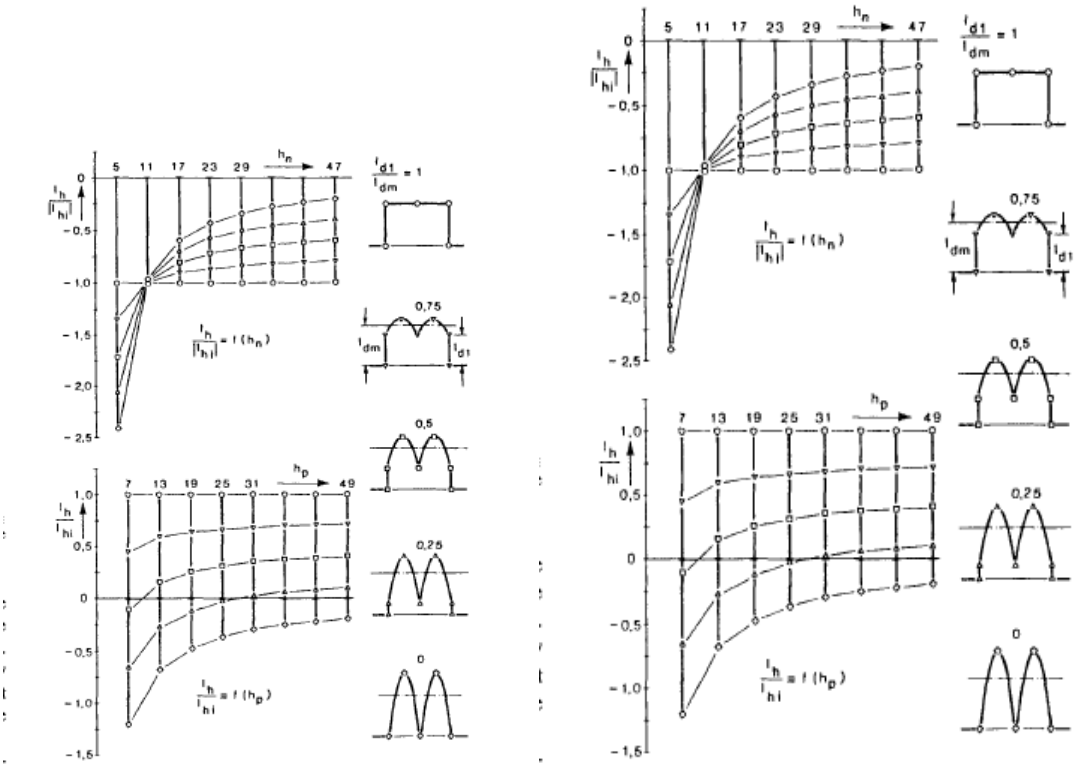

Fig. 2.2. Normalized amplitudes of the line current harmonics *I h / I h l* **for the current ratios** = **1** (o), 0.75 (v),*0.5* (U), **0.25 (A), and** 0 (0).

idealized value *I1i = l.lO.Idi,* where *Idi = Id,,,= I$* = const as shown in Fig. 1 with respect to the further treatment of current-controlled converters. For the harmonics of the positive and negative sequence systems applies [lo], and the reference to the idealized value *Ihi = f I l ; / h* according to (1) and (3) lead to the normalized harmonics of the line currents

With this, the basic effect of dc ripple on the amplitudes of the line current harmonics is represented in Fig. 3, where it is separated into negative and positive sequence systems. Thereby, the symbol " o " indicates the idealized dc smoothing *Idl/Idm = 1,* where *Idm* is the mean dc current. The other boundary case "0" characterizes the behavior at the

Fig.2.3. Working point given by a dc drive (example): *N* **versus M-Diagram and basic configuration.**

pulsating limit, i.e., *Idl/Id,* = 0. The parameter *Idl/Id,* = 0.75, *0.5,* and 0.25 corresponds to the part of the idealized dc current,

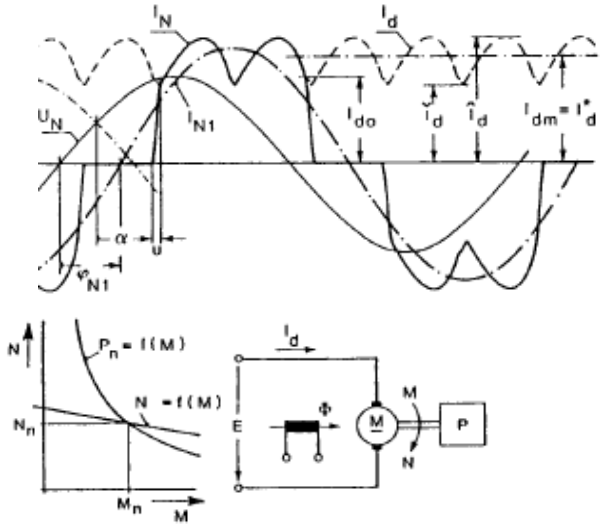

Fig.2.3. Working point given by a dc drive (example): *N* versus M-Diagram and basic configuration.

and the mean dc current ***Id m*** is kept constant. This presentation shows very clearly the distinct effect of the dc ripple; all positive sequence systems have the property of traversing a zero point at higher ripple ending in the opposite phase. The negative sequence systems retain their sign, and the strong increase of the fifth harmonic contrasts with correspondingly great reductions in the higher harmonics.

III. DETERMINATION OF THE WORKING POINT

In practical operation, the mean value of the dc current and *not* the control angle is the characteristic value for the working point of the controlled converters. As an example, the torque of a dc shunt wound motor is produced proportionally to the mean dc current. The working point of the converter follows from the mechanical requirements on the shaft (see Fig. 4), where *N* is the rotational speed, *M* is the torque, and *P* is the actual power. In the base speed range *N 5 N* , and in field-weakening range *N > N*,, the mean dc current is given.

By respectively. In both cases, the emf follows under considera-tion of the motor efficiency *q* at the working point as where *I,* , *M*,, *N*,, and *P*, are nominal motor values. In summary, the working point of the controlled converter is determined by the mean dc current *Idm* and the emf *E* . This leads to the objective, for the case under consideration of a rippled dc current, of determining the associated control and overlap angles.
The calculations are based on a current-controlled six-pulse bridge stationary-symmetrical conditions and simple commutation in continuous operation assumed; discontinuous operation was investigated. The param-eters considered are, apart from the operating point (mean dc value ***I d m = 1;*** and emf ***E)*** the circuit data (network and dc reactance ***X N = 2 r f N L N*** and ***x d = 2 T f N L d ,*** where ***f N*** is the net frequency). Usually, the ohmic resistances ***RN*** and ***Rd*** have less influence on the harmonic spectrum [121, [131; if required, they can be taken into account approximately by an additional emf ***AE = I d m (R d + 2 R N) .*** The complete calculation of the line current harmonics has already been treated in preliminary works; the most important points will now be summarized. Starting from a piecewise kalytical description, the difference equation of the dc current can be set up; its stationary value at the beginning of commutation is which agrees with the result of the conventional converter model which is valid for good dc smoothing [9], [16]. It should be noted that the

actual dc mean current ***Id m*** is always greater than the approximated dc current ***I d 0*** = ***I d ;*** compare this with the corresponding time behavior.
After the differential equations given in each time interval have been solved, the line current can be specified analytically as a function of the control and overlap angles. For these two unknown values a and *U,* two nonlinear conditions can be specified from the circuit function, ***I;*** = ***I d m (a ,*** *U)* after integration of the dc current and E = *E (a , U)* from the end of commutation [15]. In this way, the operating point specified by ***Idm*** and ***E*** determines the unknown angles a and ***U,*** which can be most conveniently calculated by Newton iteration. The spectrum of the line current can be simply determined with the aid of a standard FFT program since the line current is given in piecewise analytical form.

III. REPRESENTATION OF SELECTED RESULTS

3.1 Normalization and Assumption

To simplify the presentation, the following normalization is used: Reference for the reactances is ***R,*** = ***U N / & ,*** i.e., the normalized values ***X d*** = ***& / R ,*** and ***X N*** = ***X N / R ,*** are proportional to the mean dc current. The emf ***E*** is usually referred to the idealized dc voltage ***u d i o*** = ***2 . 34 . U N ,***i.e, e = ***E/Udio*** and Ae = ***I d m (&*** + ***2 R h r) / U d i o .*** The phase Of the complex harmonics ***I h*** refers, corresponding to Fig. 5, to the zero transition of the supply voltage, i.e., v h = *A(uN,**Ih)* **.**

In this section, the complex line harmonics will be investi-gated as a function of the dominant parameters, i.e., depending on the circuit data such as net and dc reactance as well as on the operating point given by emf and mean dc current. Using the proposed reference value ***R,*** = ***un/Idm ,*** these parameters are reduced to ***X N , x d ,*** and ***e.*** Only two network reactances ***x N*** = 7.5 and 15% are considered for reasons of space, corresponding to a usual low- and medium-voltage supply network, respectively. In order to reduce parameters, the influence of ohmic resistances is not considered here, i.e.,
Ae = 0.

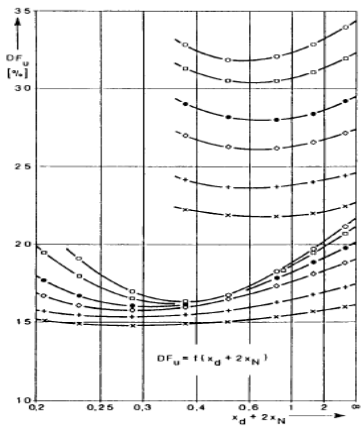

Fig. 3.1. Amplitude spectrum of the line current harmonics negative (left) and positive sequence systems (right); low-voltage supply (z,y = **7.5%) and emf** *e* = **0 assumed; parameter: reactance sum *X d*** + **22.y.**

3.1 Amplitudes of the Line Current Harmonics

The behavior of the amplitude spectrum for various values of the reactance sum *X d* + 2XN is investigated here, taking the sign into account at the operating point e = 0 but only the amplitude at e = 0.8. Figs. ***6*** and 7 represent the results for the exemplary low-voltage network. Table 1 explains the symbols used and additionally specifies the angles U and *a* as well as the dc current ripple with ***i d*** and ***I d*** as in Fig. 5. Figs. **8** and 9 show the corresponding results for the selected medium-voltage network, and Table I1 lists the relevant explanations. It should be noted that in the case of emf e = *0*, the simple relation *a* + u/2 = 90"eZ is valid for any dc ripple [**15].**

symbol		(•)	(×)	(△)	(+)	(□)	(▽)	(◇)
x_d+2x_N		16	1	0.6	0.4	0.3	0.25	0.218
u[°el]	e=0	3.5	2.8	2.4	1.8	1.1	0.5	0
r[%]		1.8	29.8	50.5	77.4	106	129	151
u[°el]	e=0.8	5.8	5.3	4.9	4.3	3.8	3.2	2.6
a[°el]		33.9	34.1	34.3	34.6	34.9	35.2	35.5
r[%]		1.1	17.3	29.4	44.5	60.0	76.1	92.8

Table 3.1 Symbols for the reactance sum *x d + 2 x n* used in Figs. 3.1 and 3.2 and corresponding specifications

The representation of the line current harmonics separated into positive and negative sequence systems permits a direct comparison with the fundamental dependencies**,** i.e., a discussion of the effect of commutation and ripple. If the waveform for good smoothing is compared with the actual behavior of the spectrum, then the greatest differences occur at the low-frequency harmonics *h* = ***5*** and 7. In addition, the deviations of the positive sequence systems

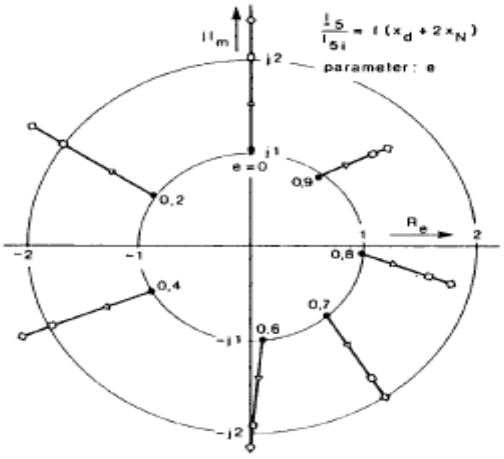

Fig. 3.2. Amplitude spectrum of the **line current harmonics negative (above) and positive sequence systems (below); low-voltage supply *(X N* = 7.5%) and emf** *e* = 0.8 **assumed; parameter: reactance sum *i d* + *2 X N* .**

symbol		(*)	(▽)	(x)	(+)	(△)	(○)	(□)
x_d+2x_N		16	2	1.2	0.8	0.6	0.45	0.35
u[°el]	coil	7.0	6.5	6.1	5.6	5.1	4.3	3.3
r[%]		1.6	13.1	22.2	33.9	46.0	63.1	88.3
u[°el]	coil sum	11.8	11.4	11.1	10.8	10.4	9.7	9.2
a[°el]		30.5	30.7	30.9	31.0	31.2	31.5	31.7
r[%]		0.9	7.4	12.5	18.8	25.7	37.6	45.5

Table 3.2 Symbols for the reactance sum *x d + 2 z n* used in Figs. 3.3 and 3.4 and corresponding specifications

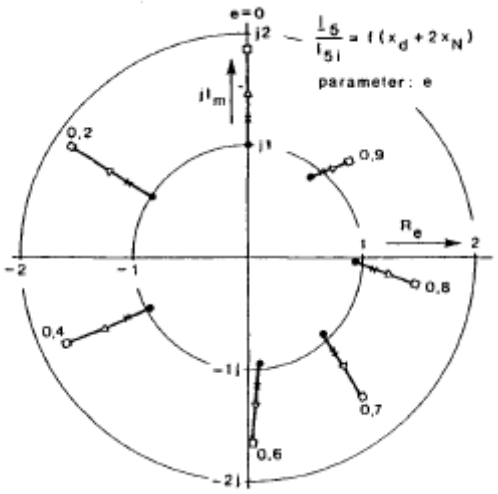

Fig. 3.3. Amplitude spectrum of the line current harmonics negative (above) and positive sequence systems (below); medium-voltage supply *(Z N* = 15%) and emf *e* = 0 assumed parameter: reactance sum *X d* + *2 X N* .

h, are generally greater than those of the negative sequence systems *h,,* which can be explained by the negative sign in(6). As a result of the dc ripple, higher harmonics can also reach greater values than those described by the conventional model assuming good dc smoothing.

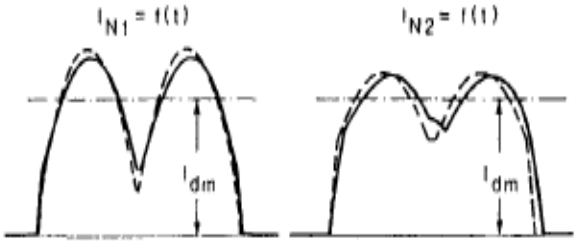

Fig. 3.4. Amplitude spectrum of the line current harmonics negative (above) and positive sequence systems (below); medium-voltage supply *(x* . =~ **15%) and emf *e*** = 0.8 **assumed; parameter: reactance sum** *X d + 2x;y* .

IV. EVALUATION AND DISCUSSION EFFECT OF DC RIPPLE AND COMMUTATION

The values marked with the symbol ***"0"*** correspond to the conventional behavior for good dc smoothing, and "()" in Fig. 12 applies to ***x d + 2 x N = 0.218,*** i.e., operation at the pulsation limit for e = 0 according to (6) and (7). In the special case of e = 0, all pointer peaks lie on the imaginary axis; with increasing values of e, the straight lines are rotated around the origin proportionally to the reduction of the control angle *a.* It should be noted that according to Fig. **3.4 ,** the positive sequence system ***hp*** = 7 shows a zero transition of the amplitude only for e = 0. For negative values of e, i.e., for inverted rotation immediately the relative deviations due to the commutation, and Fig. ***3*** lines out the results for dc ripple. With increasing emf, the approximation of the dc ripple by symmetrical sine tops [3], [4] leads to increasing errors, especially in the determination of the phase angle of the harmonics of positive sequence. An example of an asymmetry in the line current tops, which is neglected in this approximation, and leads to a corresponding rotation of the straight lines away from the origin in the loci *L7/f7*.

The evaluation proposed is based on the consideration of five dominant parameters, i.e., the operating point *(I d m , E)* and the circuit data *(X d , X N , U N)* . As a result of the cho-sen normalization, these five parameters are reduced to the following three: e = *E/Ud;*, *x d = X d / (U N I d m)* , and *X N = X N*/*(UN / I d m)* . Note that the normalized reactances depend on the operating point *x d , N N f d m* . The specified amplitude spectra refer to characteristic values of the network reactance in usual low- or medium-voltage supplies and thus permit a more realistic predetermination of the line current harmonics. It can be seen that these representations show differences from the usual assumption of a good-smoothed dc current, which are considerable in the case of higher dc ripple. Considering the results becomes clear that the worst case for the voltage distortion factor *DF,* is given by the usual calculation, assuming ideal dc smoothing. In contrast with this, higher dc ripple leads to a significant enlarged current distortion D;. from the value with good smoothing both in amplitude and especially in phase. These deviations, which are considerable,in the of high dc lead to correspondingly modified line current and voltage distortion.

REFERENCES

1. IEEE 519, *Guide for Harmonics Control and Reactive Compensation of Static Power Converters.* New York: IEEE, 1981.
2. DKE, "Electromagnetic compatibility," *DINNDE* 0839, Draft, Feb. 9, 1990 (in German).
3. L. G. Dobinson, "Closer accord on harmonics," *Electron. Power,* vol. 15, pp. 567-572, May 1975.
4. A. D. Graham and E. T. Schonholzer, "Line harmonics of converters with dc-motor loads," *IEEE Trans. Ind. Applicat.,* vol. IA-19, pp. 8 4 9 3 , Jan./Feb. 1983.
5. M. Sakui, A. Yanase, and H. Fujita, "Line harmonic current of three-phase thyristor bridge rectifier circuit with dc current ripple and over-lapping angle," *Elec. Eng.* Japan, vol. 105, no. 6, pp. 48-55, 1985.
6. S. De Haan, "Analysis of the effect of source voltage fluctuations on the power factor in three-phase controlled rectifiers," *IEEE Trans. Ind. Applicat.,* vol. IA-22, pp. 259-266, Mar./Apr. 1986.
7. M. Grotzbach and R. von Lutz, "Evaluation of converter harmonics in power systems by a direct and analytical based state variable approach," in *Proc. EPE* (Brussels), 1985, vol. 1, pp. 2.153-2.158.

8. K. R. Padiyar and P. K. Kalra, "Analysis of an HVDC converter with finite smoothing reactor," *EZec.. Power Syst. Res.,* vol. 11, pp. 171-184,1986.
9. J. Arrillaga, D. A. Bradley, and P. S. Podger, *Power System Harmonics.* Chichester: Wiley, 1985.

Multi Objective Social Spider Algorithm Based Optimal Location and Sizing of Svc Devices for Voltage Stability Improvement

Ms. M. Premalatha[1]
Assistant Professor,
Department of Electrical and Electronics Engineering,
St. Anne's College of Engineering and Technology,
Anguchettypalayam, Panruti – 607106.

Ms. R. Santhiya[2] Ms. A. Soundharya[3] Ms. B. Prithivi bala[4]
UG Scholar,
Department of Electrical and Electronics Engineering
St. Anne's College of Engineering and Technology,
Anguchettypalayam, Panruti – 607106.

Abstract— This paper presents social spider algorithm for determining the optimal location and size of Static Var Compensator (SVC) devices in power systems. The aim of SVC devices in Egyptian interconnected electrical power system is to increase the system load ability within the permissible voltage levels and to minimize the power losses and generating costs simultaneously. The proposed algorithm is applied to 500 KV interconnected electrical power system network. The numerical results achieved in MATLAB showed that the social spider technique succeeded at determining the optimal location and size of SVC with minimum power losses and minimum generating costs, as well as improvement in the system voltage profile.

Index terms: **voltage stability, FACTS, Optimal Location and Size, social spider algorithm.**

I. INTRODUCTION

Flexible AC Transmission Systems (FACTS)have been implemented in many power systems. These devices have many functions and can play important roles in the power system. They can be used for power quality improvement, voltage support, power flow control, improvement of the system stability, and an increaseinthe system reliability [1-4]. FACTS devices can be classified according to their connections to the electrical power system like series, shunt and/or combined connection. Static VAR Compensator (SVC) and Static synchronous compensator (STATCOM) are from the shunt connected FACTS types. Static Synchronous Series Compensator (SSSC) and Thyristor Switched Series Capacitor (TSSC) are from the series while Unified Power Flow Controller (UPFC) is the combined compensator type [5-7]. According to the type of connecting FACTS devices into the power system, the operation and the role of these devices in the power system is determined. The series FACTS devices are used for providing capacitive/inductive and line resistance compensation [6-9]. For the voltage support by controlling the reactive power flow, shunt FACTS devices are attained during sag/swell condition and fault operating conditions [9].The combined devices can play the role of both series and shunt compensators [4-5, 10]. SVC as a shunt compensator type is exploited in this framework to control the reactive power flow and consequently regulate the system voltage. The SVC is characterized as fast response and has high reliability in the compensation problem compared to mechanically switched capacitor

banks [7, 10]. The problem of size and location selection of SVC devices in the power systems to achieve Economic Dispatch (ED)and to minimize the generating cost has a significant role in improving the system performance, reduction of the losses and the generating costs [8]. However, typical problems such as non-linear, very large and complex mathematical programming problems can be solved using conventional computational methods or efficient algorithms [11-12]. The heuristic methods called "intelligent," as their movement between all possible solutions, are used for optimization to solve combinatorial, non-linear, complex optimization problems. These methods are not limited by restrictive expectations for the search space that includes continuity, existence of derivative of objective function, etc, [11-13].

There are many heuristic methods exploited in power system optimization and operation. One of the intelligent methods is Genetic Algorithm (GA) used for optimal tuning of PI control parameters for wind application as demonstrated in [14]. It is also used for optimal allocation of FACTS devices in power system as illustrated in [15]. Furthermore, Particle Swarm Optimization (PSO) as one of these heuristic methods is also used in optimal allocation in [15]. A modification of PSO for reactive power support and voltage stability is introduced in [8]. In addition, one of the optimization methods, Bacterial Foraging Optimization Algorithm (BFOA), has many applications in controller design of the power system [16]. This paper proposes a social spider algorithm to determine the optimal location and size of SVC. The modified approach utilizes Quadratic Adaptive Bacterial Foraging Algorithm (QABFA). The optimal location and size of SVC aims at minimizing the power losses, minimizing the generation cost by achieving the ED with improved system voltage profile.

II. SYSTEM UNDER STUDY

The studied system used in this work is a part of the Egyptian 500 KV network consists of 15 buses with their names as depicted in Appendix A, [17]. This system comprises15 buses with four generating units and 12 loads .The system also has 19 lines, three of them are double lines. The base of the data used in this system is 1775 MVA on 500 KV, the system data are given in Appendix A. In this system there is one cable under water, from bus 12 to bus 13 with length of 13.5 Km as one unit without any junctions. The depth of this cable is 800 m under the surface of the water; it is the first under water cable at this depth, such as all under water cables were designed at depth of ranges from 400-500 m as in Fig.1. The system also contains connected load between Egypt and Jordan through El Akaba gulf. This cable is four phases. In other words three of them are on-line and the fourth is off-line (spare for any problem). This cable is four phases as it will be changed into two DC cables with the extension increase in power transmitted to Jordan. There are three double reactors each of 165 MAV at buses # 1, 2 and 4 added to the reactive load power at these buses.

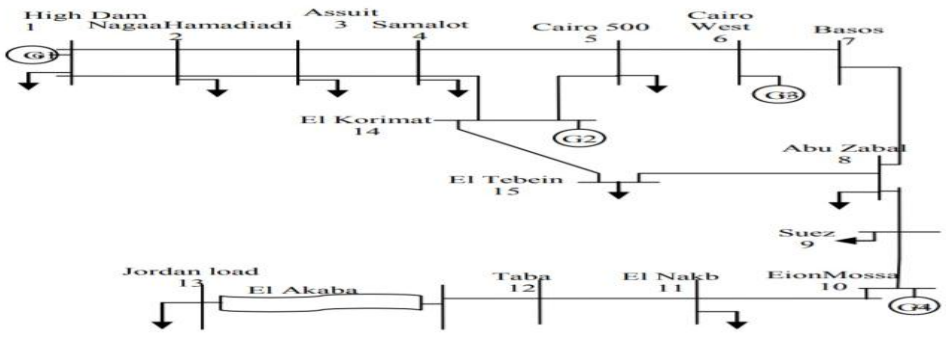

Figure 2.1 The Egyptian 500kV Interconnected Network

III. PROBLEM FORMULATION

The overall objective function in this framework is classified into two parts. First the security index is approximated as a equation

$$f1(p) = \sum_i w_i \left| v_i - v_{ref} \right|^2 \quad (1)$$

The second part of the objective function is the cost of FACTS devices represented in the form of svc. The SVC cost function in $/KVar as given in (3),

$$f_2 = 0.0003s^2 - 0.3051s + 127.38 \quad (2)$$

Where s is the operating range of SVC devicesin MVAR. The objective function is to be minimized F is given as

$$Min(F) = Min\left(f_1(p) + f_2(g)\right) \quad (3)$$

Where g is the vector that represents the variables of FACTS devices.

Subjected to the following constrains:

$$E(g,x)=0 \quad (4)$$

$$B_1(g), B_2(x) \geq 0 \quad (5)$$

Where E(g,x) represents the conventional power flow equations and $B_1(g), B_2(x) \geq 0$ are the inequality constrains for SVC devices and the optimal power flow respectively. The average value of the investment cost function of SVC is formulated as:

$$f_2(g) = f_2(g)/(4 \times 8760) \quad (6)$$

IV. SVC MODELLING

The SVC scheme mainly consists of a TCR which is connected in parallel with capacitors. From an operational point of view, the SVC, similar to a shunt-connected variable reactance, is able to generate or absorb reactive power to control the voltage magnitude at the point of connection to the AC network. Thus, it is importantly implemented to deliver fast reactive po-wer and to support voltage regulation. The thyristor's firing angle control is designed to facilitate the SVC to have virtually instantaneous speed of response. A schematic diagram of the SVC is shown in Figure 4.2, [4-6].

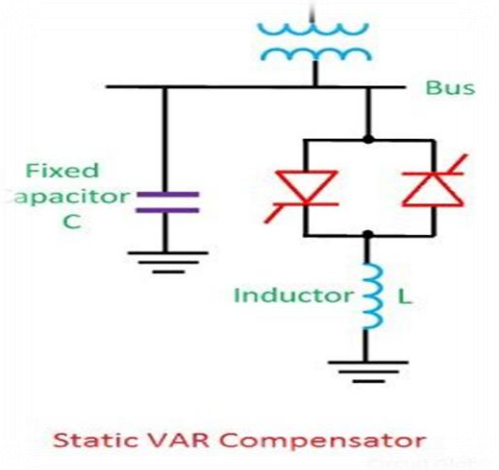

Figure 4.2 Schematic Diagrams of Static Var Compensator

V. OPTIMAL LOCATION AND SIZE OF SVC DEVICES USING SOCIAL SPIDER ALGORITHM

Social spider algorithm is swarm based nature inspired algorithm developed based on searching of prey. In SSA, we formulate the search space of the optimization problem as a hyper-dimensional spider web. Each position on the web represents a feasible solution to the optimization problem and all feasible solutions to the problem have corresponding positions

on this web. The web also serves as the transmission media of the vibrations generated by the spiders. Each spider on the web holds a position and the quality (or fitness) of the solution is based on the objective function, and represented by the potential of finding a food source at the position. The spiders can move freely on the web. However, they cannot leave the web as the positions off the web represent infeasible solutions to the optimization problem. When a spider moves to a new position, it generates a vibration which is propagated over the web. Each vibration holds the information of one spider and other spiders can get the information upon receiving the vibration.

The spiders are the agent of SSA to perform optimization. At the beginning of the algorithm, a pre-defined number of spiders are put on the web. Each spider s holds a memory, storing the following individual information:

1) The position of s on the web.
2) The fitness of the current position of s.
3) The target vibration of s in the previous iteration.

The first two types of information describe the individual situation of s, while the third type of information is involved in directing s to new positions.

Vibration is a very important concept in SSA. It is one of the main characteristics that distinguish SSA from other meta heuristics. In SSA, we use two properties to define a vibration, namely the source position and the source intensity of the vibration. The source position is defined by the search space of the optimization problem, and we define the intensity of a vibration in the range [0, +∞). Whenever a spider moves to a new position, it generates a vibration at its current position. We define the position of spider a at time t as Pa(t), or simply as Pa if the argument is t. We further use I(Pa, Pb, t) to represent the vibration intensity sensed by a spider at position Pb at time t and the source of the vibration is at position Pa. Thus I(Ps, Ps, t) defines the intensity of the vibration generated by spider s at the source position. This vibration intensity at the source position is correlated with the fitness of this position f(Ps), and we define the intensity value as follows:

$I(P_s, P_s, t)=1/(Cmax - f(Ps))$ for maximization; (1)

$I(P_s, P_s, t)=1/(f(Ps) - Cmin)$ for minimization; (2)

where C_{max} is a confidently large constant selected such that all possible fitness values of the maximization problem is smaller than C_{max}, and C_{min} is a confidently small constant such that all possible fitness values of the minimization problem is -larger than C_{min}.

INTENSITY ATTENUATION

1) Attenuation over Distance: We define the vibration attenuation over distance as follows. We define the distance between spider a and b as $D(P_a,P_b)$, and the maximum distance between two points in the search space as D_{max}. The definition of D_{max} can be problem-dependent, and we use the following equation for simplicity:

$D_{max} = ||x-x||p,$ (3)

where x is the upper bound of the search space and x is the lower bound of the search space. p indicates that we use pnorm as the method to calculate the distance between spiders, i.e., $D(P_a,P_b)=||P_a - P_b||p.$ (4)

we define the vibration attenuation over distance as follows:

$$I(Pa, Pb, t) = I(Pa, Pb, t) \times \exp\left(-\left(\frac{D(Pa,Pb)}{(Dmax \times ra)}\right)\right) \quad (5)$$

Attenuation over Time:

The vibration attenuation over time is defined as follows:

$I(P_a(t),P_a(t),t+ 1) =I(P_a,P_a,t)\times r_a.$ (6)

The algorithm then manipulates s to perform a random walk towards vtar. This random walk is conducted using the following equation:

$$P_s(t+1) = P_s + (P_{tar} - P_s)\Theta\,(1 - R\Theta R) \quad (7)$$

The probability is defined using the following equation:

$$Pj = rj/\left(\frac{D(Ps,Ptar)}{Dmax}\right) \quad (8)$$

The iteration phase loops until the stopping criteria are matched. The stopping criteria can be defined as the maximum iteration number reached, the maximum CPU time used, the error rate reached, the maximum number of iterations with no improvement on the best fitness value, or any other appropriate criteria.

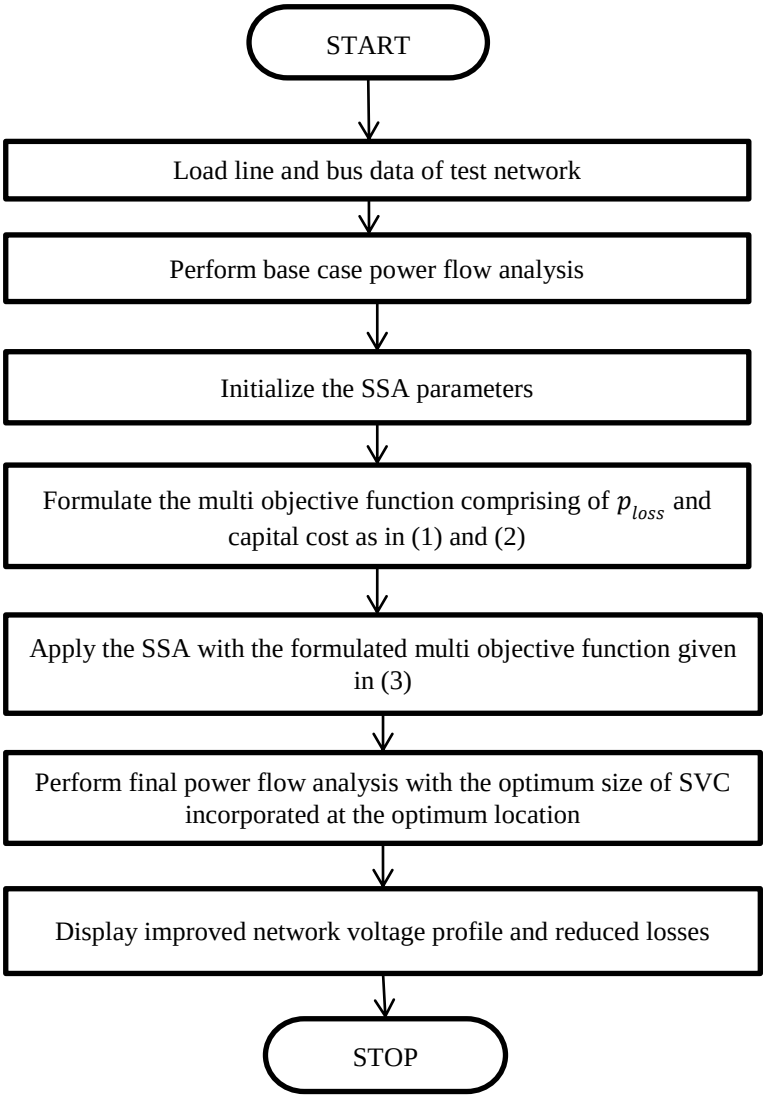

VI. SIMULATION RESULTS

The main objective of this paper is to find the best location and size of SVC in the Egyptian 500 KV network with minimum generating cost. The SSA is used in scheme to cope with this optimization problem. By re-dispatching of the load flows in electrical power system, the total generation costs can be minimized by optimal SVC allocation and size. The conventional load flow results using Newton Raphson method are given in the appendix. The base case load and line flow results are listed in Tables A.2 and A.3, respectively in the appendix. From buses 1 to 4, there are double circuit lines which they maintain the same power flow at the double circuit

Lines (lines 6, 7, 8 ,9 ,10 and 12).As a result, no circulating currents exist in these double lines. The positive active /reactive power flow means that the flow is in the right

direction, while the negative power sign shows that the flow is in the reverse direction. The negative power flow of -0.125 p.u in line 1 indicates that the power direction is basically from bus#6 to bus#5 not as resulted in the table A3 from bus #5 to bus #6. Using SSA the best location of SVC is at bus 2 with the line and load flow results illustrated in Tables 1and 2.Comparison between QABFA and SSA is illustrated through figure4 and Table 3.The results depict that the best location for SVC is at bus 2and the size is 0.289 p.u when using SSA, whereas using QABF shows the best location for SVC at bus 3 and the size becomes 0.29 p.u. Notably, there is an increase in voltage magnitude at bus 2while SVC is in service. The generated power has increased from High Dam bus as it is the cheapest generating cost (hydraulic station).

Bus	V	Phase rad	Pgpu	Q gen pu	Ploadpu	Q load pu
1	1.05	0	0.925	0.21915	0.1127	0.0563
2	1.03	-0.185	0	0.2989	0.6196	0.3943
3	1.05	-0.222	0	0	0.0451	0.0225
4	1.05	-0.240	0	0	0.169	0.107
5	1.05	-0.235	0	0	0.1127	0.1014
6	1.05	-0.231	0.338	-0.03182	0	0
7	1.05	-0.235	0	0	0	0
8	1.05	-0.247	0	0	0.0845	0.0451
9	1.05	-0.279	0	0	0.1127	0.0676
10	1.05	-0.280	0.338	0.124288	0.1127	0.169
11	1.04	-0.412	0	0	0.07664	0.02704
12	1.03	-0.419	0	0	0	0
13	1.03	-0.425	0	0	0.169	0.0563
14	1.05	-0.235	0.6759	0.106421	0.5633	0.1971
15	1.05	-0.246	0	0	0.0845	0.0563

Table 6.1 Load Flow Results of Egyptian 500kV Network With SVC

VII. CONCLUSION

The selection of size and location of SVC devices in the power systems design was an essential step. The proper selection has successfully achieved savings, enhancement of the voltage profile and the reduction in power losses. The study has presented SSA based on the economic dispatch for determining the best location and size of SVC in the interconnected electrical power system. The proposed SSA was compared with the QABFO method. The results showed that SSA scheme is far superior to QABFO in the selection of location and size as well as in the generating cost reduction and in the voltage profile improvement.

From Bus	To Bus	Line	P Flow [p.u.]	Q Flow [p.u.]	P Loss [p.u.]	Q Loss [p.u.]
5	6	1	-0.125	-0.005	0	-0.009
5	14	2	-0.001	-0.041	0	-0.079
5	4	3	0.014	-0.055	0	-0.126
14	4	4	0.019	-0.037	0	-0.095
14	15	5	0.092	-0.015	0	-0.036
3	4	6	0.068	0.001	0	0.0122
3	4	7	0.068	0.001	0	0.0122
3	2	8	-0.090	-0.012	0	-0.116
3	2	9	-0.090	-0.012	0	-0.116
1	2	10	0.406	0.081	0.006	0.137
1	2	11	0.406	0.081	0.006	0.137
6	7	12	0.213	-0.028	0	-0.005
7	8	13	0.213	-0.023	0.001	-0.015
8	15	14	-0.007	-0.021	0	-0.057
8	9	15	0.136	-0.033	0.000284	-0.066
9	10	16	0.023	-0.034	0	-0.024
10	11	17	0.248	-0.055	0.002251	-0.119
11	12	18	0.169	0.0382	0	-0.009
12	13	19	0.169	0.047	0	-0.009

Table 7.1 Flow results of Egyptian 15 bus 500kv network with SVC

Method	$P_{generated}$	P_{losses}
Base case load flow	2.279955	0.017515
QABFA	2.2783250	0.015856
SSA	2.27315	0.014875

Table 7.2 Comparison Between Ssa, Qabfa And Base Load Flow

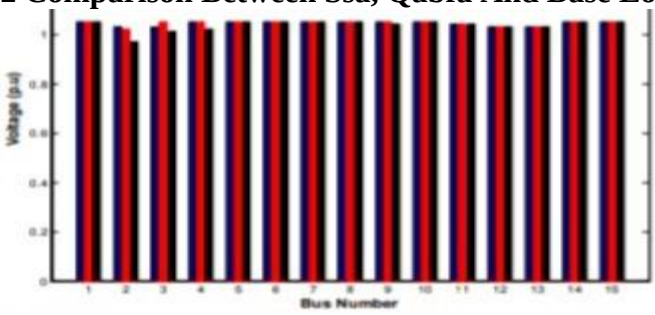

Fig.7.1 Bus voltage using QABFA, SSA and base case load flow

REFERENCES

1. IEEE FACTS working group 15.05.15, "FACTS Application", December 1995.
2. C. A. Canizares and Z. T. Faur, "Analysis of SVC and TCSC Controllers in Voltage Collapse," IEEE Trans. on Power Systems, vol. 14, no. 1, February 1999, pp. 158–165.
3. K. Habur, and D. Oleary, "FACTS - Flexible AC Transmission Systems, for cost effective and reliable transmission of electrical energy, 2018.

4. Mohamed I. Mosaad and FawzanSalem "Adaptive Voltage Regulation of Self Excited Induction Generator Using FCATS Controllers" Int. J. Industrial Electronics and Drives- Inderscience Publishers, Vol. 1, No. 4, 2014.
5. N.G. Hingorani, L. Gyugyi, Understanding FACTS – Concepts and technology of Flexible AC Transmission Systems, IEEE Press, 2000. ISBN 0-7803-3455-8.
6. Y. H. Song, A. T. Johns. Flexible AC Transmission Systems (FACTS), IEE Press, London, 1999.ISBN 0-85296-771-3.
7. A. Findley, M. Hoffman, D. Sullivan and J. Paramalingam, "Lessons learned in static var compensator protection," 2017 70th Annual Conference for Protective Relay Engineers (CPRE), College Station, TX, 2017, pp. 1-8.
8. Mohamed I. Mosaad "Constrained Particle Swarm optimization for Reactive Power And Voltage Control Considering Voltage Stability" MiddleEast Power System Conference , MEPCON 2012, pp81-86.
9. M.A ELhamedZaki , , Mohamed I. Mosaad, Mohamed G. Ashmawy , AbdElAziz Osman "Power Quality Improvement of WEGCS Using STATCOM Based EC Techniques " Int. J. of Industrial Electronics and Drives, Inderscience Publishers., 2017 Vol.3, No.4, pp.229 – 237,
10. S. Messalti, A. Gherbi and S. Belkhiat, "Assessment of power system transient stability using shunt FACTS devices: SVC and TCBR," 2014 International Conference on Electrical Sciences and Technologies in Maghreb (CISTEM), Tunis, 2014, pp. 1-6.
11. Lee KY,YomeAS,Park JH "Adaptive Hopfield Neural Network For Economic Load Dispatch "IEEE Transactions on Power Systems, 1998,13(2),pp.519-526.
12. Song YH, Wang PV ,Johns AT. "Environmental Economic dispatch using fuzzy logic controller Genetic Algorithms " IEE Proc. Gener. Transm. Distr. 1997 ;144(4),pp.377-382
13. S. Chansareewittaya and P. Jirapong, "Optimal allocation of multi-type FACTS controllers for total transfer capability enhancement using hybrid particle swarm optimization," 2014 11th International Conference on Electrical Engineering/Electronics, Computer, Telecommunications and Information Technology (ECTI-CON), NakhonRatchasima, 2014, pp. 1-6.
14. Mohamed I. Mossad, Nagy I. Elkalashy and Mohamed G. Ashmawy, "Integrating Adaptive Control of Renewable Distributed Switched Reluctance Generation and Feeder Protection Coordination" Electirc Power System Research journal, Elsevier, Volume 154, January 2018, Pages 452–462.
15. M.M.ElMetwally, A.A. El Emary, F.M.ElBendary and M.I.Mosaad, "Optimal Allocation of FACTS Devices In Power System Using Genetic Algorithms" Middle East Power System Conference ,MEPCON 2008, pp312-315.
16. Mohamed I. Mosaad, Mohamed G. Ashmawy "Short Term Load Forecasting Using Curve Fitting Prediction Optimized By Bacterial Foraging Optimization" International Review on Modelling and Simulations (IREMOS), Italy, Vol 6,no.3, August 2013, pp1150-1154.

17. A. E. Abdou, E. M. Tag Eldin, H. A. Elghazaly, A.M.K. Elmorshedy "Switching Overvoltages and Risk of Failure Assessment of The Egyptian 500 kV Power Network", world academy of science, engineering and technology(Waset 2010), Tokoyo, Japan, 2010.
18. Passino, K.M., Bacterial foraging optimization. Innovations and Developments of Swarm Intelligence Applications, 2012: p. 219.
19. Supriyono, H., &Tokhi, M. O.,"Bacterial foraging algorithm with adaptable chemotactic step size," In Computational Intelligence, Communication Systems and Networks (CICSyN), 2010 Second International Conference on (pp. 72-77), July,2010.
20. Xing, B. and W.-J. Gao, Innovative computational intelligence: a rough guide to 134 clever algorithms. Vol. 62. 2014: Springer. 469.
21. K. M. Passino, "Biomimicry of bacterial foraging for distributed optimization and control", IEEE Control Systems Magazine, June 2002, pp. 52-67.

To Improve Performance Response of Economic Load Dispatch by using Grey Wolf Optimization Technique

Mr. K. Sriram[1]
Assistant Professor,
Department of Electrical and Electronics Engineering,
St. Anne's College of Engineering and Technology,
Anguchettypalayam, Panruti – 607106.

Mr. R. Rajkumar[2], Mr. P. Pasupathi[3], Mr. R. Elumalai[4], Mr. Y. Magimai Xavi Thomas[5]
UG Student,
Department of Electrical and Electronics Engineering
St. Anne's College of Engineering and Technology,
Anguchettypalayam, Panruti – 607106.

Abstract - Economic Load Dispatch is a problem of determining the power output of each generating unit of the power system such that the total fuel cost is minimum while all the system constraints are like generation limits, valve point loading effects, etc. The problem of determining the outputs of the generating units at minimum cost is known as Optimal Power Flow (OPF) problem. The production cost of any generator is unique and is a quadratic function of power generated by it. For a given power generated by the unit, a unique cost is incurred. The minimum cost incurred for all the units combined together becomes the optimization problem which is known as the Economic Dispatch (ED) problem. The paper presents the optimal generation cost for the power system by using Grey Wolf Optimization Algorithm (GWOA). GWOA is most advanced and fastest method for optimization problem and can be implemented for any generated bus data in power system.

Index Terms— **Economic Dispatch, Optimal Power Flow and GWOA Algorithms.**

I. INTRODUCTION

The Economic Load Dispatch (ELD) can be defined as the process of allocating generation level to the generating units, so that the system load is supplied entirely and most economically. For an interconnected system, it is necessary to minimize the expenses. The economic load dispatch is used to define the production level of each plant, so that the total cost of generation and transmission is minimum for a prescribed schedule of load. The objective of economic load dispatch is to minimize the overall cost of generation. The method of economic load dispatch for generating units at different loads must have total fuel cost at the minimum point.

In a typical power system, multiple generators are implemented to provide enough total output to satisfy a given total consumer demand. Each of these generating stations can, and usually does, have unique cost-per-hour characteristic for its output operating range. A station has incremental operating cost for fuel and maintenance; and fixed costs associated with the station itself that can be quite considerable in the case of a nuclear power plant, for example things get even more complicated when utilities try to account for transmission line losses, and the seasonal changes associated with hydroelectric plants.

A major challenge for all power utilities is not only to satisfy the consumer demand for power, but to do so as to minimal cost. Any power system can be comprised of multiple generating units having number of generators and the cost of operating these generators does not usually correlate proportionally with their outputs; therefore the challenge for power utilities is to try to balance the total load among generators are running as efficiently as possible.

The Economic Load Dispatch (ELD) problem assumes that the amount of power to be supplied by a given set of units constants for a given interval of time and attempts to minimize the cost of supplying this energy subject to constraints of the generating units. Therefore it is connected with the minimization of total cost over the entire dispatch period. Therefore, the main aim in the economic load dispatch problem is to minimize the total cost of generating real power (production) at various stations while satisfying the loads and the losses in the transmission links.

The cost is usually approximated by one or more quadratic segments. The operating cost of the plant has from shown in figure2.2 for dispatching purposes, this cost is usually approximated by one or more quadratic segments. So, the fuel cost curve in the active power generation, takes up a quadratic from, given as:

$$F(P_{gi}) = a_i P_{gi}^2 + b_i P_{gi} + C_i \; Rs/hr \qquad (1.1)$$

where

ai,bi,ci are cost coefficients for ith unit

F(P_{gi}) is the total cost of generation

$P_{gi}$is the generation of i^{th} plant

II. ECONOMIC LOAD DISPATCH WITH LOSSES

Transmission losses may be neglected when transmission losses are very small but in a large interconnected network where power is transmitted over long distance, transmission losses are a major factor and affect the optimum dispatch of generation. The economic load dispatch problem considering the transmission power lossP_L for the objective function is thus formulated as:

Minimize:

$$F(P_{gi})=\sum_{i=1}^{NG} F_i(P_{gi}) \qquad (2.1)$$

$$F_i(P_{gi})= a_i P_{gi}+b_i P_{gi}+c_i \text{Rs/h} \qquad (2.2)$$

Subjected to:

The energy balance equation

$$\sum_{i=1}^{NG} P_{gi}=P_D+P_L \qquad (2.3)$$

(i) And the inequality constraints

$$P_{gi}^{min} \leq P_{gi} \leq P_{gi}^{max} \qquad (2.4)$$

The general form of the loss formula using B-coefficients is

$$P_L=\sum_{i=1}^{NG}\sum_{i=1}^{NG} P_{gi}\, B_{ij} P_{gj} \text{MW} \qquad (2.5)$$

where

P_{gi}andP_{gj} are the real power generation at i^{th} and j^{th} buses respectively

$B_{ij}$are the loss coefficients or B-coefficients

The transmission loss formula of Eq. (2.3) is known as George's formula. Using the Lagrange multiplier λ, the augmented function is,

$$L(P_{gi},\lambda)=F(P_{gi})+\lambda(P_D+P_L-\sum_{i=1}^{NG} P_{gi}) \qquad (2.6)$$

For minimization of augmented function,

$$\frac{\partial \lambda(P_{gi},\lambda)}{\partial P_{gi}}=0 \qquad (2.7)$$

$$\frac{\partial\lambda(P_{gi},\lambda)}{\partial\lambda}=0 \quad (2.8)$$

$$\frac{\partial F_i(P_{gi})}{\partial P_{gi}}=\frac{\partial F((P_{gi}))}{\partial P_{gi}} \quad (2.9)$$

The condition given by (2.20) results as,

$$\frac{\partial L(P_{gi},\lambda)}{\partial P_{gi}}= \frac{\partial F(P_{gi})}{\partial P_{gi}}+\lambda\left(\frac{\partial P_L}{\partial P_{gi}}-1\right)=0 \ ;(i=1,2,\ldots.) \quad (2.10)$$

$$\frac{\partial F(P_{gi})}{\partial P_{gi}}=\lambda\left(1-\frac{\partial P_{gi}}{\partial P_{gi}}\right); \quad (i=1,2,\ldots.,NG) \quad (2.11)$$

Or

$$\frac{\partial F(p_{gi})}{\partial P_{gi}}+\lambda(\frac{\partial P_{gi}}{\partial P_{gi}})=\lambda \ ; \quad (i=1,2,\ldots,N) \quad (2.12)$$

Where$\frac{\partial F(P_{gi})}{\partial P_{gi}}$ is called incremental fuel cost $(IC)_i$

And$\frac{\partial P_L}{\partial P_{gi}}$ is known as incremental transmission loss $(ITL)_i$, associated with i^{th} generating unit. Rearranging (2.24) results as,

$$\frac{\frac{\partial F(P_{gi})}{\partial P_{gi}}}{1-\frac{\partial P_L}{\partial P_{gi}}}=\lambda \quad (2.13)$$

$$\left(\frac{1}{1-\frac{\partial P_L}{\partial P_{gi}}}\right)\frac{\partial F(P_{gi})}{\partial P_{gi}}=\lambda \ ; \quad (i=1,2,\ldots.,NG) \quad (2.14)$$

Or

$$L_i\left(\frac{\partial F(P_{gi})}{\partial P_{gi}}\right)=\lambda; \quad (i=1,2,\ldots.,NG) \quad (2.15)$$

where$L_i$is called the penalty factor of the i^{th}plant given by

$$L_i=\frac{1}{1-\frac{\partial P_L}{\partial P_{gi}}} \quad (2.16)$$

$$(IC)_i=\lambda\,[1-(ITL)_i]\ ;\ (i=1,2,\ldots NG) \quad (2.17)$$

This equation is referred to as the exact coordination equation. Thus it is clear that to solve the economic load dispatch problem, it is necessary to complete ITL for each plant and therefore functional dependence of transmission loss on real powers of generating plants must be determined. There are several methods, approximate and exact, for developing a transmission loss model. One of the most important, simple but approximate methods of expressing transmission loss as a function of generator powers is through B-coefficients. This method is reasonably adequate for treatment of loss coordination in economic scheduling of load between plants.

$$\frac{\partial P_L}{\partial P_{gi}}=\sum_{i=1}^{NG}2B_{ij}\,P_{gj} \quad (2.18)$$

Assuming quadratic plant cost curves as given, incremental cost is obtained as,

$$\frac{\partial F_i(P_{gi})}{dP_{gi}}=2a_iP_{gi}+b_i \quad (2.19)$$

Substituting $\frac{\partial P_L}{\partial P_{gi}}$ and $\frac{\partial F_i(P_{gi})}{dP_{gi}}$ from above equation,

$$2a_iP_{gi}+b_i+\lambda\sum_{i=1}^{NG}2B_{ij}\,P_{gj}=\lambda \ ; \ (i=1,2,\ldots.NG) \quad (2.20)$$

Collecting all terms of P_{gi} and solving for $P_{gi,}$

$$(2a_i+2\lambda B_{ii})P_{gi}=-\lambda\sum_{\substack{j=1\\ j\neq 1}}^{NG}2B_{ij}\,P_{gj}-b_i+\lambda \ ; \ (i=1,2,..NG) \quad (2.21)$$

Or

$$P_{gi}=\frac{1-\frac{b_i}{\lambda}-\sum_{\substack{j=1\\ j\neq 1}}^{NG} 2B_{ij}P_{gj}}{\frac{2a_i}{\lambda}+2B_{ii}} \quad ; \text{ (i=1,2,….NG)} \qquad (2.22)$$

For any particular value of λ, above equation can be solved iteratively by assuming initial values of P_{gi}'s. Iteration are stopped when P_{gi}'s converge within specified accuracy.

III. RESULT ANALYSIS

A simple single machine infinite bus (SMIB) power system. Model is simulated in Matlab environment. The results show the implementation of whale optimization algorithm for a Six Generator Bus data for the economic load dispatch problem.

The Economic Dispatch (ED) problem is solved by the whale optimization algorithm the results obtained are discussed and compared. Two different systems, having six and fifteen generators, are taken as the test system. For simplicity, the ramp rate limits, losses, and the prohibited zones are not considered. Under the same evaluation function and individual definition, we perform 50 trials using the above methods and the quality of the solution is observed.

Six-Unit system:

The test taken into consideration system consists of six generators for a load demand of 1263 MW on the system. The characteristics of the six units are given in Table 1. The power outputs of the six generators are represented by P1, P2, P3, P4, P5 and P6. These values are randomly generated. The best solution obtained by applying these methods is shown in Table 3.2.

Unit	Pi min	Pi max	αi ($)	βi ($/MW)	γi ($/W2)
1	100	500	240	7.0	0.0070
2	50	200	200	10.0	0.0095
3	80	300	220	8.5	0.0090
4	50	150	200	11.0	0.0090
5	50	200	220	10.5	0.0080
6	50	120	190	12.0	0.0075

Table 3.1: 6 Bus Generating unit data

Unit Power Output	PSO	GA	GWOA
P1(MW)	447.9250	445.8835	426.0887
P2(MW)	170.6501	170.3555	176.8286
P3(MW)	264.7467	267.1309	262.6988
P4(MW)	120.3847	120.6641	135.45
P5(MW)	170.8557	170.3184	171.1362
P6(MW)	88.4368	88.6466	88.7916
Total Power output (MW)	1263	1263	1263
Total Generation cost ($/hr)	15,276	15,276	14,963

Table 3.2: Optimum solution of 6- unit system

Generation cost ($)		
	Max	Min
PSO	15298	15276
GA	15277	15276
GWOA	14959	14963

Table 3.3 : Comparison between three methods (50 trials)

Fifteen-Unit System:

The system consists of fifteen generators and the total load demand on the system is 2630 MW. The characteristics of the fifteen generators are given in Table 3.4. The results of the experiment are shown in Table 3.5 and Table3.6. These results are found to satisfy the system constraints.

Unit	Pi min	Pi max	αi ($)	βi ($/MW)	γi ($/W2)
1	150	455	671	10.1	0.000299
2	150	455	574	10.2	0.000183
3	20	130	374	8.8	0.001126
4	20	130	374	8.8	0.001126
5	150	470	461	10.4	0.000205
6	135	460	630	10.1	0.000301
7	135	465	548	9.8	0.000364
8	60	300	227	11.2	0.000338
9	25	162	173	11.2	0.000807
10	25	160	175	10.7	0.001203
11	20	80	186	10.2	0.003586
12	20	80	230	9.9	0.005513
13	25	85	225	13.1	0.000371
14	15	55	309	12.1	0.001929
15	15	55	323	12.4	0.004447

Table 3.4: 15 Bus Generating unit data

Unit Power Output	PSO	GA	WOA
P1(MW)	343.9627	270.8264	415.30
P2(MW)	452.0160	268.2754	351.72
P3(MW)	112.8241	118.1084	101.43
P4(MW)	127.3678	119.0828	72.99
P5(MW)	260.6972	460.6699	370.28
P6(MW)	402.4683	269.2358	416.79
P7(MW)	436.8479	269.2358	336.32
P8(MW)	60.00	60.00	124.79
P9(MW)	30.5095	147.0860	133.14
P10(MW)	30.5095	147.0860	89.26
P11(MW)	68.2176	67.5806	61.06
P12(MW)	61.9314	68.0805	49
P13(MW)	67.8161	71.3302	39.77
P14(MW)	40.8083	41.0806	40.94
P15(MW)	34.1232	41.8306	23.64

Total Power output (MW)	2630	2630	2630
Total Generation cost ($/hr)	**32,604**	**32,604**	**31,111**

Table 3.5: Optimum Solution of 15 Unit Systems

Generation cost ($)		
Method	Max	Min
PSO	15298	15276
GA	15277	15276
GWOA	**14997**	**14963**

Table 3.6: Comparison between both methods (50 trials)

SIMULATION OUTPUT WAVEFORMS

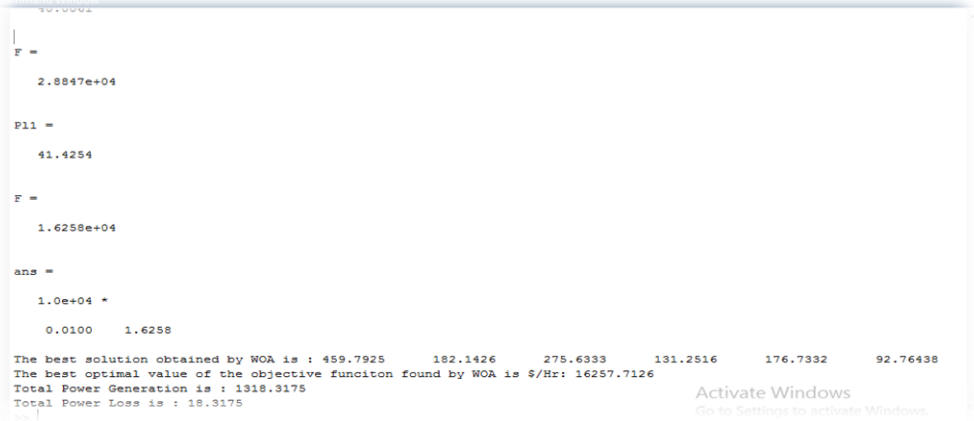

Figure 3.1 Optimal solution in command window

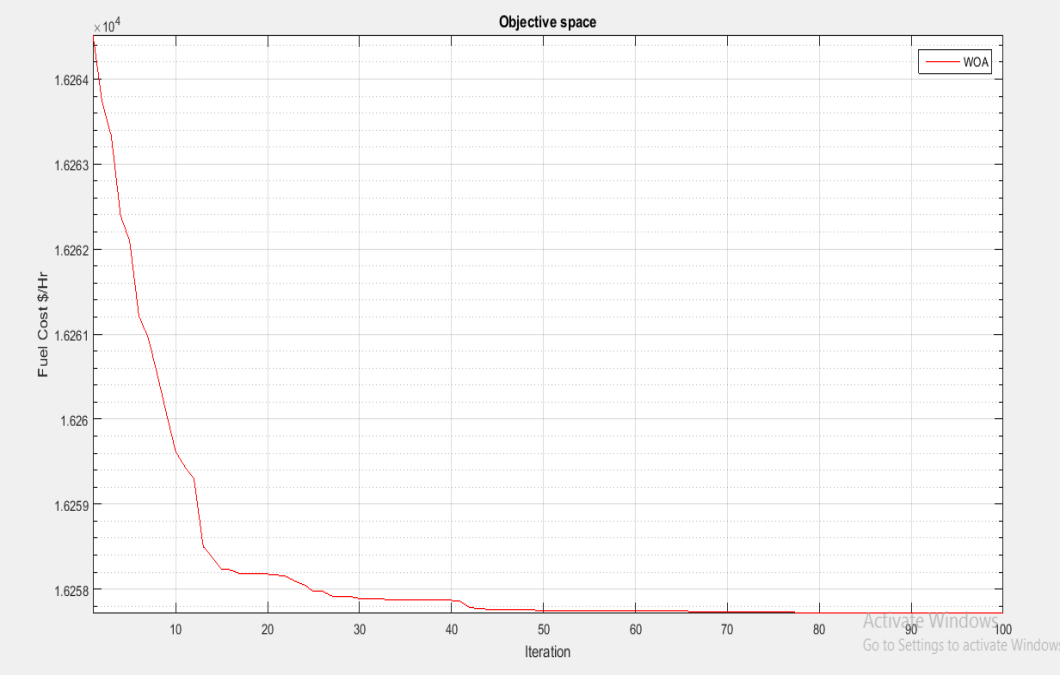

Figure 3.2 Convergence for 100 iteration

IV. CONCLUSION

According to PSO and GA approaches another nature propelled calculation is actualized for various economic load dispatch issues. The numerical comes about plainly demonstrate that the proposed calculation gives better results. The whale optimization algorithm beats the other as of late created calculations. The calculation is simple to actualize and can be coded in any computer language. Power framework administrators can likewise utilize this calculation for different enhancement issues. According to PSO and GA approaches another nature propelled calculation is actualized for various economic load dispatch issues. The numerical comes about plainly demonstrate that the proposed calculation gives better results. The grey wolf optimization algorithm beats the other as of late created calculations. The calculation is simple to actualize and can be coded in any computer language. Power framework administrators can likewise utilize this calculation for different enhancement issues.

REFERENCES

1. Simon D . Biogeography-based optimization. IEEE Trans Evol Comput 2008; 12:702–13 .
2. Rao RV, Savsani VJ, Vakharia DP. Teaching–learning-based optimization: an optimization method for continuous non-linear large scale problems. Inf Sci 2012; 183:1–15.
3. Hatamlou A. Black hole: a new heuristic optimization approach for data clus- tering. Inf Sci 2013;222:175–84 .
4. Kaveh A, Khayatazad M . A new meta-heuristic method: ray optimization. Comput Struct 2012; 112:283–94.
5. hadi hamedi, "Solving the combined economic load and emission dispatch problems using new heuristic algorithm", *Electrical Power And Energy Systems(elsvier),* Vol.46; No.1; 2013; PP:10-15
6. rui zhang et al," Economic environmental dispatch using an enhanced multi-objective cultural algorithm " *Electric Power Systems Research(elsvier),*Vol. 99; No.1; 2013; PP: 18-29
7. K. Y. Lee and M. A. El-Sharkawi (Editors), "Modern Heuristic Optimization Techniques with Applications to Power Systems", IEEE Power Engineering Society (02TP160), 2002.
8. R. C. Bansal, "Optimization methods for electric power systems: An overview", Int. J. Emerging Elect. Power Syst., vol. 2, no. 1, pp. 1-23, 2005.
9. Rao RV , Savsani VJ , Vakharia DP . Teaching–learning-based optimization: a novel method for constrained mechanical design optimization problems. Computer-Aided Des 2011;43:303–15 .
10. Feng Gao, "Economic Dispatch Algorithms for Thermal Unit System Involving Combined Cycle Units", 15th PSCC, Liege, 22-26 August 2005
11. J. H. Talaq, F. El-Hawary, and M. E. El-Hawary, "A summary of environmental/economic dispatch algorithms," IEEE Transactions on Power Systems, vol. 9, no. 3, pp. 1508–1516, 1994.
12. A. Farag, S. Al-Baiyat, and T. C. Cheng, "Economic load dispatch multiobjective optimization procedures using linear programming techniques," IEEE Transactions on Power Systems, vol. 10, no. 2, pp. 731–738, 1995
13. D. Srinivasan, C. S. Chang, and A. C. Liew, "Multiobjective generation scheduling using fuzzy optimal search technique," IEE Proceedings Generation, Transmission and Distribution, vol. 141, no. 3, pp. 233–242, 1994.

14. Baluja S (1994) Population-based incremental learning. A method for integrating genetic search based function optimization and competitive learning. Technical report, DTIC Document
15. Braik M, Sheta A, Arieqat A (2008) A comparison between GAs and PSO in training ANN to model the TE chemical process reactor. In: AISB 2008 convention communication, interaction and social intelligence, vol 1. Citeseer, p 24

PV Battery Charger Using an L3C Resonant Converter for Electric Applications

Mr. A. Sundara pandiyan[1]
Assistant Professor,
Department of Electrical and Electronics Engineering,
St. Anne's College of Engineering and Technology,
Anguchettypalayam, Panruti– 607106.

Mr. R. Manikandan[2]
UG Student,
Department of Electrical and Electronics Engineering
St. Anne's College of Engineering and Technology,
Anguchettypalayam, Panruti– 607106.

Abstract—In Electric Vehicles with rooftop PV panels, the solar irradiance and surface temperature can affect their performance and output voltages (e.g., Vpv = 24−45V DC). In these systems, the maximum energy must be extracted from the variable input voltage (PV panel), boosted by different gains, and stored in high voltage battery packs. Furthermore, depending on the battery state of charge, the charger should operate in constant voltage, constant current, or constant power modes, all the way from complete discharge condition, up to the charged floating voltage phase (Vbat = 230 − 430V DC). This combination of the variable PV input voltage and different states of charge creates a significant regulation challenge for the converter. In this paper, a high efficiency fourth order L3C resonant converter is proposed with an extreme voltage regulation capability that can effectively extract the maximum power from the PV panels and respond to the battery states of charge at different voltage and current levels. The experimental results from a 350W prototype prove the features of the proposed L3C resonant converter and demonstrate its ability to track the maximum input power while responding to the battery various states of charge.

Index Terms - **Photovoltaic panel, electric vehicle, wide DC-DC voltage regulation, full soft switching conditions**

I. INTRODUCTION

DC-DC power converters with variable voltage gain and boosting features are among the main components for PV energy systems, since the maximum power must be extracted from the low voltage, variable input source and boosted to a high voltage level [1, 2]. In PV energy systems for Electric Vehicles (EVs) with rooftop PV panel, it is also essential to employ a rechargeable battery pack to store energy and release it later [4–6]. Using battery packs for energy storage imposes challenging design constraints for the power converter, due to the different battery operating modes, including constant current, constant voltage, constant power, and no-load condition [8]. The combination of a PV panel and a rechargeable battery in an energy system requires extreme voltage gain variations from the input (Vpv = 24−45V DC) to the output (Vbat = 230 − 430V DC), and this needs to be supported by solar battery chargers. In this case, the charger should not only track the input voltage variation in order to extract the

maximum available power from the PV panel, but also boost the input voltage according to the level of variable gain and respond to the battery different states of charge. Recently, different studies have been dedicated to developing reliable and efficient non-isolated and isolated power converters for PV applications. Non-isolated power converter topologies which have been used in PV systems include boost converters, Cockcraft-Walton multipliers, coupled inductors, and switched inductors-capacitors with high voltage gain capability as the DC-DC power conversion stage for PV to grid applications (boosts a low, variable input voltage of 30 − 50V DC to a high, fixed output voltage of 400V DC) [9–13]. Although non-isolated power converters can successfully boost the PV voltage and reach high performance, they are not recommended for Electric Vehicle applications that require mandatory galvanic isolation between the PV panel and the high voltage battery pack. According to safety standards UL60950 and UL1741, isolated applications require at least 4kV galvanic isolation to be provided between the PV panel and the battery pack in order to prevent any high voltage shock path [14, 15].

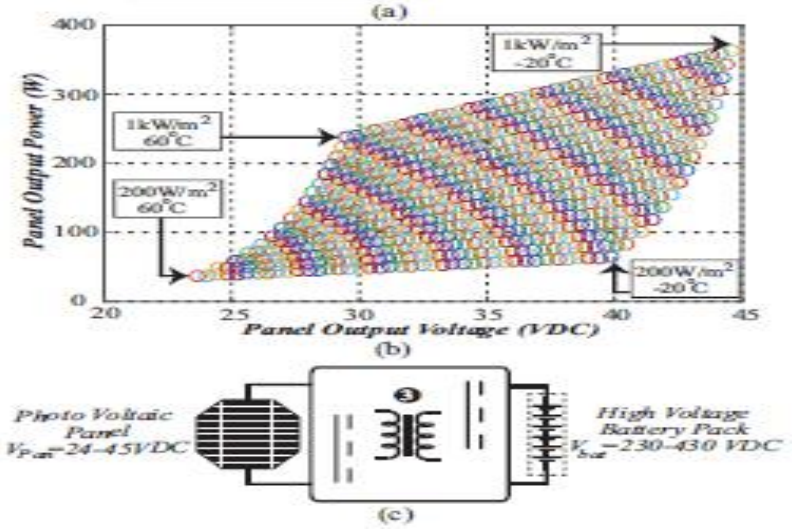

This paper proposes a high efficiency, isolated fourth order L3C resonant converter with extreme regulation capability for PV to high-voltage battery pack applications with the aim of tracking the maximum input power while responding to the battery states of charge at different output voltage and current levels. In comparison with well-known resonant power converter topologies (e.g. L3C2, LCLC, LCL2, LCC, and LCL), the proposed topology presents a steep voltage gain versus frequency, means lower frequency variation for input-output regulation, which makes it a good candidate for PV to high voltage battery pack applications. Also, the proposed resonant topology has a voltage gain of more than two for the resonant tank, which can be counted as a part of the boost action and reduces the transformer turns ratio and simplifies its structure.

II. PHOTOVOLTAIC MODULE CHARACTERISTICS AS A FUNCTION OF IRRADIANCE AND TEMPERATURE

As presented in Fig. 1(b), the PV panel maximum output power changes with respect to irradiance and temperature and the proposed L3C resonant converter should track these variations in order to transfer the maximum input power to the high-voltage battery pack [29]. In this section, the general equations for the solar PV panel will be extracted and employed to determine the variation of power-voltage characteristics of a specific PV module versus

irradiance and temperature variations. A PV module consists of a number of interconnected solar cells forming a single unit. To model Power-Voltage characteristics of PV module, the PowerVoltage characteristics of a single solar cell should be determined and then expanded to obtain the behavior of a PV array or module. In this figure, Irr is the irradiance current, which is generated when the cell is exposed to sunlight and is dependent on the solar irradiance and surface temperature.

$$Irr = Irr,ref\ (\ G\ Gref\ )[1 + \alpha T\ (T - Tref\ )] \quad (1)$$

The subscript ref represents the standard reference conditions and αT represents the rate of change of the short-circuit current with respect to temperature and is usually provided by the manufacturers. The cell temperature is a function of changes in the surface temperature and changes in the isolation [30].

$$T = Tamb + (NOCT - 20{\circ}C/\ 0.8\ )G \quad (2)$$

NOCT represents the Nominal Operating Cell Temperature provided by the manufacturer. In Fig. 2, ID is the current of the anti-parallel diode which characterizes the non-linearity of the solar cell and is a function of diodes voltage and temperature, as presented in (3).

$$ID = Io(e\ qVD\ nkT - 1) \quad (3)$$

In the recent equation, n is the ideality factor or the ideal constant of the diode and T is the temperature of the cell. The ideality factor (n) represents the different mechanisms of moving carriers across the junction. Io is the diode saturation current or cell reverse saturation current.

$$Io = Io,ref\ (\ T\ Tref\ )\ 3\ e\ (\ qEg,ref\ nkTref - qEg\ nkT\ ) \quad (4)$$

In the recent equation, Eg is the bandgap energy (eV) and depends on the materials used for manufacturing the cell. As an example, for silicon, this value can be calculated as follows [32]

$$Eg = 1.16 - 7.02 \times 10{-}4\ (\ T\ 2/\ T + 1108\ ) \quad (5)$$

Io,ref is the reference diode saturation current and can be approximately obtained using the PV cells open circuit voltage (Voc) and short circuit current (Isc) as presented in (6).

$$Io,ref = Isc\ e\ q(Vc+IcRs)\ nkT - 1 \quad (6)$$

Therefore, the relation between the voltage and current of the PV cell can be obtained as follows:

$$Icell = Irr - Io(e\ q(Vcell)\ nkNOCT - 1) \quad (7)$$

And finally, for a PV panel with Ns number of series cells and Np number of parallel cells, Eq. (7) can be rewritten as follows:

$$Icell = NpIrr{-}NpIo(e\ q(Vcell+IcellNs/Np)\ nkT\ {-}1){-}Vc + IcRsNs/Np\ RpNs/Np \quad (8)$$

The V-I relationship of a PV panel presented in (8) can be used to obtain the Power-Voltage relationship of a PV panel in different surface temperature and solar irradiance and to determine the maximum power point of the PV panel. For this specific example, the PV array consists of 72 PV cells connected in series and parallel.

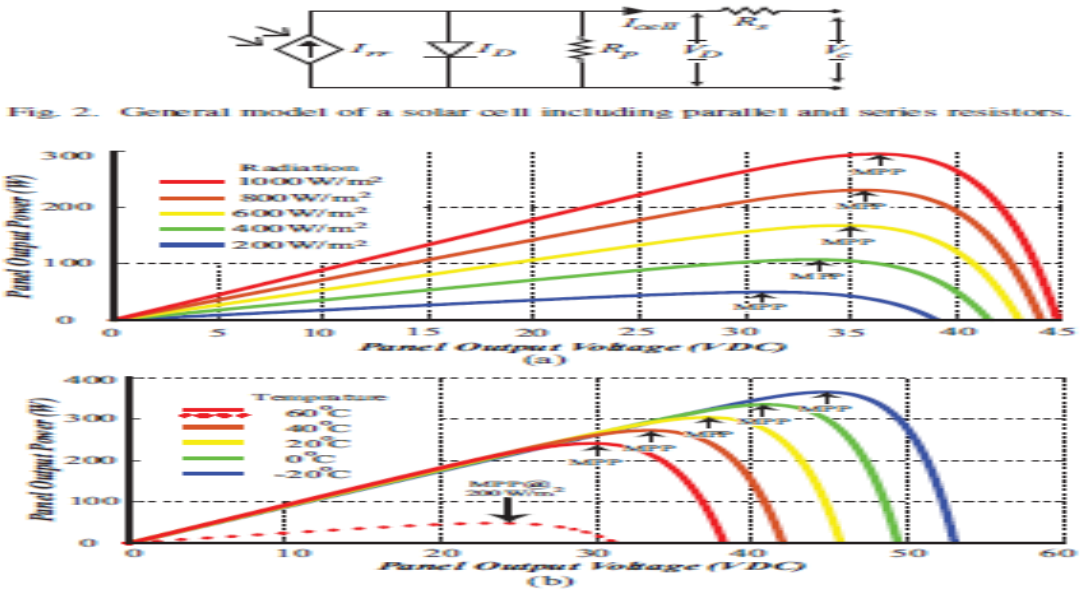

Fig. 2. General model of a solar cell including parallel and series resistors.

III. RESONANT POWER CONVERTERS REVIEW

Softly switched resonant converters are excellent candidates for DC-DC power supply design with wide regulation, due to their capability to produce variable voltage gains in different operating frequencies, while providing soft switching conditions for semiconductor devices [34]. In this section, well-known resonant power converters will be presented in order to review the application of each topology and distinguish the difference between the L3C resonant circuit and other fourth order ones. Also, this section will present and compare the voltage gain characteristics of each resonant power converter with the proposed L3C. Similar to the LCL2C resonant circuit, LCLC employs the parallel resonant capacitor in its circuit and can be used for high voltage DC-DC applications.

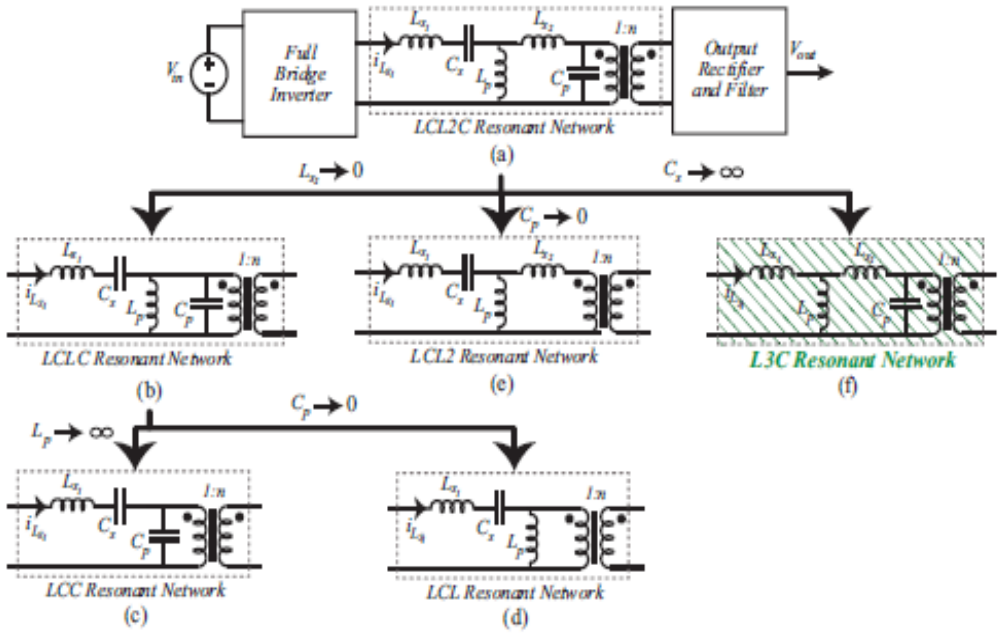

IV. STEADY STATE ANALYSIS OF L3C RESONANT CONVERTER

Fig. 7 shows a complete schematic of the proposed L3C resonant converter, including transformer secondary side and diode junction parasitic capacitances. In this figure, a fourth order model of the transformer has been employed as a model for the nonideal transformer In the proposed resonant converter, the parallel resonant capacitor in the secondary side of the transformer can merge all parasitics capacitors of the secondary side into the resonant circuit. According to Fig. 7, the proposed topology does not employ any series resonant capacitor in the primary side of the converter, which eliminates the dielectric power loss and facilitates the charger design in terms of component selection. In Fig. 7, all of the elements in the secondary side are defined with an apostrophe, but in all equations,
the variables and elements are transferred to the primary side with respect to the transformer turn-ratio, and are shown without an apostrophe. According to Fig. 7, the total amount of parallel capacitance in the secondary of the transformer can be obtained as follows

$$Ct = Cp + Cw,s + Cj \quad (9)$$

In order to model the interaction between the output side (the output rectifier, output filter, and load) and the parallel resonant capacitor, the output-side and parallel resonant elements are modeled using an equivalent impedance. The elements of the equivalent circuit are defined as follows

$$Req = \sin 2\psi\, \pi Ct\omega s\ ,\ Ceq = \pi Ct\ \psi - \sin\psi \cos\psi \quad (10)$$

The angle ψ is the interval during which the output rectifier diodes turn off and the resonant circuit is disconnected from the load (presented in Fig. 6) and is given by:

$$\psi = \cos{-1}\ (\ \pi - 2\omega sRLCt\ \pi + 2\omega sRLCt\ ) \quad (11)$$

Fig. 8 shows the AC equivalent circuit of the resonant circuit along with the equivalent impedance of the transformer secondary side. By using this equivalent circuit, it is possible to employ the FHA technique for analysis of the L3C resonant circuit. In order to calculate the output current, the second series resonant inductor current is considered purely sinusoidal. Due to the non-conduction angle of the output rectifier, the output current and output voltage can be obtained as follows

$$Io = 1\ 2\pi\ (\ \pi\ \psi\ iLs2\ d(\omega st) + 2\pi\ \pi + \psi\ iLs2\ d(\omega st)) = (1 + \cos\psi)\ \pi\ ILs2 \quad (12)$$

$$Vout = RL.Iout = RL\ (1 + \cos\psi)\ \pi\ ILs2 \quad (13)$$

According to Fig. 8, applying KVL and KCL gives the relation between output voltage and resonant circuit input current.

$$ILs2 = j\omega sLp\ j\omega sLp + j\omega sLs2 + Req + 1\ j\omega sCeq\ ILs1 \quad (14)$$

In order to calculate the resonant circuit input current, the input impedance of the AC equivalent circuit should be obtained, which can be expressed by:

$$Zin(j\omega s) = j\omega sLs1 + (j\omega sLp)||(j\omega sLs2 + Req + 1\ j\omega sCeq\ ) \quad (15)$$

One of the advantages of the proposed resonant converter is its ability to limit the output current. In this case, the L3C resonant converter can not only provide a constant current for charging the battery pack, but also protect the full-bridge inverter from over current and short circuit conditions. In over-current conditions, $Req \rightarrow 0$ and by considering (15), Zin would be as follows:

$$Zin(j\omega s) = j\omega sLs1 + j\omega sLp||j\omega sLs2 \quad (16)$$

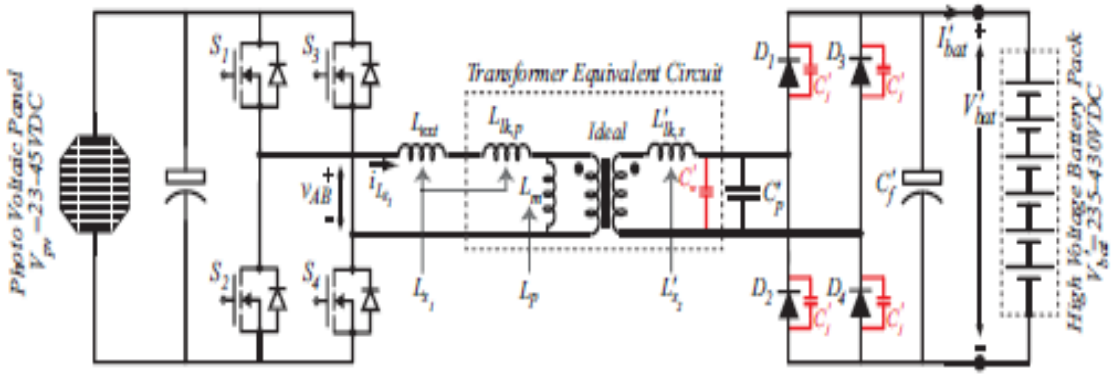

Fig. 7. Full bridge *L3C* resonant converter schematic with capacitive output filter, applicable for PV to high voltage battery applications.

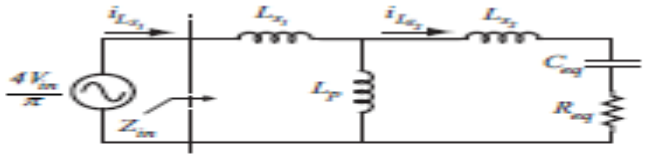

Fig. 8. AC equivalent circuit of the *L3C* resonant converter.

In this case, the inverter switches are loaded by an inductor that can limit the switches current and also load current. In fact, the resonant circuit provides an inherent short circuit protection at any operating frequency for the full-bridge inverter. In the AC equivalent circuit, the fundamental component of the resonant circuit input voltage (vAB1 (t)) can be obtained as follows:

$$v_{AB1} = 4V_{in} \pi \sin(\omega_s t) \quad (17)$$

According to Fig. 8 and Eqs. (15) and (17), the amplitude of ILs1 (MOSFETs current) can be obtained as follows:

$$I_{Ls1} = 4V_{in} \pi |Z_{in}(j\omega_s)| \quad (18)$$

The following normalized parameters are introduced for the resonant circuit.

$$L = L_p + L_{s2} , L_n = L_{s1} L_p , L_s = L_{s1} L_{s2} , Z_0 = L C_t , Q_L = R_L Z_0 , \omega_0 = 1 \sqrt{LC_t} , \omega_n = \omega_s \omega_0 \quad (19)$$

Considering Eq. (13), (14), (18) and (19) the normalized voltage gain of the L3C resonant converter is obtained as follows:

$$M_v = V_{out} V_{in} = Q L Z_0 (1 + \cos\psi) \pi V_{in} . j\omega_n L_s L_n + L_s \sin 2\psi \pi\omega_n + j(\omega_n L_s L_n + L_s + \omega_n L_n L_n + L_s - \psi - \sin\psi \cos\psi \pi\omega_n) 4 \pi |Z_{in,n}(j\omega_n)| \psi = \cos^{-1} (\pi - 2\omega_0 Q_L \pi + 2\omega_0 Q_L) \quad (20)$$

In the next section, Eq. (20) will be employed to study the voltage gain behavior of L3C resonant converter and circuit elements design.

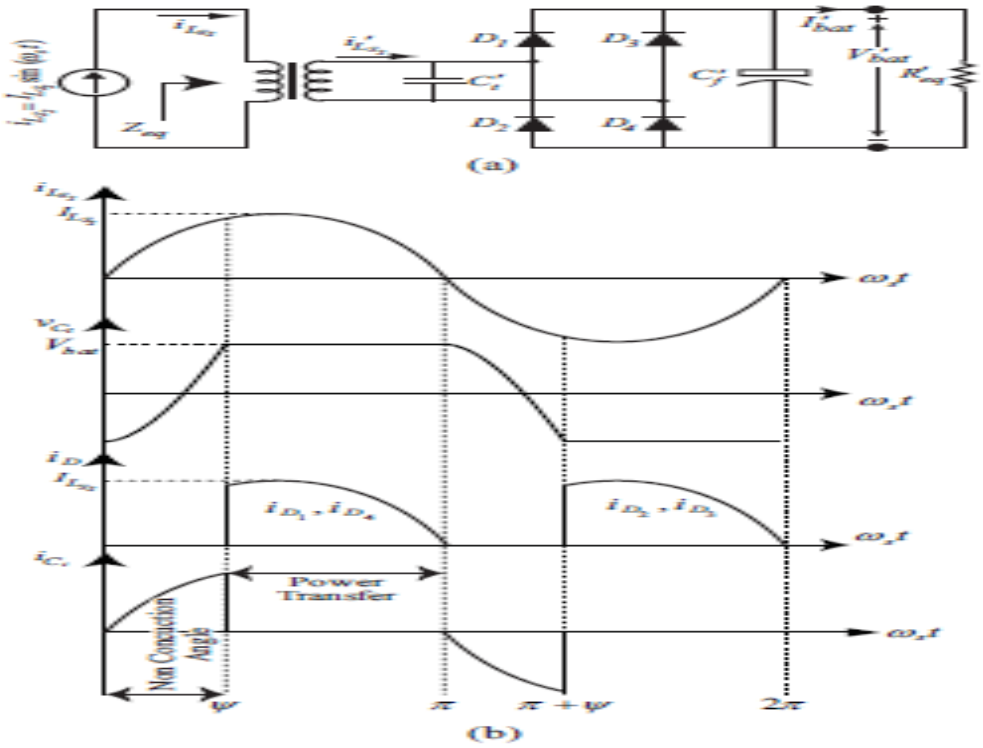

Fig. 6. a) Output rectifier with the parallel resonant capacitor, and b) main waveforms.

V. EXPERIMENTAL RESULTS AND THEORY VALIDATION

In order to investigate the performance of the proposed fourth order L3C resonant converter, a prototype platform has been employed to extract the maximum obtainable coverage of Fig. 1(b) under different output voltage and current conditions. The test setup picture is presented in Fig. 11. According to Table I, the switching frequency range is between 180 and 350kHz, and the frequency for maximum output power at maximum output voltage set to be 280kHz. Due to high current amplitude in the primary side, a high efficiency full-bridge inverter with low on-resistance MOSFET (2.5 mOhm) is used to convert the input DC voltage to a high-frequency AC voltage. The resonant tank consists of an external air-core inductor (Lext = 3.1μH placed in series with the transformer's primary side), an external parallel capacitor (placed in the secondary side of the transformer), and the parasitic components of the transformer (including primary and secondary leakage inductances and magnetizing inductance). In order to investigate the power converter performance, the power platform was tested under different input-output scenarios, and Fig. 12 shows the experimental results for the minimum and maximum output voltage under different input voltage and maximum available power conditions. Each figure contains of full-bridge inverter voltage, resonant circuit current, transformer secondary side voltage, and transformer secondary side current. The experimental results show the response of the L3C resonant converter to variation input-output voltage, which caused as a result of either changing in the PV panel, or battery state of charge. As mentioned in the introduction, the battery charger must be able to respond to different modes of the charge algorithms and track the input voltage variation in order to transfer the maximum available power. According to extracted experimental results, the proposed fourth order L3C resonant converter can regulate the output designed for this study present a maximum efficiency equal to 97.5%. Fig. 14(a) shows the

converter efficiency is above 92% from full load to 50% of the load, but due to the rculating current in light load condition, the converter efficiency decreases at light loading conditions.

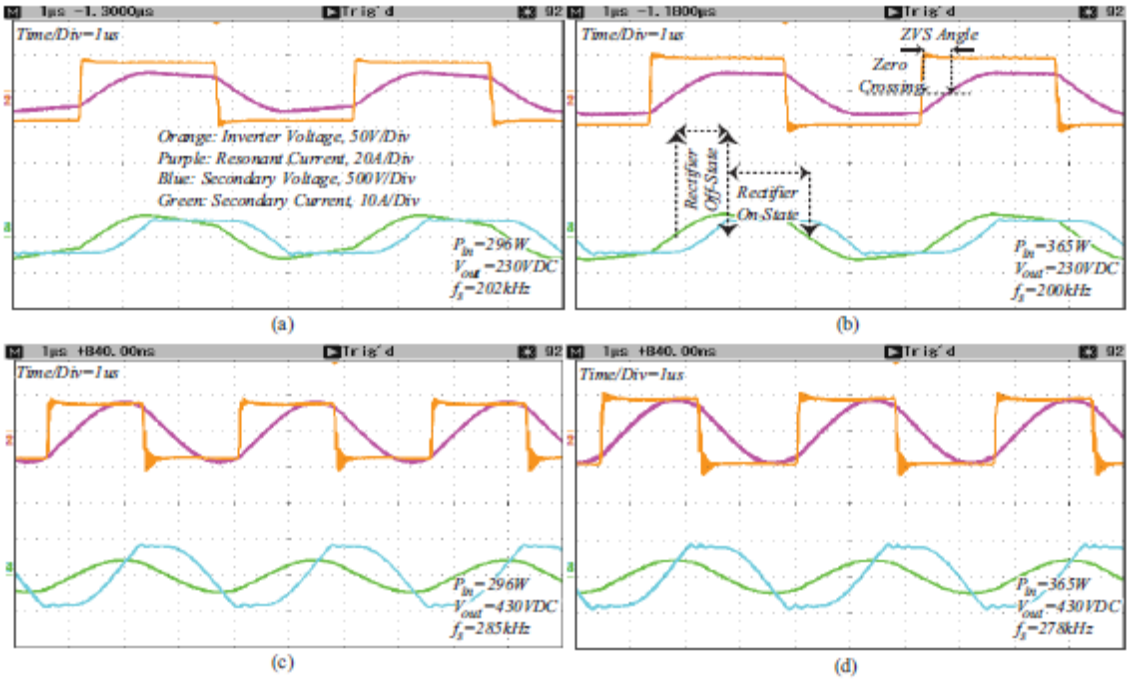

Fig. 12. Experimental results of fourth order $L3C$ resonant converter platform under different PV panel conditions and minimum-maximum output voltage, a) $1000W/m^2$ at $25°C$, b) $1000W/m^2$ at $-20°C$, c) $1000W/m^2$ at $25°C$, and d) $1000W/m^2$ at $-20°C$.

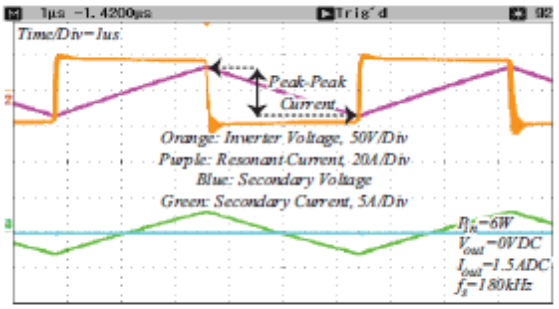

Fig. 13. $L3C$ resonant converter short circuit test at minimum switching frequency ($f_s = 180kHz$) and maximum input voltage ($V_{in} = 44V\ DC$).

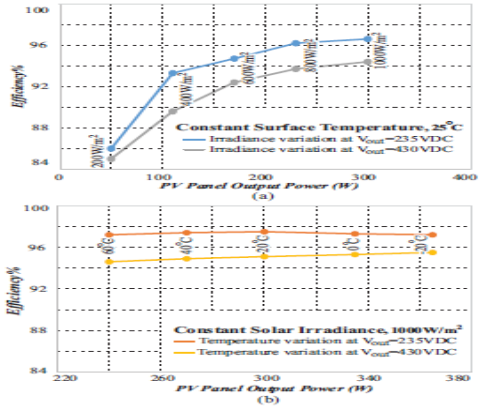

VI. CONCLUSION

This paper introduced the L3C resonant power converter with extreme regulation capability, which can be employed for solar battery charger applications. The main advantages of the proposed resonant converter are its ability to respond to different battery states of charge, while tracking the input voltage variations of the PV panel, which occur as a result of changes to the maximum power point. The proposed converter has the voltage gain of more than two, which contributes to the required voltage gain for boosting the input voltage to a high voltage one. Also, the L3C topology can provide an inherent over-current protection, which can control the battery current during constant current mode and simplifies the control and protection circuit design. In addition, soft switching of semiconductor devices provides high efficiency, and the capability of working in high switching frequency. The complete analysis of the resonant

converter along with mathematical equations were presented. The experimental results verify the theoretical analysis and the performance of the proposed converter in terms of tracking the input voltage for maximum power extraction and operating under different output voltage and current conditions.

REFERENCES

1. S. Arshadi, B. Poorali, E. Adib, and H. Farzanehfard, "High step-up DC-AC inverter suitable for AC module applications," IEEE Transaction on Industrial Electronics, vol. 63, no.11,pp.832-839, May. 2017.
2. R. Ahrabi, H. Ardi, M. Elmi, A. Ajami, "A novel step-up multiinput DC-DC converter for hybrid electric vehicles application," IEEE Transaction on Power Electronics, vol. 32, no. 5, pp. 3549-3561, Nov. 2016.
3. U. R. Prasanna, A. K. Singh, and K. Rajashekara, "Novel bidirectional single-phase single-stage isolated AC-DC converter with PFC for charging of electric vehicles," IEEE Transaction on Transportation Electrification, Early Access 2017.
4. P. He, and A. Khaligh, "Comprehensive analyses and comparison of 1kW isolated DCDC converters for bidirectional EV charging systems," IEEE Transaction on Transportation Electrification, vol. 3, no. 1, pp. 147-156, Mar. 2017.
5. VIA Motors Inc., SlTRUX Solar Cover for the 2014 VIA VTRUX, www.viamotors.com/vehicles/soltrux
6. University of Michigan's solar racing team, "Sun kings cross the outback [solar powered vehicles marathon]," IEEE Spectrum, vol. 39, no. 2, pp. 40-46, Feb. 2002.
7. M. I. Shahzad, S. Iqbal, and S. Taib, "A wide output range HB-2LLC resonant converter with hybrid rectifier for PEV battery charging,"IEEE Transaction on Transportation Electrification, vol. 3, no. 2, pp. 520-531, Jun. 2017.
8. F. Musavi, M. Craciun, D. Gautam, W. Eberle, and W. Dunford, "An LLC resonant DC-DC converter for wide output voltage range battery charging applications," IEEE Transaction on Power Electronics, vol. 28, no. 12, pp. 5437-5445, Dec. 2013.
9. M. Das, and V. Agarwal, "Design and analysis of a high-efficiency DC-DC converter with soft switching capability for renewable energy applications requiring high voltage gain," IEEE Transaction on Industrial Electronics, vol. 63, no. 5, pp. 2936-2944, May. 2016.
10. L. Muller, and J. Kimball, "High gain DC-DC converter based on the Cockcroft-Walton multiplier," IEEE Transaction on Power Electronics, vol. 31, no. 9, pp. 6405-6415, Sep. 2016.
11. W. Li, and X. He, "Review of non-isolated high-step-up DC/DC converters in photovoltaic grid-connected applications," IEEE Transaction on Industrial Electronics, vol. 58, no. 4, pp. 1239-1250, Apr. 2011.
12. G. Wu, X. Ruan, and Z. Ye, "Non-isolated high step-up DC-DC converters adopting switched-capacitor cell," IEEE Transaction on Industrial Electronics, vol. 62, no. 1, pp. 383-393, Jan. 2015.
13. Y. Tang, D. Fu, T. Wang, and Z. Xu "Hybrid switched-inductor converters for high step-up conversion," IEEE Transaction on Industrial Electronics, vol. 62, no. 3, pp. 1480-1490, Mar. 2015.
14. Underwrites Laboratories Inc., UL60950: Safety of information technology equipment, Third edition, 2000.

IoT Based Induction Motor Controlling and Monitoring by Using Raspberry-Pi

Mr. J. Ramesh[1]
Assistant Professor,
Department of Electrical and Electronics Engineering,
St. Anne's College of Engineering and Technology,
Anguchettypalayam, Panruti – 607106.

Mr. A. Prakashraj[2], Mr. M. Sindhan[3], Mr. P. Jayavel[4], Mr. P. Sivapushnam[5]
UG Student,
Department of Electrical and Electronics Engineering
St. Anne's College of Engineering and Technology,
Anguchettypalayam, Panruti – 607106.

Abstract - Now days the induction motor has remained the most popular type of motor for industrial applications. The primary advantage of the induction motor is its straightforward rotor construction leading to low cost, ruggedness, and low maintenance requirements. This paper presents a remote control and monitoring system for an induction motor based on Internet of Things (IoT) for safe and economic data communication in industrial fields. A module of transducers and sensors monitors the parameters like Temperature, external moisture RPM, vibrations, load current and voltage of induction machine and send to the processing unit (Raspberry Pi), which will analyze and display the parameters, here the processing unit also communicates with Gateway module to send information to cloud database for remote monitoring. The system also presents the Automatic and manual control methods to stop or start the induction machine to avoid system failures. To make the system fast and user friendly it provides an android application.

***Index Terms* — Induction Motor, Internet of Things, Raspberry Pi, Temperature, Vibrations, moisture, load current.**

I. INTRODUCTION

Before the invention of AC induction motors dc motors were widely used for industrial requirements. Withthe invention of AC induction motors due to their higher performance attributes over DC motor, industrialautomation is being frequently done with it. An induction motor comprises a magnetic circuit interlinking twoelectric circuits which are placed on the two main parts of the machine: (i) the stationary part called the statorand (ii) the rotating part called the rotor. Power is transferred from one part to the other by electromagneticinduction. The primary advantages of the induction motor are its straightforward rotor construction leading tolow cost, ruggedness, and low-maintenance requirements, but it is much more difficult to control.

(a) Electrical-related faults: Faults occurred due to the unbalance supply voltage or current, single phasing,under or over voltage of current, overload and etc., are come under this category.

(b) Mechanical-related faults: Faults due to broken rotor bar, mass unbalance, air gap eccentricity, bearingdamage, rotor winding failure, and stator winding failure are come under this category.

(c) Environmental-related faults: Faults under this classification are occurred due to ambient temperature aswell as external moisture and Vibrations of machine.

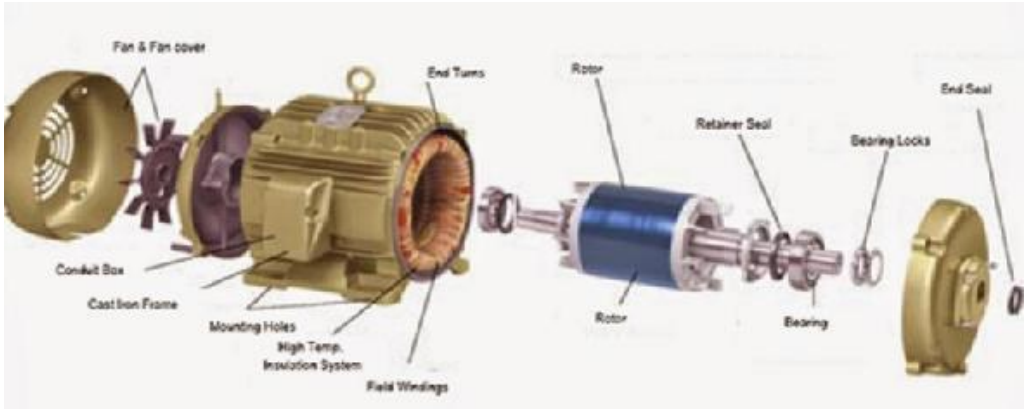

The performance of the AC Induction motor depends on above mentioned electrical, mechanical and environmental parameters of the motor, so that the controlling methods for high performance AC motor arevery sensitive to motor parameters. Parameters of an induction motor can be measured by testing's like thelocked rotor test and no load test. All electrical, mechanical and environmental parameters like current,voltage, speed, vibrations, temperature, and external moisture of the induction motors are very important for adrive system. The performance of an induction motor is directly affected by the above mentioned parameters.If any parameter of induction motor crosses its cut off levels then quality of product also changes, hencecontrolling the machines during the process of production becomes a dangerous operation in some specificindustrial applications.

Recent advances in processing technology the availability of fast-processing, stable and sensitive products provided particular benefits in industrial automation. As a result of the recent developments in Communication technologies, systems are no longer monitored and controlled by manually using classic methods, but automatically by computer controlled or remote-controlled devices. The future generation industries will be Technological developments have enabled to be taken classic systems place by Automaticand advanced systems definitely more advanced and automatic as compared with existing ones. This brings ona new terminology of "Smart Industries" in this new era of Monitoring as well as controlling of variousIndustrial applications. As an emerging technology in modern wireless telecommunication, Internet of Things(IoT) has got a lot of attention and is expected to bring benefits to many applications. The concept of "Internetof Things" (IOT) is providing a best way for Industrial automation through remote access. In IOT each deviceor devices constituting a system will be able to communicate with the other devices. Hence this leads toexchange of relevant data, statistics, logs and various other parameters information among various devices toimprove their performance, which will help industries to have better productivity, management and increasedthroughput. Here in the proposed work the IoT is used for monitoring and controlling the AC induction motor**.**

II. PROPOSED SYSTEM

The proposed system consists of Wi-Fi enabled microcontroller, Temperature sensor, vibration sensor, moisture sensor, Infra-red sensor, current and voltage measurement circuits and AC induction motor. Here we monitor and control the motor through webpage or Android application using IoT. The block diagram of proposed system is as shown in the figure-3.

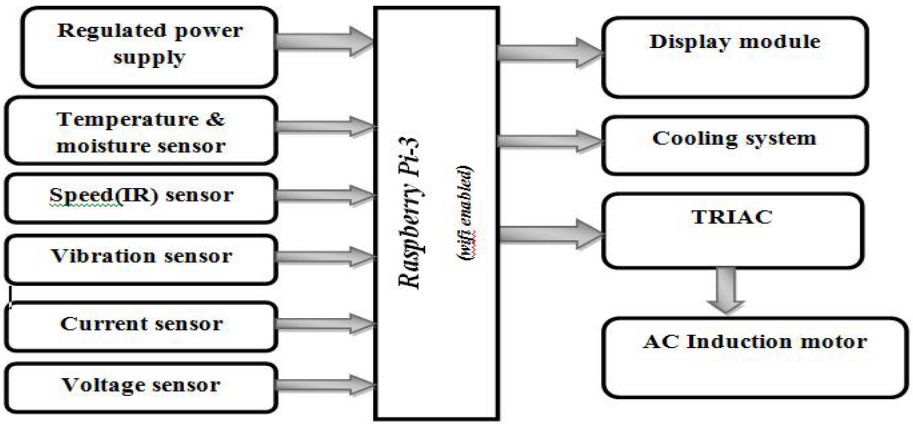

III. HARDWARE AND SOFTWARE CONFIGURATION

A. Hardware Components

For induction motor parameter monitoring we are using light weighted and easily configurable sensors like piezoelectric sensor (accelerometer) for vibration, DH11 sensor for temperature and humidity, infrared sensor for speed, ACS712 for current measurement and voltage divider for voltage measurement. Microcontroller usage is best for acquiring data. Raspberry Pi-3 board has been used for this research which has the ability to acquire sensor data, communicate with other devices, store information in local, cloud server and alert the user when fault is detected. Fig. 3 shows block diagram of the hardware connections.

Flow chart

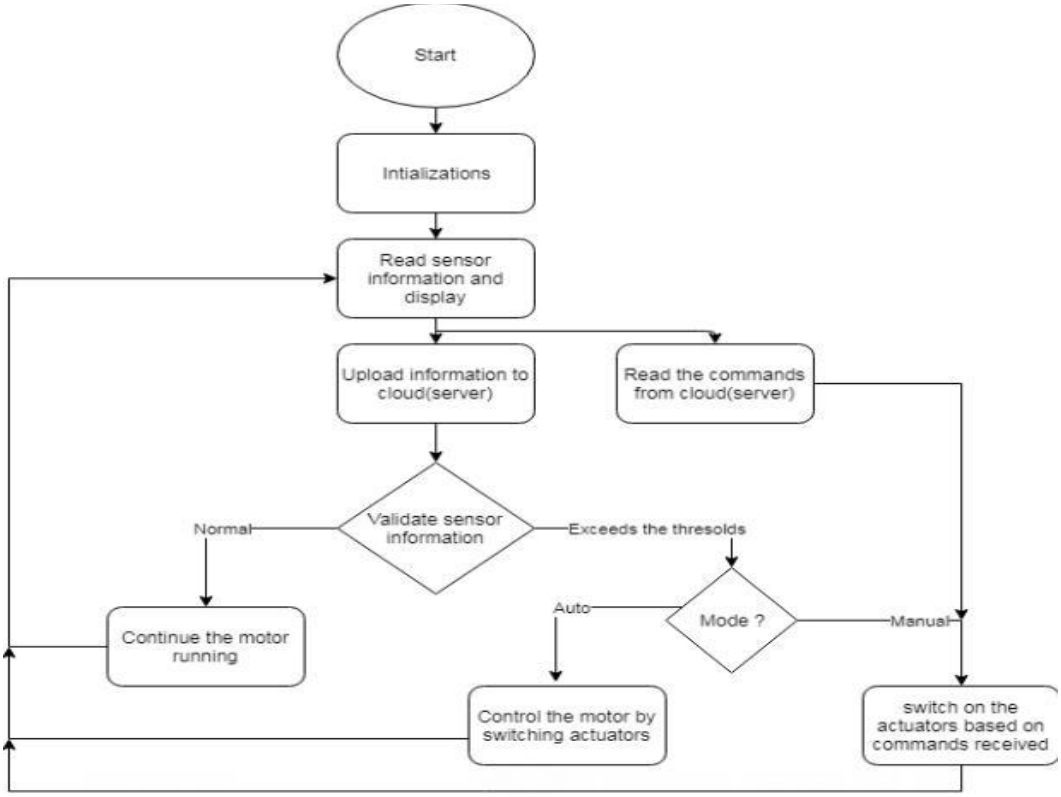

B. Cloud Storage

Data that is obtained from the sensors are transferred wirelessly to the local and cloud server for analysis. Once the data is received, a system has been devised that analyzes the raw

data. On the other hand it will also save the raw data to the SD memory. The program has been set to process real-time data and store it to the cloud with Thing speak cloud computing platform. This saved data is accessible from anywhere via internet.

IV. RESULT ANALYSIS

In this work a single phase industrial AC motor was used for experimental purpose. The motor rating is shown in Table 1 (Class A). Sensors (accelerometer, temperature, moisture, vibration, current and voltage are attached to the motor at right positions. Sensor data was collected and processed using Raspberry Pi-3 and compared with the threshold values to trigger alarm to avoid failure. The experimental setup of the proposed system is as shown in the figure4.

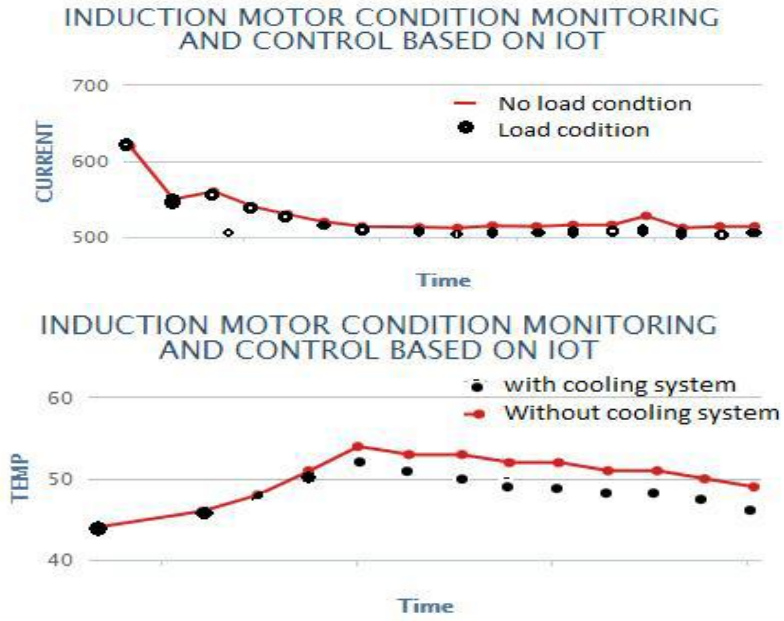

V. CONCLUSION

This paper presents the concept of Internet of Things for early detection and monitoring of motor system failures remotely. The system has been designed to combine various parameter measurements in real-time, improving the delectability of different faults. The monitoring of the motor system presents the measurement of different parameters namely vibrations, temperature, speed, moisture, voltage and current consumption. Thus, compared to conventional methods that relies solely on vibrations or temperature, this design has more information sources which can enable an alarm. The concept of IoT is presented here for remote monitoring and controlling the motor. The data received by the coordinator node is stored and graphically presented in real-time by means of a application developed in visual basics. The proposed system can be easily upgraded to add other sensors on the sensing node for the measurement of other parameters if required. The system has a high autonomy, easy installation and low maintenance costs.

REFERENCES

1. Frederic champavier, condition monitoring of induction motors using vibration and electrical signature analysis, EE mods conference, nantes, france, 14-17 september 2009.
2. L. Li et al., “The applications of WIFI-based wireless sensor network I ninternet of things and smart grid,” in Proc. 6th IEEE Conf. Ind. Electron.Appl. (ICIEA), 2011, pp. 789–793.

Dragon Fly Algorithm Based Forecasting of Substation Demands

Ms.J.Arul Martinal[1],
Assistant Professor,
Department of Electrical and Electronics Engineering,
St. Anne's College of Engineering and Technology,
Anguchettypalayam, Panruti – 607106.

Ms. D. Dhatchayani[2], Ms. R. Keerthana[3], Ms. Y. Monica[4], Ms. P. Banupriya[5]
UG Scholar
Department of Electrical and Electronics Engineering,
St. Anne's College of Engineering and Technology,
Anguchettypalayam, Panruti – 607106.

Abstract - Load forecasting is an important component for power system energy management system. Precise load forecasting helps the electric utility to make unit commitment decisions, reduce spinning reserve capacity and schedule device maintenance plan properly. Besides playing a key role in reducing the generation cost, it is also essential to the reliability of power systems. Load forecasting plays an important role in power system planning, operation and control. Planning and operational applications of load forecasting requires a certain 'lead time' also called forecasting intervals. The proposed dragonfly algorithm is implemented on real time data from 2016 to 2018. Electricity demand predictions have been made for next 5 years as one set and consecutive 5years as another set . The proposed dragonfly algorithm is found to be highly accurate with a Mean Absolute Percentage Error (MAPE) of 6.54 within a confidence interval of 2.25%. Moreover, the proposed dragonfly algorithm has a computation time of approximately 05 minutes which is favorable for offline training to forecast electricity load for a period of five years.

***Index Terms*—DA Algorithms.**

I. INTRODUCTION

Electric load forecasting is the process used to forecast future electric load, given historical load and weather information and current and forecasted weather information. In the past few decades, several models have been developed to forecast electric load more accurately. Load forecasting can be divided into three major categories:

A. Long-term electric load forecasting (LTLF): used to supply electric utility company management with prediction of future needs for expansion, equipment purchases, or staff hiring. LTLF the prediction time can be as long as 10 years and above. A precise long term load-forecasting is essential for monitoring and controlling power system operation.

B. Medium-term load forecasting (MTLF): used for the purpose of scheduling fuel supplies and unit maintenance .MTLF the prediction time is 2-5years.

C. Short-term load forecasting (LTLF): used to supply necessary information for the system management of day-to-day operations and unit commitment. LTLF the prediction time is every next hour, day by day, week by week and monthly.

With the recent trend of deregulation of electricity markets, LTLF has gained more importance and greater challenges. In the market environment, precise forecasting is the basis of electrical energy trade and spot price establishment for the system to gain the minimum electricity purchasing cost. In the real-time dispatch operation, forecasting error causes more purchasing electricity cost or breaking-contract penalty cost to keep the electricity supply and consumption balance. There are also some modifications of LTLF models due to the implementation of the electricity market.

II. LOAD FORECASTING OVERVIEW

2.1 Characteristics of the Power System Load:

The system load is the sum of all the consumers' load at the same time. The objective of system LTLF is to forecast the future system load. Good understanding of the system characteristics helps to design reasonable forecasting models and select appropriate models in different situations. Various factors influence the system load behavior, which can be mainly classified into the following categories

- Weather
- Time
- Economy
- Random disturbance

2.2 Classification of Developed Load Forecasting Methods:

In terms of lead time, load forecasting is divided into four categories:

- Long-term forecasting with the lead time of more than one year
- Mid-term forecasting with the lead time of one week to one year
- Short-term load forecasting with the lead time of 1 to 168 hours
- Very short-term load forecasting with the lead time shorter than one day

The research approaches of load forecasting can be mainly divided into two categories: statistical methods and artificial intelligence methods [1]. In statistical methods, equations can be obtained showing the relationship between load and its relative factors after training the historical data, while artificial intelligence methods try to imitate human beings' way of thinking and reasoning to get knowledge from the past experience and forecast the future load.

2.3 Requirements of the Load Forecasting Process

In nearly all the energy management systems of the modern control centers, there is a short-term load forecasting module. A good Load Forecasting system should fulfill the requirement of accuracy, fast speed, automatic bad data detection, friendly interface, automatic data access and automatic forecasting result generation.

- Accuracy
- Fast Speed
- Automatic Bad Data Detection
- Friendly Interface
- Automatic Data Access
- Automatic Forecasting Result Generation

III. DRAGONFLY ALGORITHM

Operators for exploration and exploitation

According to Reynolds, the behavior of swarms follows three primitive principles:

- Separation, which refers to the static collision avoidance of the individuals from other individuals in the neighbourhood
- Alignment, which indicates velocity matching of individuals to that of other individuals in neighbourhood.
- Cohesion, which refers to the tendency of individuals towards the centre of the mass of the neighbourhood.

The main objective of any swarm is survival, so all of the individuals should be attracted towards food sources and distracted outward enemies. Considering these two behaviours, there are five main factors in position updating of individuals in swarms .

Each of these behaviors is mathematically modeled as follows:

The separation is calculated as follows :

$$S_i = -\sum_{j=1}^{N} X - Xj \quad (3.1)$$

where X is the position of the current individual, X_j shows the position j-th neighbouring individual, and N is the number of neighbouring individuals.

Alignment is calculated as follows:

$$A_i = \sum_{j=1}^{N} Vj/N \quad (3.2)$$

where V_j shows the velocity of j-th neighbouring individual.

The cohesion is calculated as follows:

$$C_i = (\sum_{j=I}^{N} Xj/N) - X \quad (3.3)$$

where X is the position of the current individual, N is the number of neighbourhoods, and X_j shows the position j-th neighbouring individual.

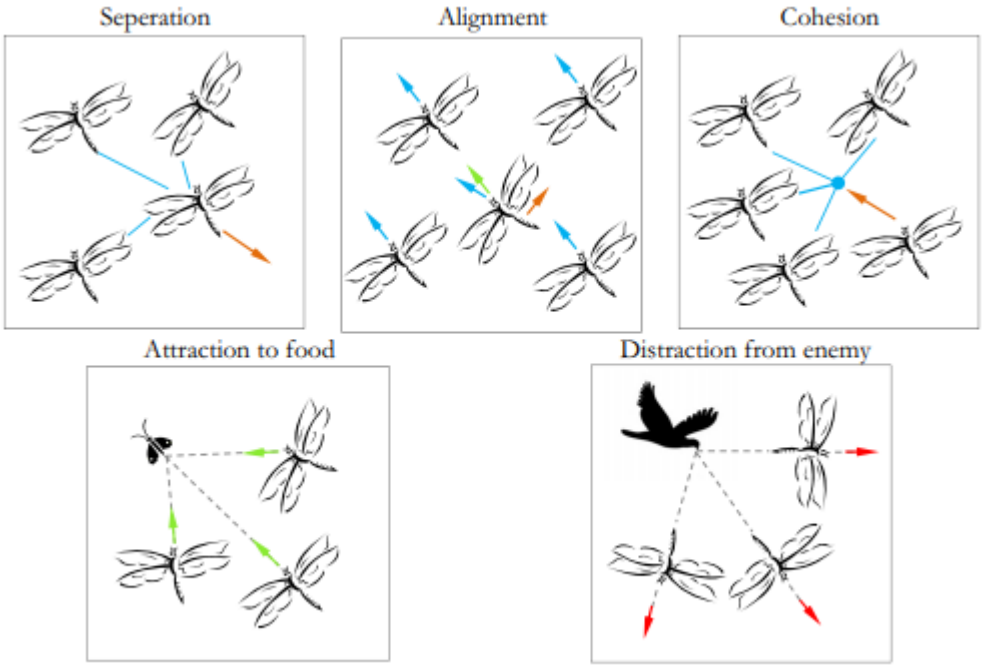

Fig. 3.1 Dragonfly algorithm structure

Attraction towards a food source is calculated as follows:

$$F_i = X^+ - X \quad (3.4)$$

where X is the position of the current individual, and X^+ shows the position of the food source.

Distraction outwards an enemy is calculated as follows:

$$E_i = X^- + X \quad (3.5)$$

where X is the position of the current individual, and X^- shows the position of the enemy.

The behavior of dragonflies is assumed to be the combination of these five corrective patterns in this paper. To update the position of artificial dragonflies in a search space and simulate their movements, two vectors are considered: step (ΔX) and position (X). The step vector is analogous to the velocity vector in PSO, and the DA algorithm is developed based on the framework of the PSO algorithm. The step vector shows the direction of the movement of the dragonflies and defined as follows (note that the position updating model of artificial dragonflies is defined in one dimension, but the introduced method can be extended to higher dimensions):

$$\Delta X_{t+1} = (sS_i + aA_i + cC_i + eE_i) + w\Delta X_t \quad (3.6)$$

where s shows the separation weight, S_i indicates the separation of the i-th individual, a is the alignment weight, A_i is the alignment of i-th individual, c indicates the cohesion weight, C_i is the cohesion of the i-th individual, f is the food factor, F_i is the food source of the i-th individual, e is the enemy factor, E_i is the position of enemy of the i-th individual, w is the inertia weight, and t is the iteration counter.

After calculating the step vector, the position vectors are calculated as follows:

$$X_{t+1} = X_t + \Delta X_{t+1} \quad (3.7)$$

where t is the current iteration.

With separation, alignment, cohesion, food, and enemy factors (s, a, c, f, and e), different explorative and exploitative behaviours can achieved during optimization. Neighbours of dragonflies are very important, so a neighbourhood (circle in a 2D, sphere in a 3D space, or hypersphere in an nD space) with a certain radius is assumed around each artificial dragonfly. An example of swarming behaviour of dragonflies with increasing neighbourhood radius using the proposed mathematical model is illustrated in fig. 3.1.

As discussed in the previous subsection, dragonflies only show two types of swarms: static and dynamic as shown in Fig. 3.2. As may be seen in this figure, dragonflies tend to align their flying while maintaining proper separation and cohesion in a dynamic swarm. In a static swarm, however, alignments are very low while cohesion is high to attack preys. Therefore, we assign dragonflies with high alignment and low cohesion weights when exploring the search space and low alignment and high cohesion when exploiting the search space. For transition between exploration and exploitation, the radii of neighbourhoods are increased proportional to the number of iterations. Another way to balance exploration and exploitation is to adaptively tune the swarming factors (s, a, c, f, e, and w) during optimization.

A question may rise here as to how the convergence of dragonflies is guaranteed during optimization. The dragonflies are required to change their weights adaptively for transiting from exploration to exploitation of the search space. It is also assumed that dragonflies tend to see more dragonflies to adjust flying path as optimization process progresses. In other word, the neighbourhood area is increased as well whereby the swarm become one group at the final stage of optimization to converge to the global optimum. The food source and enemy are chosen from the best and worst solutions that the whole swarm is found so far. This causes convergence towards promising areas of the search space and divergence outward non-promising regions of the search space.

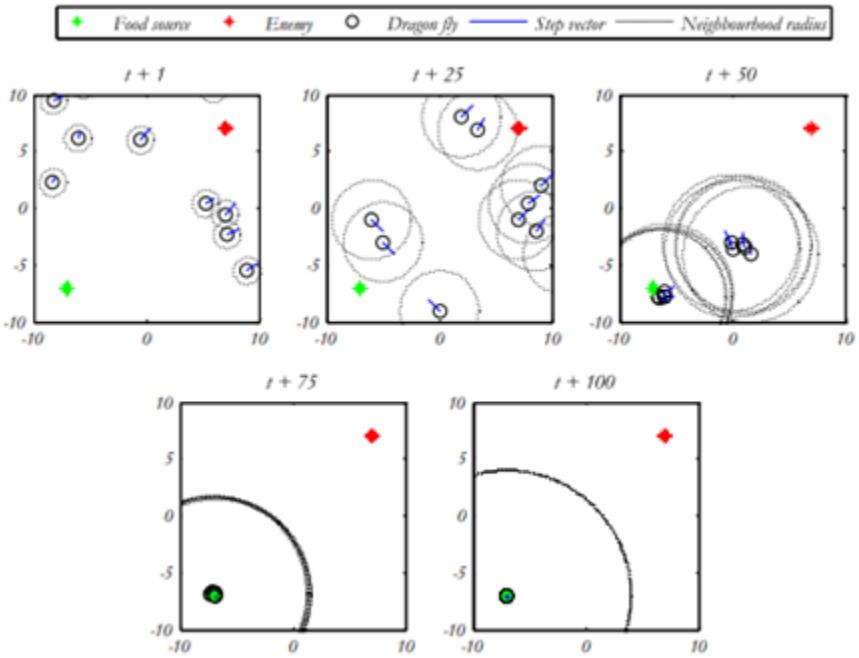

Fig. 3.2 Swarming behavior of artificial dragon flies (w = 0.9-0.2, s = 0.1, a = 0.1, c = 0.7, f = 1, e = 1)

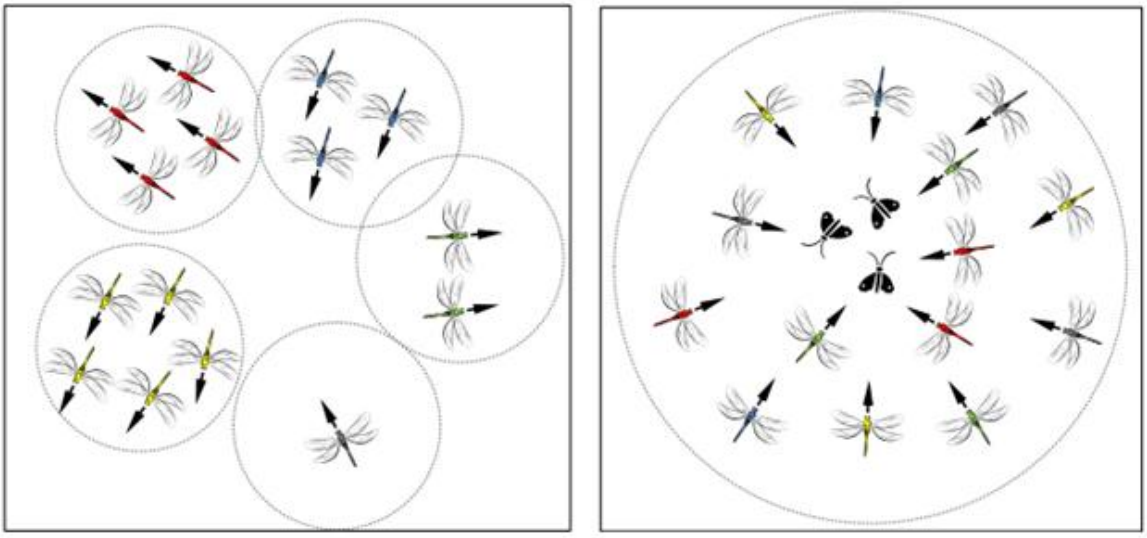

Fig. 3.3 Dynamic versus static dragonfly swarms

To improve the randomness, stochastic behaviour, and exploration of the artificial dragonflies, they are required to fly around the search space using a random walk (Le´vy flight) when there is no neighbouring solutions. In this case, the position of dragonflies is updated using the following equation:

$$X_{t+1}=X_t+Le´vy\ (d)*X_t \quad (3.8)$$

where t is the current iteration, and d is the dimension of the position vectors.

The Le´vy flight is calculated as follows :

$$\text{Le´vy}(x)=0.01r_1*\sigma/|r_2|^{1/\beta} \quad (3.9)$$

where r_1, r_2 are two random numbers in [0,1], b is a constant (equal to 1.5 in this work), and r is calculated as follows:

$$\sigma=((\Upsilon(1+\beta)*\sin(\pi\,\beta/2))/(\Upsilon(1+\beta/2)*\beta*2(\beta-1/2)))^{1/\beta} \quad (3.10)$$

where $\Upsilon(x) = (x-1)!$.

IV. ERROR METRICS

The performance of the models is also compared quantitatively using the performance metric MAPE.

MAPE is defined by the formula:

$$\text{MAPE} = (100/n)*\sum_{t=1}^{n}|(At-Ft)/At| \quad (4.1)$$

where At is the actual value and Ft is the forecast value, n is the number of observations in test set. In order to provide a more precise metric of performance, 95% confidence interval of MAPE is calculated which contains true values of MAPE with varying degrees of confidence. The 95% confidence interval of a vector X containing the hourly point absolute percentage error values is calculated by following the given steps:

Step 1: The standard error (SE) is computed using the formula:

$$SE = (X)/\sqrt{n} \quad (4.2)$$

where std(X) is the standard deviation of vector X and n is the number of elements in the vector X.

Step 2: Calculate the T-score which depends on the confidence interval needed. For 95% confidence interval, T-score is calculated as follow:

$$T = t*SE \quad (4.3)$$

where t=1.98 for 95% confidence interval and sample size 100.

Step 3: Finally calculate the 95% confidence interval (CI) using the formula:

$$CI = (X) + T \quad (4.4)$$

where mean(X) is the mean of vector X.

V. RESULT ANALYSIS

A Matlab program was written to execute the load forecasting for the 110/22 KV substation using Dragon fly Algorithm. Using the actual data for the years 2016 - 2018 the load demand for the years 2019 -2023 is forecasted.

YEAR	ACTUAL	FORECASTED
2016	39.40	37.89
2017	32.42	30.91
2018	28.47	26.96

Table.5.1 Comparison of forecasted load with actual load for the month of April from (2016 - 2018)

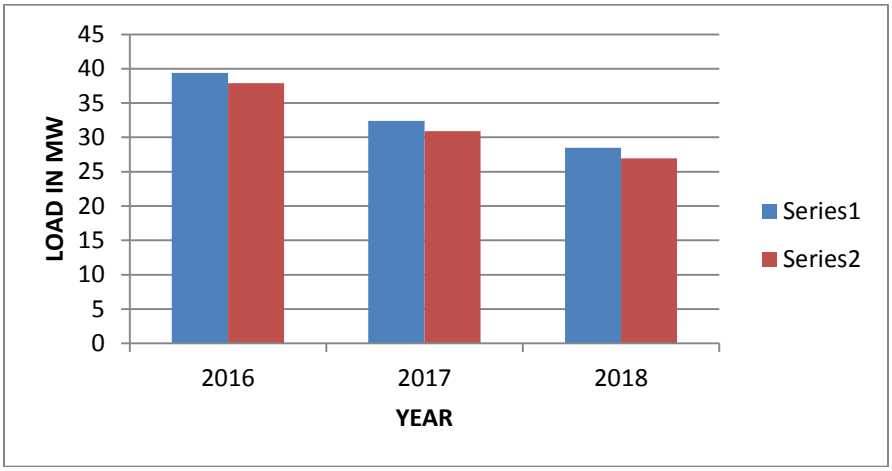

Fig. 5.1 Comparison of load in (MW) for the April month using DA algorithm

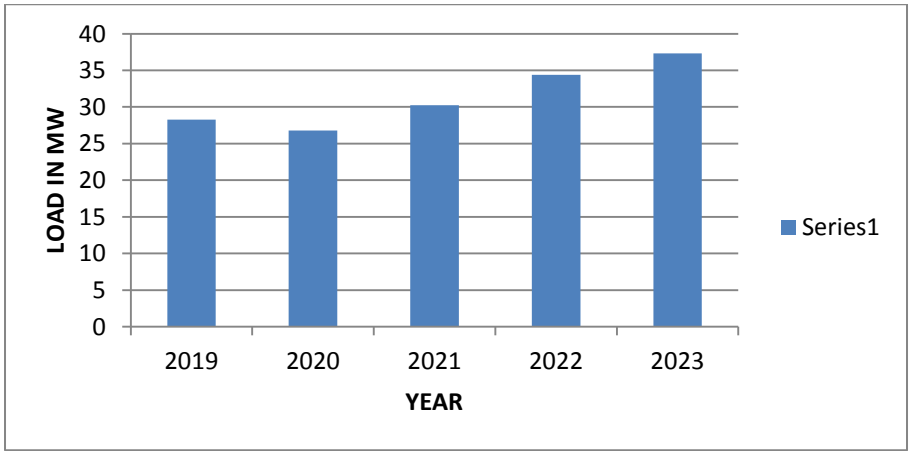

Fig. 5.2 Forecasted load in (MW) for the April month using DA algorithm

VI. CONCLUSION

This paper proposes dragonfly algorithm for long-term load forecasting. The proposed algorithm has been implemented on real time data of the 110/22 kv substation. Long term load forecast with a monthly resolution can be used by energy service providers to plan investments with minimum risks and set up of new generation facilities. The high resolution of data helps in improving the accuracy as well as allows the companies to make a more informed decision and devise an effective strategy for investments. The algorithm is found to be highly accurate with a Mean Absolute Percentage error of 6.54 and a confidence interval of 2.25%.The computation time of the proposed algorithm is calculated within 05 minutes and is appropriate for offline training.

REFERENCES

1. Rahul Kumar Agrawal1 , Frankle Muchahary2 , Madan Mohan Tripathi3, 'Long term load forecasting with hourly predictions based on long-short-term memory networks Conference Paper. February 2018 DOI: 10.1109/TPEC.2018.8312

2. Mr. K. Sriram" Short Term Load forecasting of a power System Using Plant Growth Algorithm" International Journal Of Engineering Research And Development , vol. 14, no. 09, 2018, pp 58- 60.
3. G. Gross, F. D. Galiana Short term load forecasting Proceedings of the IEEE, 1987, 75(12), 1558 – 1571.
4. Kunjin Chen, Kunlong Chen, Qin Wang, Ziyu He, Jun Hu, Member, IEEE, and Jinliang He, Fellow, IEEE,"Short-term Load Forecasting with Deep Residual Networks", arXiv:1805.11956v1 [stat.ML] 30 May 2018.
5. Vaibhav Telrandhe, V. R. Ingle,"Simulation of Electrical Load Forecasting in Substation Transformers Using ANFIS", National Conference on Innovative Paradigms in Engineering & Technology (NCIPET-2012).
6. S.Mirjalili, "Dragonfly Algorithm: A New Meta-heuristic Optimization Technique for Solving Single-objective, Discrete, and Multi-objective Problems", Neural Computing and Applications,inpress,2015, DOI:http://dx.doi.org/10.1007/s00521-015-1920-1.
7. J.Y. Fan, J.D. McDonald, _A real-time implementation of short – term load forecasting for distribution power systems', IEEE Transactions on Power Systems, 1994, 9, 988 – 994.
8. Kunjin Chen, Kunlong Chen, Qin Wang, Ziyu He, Jun Hu, Member, IEEE, and Jinliang He, Fellow, IEEE,"Short-term Load Forecasting with Deep Residual Networks", arXiv:1805.11956v1 [stat.ML] 30 May 2018.
9. Vaibhav Telrandhe, V. R. Ingle,"Simulation of Electrical Load Forecasting in Substation Transformers Using ANFIS", National Conference on Innovative Paradigms in Engineering & Technology (NCIPET-2012).

Solar Optiverter – A Novel Hybrid Approach to the Photovoltaic Module Level Power Electronics

Ms. R. Janani[1], Ms. D. Akalya[2],
UG Student
Department of Electrical and Electronics Engineering,
Krishnasamy College of Engineering and Technology,
S. Kumarapuram, Cuddalore-607 109.

Abstract— In this paper the concept of an Optiverter is proposed as a novel class of photovoltaic (PV) module level power electronics systems. Functionally, the Optiverter is a hybrid technology that combines the ultra- wide maximum power point tracking (MPPT) voltage window of the PV power optimizers with the direct AC connectivity and inherent safety of the PV microinverters. Thanks to the advanced ultimode control with variable DC-link and the shade-tolerant MPPT algorithm, the proposed Optiverter ensures efficient energy harvest from the PV module in different shading scenarios. To justify the superiority of the concept, the performance of a 300 W prototype of the PV Optiverter was experimentally compared to that of the industrial microinverters in different operation conditions, including an extreme case with opaque shading of two out of three substrings of the PV module.

Index Terms— **photovoltaic systems, module-level power electronics, microinverter, power optimizer, maximum power point tracking, partial shading, efficiency**

I. INTRODUCTION

Over the last decade, the photovoltaic (PV) module level power electronics (MLPE) has attracted increasing attention of the PV system operators and installers since it allows operation of each PV module in the maximum power point, thus ensuring the best possible energy yield from the PV installation [1]. Depending on the processed power, the PV MLPE systems can be broadly categorized as those with partial- or full-power conversion, from which the latter is more favorable due to better versatility and performance in different operating scenarios of the PV installation [2]. Today's full-power MLPE systems are mostly represented by the PV power optimizers (PVPOs) and micro inverters (PVMICs). The PVPO is an add-on component to the typical PV string installation, where the PV modules are connected in series (Fig. 1a). Attached to or integrated in the junction box of a PV module, a PVPO is designed to increase the power yield of the module before it sends an optimized DC voltage to the string inverter. The PVPO is typically a non-isolated buck- boost DC-DC converter, which continuously adapts the current drawn from the PV module to maintain a fixed string voltage regardless of string characteristics and operating conditions of the PV modules [3]. The important advantage of the PVPOs is the ultra-wide input voltage range; therefore, they can be paired with the vast majority of the PV modules, including high-power 72- and 96-cell modules and thin-film PV panels. Despite its overall simplicity, the series string installation with a PVPO still has several design constraints such as the minimal string length requirement of six to eight PV modules and impossibility of oversizing of the PVPO. Due to small component count, the PVPOs typically feature efficiencies of over 98% and high reliability [4]. However, the string inverter needed for feeding PV power

to the AC grid could potentially be a "bottleneck" of the PV installation due to the single-point-of-failure problem. Another issue could be associated with risks of fire due to arcing on the high-voltage DC wires between the PV modules and the string inverter, which is typically located in the climate-controlled space. Therefore, extra safety features are required, including arc detection and fast safety disconnection of the PV installation. In contrast to the PVPO, the PVMIC does not only maximize the energy harvest from the PV module but it also converts the output voltage of the module to the grid compliant AC voltage. The PVMICs are connected in parallel at the grid side (Fig. 1b); therefore, the requirement for a minimal number of PV modules is not a constraint any more.

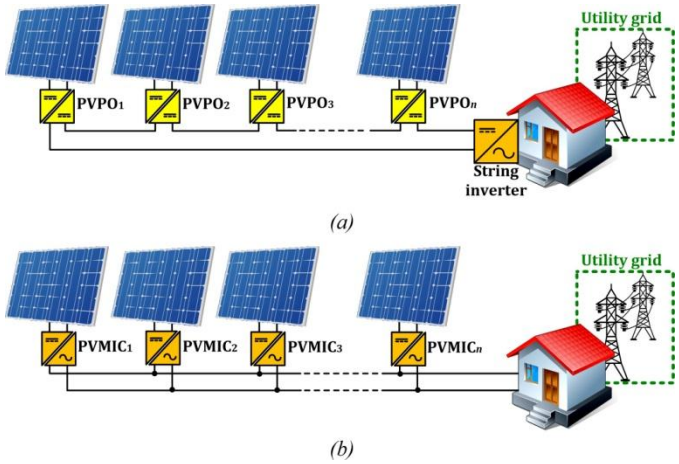

This results in excellent flexibility of sizing since the PV installation can be easily scaled up and down by adding or removing PV modules with associated PVMICs. On the other hand, the PVMIC with its multi-stage power conversion and embedded control, protection and communication systems has significantly increased component count, which penalizes their cost per watt and can have a negative impact on the power conversion efficiency. Another issue of the PVMIC is the long-term reliability since the increased number of components could potentially lead to higher failure rates, especially at the high cell temperatures, which can exceed 60 °C [5]. One of the main disadvantages of the PVMICs is the narrow maximum power point tracking (MPPT) voltage range, which is typically compromised by the tradeoff between the cost, efficiency and reliability.

This paper introduces the concept called Optiverter (PVOPT) as a novel class of PV MPLE systems. Functionally, the PVOPT is a hybrid technology, which combines the ultra- wide MPPT voltage range of the PVPOs with the direct AC connectivity and inherent safety of the PVMICs. In addition, it has the PV module level monitoring and safety cut-off, flexibility of installation and PV power system sizing, which are important features of any MLPE system. First, the paper compares the state-of-the-art MLPE technologies and explains
the essence of the proposed PVOPT technology. Next, the hardware and control system architectures of the PVOPT are presented, followed by the analysis of its advanced feature called Shade-Tolerant MPPT (ST-MPPT). To prove the concept, a 300 W PVOPT was assembled. Our test results are discussed in the experimental parts of the paper. Finally, the conclusions are drawn.

II. COMPARISON OF STATE-OF-THE-ART MLPE TECHNOLOGIES

The non-inverting buck-boost DC-DC converter (NIBBC) shown in Fig. 2a is the most popular topology for PVPOs. The benefits are the small component count and overall simplicity of realization that help to solve such important issues of MLPE systems as cost per watt and reliability. Since the NIBBC has inherent buck-boost characteristics, the multi-mode control is usually implemented where, depending on the string current, the PVPO can feature one of the three modes of operation: buck, boost and pass- through [6]. This feature allows achieving an ultra-wide range of input voltage and load regulation at high efficiency, which is one of the distinct benefits of the PVPOs over the PVMICs.

For the realization of PVMICs, two basic approaches are mainly considered, which differ by the type of the DC-link and localization of the decoupling capacitor CD. One of the most popular PVMIC topologies today is the interleaved flyback converters with an unfolding bridge shown in Fig. 2b [7]. Such configuration with a pseudo DC-link is often referred to as a single-stage PVMIC where the only way to implement the decoupling capacitor is to place it at the PV side [8]. Due to their relative simplicity, the single-stage PVMICs typically have more affordable price and efficiency than the multi-stage counterparts. In regard to the drawbacks, the localization of the decoupling capacitor at the low-voltage side results in a high capacitance values since the allowable voltage ripple must be typically kept below 5% in order to achieve the highest possible MPPT efficiency on the operating power and system specifications, the required capacitance in several cases could exceed 10 mF, which influences negatively the power density and reliability of the PVMIC because of the bulky electrolytic capacitors typically used in the design.

For the multistage PVMIC design, the main power decoupling capacitor is placed at the high-voltage DC-link, as shown in Fig. 2c [10]. As compared to the PV-side decoupling where the voltage ripple should be limited to a very small value to maximize the MPPT efficiency, the DC-link decoupling allows for a higher DC-link voltage as well as a higher voltage ripple. According to (1), this leads to the progressive reduction of the decoupling capacitance since the voltage levels at the PV-side and HV DC-link side typically differ by more than 15 times.

It can be seen that the PVPO has such important competitive advantages over the PVMIC as the ultra-wide MPPT voltage window and high rated power, which can drastically improve the energy yield of the PV system by minimizing the power losses associated with partial shading or power clipping effects. Furthermore, the PVPOs offer better versatility and PV module compatibility since the same model of the PVPO can be paired with different 60- and 72-cell modules. Contrary to that, the PVMICs are typically differentiated by the models compatible either with power maximums in the P-V curve of the module (e.g., *P-V-2* in Fig. 3).

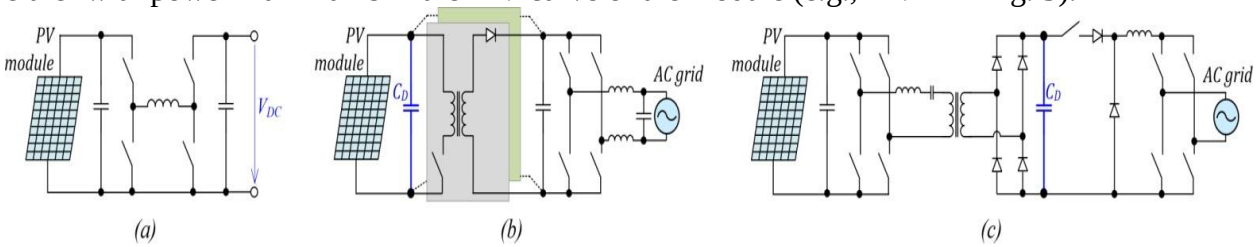

Fig. 2.1. Examples of industrial MLPE topologies: non-inverting buck-boost DC-DC converter for PVPO (a), interleaved flyback converters with unfolding bridge for PVMIC (b) and resonant full-bridge DC-DC converter with single-buck inverter for PVMIC (c).

Because of a narrow MPPT window, the typical PVMIC in that case will typically stack at the local maximum, 60- or 72- cell PV modules. In competition with the string inverters, the MLPE market today is mostly driven by the efficiency of the power conversion stage however, the MPP tracking efficiency plays also a crucial role since it strictly defines the power harvested from the PV module:

$$P = PPV \cdot \eta MPPT \cdot \eta CONV, \qquad (2)$$

where PPV is the available power of the PV module, $\eta CONV$ is the ratio of the output and the input power of the converter ($\eta CONV = PAC/PDC$) and $MPPT$ is the ratio of the input power of the converter and available power of the PV module ($\eta MPPT = PDC/PPV$). It is evident from Table I that in contrast to the PVPOs, the PVMICs have a much narrower MPPT voltage window, which is often compromised by the design tradeoffs to achieve higher efficiency of the power conversion stage at more affordable cost. As a result, the PVMICs are mainly able to track only the local power maximum similar to that indicated in the *P-V-1* curve in Fig. 3, i.e. in the conditions of uniform irradiation of cells in the PV module (Fig. 4*a*). However, in urban conditions, PV modules can often experience different partial shading effects, which could be caused by various obstructions like trees, roof top structures and neighboring buildings as well as by soiling, i.e. deposition of dust, bird droppings, snow, etc. on the surface of the PV module. Such kind of partial shading results in different irradiation of the substrings of the PV module (Fig. 4*b*), which will lead to the appearance of two or three

III. PHOTOVOLTAIC OPTIVERTER (PVOPT)

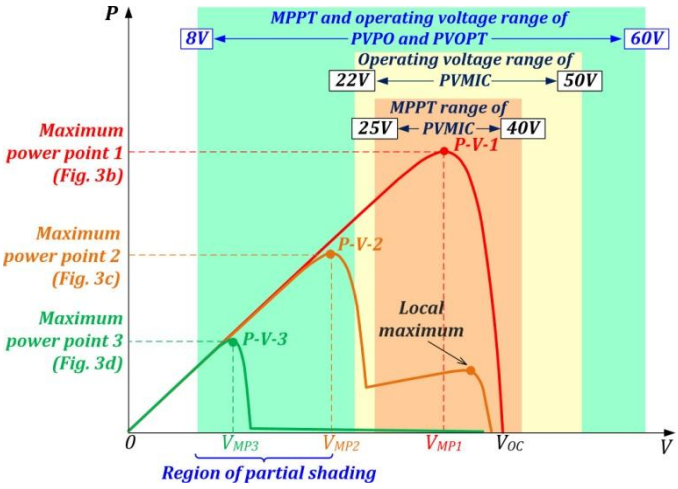

Fig. 3.1. Different shading scenarios of the PV module

To fill the existing technology gap between the PVPO and the PVMIC a hybrid approach called Optiverter (PVOPT) is proposed as a novel class of photovoltaic MLPE systems. The PVOPT combines the ultra-wide MPPT voltage range and shade-tolerant performance of the PVPOs with the direct AC connectivity and inherent safety of the PVMICs. Essentially, the concept of Optiverter proposed combines a wide-range buck-boost front-end DC-DC converter with highly efficient pass-through mode and variable DC-link voltage control, a full-bridge grid-tied inverter, and the multi-mode control. Thanks to the advanced multimode control, the MPPT voltage window of the PVOPT is more than four times wider than that of the traditional PVMIC

(Table I). Furthermore, the minimum start-up voltage of the PVOPT was shifted down to 8 V, which ensures the energy harvest from the majority of 60- and 72-cell PV modules in different shading scenarios, including extreme opaque shading of two out of three substrings of the PV module.

3.1 Design of Power Conversion Stage

Generalized power circuit diagram of the proposed PVOPT is shown in Fig. 5. To enable the ultra-wide MPPT voltage window with the possibility of tracking global maximums, the PVOPT was realized on the double-stage approach. The front-end quasi-Z-source series resonant DC-DC converter (qZSSRC) was justified as a superior solution for MLPE applications in [14]. In the given case, it is responsible for the MPPT and voltage matching between the PV module and the high-voltage DC-link. Generally, the front-end could be based on any other high-performance step-up DC-DC converter topology, allowing for input voltage and load regulation in a wide range, for example, a boost half-bridge DC-DC converter [4] or a hybrid series resonant and PWM boost converter [15]. However, as compared to its counterparts, owing to the inherent buck-boost characteristics and superior control flexibility, the qZSSRC features an unprecedented input voltage regulation capability and DC voltage gain range from 6.7 to 50 [16]. The design of the PVOPT is mainly based on the cost- performance tradeoff; therefore, special attention was paid to the integrity and hybridization of functions of the main components. For example, the transformer TX in the qZSSRC is not only providing the necessary voltage step-up and galvanic isolation but also supports the resonance and ensure the soft switching of the semiconductors. Thanks to the utilization of a series resonant tank formed by the leakage inductance Llk of the transformer TX and capacitors C1 and C2 of the voltage doubler rectifier (VDR) and proper dimensioning of the magnetizing inductance and dead time, the qZSSRC is capable of achieving high efficiency through the full-ZCS of the VDR diodes over the entire operating range, and depending on the operating mode, ZVS and/or ZCS of the primary-side MOSFETs [17].

For the simplification purposes, the grid-tied inverter is based on the simple full-bridge topology with the combination of Si and SiC MOSFETs for the low-frequency (S5, S6) and high-frequency (S7, S8) legs, correspondingly. To attenuate the switching noise and create the sinusoidal output waveform, the LCL filter was employed at the output side of the PVOPT. General specifications and top view of the developed 300 W PVOPT are presented in Table II and Fig. 6, correspondingly. As special attention was paid to the minimization of the manufacturing costs, the use of generic components was one of the main priorities of this project. For the unification purposes, all the magnetic components, including coupled inductor LqZS and hybrid isolation transformer TX, were wound on the RM14 ferrite cores.

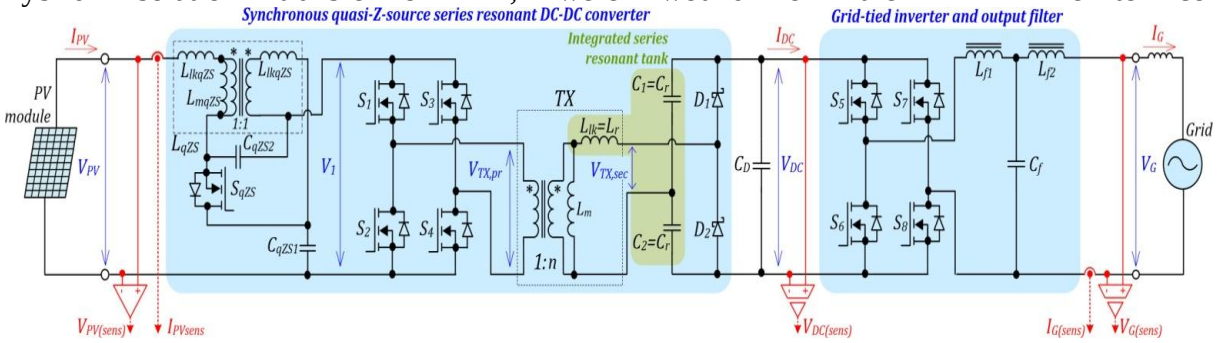

3.2 Experimental Evaluation of the Optiverter

First, the PVOPT was tested with a solar array simulator (SAS) Agilent emulating nominal operating conditions of 60-cell Si PV module Jinko Solar JKM300M-60 that is one of the leading products at the residential PV market. Current and voltage signals were measured by the oscilloscope Tektronix DPO7254, the current probe TCP0030A and the differential voltage probes P5205A. As shown in Fig. 9, the PVOPT features low input current and voltage ripple, and low grid current the total harmonic distortion (THD) of 2.6% despite the presence of the 5th harmonic in the grid voltage. The current drawn by the grid- tied inverter from the DC-link (IDC) is shifted in respect to the AC-component of the DC-link voltage, as could be expected for the single-phase system.

IV. CONCLUSIONS

The novel concept of the PV Optiverter with an ultra-wide input voltage range was proposed and justified as a shade- tolerant solution for residential and small commercial PV installations, which is compatible with a wide variety of modern residential PV modules. It outperforms conventional micro inverters under partial shading due to the implementation of the shade tolerant MPPT and can deliver power under severe opaque shading conditions, when the microinverters fail to capture any power due to their limited input voltage regulation range. Moreover, it is compatible with emerging high power PV modules due to increased power rating for avoiding the power clipping. These features result from the application of the galvanic ally isolated ultra-wide range buck-boost dc-dc converter and the novel control principle with the variable DC-link voltage that optimizes efficiency in the most probable input voltage operating range. This enables the shade tolerant MPPT through P-V curve

REFERENCES

1. S. Kouro, J. I. Leon, D. Vinnikov and L. G. Franquelo, "Grid-Connected Photovoltaic Systems: An Overview of Recent Research and Emerging PV Converter Technology," IEEE Ind. Electron. Mag., vol. 9, no. 1, pp. 47-61, March 2015.
2. M. Kasper, D. Bortis and J. W. Kolar, "Classification and Comparative Evaluation of PV Panel-Integrated DC–DC Converter Concepts," IEEE Trans. Power Electronics, vol. 29, no. 5, pp. 2511-2526, May 2014.
3. "SolarEdge Fixed String Voltage, Concept of Operation." [Online]. Available: https://www.solaredge.com [Accessed: 28-Jan-2018]
4. E. Liivik, A. Chub, R. Kosenko and D. Vinnikov, "Low-cost photovoltaic microinverter with ultra-wide MPPT voltage range," in Proc. 6th Int. Conf. on Clean Elect. Power, Santa Margherita Ligure, Italy, 2017, pp. 46-52.
5. J.K. Kaldellis, et al "Temperature and wind speed impact on the efficiency of PV installations. Experience obtained from outdoor measurements in Greece," Renewable Energy, vol. 66, pp. 612-624, June 2014.

21 Level Staircase Sine Wave Inverter with Reduced Switches and THD

Sr. A. Annai Theresa[1]
Assistant Professor,
Department of Electrical and Electronics Engineering,
St. Anne's College of Engineering and Technology,
Anguchettypalayam, Panruti – 607106.

Mr. Sinu Cleetus[2], Mr. A. Abinesh[3], Mr. C. Thamizharasan[4], Mr. S. Shanmuganatham[5]
UG student,
Department of Electrical and Electronics Engineering,
St. Anne's College of Engineering and Technology,
Anguchettypalayam, Panruti – 607106.

Abstract – Several industrial applications require high power inverter with sinusoidal waveforms and with minimum distortion. For medium and high power applications, it is difficult to attain this result using a single switch. With this background the concept of multilevel inverters were introduced in 1974. At present situation multilevel inverter is becoming more popular due to its staircase output whose characteristics are closer to the characteristics of sinusoidal waveform. But generally it has some disadvantages like, requirement of increased number of switches, complex pulse width modulation methods to reduce harmonics. The cascaded H-bridge multilevel inverter requires least number of components to achieve various voltage levels by which the quality output is obtained. However as the number of voltage levels m grows the number of active switches increases according to 2× (m-1) for the cascaded H Bridge. Here, the novel multilevel inverter topology with reduced number of power switches is proposed so that the switching losses can be reduced. The power quality of the proposed system is improved by using selective harmonic elimination (SHE) method. The whole system is numerically reformed utilizing MATLAB/SIMULINK and the simulation results are presented.

Index Terms **- Multilevel inverter (MLIs), PWM techniques and Total Harmonic Distortion (THD), Cascaded H-bridge, SHE.**

I. INTRODUCTION

Generally, the voltage source inverters generate an output voltage with a two level, so they are also called the two-level inverter. To obtain a quality output voltage or a current waveform with a minimum amount of ripple content, they require a high switching frequency along with various PWM techniques. For the high power and medium power application, these two-level inverters have some disadvantages, like switching losses due to high frequency operation, the distorted output voltage and current waveforms and the large total harmonic distortion of the voltage and current [1]. Hence multi-level inverters are used to mitigate the overall THD. In the multilevel inverter increasing the number of voltage levels without requiring higher ratings on individual devices can increase the power rating. And if the number of voltage level increases, the harmonic content of the output voltage decreases.

The multilevel inverter can be classified as flying capacitor, Cascaded H-Bridge and diode clamped multilevel inverters. Out of these technologies Cascaded H-Bridge multilevel inverter is one of the well-known, most advantageous, much simpler and basic method of multilevel inverter [2]. Multilevel inverter provides a suitable solution for medium and high

power systems to synthesize an output voltage which allows a reduction of harmonic content in voltage and current waveforms.

In the cascade multilevel H-bridge inverter, number of H bridges is connected in series, each H-bridge having a separate DC source, the capacitor or diode is not required for clamping purpose. so these are the advantages of cascade multilevel inverter over diode clamped and flying capacitor multilevel inverter, and its output waveform will be sinusoidal in nature if number of level is increased even we don't filter it [3].

In this paper, selective harmonic elimination (SHE) control strategy is used, and the 21- level cascade multilevel inverter simulation has been done in MATLAB software.

II. MULTILEVEL INVERTER

The multilevel inverter is a type of inverter circuit which is used to increase the efficiency of the inverter operation and reduce the THD level in the operation of inverter in order to reduce the losses. We also reduce the number of switches used in the circuit. The SHE technique is used to get the desired output.

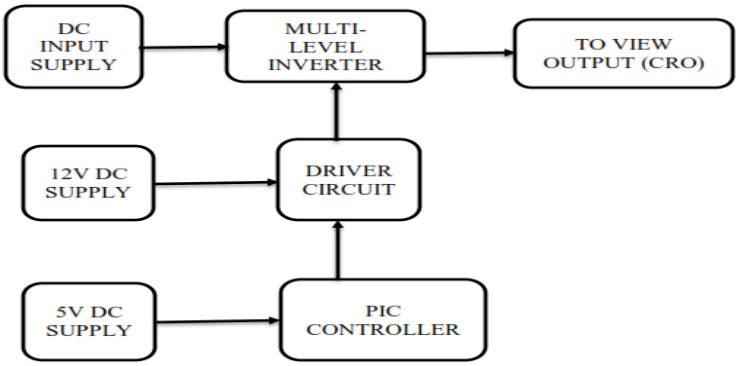

Fig.2.1 Block diagram of multilevel inverter

2.1 Cascaded H-Bridge Topology

The term H Bridge is derived from the typical graphical representation of such a circuit. An H bridge is built with four switches (solid-state or mechanical).One of the basic and well known topologies among all multilevel inverter is cascaded H-bridge multilevel inverter. It can be used for both single and three phase conversion. In Cascaded H-Bridge multilevel inverter, Number of H-Bridges is connected in series. Each H-Bridge is having separate DC source which is to be obtained from any natural sources, ultra-capacitors, fuel cells or batteries to produce inverted ac output [4].

III. PROPOSED SYSTEM

A new multilevel inverter with reduced number of switches are proposed and the switching losses also get reduced and level is increased up to 21 level with reduced (THD). In conventional approach, PWM techniques are used by the comparison of reference and carrier signals to provide the required gating signals for the inverter switches. The number of output voltage levels obtained from this approach is given in the following equation: $m = 2Ns + 1$ where m denotes the output voltage levels and Ns is the individual inverter stages. The number of switches required to achieve m levels is given in the following equation: $l = 2(m - 1)$ for the implementation of 21-level CMLI, the number of switches required is 40.

The proposed ACMLI topology for 21-level inverter requires twelve semiconductor switches and four isolated dc sources which separate output voltage in two parts. One part is called level generation part (left side) and is responsible for level generating in positive polarity & negative polarity. The other part is called polarity generation part (right side) and is

responsible for generating the polarity of the output voltage. This topology combines the two parts (left part and right part) to generate the multi-level output voltage waveform. The main purpose of this proposed ACMLI topology is to control the EMI, minimize the total harmonic distortion with selective harmonic elimination (SHE) technique and it also minimizes power semiconductor switches than conventional multilevel inverter. For a conventional single-phase 21-level inverter, it uses 40 switches, whereas the proposed topology uses only 12 switches with the same principle. PIC microcontroller PIC16F877A is used to generate pulse for Switches.

3.1 Operation of the proposed topology

The proposed single-phase asymmetrical cascade 21-level inverter for line to ground voltages is shown in figure 2. With this inverter, 21 levels (0, ±10V) of output voltage as a staircase waveform is obtained.

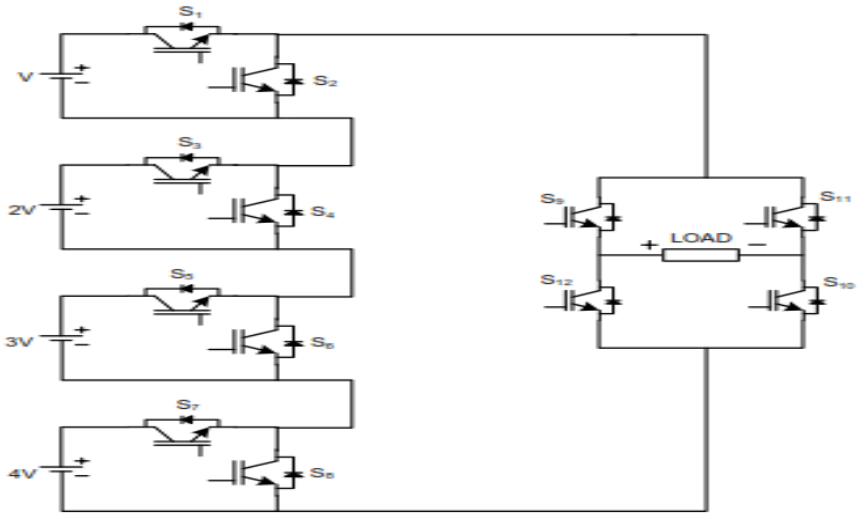

Fig.3.1 Proposed Multilevel Inverter Topology

The different switching states (i.e) ON, OFF states of different switches for obtaining different voltage levels are given in the table.1 and are explained as follows.

Switches S9, S10, S11 and S12 are used for complementary pair. When S9, S10 are turned ON together, positive half cycle (level: +1, +2, +3, +4…) can be generated and when S11, S12 are turned ON together, negative half cycle (level: -1, -2, -3 and -4…) can be generated across load. When switches S2, S4, S6 and S8 switches are turned ON the output voltage will be "zero" (level 0). When S1, S4, S6 and S8 switches are turned ON the output voltage will be "Vdc" (level +1). The output voltage will be "2 Vdc" (level +2) when switches S2, S3, S6, and S8 are turned ON. When switches S1, S3, S6 and S8 are turned ON, the output voltage will be "3 Vdc" (level +3). When switches S1, S4, S6, S7 are turned ON, the output will be "4Vdc (level +4). When switches S1, S3, S5, S7 are turned ON, the output will be "5Vdc (level +5). When switches S1, S3, S5, S8 are turned ON, the output will be "6Vdc (level +6). When switches S2, S4, S5, S7 are turned ON, the output will be "7Vdc (level +7). When switches S1, S4, S5, S7 are turned ON, the output will be "8Vdc (level +8). When switches S2, S3, S5, S7 are turned ON, the output will be "9Vdc (level +9). When switches S1, S3, S5, S7 are turned ON, the output will be "10Vdc (level +10). So, for all these positive 10 levels complementary pair S9, S10 are in ON condition. The same switches are in ON condition for all the negative 10 levels, but the complementary pair in ON condition is S11, S12.

VOLTAGE LEVEL	SWITCHING STATE												OUTPUT VOLTAGE
	S_1	S_2	S_3	S_4	S_5	S_6	S_7	S_8	S_9	S_{10}	S_{11}	S_{12}	
+10	1	0	1	0	1	0	1	0	1	1	0	0	10V
+9	0	1	1	0	1	0	1	0	1	1	0	0	9V
+8	1	0	0	1	1	0	1	0	1	1	0	0	8V
+7	0	1	0	1	1	0	1	0	1	1	0	0	7V
+6	1	0	1	0	1	0	0	1	1	1	0	0	6V
+5	1	0	0	1	0	1	1	0	1	1	0	0	5V
+4	0	1	0	1	0	1	1	0	1	1	0	0	4V
+3	1	0	1	0	0	1	0	1	1	1	0	0	3V
+2	0	1	1	0	0	1	0	1	1	1	0	0	2V
+1	1	0	0	1	0	1	0	1	1	1	0	0	V
0	0	1	0	1	0	1	0	1	1	1	0	0	0
-1	1	0	0	1	0	1	0	1	0	0	1	1	-V
-2	0	1	1	0	0	1	0	1	0	0	1	1	-2V
-3	1	0	1	0	0	1	0	1	0	0	1	1	-3V
-4	0	1	0	1	0	1	1	0	0	0	1	1	-4V
-5	1	0	0	1	0	1	1	0	0	0	1	1	-5V
-6	1	0	1	0	1	0	0	1	0	0	1	1	-6V
-7	0	1	0	1	1	0	1	0	0	0	1	1	-7V
-8	1	0	0	1	1	0	1	0	0	0	1	1	-8V
-9	0	1	1	0	1	0	1	0	0	0	1	1	-9V
-10	1	0	1	0	1	0	1	0	0	0	1	1	-10V

Table. 3.1 Switching States of Proposed Scheme

3.2 Modulation strategies

In this proposed scheme, the selected harmonic elimination technique is used and by which the lower order harmonics are eliminated. The harmonic elimination is performed for several reasons. The first reason is harmonics are a source of EMI. Without harmonic elimination, designed circuits would need more protection in the form of snubbers or EMI filters [5], as result, designed circuits would cost more. The second reason is that EMI can interface with control signals used to control power electronics devices and radio signals. The third reason is that harmonics can create losses in power equipment. The fourth reason is that harmonics can lower the power factor of a load. Increased harmonic content will decrease the magnitude of the fundamental relative to the magnitude of the entire current, as a result the power factor would decrease. There are four kinds of control methods for multilevel converters. They are the selective harmonic elimination method, traditional PWM control method and space vector PWM method. The traditional PWM, space vector PWM and space vector modulation methods cannot completely eliminate harmonics. Of these four kinds we use here the selective harmonic elimination technique which is very important and efficient method. This technique is widely used in control of the conventional VSIs, in order to improve much more their output voltages quality.

3.3 Selective harmonic elimination technique

Selective Harmonic Elimination technique SHE is used to increase MLI efficiency by reducing output Total Harmonic Distortion THD associated with MLI switched output [6], [7]. It is rather simple to be applied to proposed topology by selecting suitable switching angles α1, α2, α3, etc….α21. The Fourier series expansion of the (stepped) output voltage waveform of the proposed topology in twenty one levels configuration is

$$V(\omega t) = \sum_{n=1,3,5}^{\infty} \binom{n4V_{dc}}{n\pi} [cos(n\alpha_1) + cos(n\alpha_2) + cos(n\alpha_3) \ldots\ldots cos(n\alpha_{21})]\sin(n\omega t)$$

This waveform has 10 step angles $\alpha_1\alpha_2\alpha_3 \ldots\ldots \alpha_{10}$, therefore the switching angles are chosen so as not to generate the 3rd, 5th, 7th and 9th order harmonics while achieving the desired fundamental voltage.

The mathematical statements of these conditions are:

$$\frac{4V_{dc}}{\pi[cos(\alpha_1) + cos(\alpha_2) + cos(\alpha_3) + \cdots \ldots cos(\alpha_{10})]} = V_f$$

$$\frac{4V_{dc}}{\pi[cos(3\alpha_1) + cos(3\alpha_2) + cos(3\alpha_3) + \cdots \ldots cos(3\alpha_{10})]} = 0$$

$$\frac{4V_{dc}}{\pi[cos(5\alpha_1) + cos(5\alpha_2) + cos(5\alpha_3) + \cdots \ldots cos(5\alpha_{10})]} = 0$$

$$\frac{4V_{dc}}{\pi[cos(7\alpha_1) + cos(7\alpha_2) + cos(7\alpha_3) + \cdots \ldots cos(7\alpha_{10})]} = 0$$

$$\frac{4V_{dc}}{\pi[cos(9\alpha_1) + cos(9\alpha_2) + cos(9\alpha_3) + \cdots \ldots cos(9\alpha_{10})]} = 0$$

By using these mathematical statements we eliminate the low-order harmonics 3, 5, 7, and 9.

IV. RESULT ANALYSIS

The circuit for 21 level inverter is simulated in MATLAB/ SIMULINK and its outputs (i.e) load current and voltage are obtained as given below.

4.1 Circuit diagram

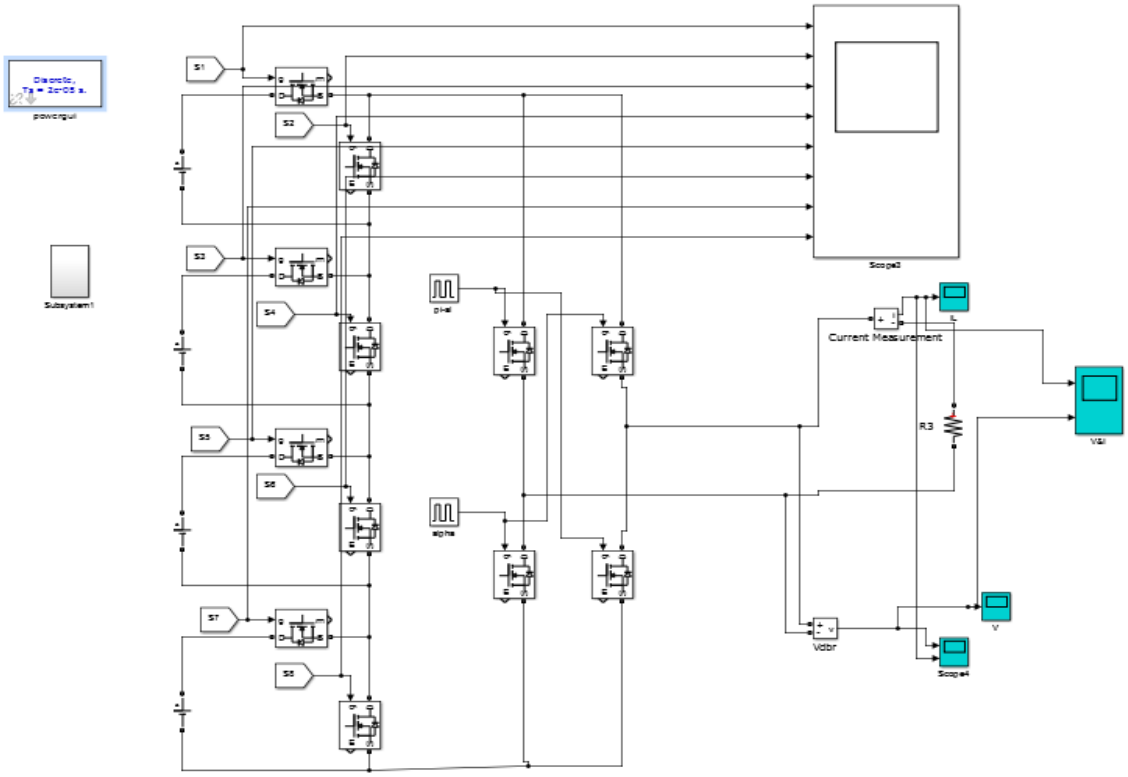

Fig 4.1 Circuit diagram

4.2 Gate pulses for MOSFET

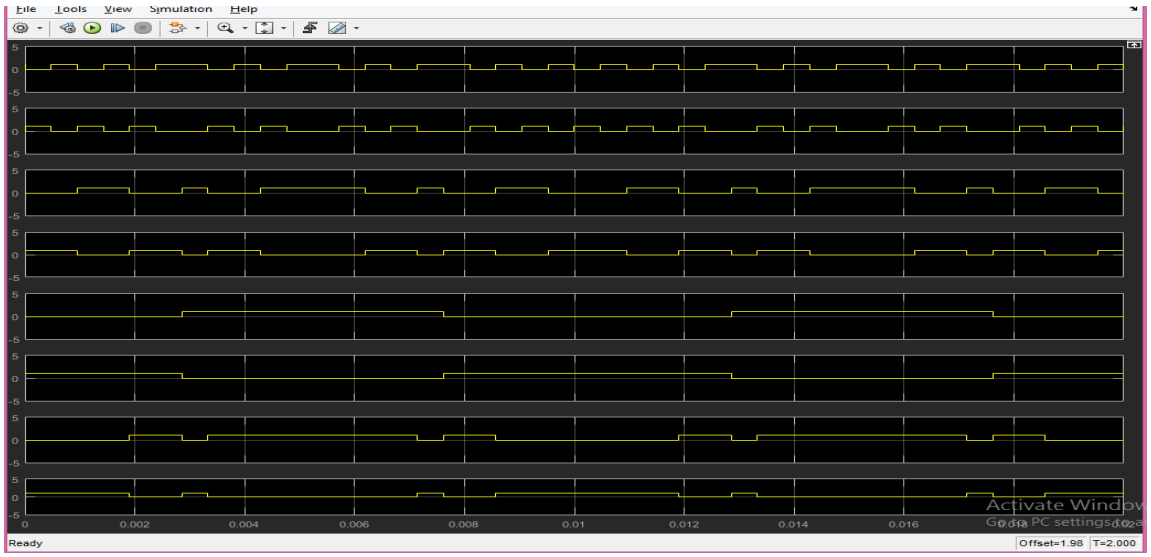

Fig 4.2 Gate pulses for MOSFET

4.3 Load Current

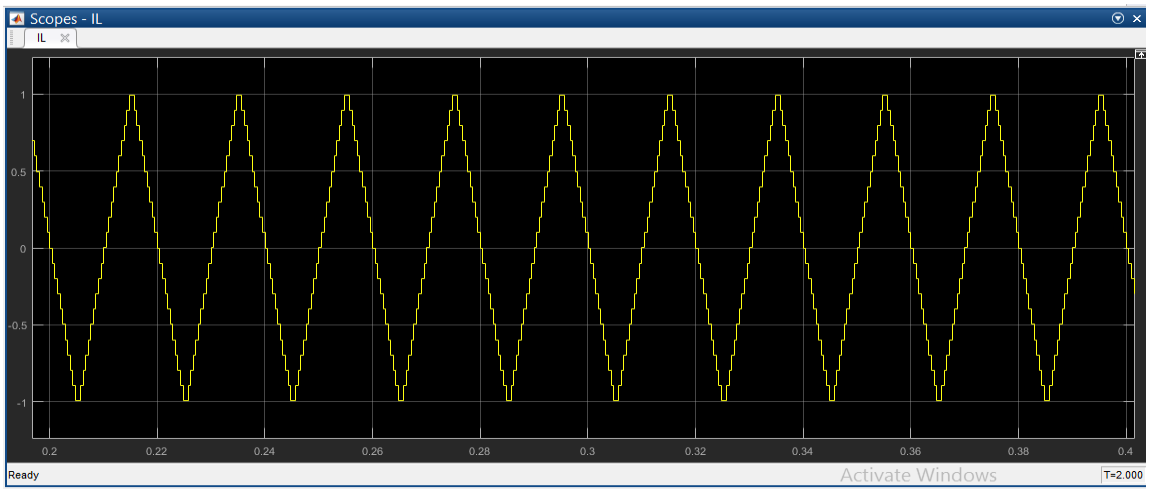

Fig 4.3 Load Current

4.4 Load current and voltage

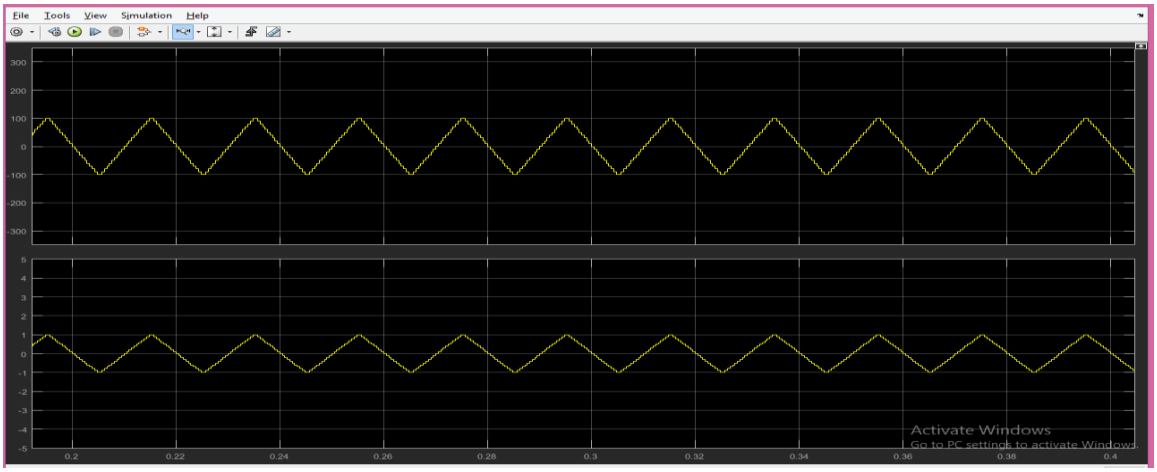

Fig 4.4 Load current and voltage

V. CONCLUSION

This paper introduces a new MLI topology based on conventional asymmetric cascaded half H-bridge inverter. Asymmetric DC sources configuration is utilized in order to maximize number of output voltage levels. DC sources are sized and interconnected in order to allow the proposed topology to produce both negative and positive half cycles. Thus, this eliminates the need for conventional polarity changer H-bridge. And also, instead of using 40 switches, the numbers of switches are reduced to 12 so that the switching losses are getting reduced and the cost required for the devices becomes less. In addition to that the THD is reduced to a reasonable value by using selective harmonic elimination (SHE) technique. Harmonic analysis is carried out using MATLAB R2012a version software. The scheme has successfully been implemented and tested by using R2012a version of MATLAB/Simulink software.

REFERENCES

1. Dr. Asha Gaikwad, Pallavi Appaso Arbune (2016). Study of Cascaded H-Bridge Multilevel Inverter. In: International Conference on Automatic Control and Dynamic Optimization Techniques (ICACDOT)
2. Mohammad Ahmad and B.H. Khan, Senior Member, IEEE (2012). New Approaches for harmonic reduction in solar inverters
3. Jigarkumar.V. Patel, N. G. Mishra, wjter 2018, Analysis of Five- Level Cascade Multilevel Inverter Using SPWM Technique
4. Pravin T. Jadhav Swapnil Y.Gadgune, and Lohit R. Chaudhary "Implementation of Shunt APF based on Diode Clamped and Cascaded H-Bridge Multilevel Inverter" IEEE 2015.
5. K.J.Mckenzie, onverter using resultant theory, Symmetric polynomials, and Power Sums ", Master thesis,2004.
6. Kamaldeep, J. Kumar, Performance analysis of H-Bridge multilevel inverter using Selective Harmonic Elimination and Nearest Level Control technique, in: 2015 International Conference on Electrical, Electronics, Signals, Communication and Optimization (EESCO), 2015, pp. 1–5.
7. L.M. Tolbert, F.Z. Peng, T.G. Habetler, Multilevel converters for large electric drives, IEEE Trans. Ind. Appl. 35 (1) (1999) 36–44.

.

Smart Prepaid Energy Meter using GSM and Arduino

Sr. A. Annai Theresa[1]
Assistant Professor,
Department of Electrical and Electronics Engineering,
St. Anne's College of Engineering and Technology,
Anguchettypalayam, Panruti – 607106.

Ms. M. Nirmala[2], Ms. J. Santhini[3], Ms. V. Dhivya[4], Ms. M. Suvedha[5]
UG Student,
Department of Electrical and Electronics Engineering
St. Anne's College of Engineering and Technology,
Anguchettypalayam, Panruti – 607106.

Abstract - The aim of paper is to propose a different method for measuring and billing of the energy consumed rather the conventional method. Here a new procedure is followed based on ATmega 328P microcontroller for controlling and detecting energy consumed. It is possible to recharge the electricity balance through this system jus by sending an SMS. It also continuously reads the energy meter readings and automatically sends some updates like low-balance alert, zero-balance alert, recharge alert when necessary to the registered number through GSM modem. Illegal usage of power is detected and alert message is sent to the authorities immediatelyt.

***Index Terms*— smart meters; Arduino; energy meter; GSM.**

I. INTRODUCTION

In a world where everything is automated, the automation of the energy payments is much needed. The world is being digitized and it is important that we should be able to move along with trends and changes. Energy is the most common and most important resource and the need for it use it in a controlled manner is crucial where the resources for it are scarce. So, using Prepaid Energy meters helps us to avoid the wastage of power consumed in our daily lives. Moreover, it is also important to protect the revenue of the government from the loss occurs due to the illegal usage of power. Hence, there is a definite need for us to use an advanced energy meters, which can both monitor the consumption and theft.

II. EXISTING SYSTEM

The energy meters used now-a-days are modified version of the older system, the digital meters doesn't have a prepaid system, where the power to be consumed is estimated prior to its usage and recharged, similar to that of a prepaid talk time for a mobile. Moreover to it, there is no proper equipment which can detect the illegal power usage, using power without actually paying for it. However, in some energy meters an LED is provide which blinks whenever someone tries to open the energy meter box, but this can be stopped using a button which is provided at it backside, which doesn't guarantee security.

III. PROPOSED SYSTEM

Smart Prepaid Energy meter using Arduino and GSM can provide the solution to problems discussed. This project helps in not only automating but also for controlled managing of the energy consumed, which results in efficient usage of power. GSM modem is helpful for the message alerts and notifications needed for these purposes. The different components used are controlled by ATmega 328P microcontroller in Fig 3.1.

Illegal usage of power, in other words power theft, is a loss to the government's revenue. This problem, up to some extent, can be solved with this project. Whenever power theft is detected, the system notifies the authorities.

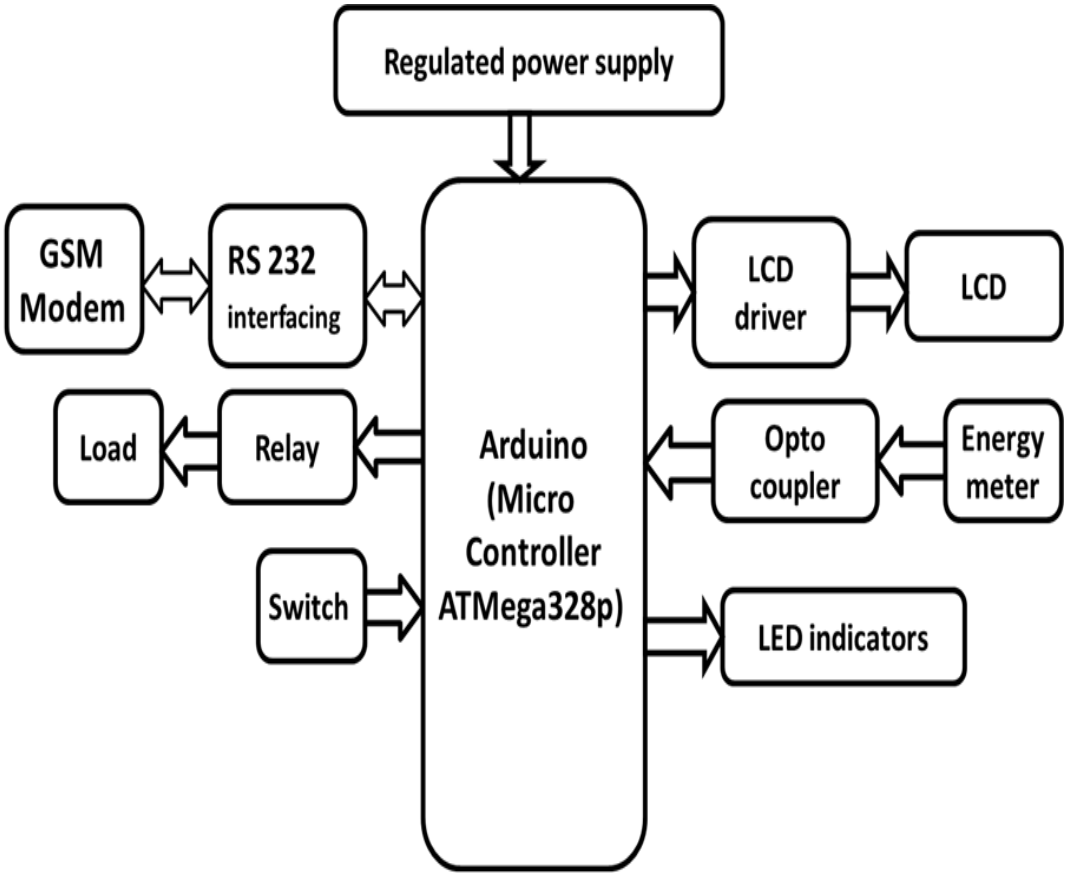

Fig 3.1. Block diagram of prepaid energy meter with power theft detection and control

IV. ANALYSIS OF HARDWARE COMPONENTS

4.1 Regulated Power Supply:

The microcontroller and the circuit associated with it requires 5V supply where as the relay used requires 12V supply for its operation. Usage of two separate power supplies for arduino and relay will increase the size and cost of the project. Hence, a single 12V adapter is connected to the mains, which produces 12V output usable for the relay and then this voltage is passed through a LM7805 voltage regulator resulting in a 5V DC output usable for the arduino and the associated circuitry. The adaptor works as a filter and rectifier. Load is connected across 220V AC supply

.

4.2 Microcontroller:

Microcontroller is a programmable device which consists of a processor RAM, ROM, I/O ports, and a timer all on a single chip. ATmega 328P microcontroller is used in this project. It is highly reliable and virtually low cost. The software used to program the ATmega 328P to do specific tasks is Arduino IDE. It has a total of 28 pins out of which 23 are multi-functional. The device operates between 1.8-5.5 volts

4.3 GSM Modem:

GSM in this project is used for the communication between the device and the user. We used SIM800L module. This module supports quad-band GSM/GPRS network, available for GPRS and SMS message data remote transmission. The SIM800L communicates with microcontroller via UART port, supports command including 3GPP TS 27.007, 27.005 and SIMCOM enhanced AT Commands. SIM800L is a miniature cellular module which allows for GPRS transmission, sending and receiving SMS and making and receiving voice calls. After connecting power module boots up, searches for cellular network and logins automatically. On board LED displays connection state (no network coverage-fast blinking, logged in-slow blinking).

.

4.4 Energy Meters:

In this project Digital Energy Meters. These meters have microprocessors which are used to calculate phase angle between voltage and current, so that it also measures and indicates reactive power. It is programmed in such a way that it calculates energy according to the tariff and other parameters like power factor, maximum demand, etc. and stores them in EEPROM. It also contains real time clock (RTC) for calculating time for power integration, maximum demand calculations and also time and date stamps for particular parameters.

4.5 Optocoupler:

An Optocoupler is an electronic device that interconnects two separate electrical circuits by means of a light sensitive optical interface. It acts to break ground loops used in eliminating common-mode noise, especially for systems working at the higher operating voltages. Here we are using PC817 Optocoupler

.

4.6 Relay:

A relay is an electrically operated switch. In this project relay is used to control the power to the energy meter. The relays are controlled using a low-power signal. All relays contain a sensing unit, the electric coil, which is powered by AC or DC current. When the applied current or voltage exceeds a threshold value, the coil activates the armature, which operates either to close the open contacts or to open the closed contacts. When a power is supplied to the coil, it generates a magnetic force that actuates the switch mechanism. The magnetic force is, in effect, relaying the action from one circuit to another. The first circuit is called the control circuit; the second is called the load circuit.

V. WORKING

The 230V AC power supply is given to operate the loads. A 20V adapter is used to provide 5V to the Arduino board and from here it is interfaced with relay, GSM and LCD. The transmitter and receiver pins of GSM are connected to the receiver (Rx 0) and transmitter (Tx 1) pins of Arduino board. The optocoupler is given to the 8 pin of Arduino Uno and the other end is given to the energy meter. The relay is connected to the 12 pin of the Arduino

board and to the energy meter as well as the load. The load in turn is connected to the energy meter. The LCD 6 pins i.e. RS, Rw, E, D0-D2 are given to the 2, 3, 4,5,6,7 pins and the

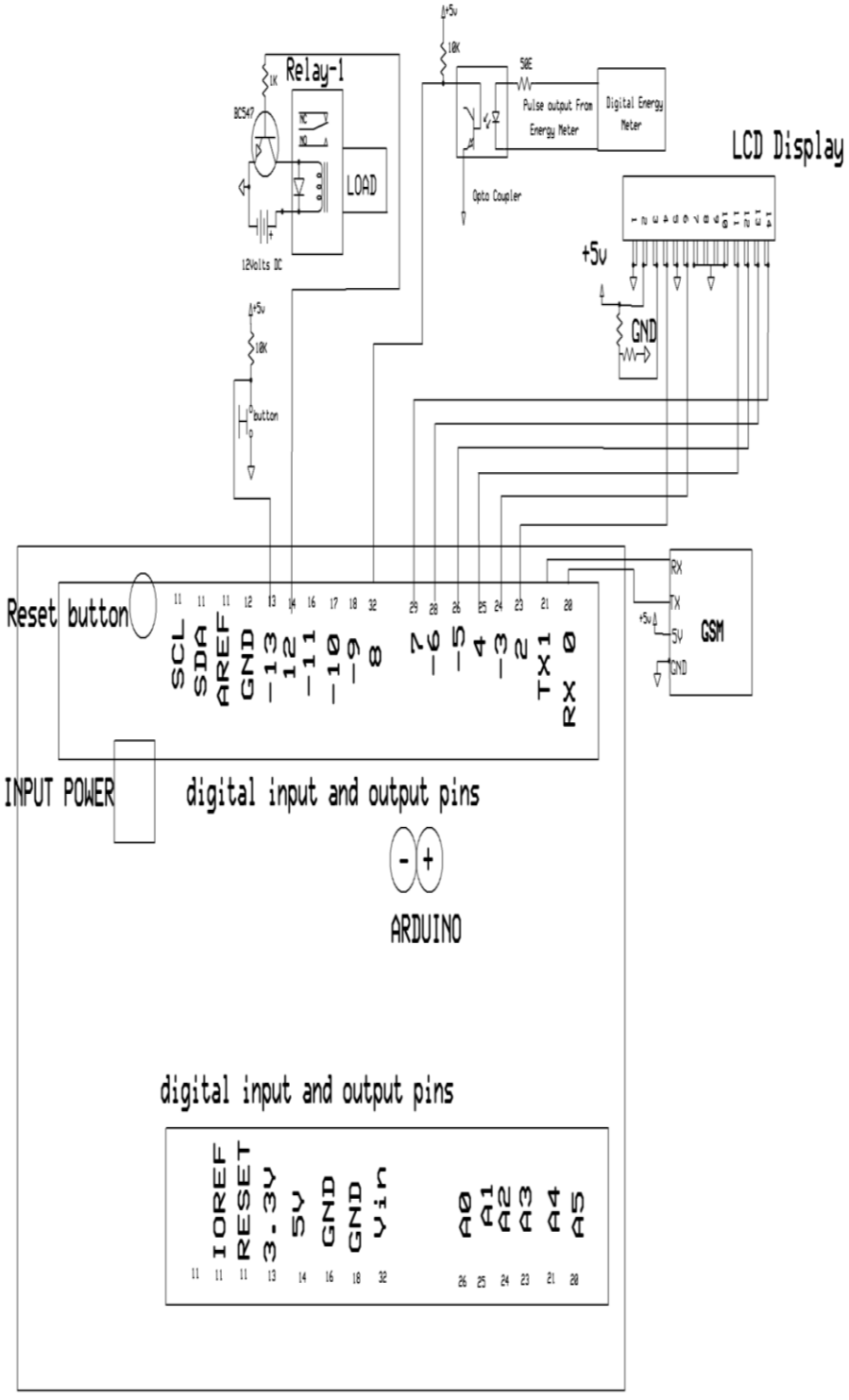

Fig 5.1. Circuit diagram of prepaid energy meter

switch is connected to the 13 pin of the Arduino board. Here we are representing the switch outside of the energy meter just to represent the power theft in real life as shown in Fig 5.1.

VI. FLOWCHART

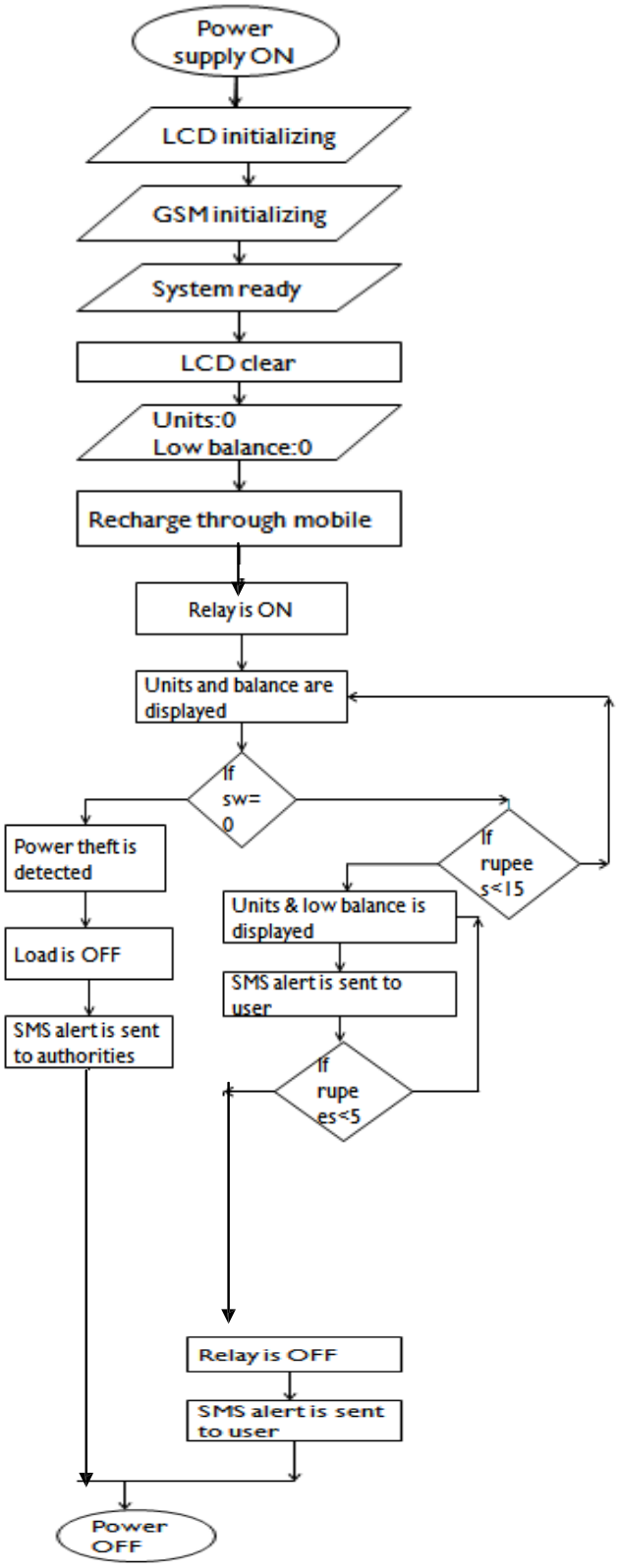

Fig 6.1. Circuit diagram of prepaid energy meter

VII. ALGORITHM

Step1: Switch ON the power supply.
Step2: Initialize the LCD and GSM and display System Ready message.
Step3: Clear LCD and display units and balance.
Step4: Recharge through mobile so that Relay is turned ON.
Step5: Display the new units and balance available.
Step6: If switch is ON go to step11 else go to step 7.
Step7: If rupees<15, go to step 8 else go to step 5.
Step8: Send the SMS alert and display the same in LCD.
Step 9: If rupees<5, go to step 10 else go to step 7.
Step10: Turn OFF the Relay, send alert message and go to step 13.
Step11: Turn OFF the load.
Step12: Send the SMS alert to the authorities and go to step 13.
Step 13: Turn OFF the power..

VIII. RESULTS

When the supply is provided to meter, initially LCD gets initialized. Text SMS is sent to consumer as "System Ready". The meter can be recharged by messaging from the any number to the GSM modem that is fixed with meter and user will get message that the energy meter has been recharged by some amount shown in Fig 8.1. The consumer can recharge the meter according to his requirement. If the consumer wants to know the left out balance in meter then it can be checked in LCD display of Meter. If the switch is ON, it indicates the power theft.

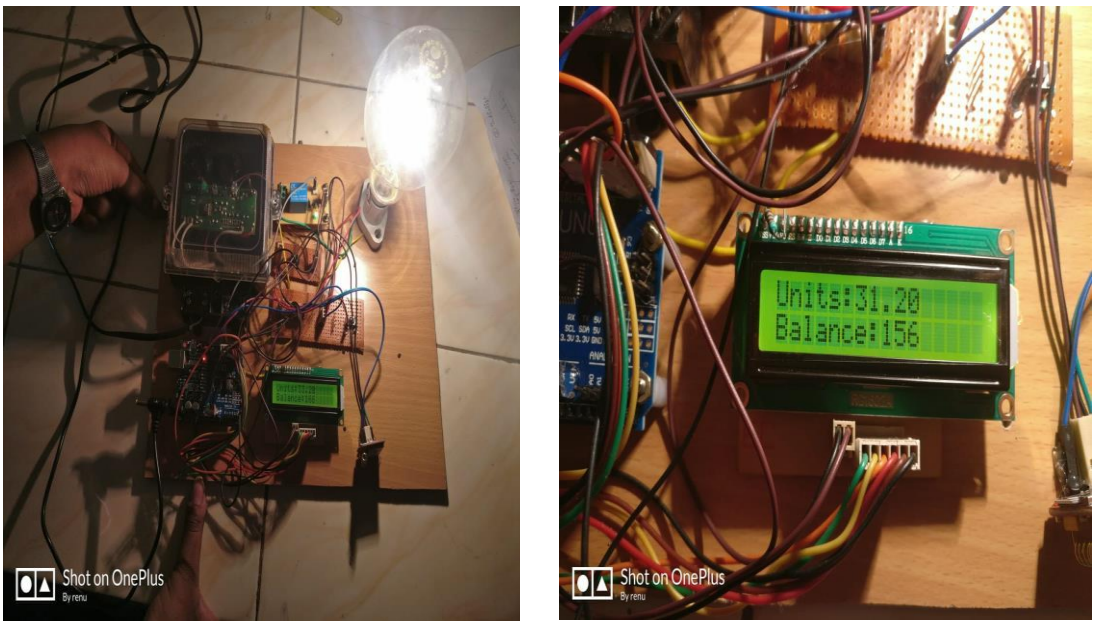

Fig. 8.1. Recharge is done and the balance & units goes on decreasing as the load consumes energy

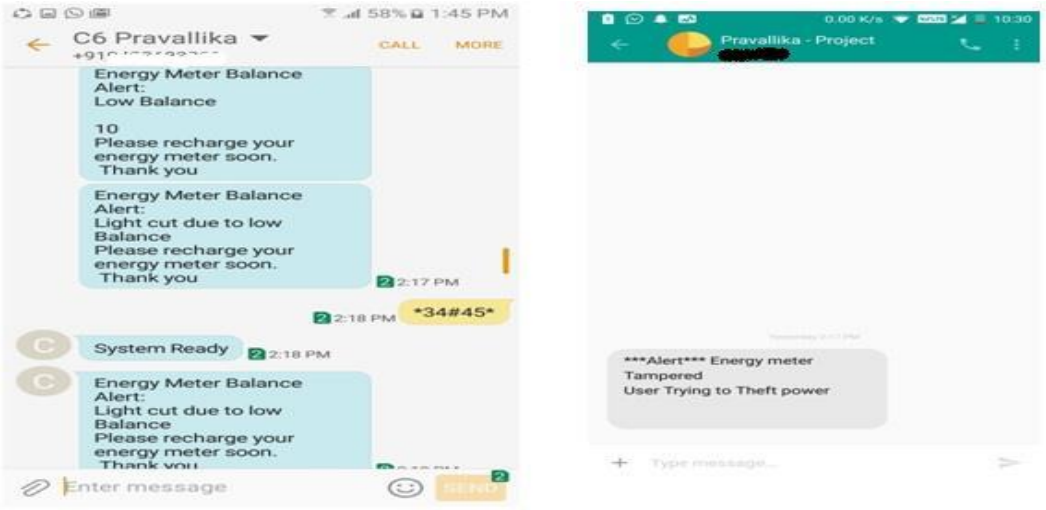

Fig 8.2. The message alerts to the user mobile when there is low balance and no balance

IX. CONCLUSION

Prepaid energy meter with power theft detection is easy to install and beneficial for both energy provider and consumer. This project reduces the manual efforts and human errors, by monitoring all the parameters and functioning of the connections. Also by implementing this system we can control the usage of electricity on consumer side to avoid wastage of power. An attempt is made in this work to develop a system, which when interfaced with static electronic energy meter is avoided where in complexity of the circuit is reduced and cost also gets reduced of the meter. This system avoids electricity theft to large extent and makes the energy meter tamper proof. This meter increases the revenue of the Government by detecting the unauthorized tampering in the power lines

REFERENCES

1. Smart energy metering and power theft control using Arduino & GSM Automated Smart Metering ; (IEEE- 2017)
2. Hashmi, M.U., & Jayesh, G.P. (2015). Anti-theft Energy Metering for Smart Electrical Distribution System. International Conference on Industrial Instrumentation and Control(ICIC) ,May 28-30
3. Ganurkar, S., & Gour, P. (2014). Prepaid Energy Meter for Billing System Using Microcontroller and Recharge Card. International Journal Of Core Engineering & Management (IJCEM) 1, Issue 1, April.
4. Pradeep Mittall 2015, Wireless Electricity billing system, International Research Journal of Engineering Technology (IRJET) Volume: 02,pp.21-34.
5. J.L.Parra and E.A.S.Calderon 2013, Use of shunts detecting equipment for the identification of illegal power outlets, International Journal of Innovative research in science, engineering and technology, pp. 1

Control strategy of Permanent Magnet Brushless DC Motor with Snubber circuit using Fuzzy Logic Control

Mr. V. C. Eugin Martin Raj[1]
Associate Professor,
Department of Electrical and Electronics Engineering,
St. Anne's College of Engineering and Technology,
Anguchettypalayam, Panruti – 607106.

Mr. P. Harish[2], Mr. M. Praveen Kumar[3], Mr. S. Anbumathi[4], Mr. S. Selvaraj[5]
UG Students,
Department of Electrical and Electronics Engineering
St. Anne's College of Engineering and Technology,
Anguchettypalayam, Panruti – 607106.

Abstract - Brushless DC (BLDC) motors are widely used for many industrial applications because of their reliability, high efficiency, high starting torque, and less electrical noise. For the speed control of BLDC motor, different controllers are used. In this work, the performances of BLDC motor have been evaluated without controller and with conventional controllers PI and PID. The results have been compared with fuzzy based controller. In comparison with conventional controllers, fuzzy controller gives effective speed response but conventional controllers provide better response with changing load. At the same time the additional snubber circuit will be used to increase the dv/dt and di/dt proctetion. MATLAB/SIMULINK software is used to carry out the above investigation.
***IndexTerms*—BLDC motor, PI controller, PID Controller, Fuzzy controller, Snubber Circuit.**

I. INTRODUCTION

Industries use mainly two types of motors: (i) dc motors where the flux is produced by the current through the field coil of the stationary pole structure, (ii) permanent magnet brushless dc motors where the permanent magnet provides the necessary air gap flux instead of wire wound field poles. As the brushless DC motors do not have brushes, the commutation takes place electronically. BLDC motor is actually a permanent magnet synchronous motor (PMSM) with trapezoidal back EMF [1].

BLDC motors comprise several attractive properties such as smooth speed control and torque –speed characteristics [1]. Moreover, the control of DC motor also simple and does not requires complex Hardware [2] and [3]. But, DC motors have main disadvantages regarding to lifetime of brushes are the limited. A lower reliability occurs caused by the brushes and the operation need time to time maintenance of replacement [4].

Proportional Integral and Derivative (PID) controllers have been used in industrial control applications for a long time. PID controllers date to 1890s governor design. Despite having been around for a long time, majority of industrial applications still use PID controllers. According to a survey in 1989, 90% of process industries use them. This widespread use of PID in industry can be attributed to their simplicity and ease of re-tuning on-line.

The PID controller is so named because its output sum of three terms, proportional, integral and derivative term. Each of these terms is dependent on the error value e(t) between the input and the output,

$$output = k_p e(t) + k_i \int_0^t e(t)dt + k_d \frac{de(t)}{dt}$$

where Kp, Ki and Kd are the P, I and D parameters respectively. These terms determine the type of system response. The properties of P, I and D are discussed briefly here.

The effects of each of controller parameters, Kp, Ki and Kd on a closed-loop system are summarized in the table below.

Control Parameter	**Rise Time**	**Overshoot**	**Settling Time**	**Steady State Error**
Kp	Decrease	Increase	Small Change	Decrease
Ki	Decrease	Increase	Increase	Eliminate
Kd	Small Change	Decrease	Decrease	No Change

Table 1.1: Effects of control parameters

There have been various types of techniques applied for PID tuning, one of the earliest being the Ziegler Nichols technique. These techniques can be broadly classified as classical and computational or optimization techniques. This paper discusses about modeling and speed control techniques of BLDC motor using open loop and closed loop with conventional controllers-PI, PID controller and fuzzy controller also. The performance of speed control of BLDC motor is verified through simulation analysis on MATLAB Simulink platform.

II. BLDC MOTOR OPERATIONAL PRINCIPLE

BLDC motors use mechanical commutator and brushes to achieve the commutation. However, BLDC motors are truly an inside-out DC Commutator with the mechanical commutator replaced by an electronic switching converter. The stator of BLDC motors is the coil, and the rotor is the permanent magnet. The stator develops the magnetic field to make the rotor rotating. Hall Effect sensors detect the rotor position as the commutating signals. Therefore, BLDC motors use permanent magnet instead of coil in the armature and do not need brushes. For the three phases BLDC motors, the back-EMF and phase current waveforms with 120° conduction mode are shown in Figs. 1, 2, [5] and [6].

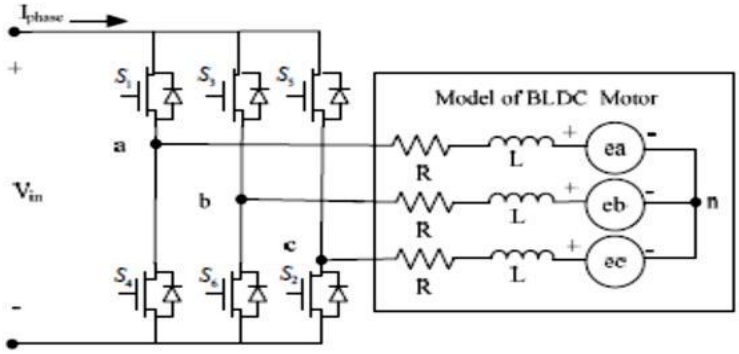

Fig 2.1: Circuit diagram of BLDC motor drive system

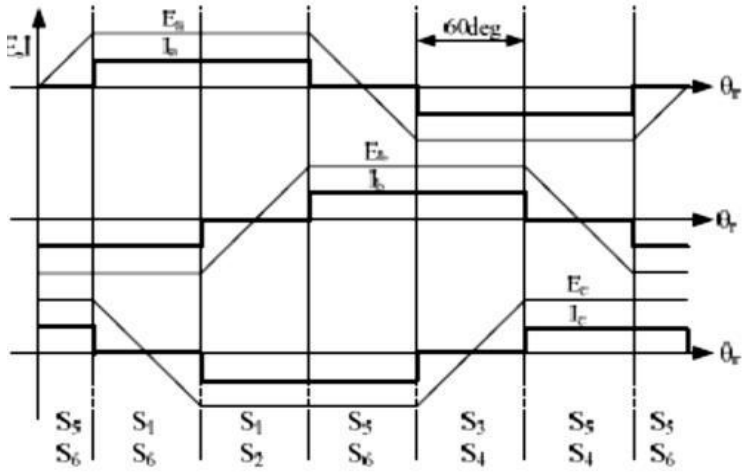

Fig2.2: Trapezoidal back emf pattern and referencecurrent generation

III. MATHEMATICAL MODELING OF BLDC MOTOR

Dynamic equations BLDC motor is represented as following:

$$\begin{bmatrix} v_a \\ v_b \\ v_c \end{bmatrix} = \begin{bmatrix} R & 0 & 0 \\ 0 & R & 0 \\ 0 & 0 & R \end{bmatrix} \begin{bmatrix} i_a \\ i_b \\ i_c \end{bmatrix} + \begin{bmatrix} L-M & 0 & 0 \\ 0 & L-M & 0 \\ 0 & 0 & L-M \end{bmatrix} \frac{d}{dt} \begin{bmatrix} i_a \\ i_b \\ i_c \end{bmatrix} + \begin{bmatrix} e_a \\ e_b \\ e_c \end{bmatrix}$$

where v_a, v_b, v_c are the phase voltages, i_a,i_b, i_c are the phase currents, e_a, e_b, e_c are the phase back-EMF waveforms, R is the phase resistance, L is the self inductance of each phase and M is the mutual inductance between two phases. So electromagnetic torque can be obtained as:

$$T_e = \frac{1}{\omega_r}(e_a i_a + e_b i_b + e_c i_c)$$

where ωr is the mechanical speed of the rotor. The equation of motion is:

$$\frac{d}{dt}\omega_r = (T_e - T_L - B\omega_r)/J$$

The electrical speed ω_e is related to the mechanical speed for a motor with P numbers of poles as following:

$$\omega_e = (P/2)\omega_r$$

where P is the number of poles, ω_r is the rotor speed in rad/sec.

IV. CONTROL OF BLDC MOTOR

The speed control of BLDC motor with conventional controller and fuzzy controller has been investigated.

4.1 P-I Controller

P-I Controller is mainly used to eliminate the steady state error. Since P-I controller has no ability to predict the future errors of the system it cannot decrease the rise time and eliminate the oscillations. The output of the PI controller in time domain is defined by the following equation:

$$output = k_p e(t) + k_i \int_0^t e(t)dt$$

where Kp is the proportional gain, Ki is the integral gain and e(t) is the instantaneous error in the signal.

4.2 P-I D Controller

P-I-D controller has the optimum control dynamics including zero steady state error, fast response (short rise time), no oscillations and higher stability. The necessity of using a derivative gain component in addition to the PI controller is to eliminate the overshoot and the oscillations occurring in the output response of the system. Its output sum of three terms, proportional, integral and derivative term. Each of these terms is dependent on the error value e(t) between the input and the output:

$$output = k_p e(t) + k_i \int_0^t e(t)dt + k_d \frac{de(t)}{dt}$$

where K_d is the derivative gain.

4.3 Fuzzy Logic Controller

MATLAB Fuzzy logic Toolbox is use to design fuzzy logic controller. Basically, the Fuzzy Logic controller consists of four basic components: fuzzification, a knowledge base, inference engine, and a defuzzification interface. The addition of fuzziness to data in fuzzy logic is called the fuzzification. fuzzy linguistic descriptions are formal representation of system made through fuzzy IF-THEN rules. They encoded knowledge about a system in statements of the form- IF (a set of conditions) are satisfied then (a set of consequents) can be inferred. The conversion of a fuzzy set to single crisp value is called defuzzification. [7] and [8]. In Mamdani type FIS the crisp result is obtained by defuzzification, in the Mamdani FIS can be used for both multiple inputs and single output and multiple inputs multiple outputs system [9].

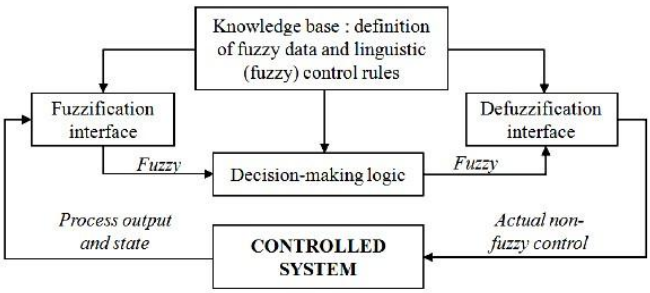

Fig 4.1: Block diagram of Fuzzy Logic Controller

The BLDC motor has been simulated in the MATLAB/SIMULINK environment. Fig.4.2 shows the Simulation model of BLDC motor wihout controller. The motor is fed by a PWM inverter. The inverter gates signals are produced by decoding the Hall Effect signals. Various parameters used for simulation shown in Table 4.1

Stator phase resistance	2.8750 ohm
Stator phase inductance	8.5 mH
Number of Slots	18
Voltage constant	40 V/Krpm
Number of poles	16
Number of phases	3
Voltage input	24 V
Power input	40 W
Proportional constant	0.0015
Integral constant	0.25

Table 4.1: Parameters used for simulation of BLDC motor

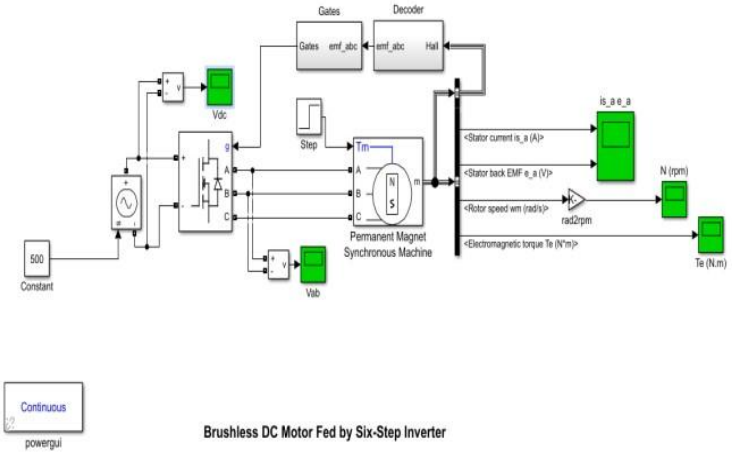

Fig 4.2: Simulation model of BLDC motor without controller

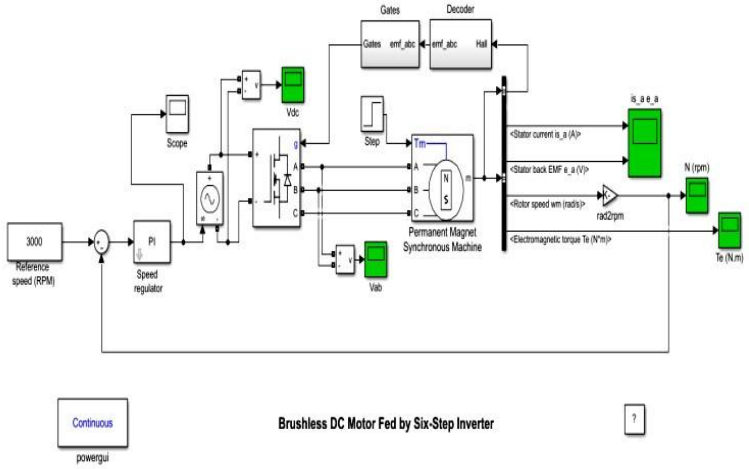

Fig 4.3: Simulation model of BLDC motor with PI controller

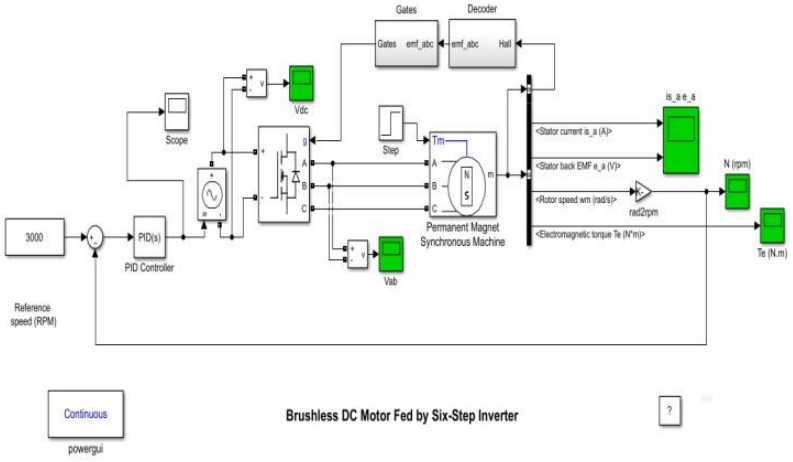

Fig 4.4: Simulation model of BLDC motor with PID controller

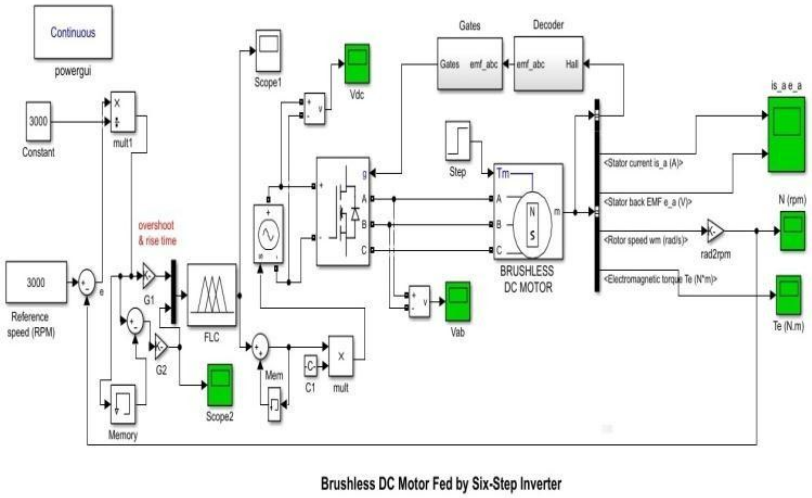

Fig 4.5: Simulation model of BLDC motor with Fuzzy controller

From speed time waveform it can be seen that speed of motor is directly proportional input voltage. Speed is a function of voltage. Speed of BLDC motor can be controlled by applied voltage. The speed of BLDC motor can be controlled using proportional integral (PI) controller, PI controller can regulate the duty cycle hence control the voltage applied to BLDC motor. Speed of BLDC motor is directly proportional to applied voltage. Speed of BLDC motor can be set to reference speed. Any diversion from this speed will be given as an error signal to PI controller. PI controller will take appropriate signal on receiving of this error signal; it can increase as well as decrease the duty cycle of applied gate signal.

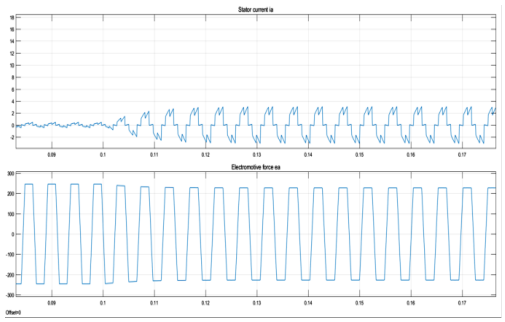

(a)

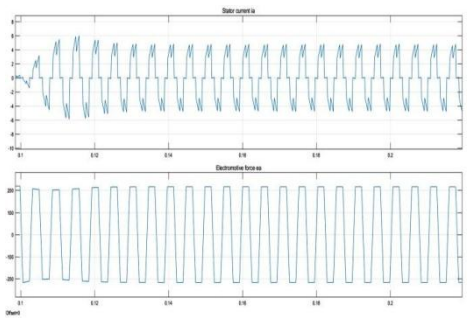

(b)

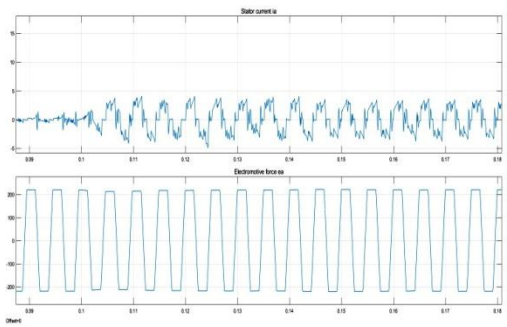

(c)

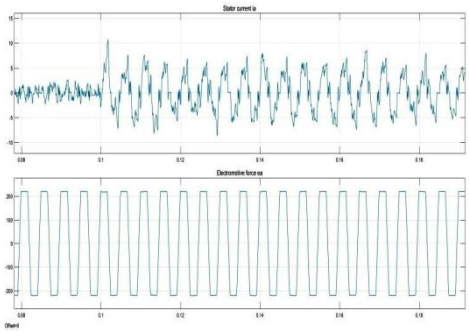

(d)

Fig 4.6: Stator Current and Back EMF of Phase A (a) without controller (b) PI controller (c) PID Controller (d) Fuzzy Controller

The Fuzzy Logic Controller has been designed using the MATLAB Fuzzy Toolbox and the membership function editor developed is as shown in Fig.4.7. In the present work, Mamdani based fuzzy system has been used. For controlling the speed of BLDCM, error in speed and rate of change in speed are taken as the input variables:

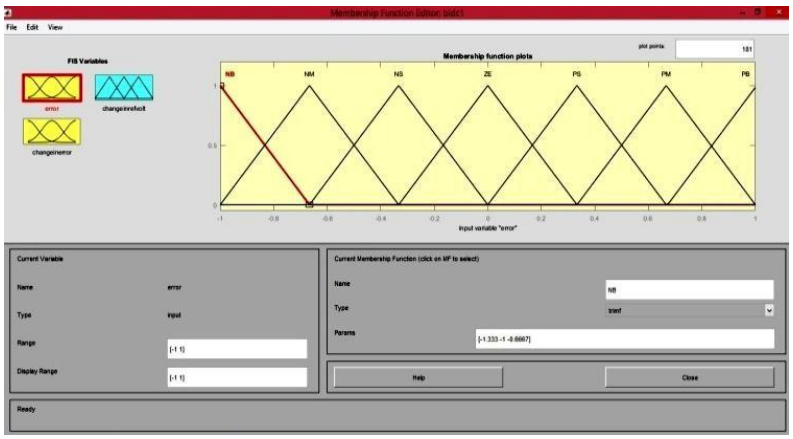

Fig 4.7: Membership function editor for fuzzy controller

Hence in the present work, a fuzzy system with two inputs and one outputs are simulated. The triangular membership has been used for its simplicity and great performance. Each universe of discourse has been divided into seven fuzzy sets such as Negative Big (NB), Negative Medium (NM), Negative Small (NS), Zero (ZE), Positive Small (PS), Positive Medium (PM), Positive Big (PB). A rule base consisting of forty nine fuzzy rules has been developed based on the pre-defined membership functions of the two inputs (e is the error; ce is the change in error). The rule base has been included in the Fuzzy Interface System Editor of the present work by means of the Rule Editor.

de \ e	NB	NM	NS	ZE	PS	PM	PB
NB	NB	NB	NB	NB	NM	NS	ZE
NM	NB	NB	NB	NM	NS	ZE	PS
NS	NB	NB	NM	NS	ZE	PS	PM
ZE	NB	NM	NS	ZE	PS	PM	PB
PS	NM	NS	ZE	PS	PM	PB	PB
PM	NS	ZE	PS	PM	PB	PB	PB
PB	ZE	PS	PM	PB	PB	PB	PB

Table 4.2: Fuzzy rule matrix

Parameter\ Controller	PI Controller	PID Controller	Fuzzy Controller
Rise Time	14.580 ms	12.288 ms	11.850 ms

Overshoot (%)	4.737%	No overshoot	0.274%

Table 4.3: Comparison of different controller parameters

V. CONTROL OF BLDC MOTOR USING ADDITIONAL SNUBBER

Snubbers are used in electrical systems to reduce the transient across the device while switching ON/OFF the device. While having a transient this may cause electromagnetic disturbance which in turn creates interference with nearby circuits. The snubber prevents this undesired voltage by conducting transient current around the device.

Semiconductor switch turns on from 10µs to 100µs. At that time the voltage across them falls and the current through the switch rises. These extremely large and fast edges create massive amount of trouble, as a result semiconductor switch may actually burns itself and the EMI contaminates the entire power distribution system. The solution is to add a few components to snub these transients, slowing them or diverting them while protecting the power system from interference. In general snubbers used for load line shaping, to reduce switching losses, reduces turn off dv/dt, controllable working current is much greater, device heating is minimized, reduces the peak power and average power dissipate, power dissipation is avoided, reduces voltage transients.

Snubber circuit basically consists of a series connected resistor and capacitor placed in shunt with semiconductor switch. Generally snubbers to slow the rate of rise of this current. Inductor opposes a change of current, so placing an inductor in series with the semiconductor switch

Closed loop system is simulated using Matlab/Simulink. The simulink model of closed loop controlled buck converter fed PMBLDC drive system without and with snubber is shown in Figure 4.18 and Figure 4.23. Here 48V DC is stepped down to 24V DC using a buck converter. The output of buck converter is filtered using pi-filter. The output of the pi-filter is applied to the three phase inverter, the inverter produces three phase voltage required by the PMBLDC motor. The technical specifications of the drive systems are as follows

Input voltage	:	48 V DC
Buck output voltage	:	24 V DC
Pulse width to Buck MOSFET	:	0.5 duty cycle (50%)
Toff	:	50%
Pulse width (33%) to Inverter MOSFET	:	120 mode of operation.

5.1 Parameters of BLDC Motor.

The inverter is a MOSFET bridge.

Stator resistance Rs	:	2.8750 ohms
Stator Inductance Ls	:	$8.5e^{-3}$ Henrys
Flux induced by magnets	:	0.175 Weber's
Back EMF Flat area	:	120 degrees
Inertia	:	0.8x10-3
Friction factor	:	1x10-3
Pole pairs	:	4

Stator windings are connected in star to an internal neutral point.

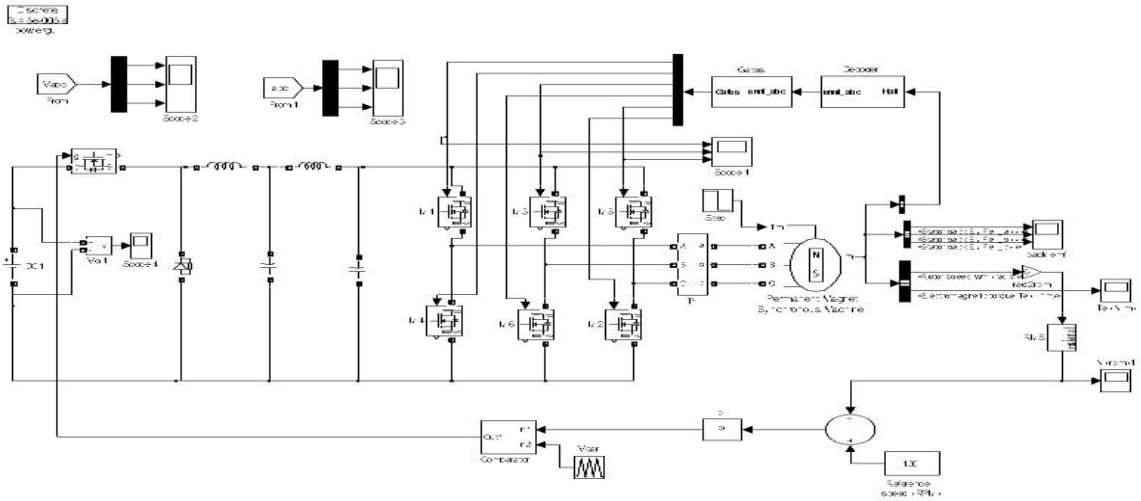

Fig 5.1: Simulink diagram of the closed loop controlled Buck converter fed PMBLDC drive system without snubber

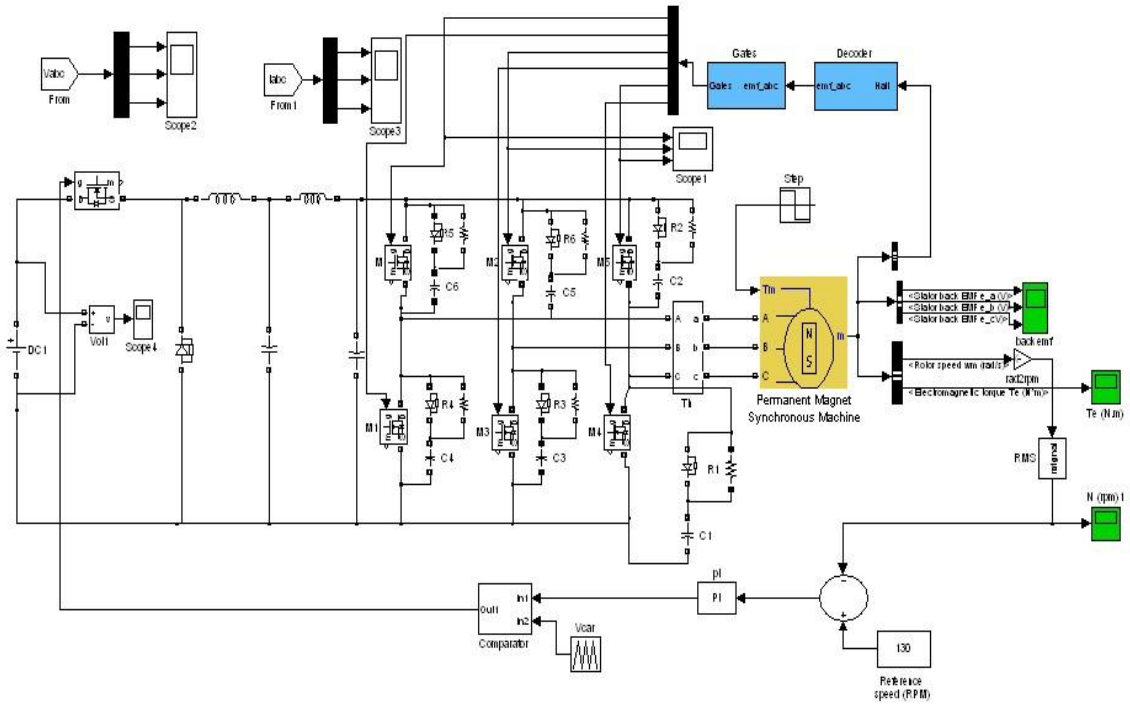

Fig 5.2: Simulink diagram of the closed loop controlled Buck converter fed PMBLDC drive system with snubber

Buck Converter	Voltage Spike (Volts)	Current Spike (Amps)
Without Snubber	1.8	1.2
With Snubber	0.5	0.8

Table 5.1 Comparison of Buck Converter with and without snubber

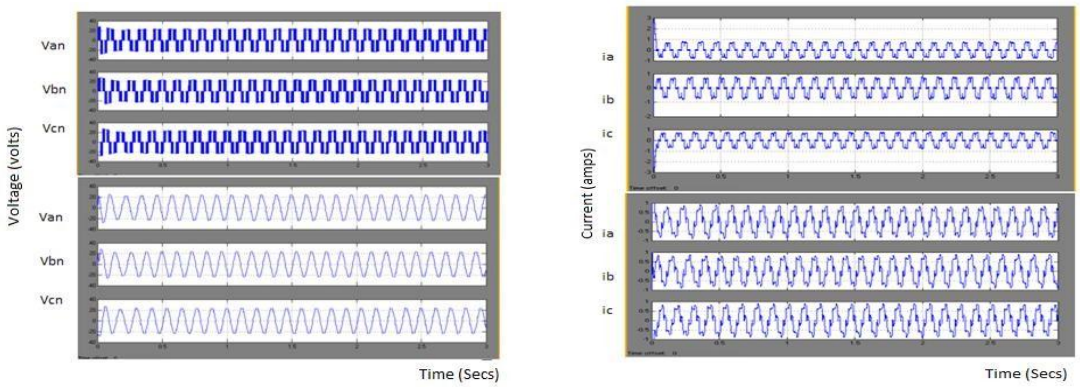

(a) **(b)**

Fig 5.3: (a) Inverter phase voltages without snubber and with snubber; (b) Inverter output current without snubber and with snubber

VI. CONCLUSION

The currents are balanced and they are displaced by 120º. The comparison of voltage and current spikes with and without snubber are given in Table 4.1. The height of the spike is reduced by introducing the snubber.

Closed loop controlled PMBLDC drive system is simulated using MATLAB/SIMULINK and the above results were derived. Buck converter is proposed to reduce the input voltage to the required value. Closed loop Buck controlled PMBLDC drive systems with and without snubber is modeled and simulated using MATLAB/SIMULINK and the results are presented. This drive system has advantages of reduced switching losses. With the presence of snubber circuit the voltage spikes are reduced by 72% and current spikes are reduced by 33%, which in turn improves the output response.

REFERENCES

1. Lokesh Kumar Agarwal, Bhavesh Kumar Chauhan, G. K. Banerjee., "Speed Control of Brushless DC Motor Using Fuzzy Controller", International Journal of Pure and Applied Mathematics, Volume 119, No. 15, 2018, 2689-2696.
2. Balogh Tibor,Viliam Fedak, Frantisek Durovsky., "Modeling and Simulation of the BLDC Motor in MATLAB GUI", Proceedings of the IEEE Fifth International Conference on Fuzzy Systems and Knowledge Discovery, US, pp. 1403- 1407, 2011.
3. J.R.Hendershot and T.J.E.Miller, Design of brushless Permanent-magnet Motors; Oxford, UK: Oxford Science, 1994.
4. P.Pillay and R.Krishnan, Modeling, Simulation and Analysis of Permanent-magnet Motor Drives, part II: The brushless DC Motor Drive, IEEE Transactions on Industry applications, vol.25,no.2,march/April 1989.
5. A. K. Wallace and R.Spee, The effects of motor parameters on the performance of brushless DC drive, IEEE Transactions on Power Electronics, vol.5, no.1, pp.2-8, January 1990.
6. Grasblum P., "3-phase BLDC motor contents control with Hall sensors using DSP56F80x,", Motorola App Note AN1916/D, 2004.

7. Ji Hua, Li Zhiyong, "Simulation of Sensorless Permanent Magnetic Brushless DC Motor Control System", Proc. of the IEEE International Conference on Automation and Logistics, Qingdao, China, pp. 2847-2851, September 2008.
8. Mohd Shahrieel Mohd Aras, Eric Chee Sai Hoo, Mohd Hendra bin Hairi, Syed Najib Bin Syed Salim, Intan Azmira binti Wan Abd Razak, "Comparison of Fuzzy Control Rules using MATLAB Toolbox and Simulink for DC Induction Motor-Speed Control", 2009 International Conference of Soft Computing and Pattern Recognition.
9. S. Rajasekaran, G.A. Vijaylakshmi Pai"Neural Networks, fuzzy logic, and genetic algorithms synthesis and applications", Prentice Hall India, Eastern Economy Edition,(2005).
10. Trapti Yadav, Deepti yadav, Nidhi Singh"Self Tuning PID Controller using Fuzzy Inference Mamdani and Sugeno method on the AVR System". International Journal of Applied Engineering Research ISSN: 0973-4562, Volume 8, No.12, 2013.

Carrier level shifted based control method for the PWM 3L-T-type qZS with capacitor imbalance compensation

Mr. V. Balaji[1]
Assistant Professor,
Department of Electrical and Electronics Engineering,
St. Anne's College of Engineering and Technology,
Anguchettypalayam, Panruti– 607106.

Mr. C. Vignesh[2], Mr. M. Vignesh[3], Mr. G. Ragul[4], Mr. Mohamed Shaffiullah[5]
UG Student,
Department of Electrical and Electronics Engineering
St. Anne's College of Engineering and Technology,
Anguchettypalayam, Panruti– 607106.

Abstract - ***This paper presents a modified carrier level- shifted based control method for a pulse width modulation controlled three-phase three-level T-type quasi-impedance source inverter. The benefits of the proposed strategy are a uniform distribution of shoot-through states of constant width throughout the fundamental period and the mitigation of the inner capacitors' voltages imbalance. The latter is achieved by means of a proportional-integral controller, which adjusts the relative time application of redundant states. The improved performance is demonstrated in terms of reliability, as the capacitors do not suffer from neutral point imbalance. The control method can also be implemented in a different multilevel inverter configuration with an impedance-source network. A comprehensive simulation study and several experiments were performed in order to validate the adopted method in situations of imbalanced capacitor voltages.***

***Index Terms*— Quasi and T - type.**

I. INTRODUCTION

An increasing energy demand, lack of conventional energy resources, growing concern over environmental pollution, and concept of on-site energy generation have led to the rapid rise in renewable energy generators. Most of these generators are inverter-based, both in connection to the lowvoltage distribution network and in islanded operation. As of2015, many of them interact with photovoltaic (PV) modules [1], considered one of the most promising technologies, with a cumulative installation capacity of 227 GW [2]. Some studies have identified benefits in PVsystems without galvanic isolation [3], as well as in the use of three-level inverter (TLI) topologies within the residential sector [4], [5]. The main advantages of the former include higher performance, higher power density, and lower cost—due to the absence of the transformer. In comparison with their two-level counterparts, TLIs show advantages in lower power switching losses from commutating only half of the dc-link voltage, better harmonic performance at the output, and a reduced ac output filter [4]. A relatively recent multilevel topology is that of the T-type inverter [6], [7], causing several manufacturers to compete for a lead in the market. In comparison with the more mature neutral point- clamped (NPC) [8], the T-type inverter only needs a single power switch to clamp the middle point to the positive or negative dc rail. This reduces conduction losses, consequently lowering power switching losses at lower switching frequencies [5]. However, because the outer switches of the T-type inverter have to block the full dc-link voltage, the

NPC inverter may be a better solution at higher switching frequencies, when switching losses become more significant [5]. Though the T-type is also constrained by performing just voltage-buck operations, recent solutions based on impedance-source (IS) networks [9]–[12] are able to overcome this limitation. IS-based inverters do not suffer from shoot-through (ST) states, and most of them have a continuous input current. This family of converters increases the input voltage range regulation [13], a typical requirement in PV installations, avoiding an intermediary dc–dc boost converter. The three-level T-type quasi-impedance-source inverter (3LT- type qZSI) has been proposed and analyzed in only a few pieces of literature [14], [15] but is considered a potential and competitive design in the field of PV inverters. Fig. 1(a) presents the considered topology and Fig. 1(b) shows its simplified switching circuit. The control and switching signal generation for this configurationmust be carefully analyzed and the balance of the neutral point assured. There are several pulsewidth modulation (PWM) techniques that can be applied to IS-based inverters, such as simple boost control [16], maximum boost control [17], and maximum constant boost control [18]. These were later extended to control other IS multilevel inverters.

II. OPERATION WITH UNBALANCED CONDITIONS

Second simulation test is conducted to analyze the operation of the inverter in situations of imbalanced capacitor voltages. Different load and output filter values per phase are connected to the system in order to generate intentionally unbalanced voltages (vC2 and vC3). At the same time, to produce a greater imbalance, capacitors C2 and C3 have slightly different as well as the estimated constant values of the proposed PI controller, which will be further discussed in details. The rest of the parameters remain the same as in Table I. In this simulation case, input voltage is set to 220 V and the same Ds was also considered. The main simulated waveforms are presented in Fig. 8. Fig. 8(a) shows the input current and voltage, where a low-frequency pulsation is appreciated. The low-frequency pulsation, resulting from imbalanced conditions, is also seen in the dc-link voltage, depicted in Fig. 8(c). Fig. 8(b) shows the voltages across inner capacitors (vc2 and vc3) and their difference. As expected, C2 exhibits a higher voltage, while C3 has a higher ripple. The difference between them represents the voltage imbalance of the neutral point. If this situation is not controlled, the converter may be damaged. The output current per phase [see Fig. 8(d)] demonstrates the high degree of imbalance.

2.1 Compensation With Neutral-Point Unbalanced Conditions

The stability of our system with the proposed closed loop control scheme based on a PI controller, for mitigating the capacitor voltage imbalance is discussed in this section. The equivalent circuit for this situation is presented in Fig. 9(a), which allows different charge/discharge ratings of inner capacitors. The block diagram of the proposed PI-based control is depicted in Fig. 9(b), where Δvc is the measured variable, C(s) and G(s) represent the transfer functions of the controller and plant, respectively, and γ is the common compensation control action.

III. EXPERIMENTAL VERIFICATION

An experimental prototype was built to further validate the proposed modulation method with imbalance compensation. This section summarizes the assembling procedure of the 3L-Ttype qZSI and describes the main components for experimental verification. The 3L-T-type inverter assembly is based on the 12MB150VX-120-50 IGBT module from Fuji Electric [see Fig. 12(a)]. It is configured to have 1200 V and 50 A 12 RBIGBT in one package with highlighted advantages as size reduction and significant low power loss. The values of the passive elements (qZSN and output filter) are the same than the ones calculated for the simulation study. Diodes for the qZSN are based on the silicon carbide Schottky diode

C3D10060G from CREE. A driver board [see Fig. 12(b)] for the AT-NPC 3-level 12in1 IGBT module is used to drive the power module, provided by Fuji Electric as well. Gate peripheral circuits are based on the ACPL-333J driver from Avago Technologies with a builtin function for short-circuit protection. The control unit is the dSPACEMicroLabBox [see Fig. 12(c)] with a 2-GHz dual-core real-time processor, programmable field-programmable gate array (FPGA), and analogical/digital channels. The proposed carrier level-shifted modulation technique was programmed on a host PC in MATLAB/Simulink to run on ControlDesk software in real time at a sampling rate of 10 kHz. In order to embed the ST states into the conventional ones, another board with 74AC11032 chips (or gates) from Texas Instruments was designed. Finally, the measurement board (with the aim of implementing the common compensation tomitigate the neutral-point imbalance) includes two LEM LV 25-P voltage sensors. A general schematic of implementation of the proposed modulation technique and its different stages are presented in Fig. 13.

3.1 Experimental Results With Unbalanced Neutral-Point Conditions

This test analyzes the unbalanced situation without the PI controller for common compensation. Input voltage is set to 220 V, and the intentional imbalance is produced as in the corresponding simulation case (parameters are presented in Table II). The main waveforms are depicted in Fig. 16. Fig. 16(a) shows the input current and voltage, with the expected low-frequency pulsation resulting from imbalanced conditions. This effect is also transferred to the dc-link voltage, depicted in Fig. 16(c). Fig. 16(b) shows the voltages across inner capacitors (vc2 and vc3) and their difference. This neutral-point imbalance may be. the cause of potential fault on the converter performance. The different output currents per phase are presented shows the experimental results obtained after PI controller operation.

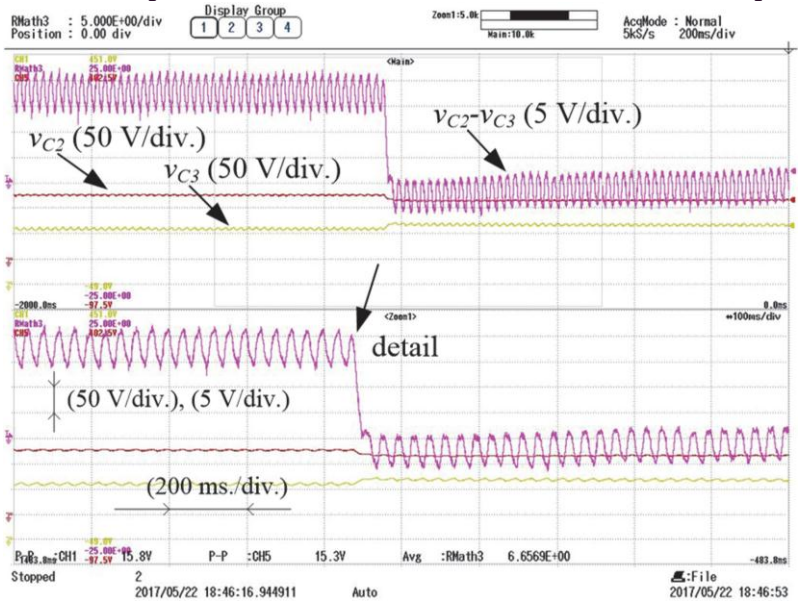

Fig 3.1 Experimental results obtained after PI controller operation

The ripples of input current and dc-link voltage are quite similar to those in the situation without the controller [see Fig. 17(a) and (c)], but the difference (vc2 − vc3) [see Fig. 17(b)] has been reduced adequately. The output current shown in Fig. 17(d) has a little bit more distortion than in the previous case without the common compensation. THDI of each measured current was calculated and is presented in Table III. It is worth to notice the good agreement between simulation and experimental studies. Finally, the transient process of the PI controller action is presented in Fig. 18. The reduction of the voltage difference (vc2 − vc3) is achieved very quickly.

V. CONCLUSION

This study proposed a new modulation technique that can be applied to any IS-based multilevel inverter. Its main capabilities include generating ST states of constant width throughout the entire fundamental period and balancing the neutral-point voltage altogether. These advantages allowed the reduction of the passive component rating and increased reliability in comparison with previously reported methods. The proposed idea was successfully validated by simulations and by a prototype based on the 3L-T-type qZSI topology. The selection of the controller parameters directly affected the quality of the output current. The method also presented a high level of simplicity in its implementation.

REFERENCES

1. E. Romero-Cadaval, G. Spagnuolo, L. G. Franquelo, C. A. Ramos-Paja, T. Suntio, and W. M. Xiao, "Grid-connected photovoltaic generation plants: Components and operation," IEEE Ind. Electron. Mag., vol. 7, no. 3, pp. 6–20, Sept. 2013.
2. REN21, "Renewables 2016: Global status report," 2016. [Online]. Available: http://www.ren21.net
3. T. Kerekes, R. Teodorescu, P. Rodriguez, G. Vazquez, and E. Aldabas, "A new high-efficiency single-phase transformerless PV inverter topology," IEEE Trans. Ind. Electron., vol. 58, no. 1, pp. 184–191, Jan. 2011.
4. R. Teichmann and S. Bernet, "A comparison of three-level converters versus two-level converters for low-voltage drives, traction, and utility applications," IEEE Trans. Ind. Appl., vol. 41, no. 3, pp. 855–865, May 2005.
5. M. Schweizer, T. Friedli, and J. Kolar, "Comparative evaluation of advanced three-phase three-level inverter/converter topologies against twolevel systems," IEEE Trans. Ind. Electron., vol. 60, no. 12, pp. 5515–5527, Dec. 2013.
6. M. Schweizer and J. Kolar, "Design and implementation of a highly efficient three-level T-type converter for low-voltage applications," IEEE Trans. Power Electron., vol. 28, no. 2, pp. 899–907, Feb. 2013.
7. Nabae, I. Takahashi, and H. Akagi, "A new neutral-point-clamped PWM inverter," IEEE Trans. Ind. Appl., vol. IA-17, no. 5, pp. 518–523, Sept. 1981.
8. O. Ellabban and H. Abu-Rub, "Z-source inverter: Topology improvements review," IEEE Ind. Electron. Mag., vol. 10, no. 1, pp. 6–24, Mar. 2016.

TABLE OF CONTENT

Investigation on Utilization of Biogas & Prosopis Juliflora Biodiesel in Dual Fuel Mode in a Single Cylinder Diesel Engine

Mr. R. Sasikumar,
Assistant Professor,
Department of Mechanical Engineering,
St. Anne's College of Engineering and Technology,
Anguchettypalayam, Panruti – 607106.

Mr. K. Shanmugaelango
Associate Professor,
Department of Mechanical Engineering
St. Anne's College of Engineering and Technology,
Anguchettypalayam, Panruti – 607106.

Mr. R. Jayakumar
Assistant Professor,
Department of Mechanical Engineering
St. Anne's College of Engineering and Technology,
Anguchettypalayam, Panruti – 607106.

Abstract - In this work, experiments were accomplished on a single cylinder DI diesel engine by means of using bio-gasoline as a primary gas and prosopis juliflora biodiesel and diesel oil as secondary fuels in twin gas operation. the experiments were executed to degree overall performance parameters i.e. (brake specific fuel consumption, brake thermal efficiency and exhaust gas temperature) and emission parameters together with carbon monoxide, carbon dioxide, nitrogen oxide unburned hydro carbon and smoke and so forth. At one-of-a-kind load conditions. For the twin-fuel system, the consumption device of the check engine became changed to convert into biogas and biodiesel of a twin-fuelled combustion engine. Biogas turned into injected during the consumption procedure by means of gas injectors. the take a look at confirmed that, the engine performance parameters like BP, BTE and EGT gradually increase with increase in engine load for all check situations the usage of both pilot fuels diesel and PJFO. However, the BSFC of the engine confirmed lowering slope with increase in engine load for all check conditions. Above 40% engine load the BSFC values for all check fuels are very near every other. The engine emission evaluation confirmed that the CO2, CO and NOX emissions increase with boom in engine load for each single and twin gasoline mode operation the usage of both pilot fuels. The NOX awareness of exhaust gases in dual gasoline mode is superior than that of single mode.

Keywords: Biodiesel; Biogas; Dual fuel; Engine performance; Exhaust emission.

I. INTRODUCTION

These days, due to the rapid depletion, rising charges, uncertainty in supply and ever increasing demand of petroleum and most importantly stricter emission norms have triggered an extensive research for alternative fuels. Subsequently fuels which can be renewable, smooth burning and can be produced in a decentralized manner are being investigated as alternative fuels. Over few decades, lot of studies has gone into use of alternative fuels in IC engines. Diesel fuel is essentially fed on via the transportation quarter, agriculture & power manufacturing. Thermodynamic tests based on the engine overall performance opinions have hooked up the feasibility of the usage of distinct bio-fuels [1]. It far biodegradable, non-poisonous and possesses low emission profiles. The term bio-gas is noted opportunity fuel which is produced from biomass. Bio-diesel is a surroundings pleasant alternative liquid gasoline for the diesel. Biodiesel is produced by a transesterification process of vegetable oils, animal fats and waste oils. Chemically, bio-diesel is known as the mono-alkyl-esters of lengthy-chain-fatty acids derived from renewable liquid gasoline. The benefits of biodiesel are that it reduces the formation of sulphur dioxide (SO2), CO, HC and pm emissions throughout the combustion system due to its low sulphur, low fragrant, and the presence of oxygen-containing compounds [2]. Similarly to this, biodiesel has appropriate ignition potential in engine due to its extraordinarily excessive cetane range as compared to that of traditional diesel gasoline [2, 3]. Biogas is produced from anaerobic biodegradation of natural fabric within the absence of oxygen and the presence of anaerobic micro-organisms. it may be created from animal manure waste, waste water and stable waste. It is able to be seemed as an alternative clean power aid in view of its friendly environmental nature in CI engine as it has decrease effect on pollution as compared to fossil liquid fuels. In preferred, it's far produced through the anaerobic fermentation of natural waste in landfills and the anaerobic digestion of sludge, plants, and agro-commercial by-products and animal organic waste. The primary composition of biogas is methane (ch4) (about over 65% via vol.). Due to its higher octane wide variety and automobile-ignition temperature it posses excessive knock resistance [3, 4]. As a result it is suitable for CI engines. Similarly to this, the carbon content material of methane is likewise distinctly low as compared to that of conventional diesel fuel, ensuing in a considerable lower in pollutant exhaust emissions [4, 5]. Due to restricted sources of fossil fuels, alternative solutions had been proposed via many researchers. The ''twin-gas concept'' is one of them that use each conventional diesel and gaseous fuels. Diesel engines, with minor change can be made to perform on gaseous fuels correctly. Such engines commonly have the gaseous gasoline blended with the air in the engine cylinders, both via direct mixing within the intake manifold with air or thru injection at once into the cylinder [5]. Twin fuel CI engines introduce a premixed air–gaseous gas mixture that is ignited at the very last degree of the compression stroke with the aid of a liquid fuel injection (pilot fuel) with excellent ignition homes. Induction of gaseous gasoline, referred to as primary fuel, reduces the consumption of diesel for energy era, which increases the premixed combustion and decreases NO_X and pm emissions compared to diesel engine operation [6]. Many researchers have studied the performance and emission characteristics of the dual-fuel engines fuelled with gaseous-liquid fuels. it became experimentally mentioned that the usage of CNG in a twin gas mode reduces the noise degree, specific fuel intake, and NO_X emissions [6]. But, the hydrocarbon emission extended with a substitution of CNG for seventy five% of the diesel gas. Investigations showed that via taking biogas diesel and biogas biodiesel of soybean oil in a twin gasoline engine the BSFC and BTE of twin gas mode are better and decrease respectively in comparison to single mode operation [7]. However, NO_X and CO_2 emission of biogas-biodiesel is extra than biogas-diesel dual fuel mode, whereas CO and HC emission is lower. it turned into claimed that dual gas operation outcomes in higher output, higher precise gas consumption, superior emissions and

quieter and smoother operation [8]. Experiments have been performed by using thinking about diesel and coir-pith producer fuel in dual fuel mode and it changed into observed that BSFC is greater and BTE is decrease. CO and smoke emissions are higher in dual gasoline mode compared to single mode operation [9].

II. MATERIALS AND METHODOLOGY

2.1 The experimental setup

The equipment used for this have a look at was primarily based on a vertical, four-stroke, single cylinder, regular speed, direct injection, water cooled, and compression ignition engine. It has a bore of 80 mm, a stroke length of 110 mm, a displacement quantity of 553 cm^3 and a compression ratio of 16.5:1.the rated most energy become 3.78 kw at 1500 rpm. The engine becomes coupled with an electrical dynamometer rated at 10 kw and 43.5A. The targeted specs and dimensions of the check engine are summarized in desk 1. The experimental equipment for the twin-gasoline engine consisted of the check engine, the dynamometer and manipulates structures, the exhaust emission analyzer, and the fuel injection machine as proven in Figure 1 and Figure 2. The engine load and velocity have been controlled the usage of an eddy current dynamometer system with a most braking electricity of 10 kw. The exhaust gasoline was analyzed through multi-gas analyzer. The smoke intensity became measured with a Bosch kind smoke meter. The engine oil sump became packed with clean lubricating oil earlier than the begin of test. The diesel and biodiesel fuels have been pressurized with the aid of the excessive stress injector system and the drift price of the biodiesel and diesel fuels become measured with the aid of the gas go with the flow meter. The consumption machine of the test engine changed into modified for a dual-fuel mode. Biogas became injected at some point of the intake method by using a gas injector which became established within the intake pipe (Figure 3). The gasoline waft fee is controlled with the aid of a manage valve. The intake of biogas gasoline was measured the use of a gasoline glide meter.

2.2 Test fuel

The pilot fuels injected into the combustion chamber which acts because the source of ignition, have been traditional diesel gasoline and neat biodiesel. Diesel gasoline became used because the reference gas. The biodiesel used in this study changed into 100% methyl ester of prosopis juliflora oil. The neat prosopis juliflora biodiesel is bought from a commercial biodiesel dealer. The houses of prosopis juliflora oil biodiesel are tested according to ASTM standards within the laboratory and proven in Table 2. The bodily homes of biodiesel are really one-of-a-kind in comparison to diesel gas. It has higher density, viscosity, cetane wide variety and lower LHV (lower heating value) than diesel gas. Biogas is constituted of anaerobic biodegradation of natural solid waste within the absence of oxygen and the presence of anaerobic micro-organisms. The above process is accomplished in a biogas reactor inside a designated time period. The method yields normally methane, carbon dioxide and a stable compost. The homes and composition of biogas depend on the nature and form of the anaerobic digestion reactor in addition to on the character of natural fabric use. Table 3 suggests the homes of biogas.

Table 1. Test engine specification

S. No.	Parameters	Description
1	Make	Kirloskar oil Engines Ltd, India
2	Engine type	4- stroke Single Cylinder Direct Injection Compression Ignition
3	Engine Model	AV-1
4	Rated power	5.2 kW at 1500 rpm
5	Compression ratio	16.5:1
6	Bore x stroke	80 mm x 110 mm
7	Displacement volume	553 cc
8	Injection pressure	220 bar
9	Injection Nozzle Opening	23°BTDC
10	Cooling type	Water-cooled
11	Dynamometer	Eddy Current Type (10kW, 43.5 A)

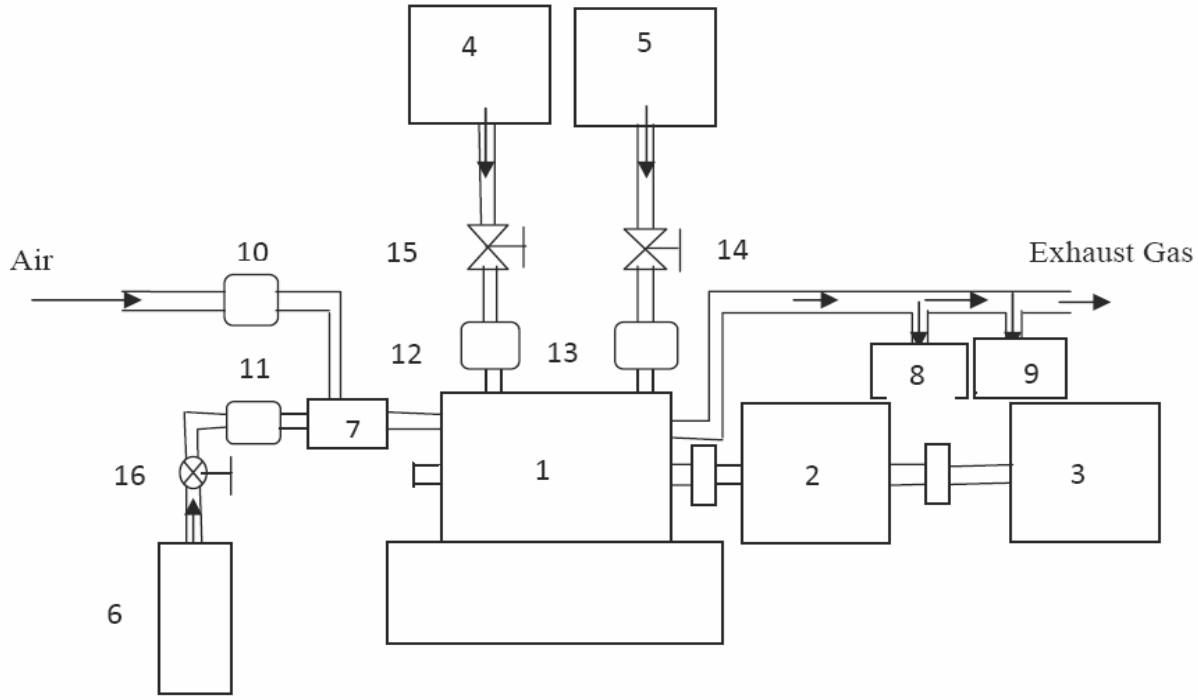

Fig 1. Schematic diagram of the experimental setup

1. Engine, 2. Dynamometer, 3. Loading unit, 4. Diesel Tank, 5. Biodiesel Tank, 6. Biogas Container, 7.Mixing Unit, 8.Exhaust Gas Analyzer, 9.Smoke Meter, 10-13. Flow Meters, 14-16. Control Valve

Table 2. Properties of diesel and PJFO

S. No.	Properties	Diesel	PJFO
1	Density at 20ºC(kg/m3)	850	886
2	Calorific Value (kJ/kg)	44000	41200
3	Viscosity at 40ºC (cSt)	2.87	5.35
4	Flash point (ºC)	76	172
5	Cloud point (ºC)	6.5	14.2
6	Pour point (ºC)	3.1	5.2
7	Iodine No. (g I2/100gm)	-	86.5
8	Acid Value (mg NAOH/g)	-	0.43
9	Cetane Index	52	57.3
10	Moisture Content (mg/kg)	-	0.036

Table 3. Properties of biogas [10-13]

S. No.	Properties value	
1	Methane (%, by vol.)	30–73
2	Carbon dioxide (%, by vol.)	20–40
3	Hydrogen (%, by vol.)	1–3
4	Oxygen (%, by vol.)	0–5
5	Nitrogen (%, by vol.)	5–40
6	Octane number	130
7	Auto-ignition temperature (°C)	632–813
8	Lower heating value (KJ/kg)	26170
9	A/F ratio (by vol.)	17.2
10	Density(kg/m3)	0.65–0.91
11	Boiling point(°C)	(-)126–162

2.3 Experimental procedure

First of all, the engine become began with diesel oil for 15 minutes in single mode operation. As soon as the engine has warmed up, and stabilize then it was converted to twin gas mode in which biogas is furnished because the inducted gasoline and diesel is provided as an induction gasoline. Readings were taken, when the engine changed into operated the use of an

eddy contemporary dynamometer at a constant engine pace of 1500 rpm with different engine loads. The engine masses were 20%, 40%, 60%, 80% and 100%. The performance of the engine became evaluated in phrases of brake thermal performance, brake strength, precise electricity consumption, and emission traits like CO, HC, NO_X and smoke. under biogas/diesel twin-gasoline operation, an attempt has been made to keep the pilot amount of diesel fuel steady, even as the engine strength output become adjusted through the quantity of biogas. After the cease of first observations, the second observations have been taken through thinking about biodiesel and biogas in dual fuel mode below same check conditions. The performance and emissions traits have been also computed.

III. RESULTS AND DISCUSSION

3.1 Brake power

Figure 3 indicates the version in engine power output at exceptional engine loads for single fuel mode and dual gas mode operations of the engine. the parent explains that the energy output of the engine is barely higher during single fuel mode than that of dual fuel mode below all check situations. this is due to better heating cost of diesel and pjfo compared to biogas. the parent also suggests that with growth in engine load, the brake electricity will increase linearly and this is due to the better gasoline consumption price of the engine with growth in load

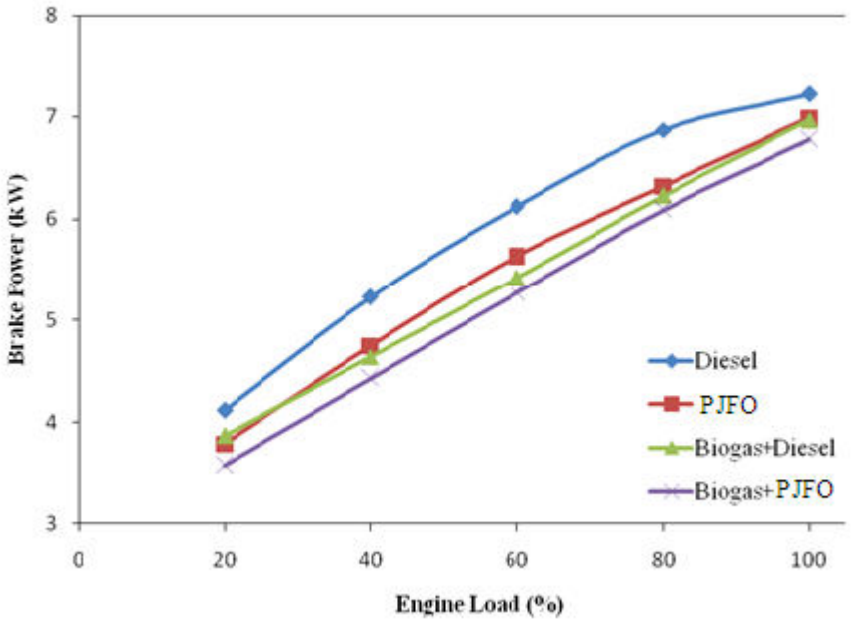

.

Fig.3. Variation of brake power with engine load

3.2 Brake specific fuel consumption

Figure 4 indicates that the BSFC acquired is the sum of the biogas and the liquid fuels i.e. PJFO and petro diesel. At low engine load situations of 20% and 40%, the BSFCs for twin-fuel combustion for both fuels were better than for single-fuel combustion. Those consequences received indicate the lower price of combustion of gaseous fuel because of the lower air–fuel ratio in the combustion chamber and a lower combustion temperature. While the differences in the BSFCs between single and dual-gas combustions are an awful lot decrease at higher engine loads. it become seen that at engine loads over 60%, where a excessive thermal load changed into imposed at the engine, the boom in combustion rate of biogas caused a widespread improvement within the BSFC with twin-gasoline combustions.

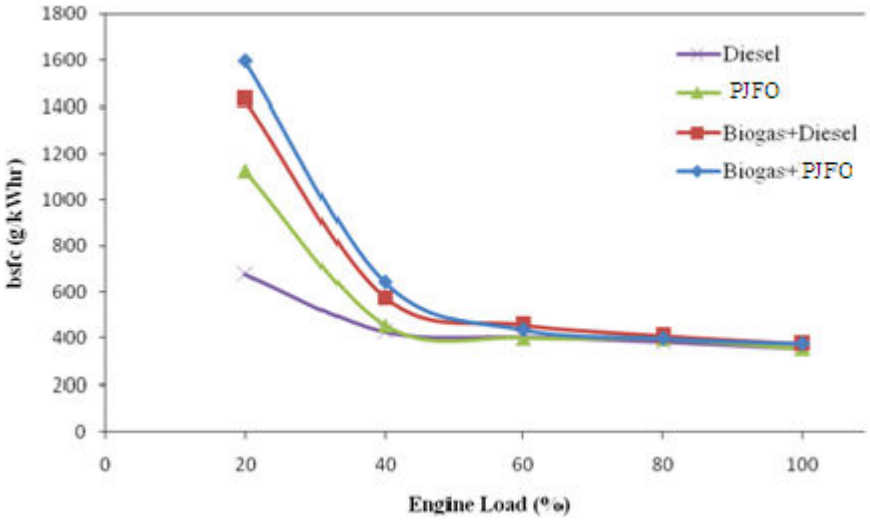

Fig.4. Variation of BSFC with engine load

3.3 Brake thermal efficiency

Figure 5 indicates that the thermal performance of twin-gas combustion for each pilot fuels become decrease as compared to single-gasoline mode at all engine masses. It's been stated that the decrease thermal performance of the dual-fuel combustion is due to the effect of biogas residuals, combustion fuel residuals and occasional combustion temperatures at some stage in the combustion manner [14]. the determine also shows that below excessive load conditions, the brake thermal efficiency is higher in single gas mode operation for diesel as that of PJFO, which is due to the fact the heating value of PJFO is pretty decrease than that of diesel.

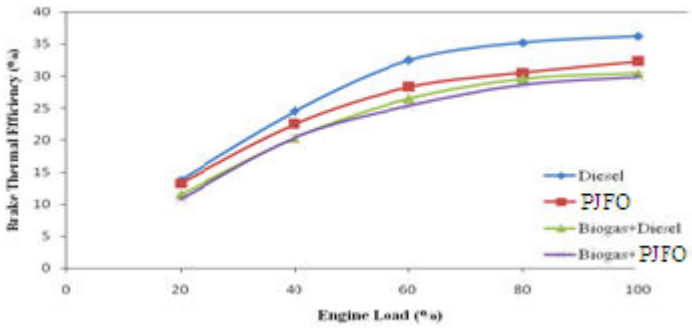

Fig.5. Variation of BTE with engine load

3.4 Exhaust gas temperature

Figure 6 shows the variant of the exhaust gasoline temperature with engine load for all of the gasoline modes. The exhaust temperature measurements have been performed using a thermocouple established on the stop of the exhaust port. On this determine, the exhaust gas temperature will increase linearly as the engine load is expanded due to the increase of general electricity input that's due to better precise gas intake. However, the exhaust fuel temperatures have been observed slightly lower for twin-fuel combustions as compared to single-fuel modes and these differences expanded at higher engine hundreds. The low gas temperature can be explained through the decreased fee temperature with induction of biogas in the engine which acts as warmness sink. It may also be because of that the flame propagation pace of the pilot fuel in intake rate is reduced and then the fuel within the combustion chamber changed into no longer burnt absolutely and consequently the combustion strain and temperature are reduced.

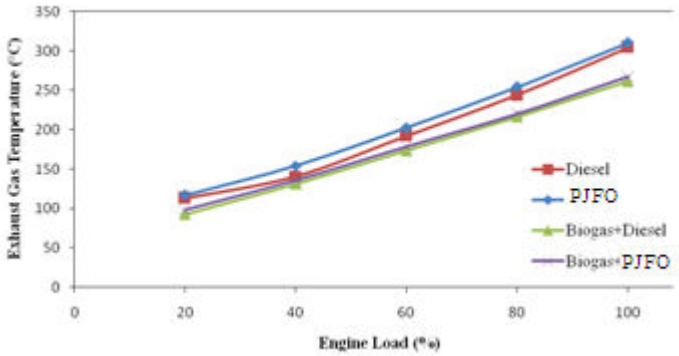

Fig.6. Variation of EGT with engine load

IV. CONCLUSION

To investigate about diverse results of dual-gas combustion of PJFO and biogas alongside diesel on

The overall performance and exhaust emission traits of a single cylinder four stroke DI diesel engine

Under various experimental situations. The following conclusions have been drawn from the evaluation:

1**.** The take a look at outcomes confirmed better brake precise fuel consumption of the engine at 20% and 40% load and comparatively a lot lower BSFC at better engine hundreds. Also the BSFC in twin fuel mode was higher than that of single gasoline mode operation at 20% and 40% loads but it's far almost equal for both modes at higher engine masses.

2. the brake thermal efficiency of the test engine in twin-gas combustion mode for both pilot fuels changed into decrease compared to that during single-fuel combustion mode at all engine loads. it become additionally determined that beneath high load situations i.e. above 60% engine load, the BTE become better in single fuel combustion mode than that of dual gasoline combustion mode.

REFERENCES

1. Murugesan A, Umarani C, Subramanian R, Nedunchezhian N. Bio-diesel as an alternative fuel for diesel engines-a review. Renewable and Sustainable Energy Reviews13 (2009) 653-662.
2. S.H. Yoon, H.K. Suh, C.S. Lee, Effect of spray and EGR rate on the combustion and emission characteristics of biodiesel fuel in a compression ignition engine, Energy and Fuels 23 (2009) 1486-1493.
3. S.H. Park, S.H. Yoon, C.S. Lee, Effect of the temperature variation on properties of biodiesel and biodiesel–ethanol blends fuels, Oil & Gas Science and Technology 63 (6) (2008) 737-745.
4. C. Tricase, M. Lombardi, State of the art and prospects of Italian biogas production from animal sewage: technical-economic considerations, Renewable Energy 34 (2009) 477-485.
5. B.B. Sahoo, N. Sahoo, U.K. Saha, "Effect of engine parameters and type of gaseous fuel on the performance of dual-fuel gas diesel engines-A critical review", Renewable and Sustainable Energy Reviews 13 (2009) 1151-1184.

6. S. Maji, Amit Pal, B.B. Arora, Use of CNG and diesel in CI engines in dual fuel mode, SAE 2008- 28-0072, 2008.
7. Bedoya I.D, Arrieta A.A, Cadavid F.J. Effects of mixing system and pilot fuel quality on dieselbiogas dual fuel engine performance. Bioresource Technology 100 (2009) 6624-6629.
8. Karim GA. The dual fuel engine. In: Evans RL, editor. Automotive alternatives. New York: Plenum Press; 1987. p. 83-104.
9. Ramadhas A.S, Jayaraj S, Muraleedharan C. Dual fuel mode operation in diesel engines using renewable fuels: Rubber seed oil and coir-pith producer gas. Renewable Energy 33 (2008) 2077- 2083.
10. C. Rahmouni, M. Tazerout, O. Le Corre, A method to determine biogas composition for combustion control, SAE 2002-01-1708, 2002.
11. S. Maji, Amit Pal, B.B. Arora, Use of CNG and diesel in CI engines in dual fuel mode, SAE 2008- 28-0072, 2008.
12. M.D. Phan, W. Kanit, Study on biogas premixed charge diesel dual fuelled engine, Energy Conversion and Management 48 (2007) 2286-2308.
13. N. Bahman, P. Vahab, N. Gholamhassan, Y. Talal, G. Barat, Experimental investigation of performance and emission parameters of a small diesel engine using CNG and biodiesel, SAE 2007-32-0075, 2007.
14. Yoon Seung Hyun, Lee Chang Sik Experimental investigation on the combustion and exhaust emission characteristics of biogas–biodiesel dual-fuel combustion in a CI engine. Fuel Processing Technology 92 (2011) 992-1000.
15. G.A. Karim, A review of combustion processes in the dual fuel engine-the gas diesel engine, Progress in Energy and Combustion Science 6 (1980) 277-285.
16. N.N. Mustafi, R.R. Raine, A study of the emissions of a dual fuel engine operating with alternative gaseous fuels, SAE 2008-01-1394, 2008.
17. N. Bahman, P. Vahab, N. Gholamhassan, Y. Talal, G. Barat, Experimental investigation of performance and emission parameters of a small diesel engine using CNG and biodiesel, SAE 2007-32-0075, 2007.

A Review on The Development of Nanotechnology and Nano Materials in Civil Engineering

Mrs. Annie John
Associate Professor,
Department of Electrical and Electronics Engineering,
St. Anne's College of Engineering and Technology,
Anguchettypalayam, Panruti – 607106.

Abstract-Nanotechnology and Nanomaterials is one of the most active research areas with both science and engineering. Thus, this is nanotechnology will help us control the smallest of the material, therefore, avoid the errors occurs or problems in the field of civil engineering. The Architecture, Engineering, and Construction industry can take the advantage of applications of nanotechnology and nanomaterial. This review Paper shows there are different uses of nanotechnology in building materials like concrete, carbon, nanotube, steel, wood, coating, glass ,fire protection ,thermal insulation and green building etc. different nanomaterial are used in the construction material like Titanium dioxide (TiO2), nano silica(ns), polycarboxilates,Zirconium Oxide Nanoparticles (ZrO2),Silver Nanoparticles (Ag),Aluminum Oxide Nanoparticles (Al2O3),Zirconium Oxide Nanoparticles (ZrO2),Wolfram (Tungsten) Oxide Nano particles (WO3)etc.by using these materials and nanotechnology we can save time and also energy .this is the advanced technology which can very useful in the civil or construction industry.

Keywords: Nanotechnology , Nano material, Titanium dioxide (TiO2), nano silica(ns), polycarboxilates, (ZrO2),(Ag), (Al2O3), (ZrO2), (WO3)

I. INTRODUCTION

Nanotechnology is the use of very small particles of material to create new large scale materials. Nanotechnology is use in science as well as in technologies also. It have already been in development for many years.The Architecture, Engineering, and Construction industry might accommodate broad applications of nanotechnology and nanomaterial. These products can be used for design and construction processes in many areas. Nanotechnology is the area which is used to improve the mixture design, performance and production of cement-based materials. Materials composed of nano-sized particles displays unique physical and chemical properties compared to those with normal particle sizes. Concrete is stronger, more durable and more easily placed, steel tougher and glass self-cleaning. Increased strength and durability of the product. Nanomaterials can be defined as those physical substances with at least one dimension between 1…150 nm (1 nm = 10–9 m). Currently, the use of nanomaterials in construction is reduced, mainly for the following reasons: the lack of knowledge concerning the suitable nanomaterials for construction and their behavior; the lack of specific standards for design and execution of the construction elements using nanomaterials; the reduced offer ofnanoproducts; the lack of detailed informations regarding the nanoproducts content; high costs; the unknown of health risks associated with nano materials.

II. NANO TECHNOLOGY IN CONSTRUCTION INDUSTRY

Nanotechnology can be used for design and construction processes. Nanotechnology can generate products with their characteristics to improve the current construction materials. For example, new structural materials with unique properties, lighter and stronger composites, fire insulator, sound absorber, low maintenance coating Nano sized sensors solar cells etc.

The areas of application of nanotechnology in civil engineering and the science & technology behind the improved performance.

2.1 Nanotechnologies for Concrete

Concrete is a macro-material which has its nano-properties. The additions of nano-silica (SiO2) to cement for control the degradation of the calcium-silicate hydrate reaction to improve in durability. Micro and nanostructure resulting in improved mechanical properties. Nanotechnology is used to studying its properties like hydration reaction, alkali silicate reaction (ASR) and fly ash reactivity. For concrete containing large volume fly ash, at early age it can improve pore size distribution by filling the pores between large fly ash and cement particles at Nano scale. It is also been reported that adding small amount of carbon nanotube (1%) by weight could increase both compressive and flexural strength (Mann,2006)

2.2 Nanotechnologies for Steel

Steel is major part in the construction industry since 19th to 20th century and it is widely available for the construction purpose. Fatigue is a issue that can lead to the structural failure of steel subject to cyclic loading, such as in bridges or towers. The stress is lower than the yield stress of the material and due to that shortening of useful life of the structure is occurs. this can be avoided by taking the regular inspection. The addition of copper nanoparticles reduces the surface unevenness of steel and it is more efficient materials use in construction subjected to fatigue issues (Mann, 2006) and The addition of nanoparticles of magnesium and calcium leads to an increase in weld toughness. The carbon nanotubes have little use as an addition to steel because of their inherent slipperiness is occurs ,due to the graphitic nature, making them difficult to bind to the bulk material (Mann, 2006).

2.3 Nanotechnologies for Wood

Wood is composed of nanotubes surfaces at the nanoscale. It is sustainable construction as both the production and the part of a renewable cycle. Due to its natural origins, wood is leading the way in cross-disciplinary research and modelling techniques. wood is highly water repellent coating which result of the combination of silica and alumina nano particles and hydrophobic polymers.

2.4 Nanotechnologies for Glass

Glass is Fire-protective which another application of nanotechnology. Glass panel (an interlayer) is formed of fumed silica (SiO2) nano particles which turns into a rigid and fire shield when heated. Because of the hydrophobic properties of TiO2, it can be applied in self-cleaning windows. To prevent sticking of pollutants, and thus reduce a maintenance costs .Nano-TiO2 coatings can be applied to building exteriors.

2.5 Nanotechnologies for Coatings and Paintings

Nanotechnology is applied to paints in order to avoid the corrosion under insulation because of hydrophobic and repels water from the metal pipe and can also protect metal from salt water attack. Coatings have self healing capabilities through a process of "self assembly". Eg. Glazing. The coatings have Nano particles or Nano layers have been developed for different purposes like protective or anti-corrosion coatings for mechanism; self-cleaning, thermal control, energy saving, anti-reflection coatings for glass/windows; easy-to-clean, antibacterial coatings for work surfaces; and more durable paints. The coating is consist of two stages. First, using a „photo catalytic" process, nano sized TiO2 particles in the coating react with ultra-violet

rays from natural daylight to break down and disintegrate organic dirt. Secondly, the surface coating is hydrophilic, which lets rainwater spread evenly over the surface and „sheet" down the glass to wash the loosened dirt away. It can therefore reduce airborne pollutants when applied to outdoor surfaces. TiO2 is used to coat glazing because of its sterilizing and anti-fouling properties.

2.6 Nanotechnologies for Thermal Insulation

Moisture is obtained from Micro and nonporous aerogel materials. The uses hydrophobic nano porous aerogel structure is for ultra-thin wall insulation. Aerogel is form of silica which has application for transparent insulation. The energy saving product is nothing but use of Micro systems offer the possibility of monitoring and controlling the internal environmental condition of buildings.

2.7 Nanotechnologies for Fire Protection

Fire protection is done by providing coating produced by a spray-on cementitious process. Nano-cement some properties to create a tough, durable, high temperature coatings. This is achieved by the mixing of carbon nanotubes with the cementious material.

2.8 Nanotechnologies for Structural Monitoring

Nano and micro electrical mechanical systems (MEMS) sensors have been developed and used in construction to monitor and/or control the environment condition and the materials/structure performance. One advantage of these sensors is their dimension. Nano sensor ranges from 10-9 m to 10-5m. The micro sensor ranges from 10-4 to 10-2 m (Liu *et al.,* 2007). These sensors could be embedded into the structure during the construction process. The sensors can also be used to monitor concrete corrosion and cracking. The smart aggregate can also be used for structure health monitoring. The disclosed system can monitor internal stresses, cracks and other physical forces in the structures during the structures' life. It is capable of providing an early indication of the health of the structure before a failure of the structure can occur.

2.9 Nano Technology and Green Building

Nanotechnology, the manipulation of matter at the molecular scale, is bringing new materials and new possibilities to industries as diverse as electronics, medicine, energy and aeronautics. Our ability to design new materials from the bottom up is impacting the building industry as well. New materials and products based on nanotechnology can be found in building insulation, coatings, and solar technologies. Work now underway in nanotech labs will soon result in new products for lighting, structures, and energy. In the building industry, nanotechnology has already brought to market self-cleaning windows, smog-eating concrete, and many other advances. But these advances and currently available products are minor compared to those incubating in the world's nanotech labs today. There, work is underway on illuminating walls that change colour with the flip of a switch, nano composites as thin as glass yet capable of supporting entire buildings, and photosynthetic surfaces making any building facade a source of free energy.

III. NANO MATERIALS

Nano material is defined as the smallest material which has less than 100nm in size. One nanometer is 10-9 meters or about 3 atoms long. For comparison, a human hair is about 60-80,000 nanometers wide. In general in nanotechnology, following points are to be considered that is Small size, measured in 100s of nanometers or less, Unique properties because of the small size ,Control the structure and composition on the nm scale in order to control the properties. Currently, the use of nano materials in construction is reduced, mainly for the different reasons

3 Types of Nano Materials

There are different types of nano materials are available for different purposes which is for the construction or any other purpose which is belonging to nano technology.

- Titanium dioxide (TiO2)
- Carbon nano tubes (CNT's)
- Nano silica(ns)
- Poly carboxilates
- Zirconium Oxide Nano particles (ZrO2)
- Silver Nanoparticles (Ag)
- Aluminum Oxide Nano particles (Al2O3)
- Zirconium Oxide Nano particles (ZrO2)
- Wolfram (Tungsten) Oxide Nano particles (WO3)

3.1Titanium dioxide (TiO2)

TiO2 is a white pigment and can be used as an excellent reflective coating. It is incorporated, as nano particles and it is added to paints, cements and windows for its sterilizing properties since TiO2 breaks down organic pollutants, volatile organic compounds and bacterial membranes through powerful catalytic reactions. It can therefore reduce airborne pollutants when applied to outdoor surfaces. Additionally, it is hydrophilic and therefore gives self cleaning properties to surfaces to which it is applied. The process by which this occurs is that rain water is attracted to the surface and forms sheets which collect the pollutants and dirt particles previously broken down and washes them off. The resulting concrete, already used in projects around the world, has a white colour that retains its whiteness very effectively unlike the stained buildings of the material's pioneering past.

3.2Carbon nanotubes (CNT's)

A further type of nanoparticle, which has remarkable properties, is the carbon nano tube (CNT) and current research is being carried out to investigate the benefits of adding CNT's to concrete. Carbon nanotubes are a form of carbon that was first discovered in Russia but came into use in the late ninety's in Japan. They are cylindrical in shape, as shown in figure below, and their name comes from their nanometre diameter. They can be several millimetres in length and can have one "layer" or wall (single walled nanotube) or more than one wall (multi walled nanotube). They have 5 times the Young's modulus and 8 times (theoretically 100 times) thestrength of steel while being 1/6th the density. The addition of small amounts (1% wt) of CNT's can improve the mechanical properties of samples consisting of the main Portland cement phase and water. Oxidized multi-walled nanotubes (MWNT's) show the best improvements both in compressive strength (+ 25 N/mm2) and flexural strength (+ 8 N/mm) compared to the reference samples without the reinforcement. It is theorized the high defect concentration on the surface of the oxidized MWNTs could lead to a better linkage between the nanostructures and the binder thus improving the mechanical properties of the composite rather like the deformations on reinforcing bars.

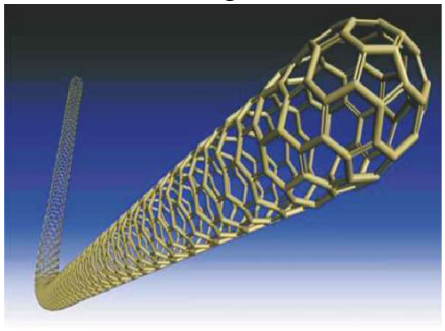

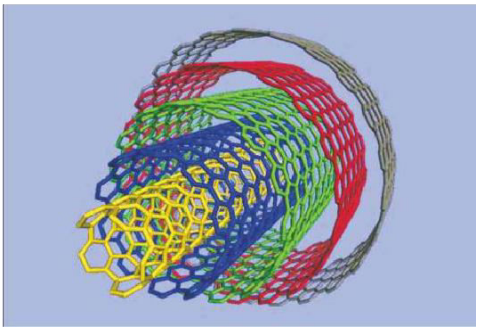

Fig.3.2.1computer-generated model of a carbon nanotube fig.3.2.2computer-generated model of multiwalled carbon nanotubes

3.3 Nano Silica(ns)

Fially, fibre wrapping of concrete is quite common today for increasing the strength of pre- existing concrete structural elements. Advancement in the procedure involves the use of a fibre sheet containing nano-silica particles and hardeners. These nanoparticles penetrate and close small cracks on the concrete surface and, in strengthening applications, the matrices form a strong bond between the surface of the concrete and the fibre reinforcement. In the strengthening process pre-cut carbon tows (fibres) and sheets impregnated with the matrix are placed on the prepared concrete surface and bonded using grooved rollers. The ability of the samples to sustain load after cracking is greatly improved by the carbon tows and both the matrix and the interface are durable under wetting and drying and scaling (scraping) conditions. Additionally, there is no decrease in the maximum load capacity after repeated cycles of wetting and drying or scaling.

3.4 Polycarboxilates

The material behaves like a thick fluid and is made possible by the use of polycarboxylates (a material similar to plastic developed using nanotechnology). SCC mixes, which contain a high content of fine particles, need a very effective dispersing system in order to be fluid and workable overtime at low water/cement ratio (high W/C ratios would lead to risk of segregation) and only polycarboxylates can meet these requirements. In addition, while long term strengths of conventionally super plasticized concrete are very high, the very early strengths, especially in winter, are not high enough for a quick and safe removal of formwork and steam curing is therefore used to accelerate the hydration of cement. This can be eliminated in the precast industry through the use of the latest generations of polycarboxylates resulting in further time and energy savings.

3.5 Silver Nanoparticles (Ag)

Silver Nanoparticles will affect, in contact with bacteria, viruses and fungi. The nanosilver inhibits multiplication and growth of bacteria and fungi, which causes infection, odour, itchiness. In this nanosilver produce the small particles and it varies uniformly. When the nanoparticles are bonded together with other material, the surface area is increasing several million times than the normal silver particles.

3.6Aluminum Oxide Nanoparticles (Al2O3)

Hydration of calcium silicate is occurs due to reaction between Alumina (Al2O3) with calcium hydroxide.

The rate of the pozzolanic reaction is same as amount of surface area available for reaction. It improves higher split tensile and flexural strength due to addition of nano-Al2O3 . The cement could be beneficially replaced in the concrete mixture with nano-Al2O3 particles up to maximum limit of 2.0% with average particle sizes of 15 nm, the optimal level of nano-Al2O3 particles content being achieved with 1.0% replacement (Nazari *et al*., 2010).

IV. CONCLUSION

Nanotechnology has help improve the quality of and solved many issue with building materials such as concrete and steel. The comparison between the construction material concrete,steel,timber or wood and glass with the properties of carbon nanotube then we get that carbon nanotube has a Young's modulus of 1054 GPa, a tensile strength of 150 GPa and a density of 1.4 g-cm^{-3}. So from this we can conclude that carbon nanotube has strength of 150 times that of steel and at the same time it is six times more lighter than other material. The use of CNTs to improve the efficiency of energy transmission, lighting, and or heating devices.

The use of nanotechnology has also helped to form more efficient and also sustainable materials such as self-cleaning and self-repairing concrete. The use of coatings made from nanotechnology helps to get better fire-resistance, corrosion protection, insulation, and innumerable other applications. Nanotechnology can even help improve the quality and availability of water. In other words, it creates an environmental challenge to the construction industry as well. Nanotechnology is an extension of the sciences and technologies .The use of micro nano materials (MNMs) in the construction industry should be considered not only for enhancing material properties and functions but also in the context of energy conservation. Using silica nano particles in insulating ceramics and paint/coating that enable energy conservation and solar-powered self-cleaning nano-TiO2-coated surfaces. It is necessary to establish a system to identify the environmentally friendly and sustainable construction nano materials and to avoid the use of harmful materials in the future.

REFERENCES

1. Zhi Ge, Zhili Gao "Applications of Nanotechnology and Nanomaterials in Construction" (ICCIDC–I) August 4-5, 2008, Karachi,, Pakistan
2. Saurav "Application Of Nanotechnology In Building Materials" (IJERA) ISSN: 2248-9622 Vol. 2, Issue5, September- October 2012, pp.1077-1082
3. Syed Sabihuddin "Application of Nanotechnology in Civil Infrastructure" ISSN : 2248-9622, Vol. 4, Issue 3(Version 1), March 2014, pp.92-95

Analysis of Strength in Unidirectional Grpf Based Fiber Orientations Under Static Loading Using Ansys

Mr. K. Shanmugaelango,
Associate Professor,
Department of Electrical and Electronics Engineering,
St. Anne's College of Engineering and Technology,
Anguchettypalayam, Panruti – 607106.

Mr. R. Sasikumar ,
Assistant Professor,
Department of Electrical and Electronics Engineering,
St. Anne's College of Engineering and Technology,
Anguchettypalayam, Panruti – 607106.

Mr .P. Murugan
Assistant Professor,
Department of Electrical and Electronics Engineering,
St. Anne's College of Engineering and Technology,
Anguchettypalayam, Panruti – 607106.

Absract-The Composite materials have found widespread applications in various fields of engineering such as aerospace, marine, automobile and mechanical applications. The strength of the composites are depends on two factors which are fiber orientation and length. In our project we are analyzing the effect of fiber orientation in a rectangular composite lamina under transverse static loading by using the finite element method. The results are obtained with the help of five different angle of orientation of GRPF/epoxy. For analysis ANSYS software were used. By comparing the results of five different orientations finally conclude the better one which will utilize full strength of the fiber composite. It is observed that the stress value is maximum of 14384 N/mm^2 while considered the boundary condition 2 at 30^0. Also the stress value is minimum of 412 N/mm^2 while considered boundary condition 4 at 45^0. It is also observed that displacement value is maximum of 125.409 mm while considered boundary condition 2 at 60^0. From the result it is observed that the orientation at 30^0 with boundary condition 2 is safe while comparing other boundary conditions.

Keywords: Glass reinforced plastic fiber, Epoxy, Stress, ANSYS.

I. COMPOSITE MATERIAL AND ITS CONSTITUENTS

Composites are a combination of two or more constituent materials with significantly different physical or chemical properties. The performance of composites is superior to their constituent materials acting alone. The characteristics of resultant composite material are totally different from the individual constituents and unique. Within the composite, the different materials are apart and they do not dissolve or blend into each other. .

Fillers are added to reduce the cost and increase the modulus. They also reduce the mould shrinkage and control viscosity. They provide smooth surface to composite produced. Also

toughness, colorants, flame retardants, ultraviolet absorbers, coupling agents, lubricants, heat stabilizers, and forming agents may also be added to the matrices..

II FILLERS AND OTHER ADDITIVES

Fillers are added to a polymer matrix to reduce the cost (as fillers are less expensive than most of the resins) and to increase the modulus. They produce smooth surface. They control viscosity and reduce mould shrinkage during fabrication. But the problem is they tend to reduce its strength and impact resistance. The most common filler for polyester and vinyl ester resins is calcium carbonate ($CaCO_3$), which is used to reduce cost as well as mold shrinkage. Examples of other fillers are clay, mica, and glass micro spheres (solid as well as hollow).

Also toughness, colorants, flame retardants, ultraviolet absorbers, coupling agents, lubricants, heat stabilizers, and forming agents may also be added to the matrices. Coupling agents act as compatibilizers between the hydrophilic fibers and the hydrophobic polymers and improve the bond between materials by different ways; that is by eliminating weak boundary layers, by producing tough, deformable layers, by developing a highly cross-linked interphone region with an intermediate modulus, by improving the wettability (critical surface tension factor), by forming covalent bonds with both materials, and by altering surface acidity.

III. MATRIX AND ITS TYPES

The high strength of composites is largely due to the fiber reinforcement. But the importance of matrix material cannot be underestimated. Matrix provides support for the fibers and assists the fibers in carrying the loads. It also provides stability to the composite material.

The major types of matrix are metal matrix, ceramic matrix and polymer matrix. Accordingly composites are classified into metal matrix composite (MMC), ceramic matrix composite (CMC) and polymer matrix composite (PMC). Table 1.1 gives the applications of composites classified on the basis of the matrix used.

Following are the requirements of a good matrix material.

- Excellent chemical resistance.
- Low coefficient of thermal expansion.
- Strength at elevated temperature (depending on application).
- Should be easily process able into the final composite shape.
- Dimensional stability (maintains its shape) and Reduced moisture absorption
- Low shrinkage.

IV. SUPERIOR CHARACTERISTICS OF COMPOSITE MATERIALS OVER OTHER MATERIALS

Majority of the composite materials provide a combination of strength and modulus that are either comparable to or better than many traditional metallic counterparts. Owing to their low density, the strength–weight ratios and modulus– weight ratios of these composite materials are superior to most of the other known metals. Fatigue strength as well as fatigue damage tolerance of many composite laminates are extremely good and because of this reason there are emerged as an important class of structural materials and found applications in aerospace, military, marine automotive industry. They are useful for making sporting goods and even have bio-medical applications.

V. RESULTS AND DISCUSSIONS

In this chapter, the modeling of the layer using ANSYS and the steps used to solve them were discussed and the results of boundary conditions were analyzed.

VI. MODELING OF STRUCTURE

To study influences of fiber orientation upon deflection and for different stresses. A laminated composite plate of dimension 200mm×100mm×1mm with a unidirectional cross section using the finite element analysis software.

Maximum stress is easily found out by using the ansys solve command. But it is difficult to estimate the stress directly from the results. For that stress gradient graph is developed by means of path operations. By using the path operations the stress is easily calculated.

VII. MESHING MODEL

In this method, a body or structure in which the analysis is carried out is subdivided in to smaller elements of finite dimensions called finite elements. Then the body is considered as an assemblage of these elements connected at finite number of joints called nodes or nodal point. The meshed view of lamina plate is as shown in fig 5.2.

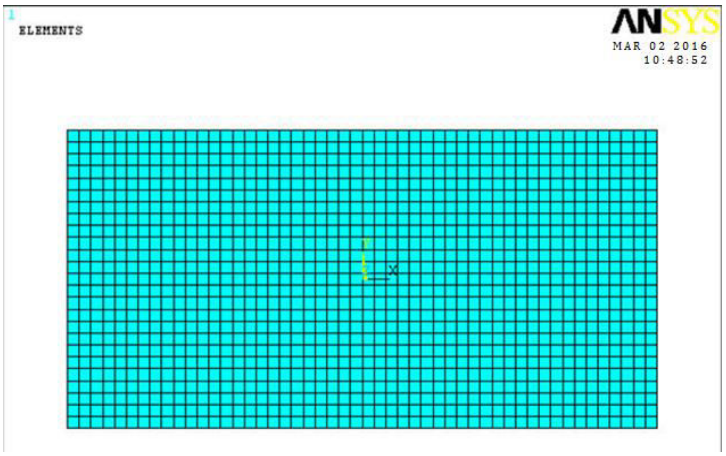

Fig 1.2 Meshed View of Lamina Plate

VIII SOLVING MODEL:

From fig 5.3 and 5.4 The properties of each type of finite element is obtained and assembled together and solved as whole to get solution.

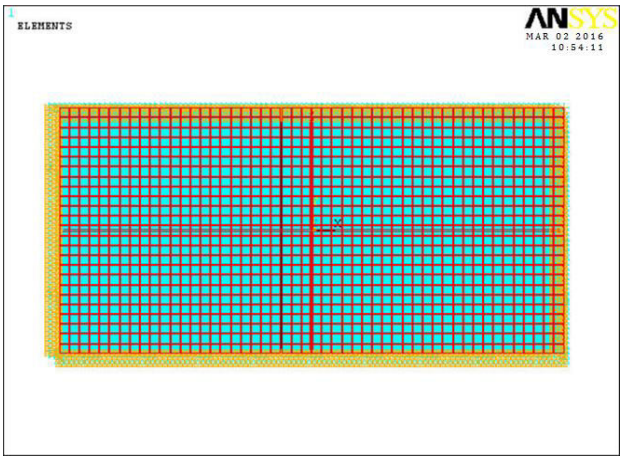

Fig 1.1 Solved Lamina Plate

The shear strength of the glass fibre/epoxy composite was quite sensitive to strain rate and the shear strength increased as strain rate increases. sThe table 5.1 and 5.2 explains the stress and displacement results of GRPF/Epoxy.

a) GRPF /EPOXY STRESS RESULTS

The stress values of the lamina at different boundary conditions at different orientations are as shown in the Table 5.1.

BOUNDARY CONDITIONS	0 DEGREE	30 DEGREE	60 DEGREE	90 DEGREE
B1	624.372	679.378	677.546	628.382
B2	11874	14384	14284	11884
B3	692.412	623.521	625.521	698.842
B4	476.651	437.242	435.24	484.601

Table 1.1 Stress Result of GRPF/Epoxy

b) GRPF/EPOXY DISPLACEMENT RESULTS

BOUNDARY CONDITIONS	0 DEGREE	30 DEGREE	45 DEGREE	60 DEGREE	90 DEGREE
B1	0.469255	0.448734	0.438342	0.468734	0.475953
B2	79.751	115.409	120.875	125.409	81.851
B3	0.391136	0.37362	0.366702	0.35363	0.381146
B4	0.194586	0.117971	0.122807	0.11880	0.124586

The displacements values of the lamina at different boundary conditions at different orientations are shown in the Table 5.2.

Table 1.2 Displacement Result of GRPF/Epoxy

IX. CONCLUSION

This experimental analysis of GRPF/epoxy based composites using ANSYS leads to the following conclusions

- Modeling of the composite lamina in ANSYS is possible.
- Analysis of the composite at different orientations is possible using ANSYS.
- The stress and displacement curves are obtained are analysed using ANSYS.
- It is observed that the stress value is maximum 14384 N/mm^2 while considered the boundary condition 2 at 30^0.
- Also the stress value is minimum 412 N/mm^2 while considered boundary condition 4 at 45^0.
- It is also observed that displacement value is maximum 125.409 mm while considered boundary condition 2 at 60^0.
- From the result it is observed that the orientation at 30^0 with boundary condition 2 is safe while comparing other boundary conditions.
- From this it is concluded that we can use the safe orientation for better performance. The default orientation of material is replaced by safe orientation are show above results

REFERENCES

1. Alnefaie, A., (2009) 'Finite Element Modeling of composite plates with internal delamination', Composite Structures, Vol. 90, pp. 21-27.
2. Ankur and Anish Gandhi, H., (2014) 'Investigation of the Effect of Fiber Orientation on Mechanical Properties of Composite Laminate Using Numerical Analysis', International Journal of Advanced Mechanical Engineering, Vol. 4, No 5, pp. 501-508.
3. Gubran and Gupta, K., (2005) 'The effect of stacking sequence and coupling mechanisms on the natural frequencies of composite shafts', Sound and Vibration, Vol. 282, pp. 231-248.
4. Jun.L and Rongying, S., (2008) 'Dynamic finite element method for generally laminated composite beams', Mechanical Sciences, Vol. 50, pp. 466-480.
5. Qu.Y and Meng, G., (2013) 'A unified formulation for vibration analysis of composite laminated shells of revolution including shear deformation and rotary inertia', Composite structures, Vol. 98, pp. 169-191.
6. Rarani, S., Sharifi and Shokrieh, M., (2014) 'Effect of ply stacking sequence on buckling behavior of E-glass/epoxy laminated composites', Computational Material Science, Vol. 89, pp. 89-96.
7. Sahoo, R., and Singh, B., (2014) 'A new trigonometric zigzag theory for static analysis of laminated composite and sandwich plates', Aerospace science and technology, Vol. 35, pp. 15-28.
8. Xiang Xie and Zhigang Liu., (2014) 'Free vibration analysis of composite laminated cylindrical shells using the Haar wavelet method', Composite Structures, Vol. 109, pp. 167-199.

Design and Fabrication of Elliptical Bicycle and Save Electrical Energy With The Help of Piezoelectric Transducers

Mr. K. Saravanan
Assistant Professor,
Department of Mechanical Engineering,
St. Anne's College of Engineering and Technology,
Anguchettypalayam, Panruti – 607106.

Mr. M. Balamurali
UG Student,
Department of Mechanical Engineering,
St. Anne's College of Engineering and Technology,
Anguchettypalayam, Panruti – 607106.

Mr. V. Balamurugan
UG Student,
Department of Mechanical Engineering,
St. Anne's College of Engineering and Technology,
Anguchettypalayam, Panruti – 607106.

Abstract – ElliptiMove is tool used in training by fitness enthusiasts and athletestoimprove their performance with an innovative engineering concept that combines the motion of running, bicycling and elliptical machine. Elliptical cycling is for people who want to get physically fit, achieve their fitness goal and recover from hip and knee injuries. Its unique mechanism encourages maximum people to use this bike. Our aim is to design the elliptical bicycle in an optimized manner by reducing it's weight and cost in a such a way that it has low impact, high performance, exciting outdoor workouts and has an significant role in human welfare.

Index Terms— **elliptical bicycle, piezoelectric transsducers**

I. INTRODUCTION

The ElliptiMove is an elliptical bicycle. By modifying the elliptical trainer motion and combining it with the functionality of a bicycle, the ElliptiMove bicycle delivers a high-performance workout experience that closely mimics running outdoors while eliminating the impact. It provides the most comfortable, fun and efficient way to get out and stay active.ElliptiGO co-founder and former Ironman tri-athlete Bryan Pate was inspired to create the world's first elliptical bicycle after injuries plagued him to the point where he could no longer run for fitness. Although he was an experienced cyclist, Pate chose instead to use the elliptical trainer to stay fit because it was more comfortable than sitting on a bike. Unsatisfied with the experience of working out in a gym, however, Pate had a vision of creating a product that would allow him to have both the outdoor "running experience"

and the low-impact workout of the elliptical machine. In 2005, Bryan partnered with ElliptiGO co-founder Brent Teal, a mechanical engineer and ultra-marathoner, to design and develop the world's first elliptical bicycle. Five prototypes and thousands of test miles later, the ElliptiGO was born. The ElliptiMove is perfect for anyone who wants to get a great cardiovascular workout outdoors without damaging their body. It is particularly well-suited for runners who want to enjoy a running-like experience while giving their knees and joints a break from the wear and tear caused by running. The ElliptiMove is also ideal for cyclists who want to get the experience of cycling without the discomfort caused by sitting on a conventional bike seat or riding in a hunched-over position. The ElliptiMove is easy to ride and more stable than it looks. Riding an ElliptiMove requires the same amount of balance as is required to ride a traditional bike or scooters

II. PROBLEM DEFINITION

Most of the people use fitness equipments for workouts and to stay fit, however as the fitness equipments are placed in closed/ confined spaces, unfortunately the user ends up working out in an artificial environment and misses the opportunity to explore the nature. Another problem associated with fitness equipments is, the person using the fitness equipment has to perform a single exercise and is committed to that workout until it gets completed. So the aim of our project is to develop an elliptical bicycle or a fitness tool in minimum cost, which allows the user to work out as well as carry out his chores, commute from one place to another and can be used for general recreation.

2.1 Project Plan

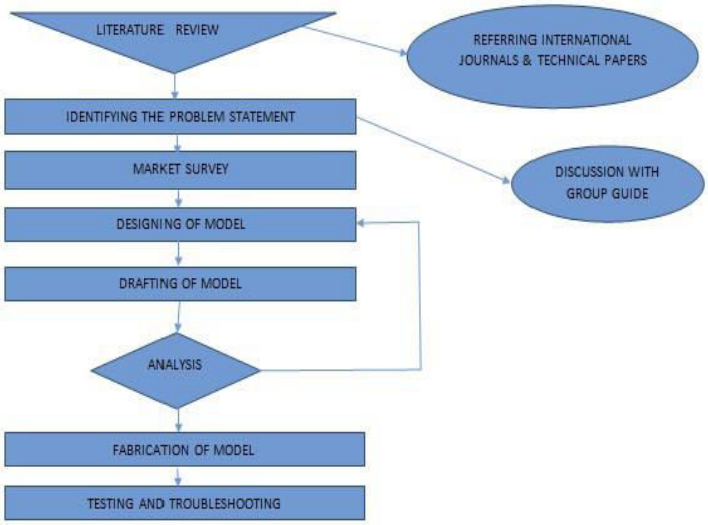

2.2 Literature Review

A Bi-cycle frame should have low weight, high lateral stiffness and moderate vertical stiffness. Because of chain load, frame lateral deformation during pedaling is bigger when the rider pushes on right pedal (a pro rider may apply a force up to two times his weight). Most of the bicycles built today utilize heat treated steel or aluminum or titanium alloy tubing to minimize their weight. The tubes are then welded together to create the desired fork or frame geometry. It is Notable part in whole racing cycle system which is subjected to static and dynamic loads. Historically, the most common material for the tubes

of a bicycle frame has been steel. Steel frames can be very inexpensive carbon steel to highly specialize using high performance alloys. Frames can also be made from aluminum alloys, titanium, carbon fiber, and even bamboo and cardboard. Occasionally, diamond (shaped) frames have been formed from sections other than tubes. These include I-beams and monocoque. We will also obtain the knowledge how to make a finite element model in Hyper mesh by going through literature papers. The conditions required for applying various Constraints and how the loads are applied is briefed about in the technical papers referred. By using composite materials we can reduce the cost of cycle. Reverse engineer and extract dimension of frame Make a 2D model of Chassis, Designing the chassis using CATIA V5R19. Get the exact parameters of the material used. Meshing the CAD model, Apply the Boundary conditions, Solve for the solution of meshed model using ANSYS '15.

IV. Testing of the Fabricated Model:-

Followed by the fabrication of the actual model, the model has been tested for different road, different load and various environmental conditions to identify any defects or flaws in the design or fabrication processes, and eventually no defects or flaws where noticed or observed. The model was tested on smooth, rough, dirt and uneven road surfaces to observe the behavior of the bicycle on the above mentioned road conditions, and fortunately the bicycle behaved in a well mannered way, hence eliminating any chances of misbalance or mishap

V. CONCLUSION

Thus we conclude that ElliptiMove is designed and fabricated with the 80% cost optimization hence satisfying our aim of the project which was to design and fabricate the model while optimizing the cost which is successfully achieved with an added advantage of introducing this concept in the Indian market. ElliptiMove is designed in such a way that we have also achieved weight optimization up to 1 kg. ElliptiMove provides the rider a workout experience while eliminating the impact on the joints of the human body caused during running, bicycling or working on a elliptical trainer in the gym. The comfortable and better ergonomics of ElliptiMove ensures that the rider workouts with ease eliminating the pain caused due to constant cycling during the use conventional bicycle. Thus we have developed a fitness tool which allows the rider to work out and simultaneously explore the nature or carry out his daily chores without any problem of injuries or damage to the body. Thus ElliptiMove emulates the natural running movement, so the rider stands upright, in a very comfortable position and propels the ElliptiMove using a very comfortable motion. The upright riding position drastically improves the rider's ability to see over traffic and obstacles as compared to road cycling. The less aerodynamic upright position makes ElliptiMove riders work harder than cyclists to maintain the same pace, allowing ElliptiMove riders to get their workout done in less time and while covering less distance.

REFERENCES

1. Sagar Pardeshi, Pankaj Desle "Design and Development of Effective Low Weight Racing Bicycle Frame", International Journal of Innovative Research in Science, Engineering and Technology (IJIRSET).

2. Matthew N. Godo, David Corson, Steve M. Legensky, "A Practical Analysis of Unsteady Flow Around a Bicycle Wheel, Fork and Partial Frame Using CFD" American Institute of Aeronautics and Astronautics.
3. Stephen Smaldone, Chetan Tonde, Vancheswaran K. Ananthanarayanan, Ahmed Elgammal, and Liviu Iftode, "Improving Bicycle Safety through Automated Real-Time Vehicle Detection" Department of Computer Science Rutgers University 110 Frelinghuysen Rd, Piscataway, NJ 08854
4. Shih-Wen Hsiao, Rong-Qi Chen, Wan-Lee Leng, "Applying riding-posture optimization on bicycle frame design" Department of Industrial Design, National Cheng Kung University, Tainan 70101, Taiwan, ROC
5. Henri P. Gavin, "Bicycle Wheel Spoke Patterns and Spoke Fatigue", ASCE Journal of Engineering Mechanics, vol 122, no. 8, (August 2014) pp. 736-742.

Comparison of Mechanical Characterization of Glass and Chicken Feather Epoxy Composite Natural Fiber Composite

Mr. K. shanmuga elango
Associate Professor,
Department of Mechanical Engineering,
St. Anne's College of Engineering and Technology,
Anguchettypalayam, Panruti – 607106.

Mr. J. Manikandan , Mr. B. Prasanth,
UG Student,
Department of Mechanical Engineering
St. Anne's College of Engineering and Technology,
Anguchettypalayam, Panruti – 607106.

Abstract - This research demonstrates that chicken feathers can be used as matrix to develop completely biodegradable composites with properties similar to that of composites having polypropylene (PP) as matrix. Feathers are ubiquitous and inexpensive but have limited industrial applications. Feathers have been preferably used for composite applications due to their low density and presence of hollow structures that facilitate sound absorption. However, previous approaches on using feathers for composites have used the whole feather or the feather fractions as reinforcement with synthetic polymers as matrix resulting in partially degradable composites. In addition, the hydrophilicity of the feathers and hydrophobicity of the synthetic matrix results in poor compatibility and therefore less than optimum properties. Although it has been shown that feathers can be made thermoplastic and suitable to develop films and other thermoplastics, there are no reports on using feathers as matrix for composites. In this research, chicken feathers were used as matrix and Glass fibers as reinforcement to develop com pletely biodegradable composites. Tensile, flexural and acoustic properties of the feather-Glass composites were compared to PP-Glass composites. Utilizing feathers as matrix could enable us to develop low cost 100 % biodegradable composites containing feathers or other biopolymers as the reinforcement.

Keywords - Chicken feathers, Matrix , Composites, Biodegradable.

I. INTRODUCTION

Polymers have generated wide interest in various engineering, in view of their good strength and low density as compared to monolithic metal alloys. As lighter in weight they are suitable materials for weight sensitive uses, but the limitation is the high cost. Considering cost factor, one can use of low cost fillers materials viz., chicken feather, jute, flying ash etc., which available with least effort. The mechanical properties of the composites are not changed by the addition of such fillers, as many researcher have studied the same. There have been various outputs on use of filler materials like minerals and inorganic oxides. But minimal attempts have been made to utilize cheap materials like industrial wastes; feathers from poultry are in preparing polymer reinforced composites. S Mishara et. al., worked and quoted that, the degree of mechanical reinforcement that could be obtained by the introduction of glass fibres

in biofibre (pineapple leaf fibre/sisal fibre) reinforced polyester composites has been assessed experimentally. Addition of relatively small amount of glass fibre to the pineapple leaf fibre and sisal fibre-reinforced polyester matrix enhanced the mechanical properties of the resulting hybrid composites. Vithal Rao Chauhan et.al., worked on the mechanical properties of glass/orthophthalic polyster resin with hematite ore filled composites and observed that the inclusion of hematite ore in composites with increased tensile strength, impact strength, hardness and flexural strength. Increase filler percentage till 6% weight fraction in composites got beneficial mechanical properties, further increase of filler material with matrix material improper bonding, interface and embrittlement of the composites causes detrimental effect. V. Ananda Rao, Alok Satapathy, S.C. Mishra were worked on the Polymer composites reinforced with short fibers obtained from poultry feathers based on the erosion characteristics and gave a result. Hence by this research survey, it is motivated to make some experiments to investigate the effect of the varied volume fraction of chicken feather as filler content on glass /unsaturated polyester resin. The objective is to investigate the mechanical properties.

II. MATERIALS AND METHODS

2.1 Materials

Chicken feathers used for the study were obtained from Feather Fiber Corporation (Nixa, MO) and included both the barbs and the quill. Glass fibers with an average fineness of 32 denier, breaking strength of 312 MPa, breaking elongation of 1.4 % and Young's modulus of 24.3 GPa were purchased from Bast Fibers LLC (Cresskill, NJ). PP fibers with fineness of 15 denier, breaking tenacity of 4 g/denier and melting temperature of 162 C were obtained from Drake Extrusion (Martinsville, VA). Glyc- erol and other chemicals used were reagent grade and used as received.

2.2 Preparation of Feathers

Feathers were powdered in a Wiley mill to pass through a 20 mesh screen before using as the matrix for composites. Glycerol (5 % w/w) was added to facilitate melting of the matrix. Feathers were thoroughly mixed with water con- taining a known amount of glycerol, dried in an oven and later used for compression molding.

2.3 Fabricating the Composites

Glass fibers were carded into mats and several mats were used as reinforcement depending on the density of the composites. Powdered feathers were then evenly sprayed on the layers of Glass fibers. The Glass-feather prepreg was placed between two aluminum foils and compression molded at the desired temperature (205–215 C) for a pre-determined time. For the PP-Glass composites used as control, the two fibers were mixed in the desired ratio and carded several times to achieve uniform mixing. Carded fibers were cut into mats (25 cm 9 22 cm) and several mats were placed between aluminum sheets andB compres- sion molded in a Carver Press at different temperatures and times. The PP Glass composites were compression molded at 185 C for 90 s based on our previous researches After compression molding, the press was cooled down by running cold water and the composites were collected for analysis. The weight of the matrix and reinforcement was controlled to obtain a density of 1 g/cm^3.

III. TESTING THE COMPOSITES

3.1 Flexural Properties

Composite samples were conditioned at 21 C and 65 % relative humidity for at least 24 h before testing. Flexural properties of the composites were determined based on ASTM standard D790-03 using 3-point bending on speci- mens with dimensions of 20.3 cm long and 7.6 cm wide. Crosshead speed during testing on a MTS tensile tester (Model Q Test 10) was 10 mm/min. At least five samples from three different composites were tested and the aver- age and standard deviations are reported.

3.2 Tensile Properties

Tensile properties of the samples (165 mm in length, 19 mm wide at the widest section and 13 mm at the narrow section) were determined according to ASTM standard D638-03 on an Instron (Model 4000, Instron, Norwood, MA). Gauge length was 115 mm and crosshead speed was 5 mm/min. At least 15 samples from three different com- posites were tested for each condition and the average and standard deviation is reported.

3.3 Stability Under High Humidity

Tensile and flexural properties of the composites were also measured at high humidity by conditioning the samples at 21 C and 90 % humidity in a conditioning chamber from 0 to 48 h. After conditioning, the samples were immedi- ately tested for tensile and flexural properties as described earlier.

3.4 Acoustic Properties

Acoustic properties of the feather-Glass and PP-Glass com- posites were tested according to ASTM standard C423-99A on a Bruel and Kjaer small size impedance tube. Absorp- tion coefficients were recorded on three different com- posites for each condition and the average values were used to plot the sound absorption curves. Noise reduction coefficients (NRCs) were calculated to evaluate the ability of the composites to absorb noise.

3.5 Morphology

Interaction between the matrix and reinforcement was observed using a variable pressure scanning electron microscope (VP-SEM) (Hitachi Corporation, Model S-3000N). Samples were sputter coated with gold palla- dium and observed under the SEM at a voltage of 20 kV.

3.6 Statistical Analysis

An ANOVA was used to determine the statistical signifi- cance in the results at a significance level of a = 0.05 with the help of SAS package. A Tukey's pair-wise comparison was used with 5–15 replications for each experiment.

IV. TESTING ANALYSIS

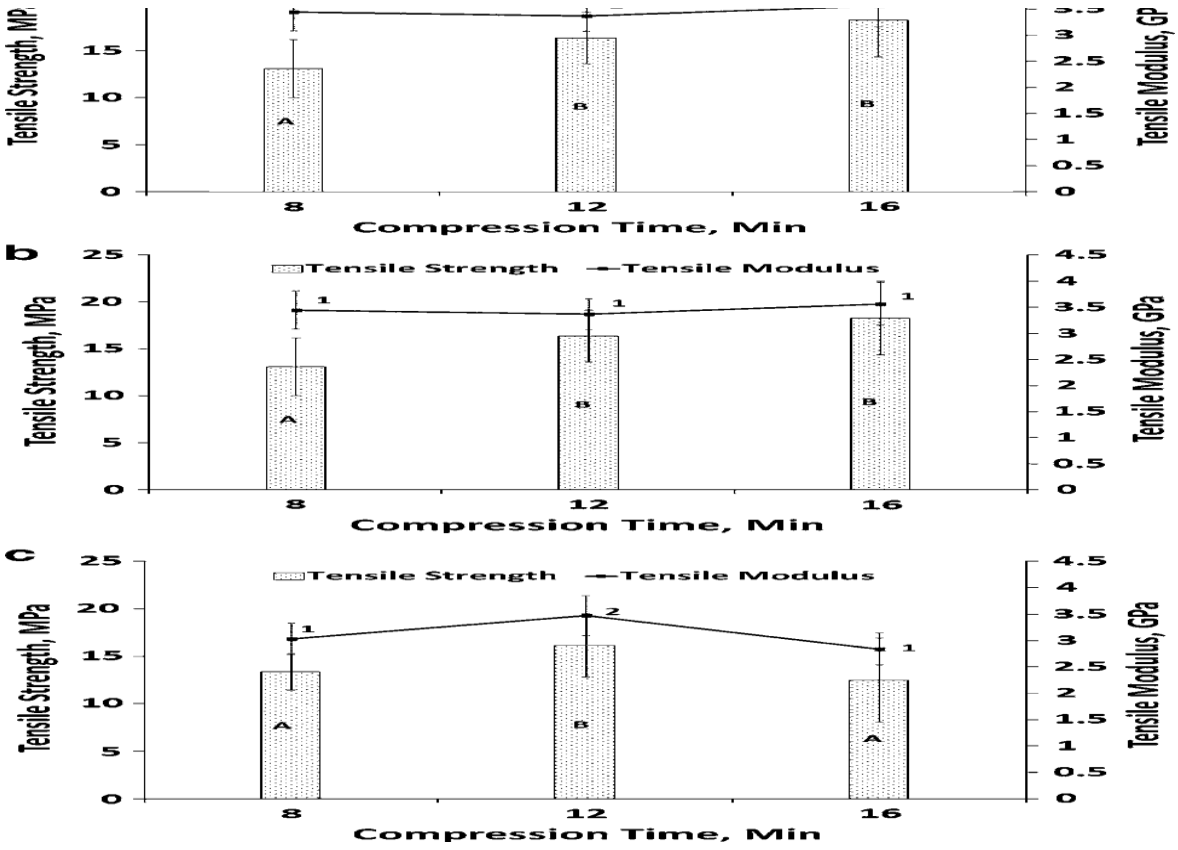

Fig: Testing analysis of compression, Tensile.

V. RESULTS AND DISCUSSION

5.1 Morphology of the Composites

Most of the feather powder used as matrix had melted uniformly and adhered to the Glass fibers together as seen from. Cross-section of the 50 % feather/50 % Glass composites in also showed that the matrix was distributed evenly and melted throughout the composite. It should also be noted that the composites were considerably consolidated without much space between the matrix and reinforcement and the feather powder did not reveal the presence of the characteristics honeycomb structures that facilitate sound absorption.

5.2 Influence of Process Parameters on Tensile Properties

It is illustrate the effects of temperature, time of compression molding and the concentration of feather as matrix on the tensile properties of the composites. With 50 % matrix and compression molding at 205 C, increasing compression time steadily increased the strength of the composites but the modulus did not show any sig- nificant changes. Compression time of 8 min could not melt the matrix sufficiently and we therefore obtained composites with lower strength and modulus. Increasing time provides sufficient time for the matrix, provides better adhesion between the matrix and reinforcement and therefore improved the strength. However, prolonging the heating to 16 min damages the

matrix due to thermal decomposition and therefore the strength decreased. Modulus was mostly related to the reinforcement which should not be damaged under the compression temperature

VI. CONCLUSION

Chicken feathers as matrix provided higher tensile and flexural properties to the composites compared to using PP as matrix. A compression temperature of 215 C and time of 8 min was required to achieve optimum tensile and flexural properties for the feather/Glass composites. Feathers and Glass absorb considerable amounts of water resulting in 50–60 % lower tensile and flexural properties at high (90 %) humidity. Acoustic properties of the feather matrix consolidated composites developed here were similar to that of the PP/Glass composites. Further studies on chemical modifications of the feathers are necessary to obtain com- posites with good performance properties at high humidi- ties. Also, feathers could be used as matrix and reinforcement to develop 100 % protein based composites.

REFERENCES

1. Mishra, S., A. K. Mohanty, L. T. Drzal, M. Misra, S. Parija, S. K. Nayak, and S. S. Tripathy. "Studies on mechanical performance of biofibre/glass reinforced polyester hybrid composites." Composites Science and Technology 63, no. 10 (2003): 1377-1385.
2. Chauhan, Vithal Rao, K. R. Dinesh, K. Veeresh, Veerabhadrappa Algur, and Manjunath Shettar. "Analysis of Mechanical Properties of Glass/Orthophthalic Polyster Resin with Hematite Ore Filled Composites." International Journal of Research 1, no. 7 (2014): 167-171.

Observe The Calorific Value of Distinct Biomasses Production From The Waste of Biogas Production Plant

Mr. T. Elangovan
Assistant Professor,
Department of mechanicalEngineering,
St. Anne's College of Engineering and Technology,
Anguchettypalayam, Panruti – 607106.

Ms. D. shaliya, Ms. A. Anu
UG Student,
Department of mechanical Engineering
St. Anne's College of Engineering and Technology,
Anguchettypalayam, Panruti – 607106.

Abstract - A study of the biomass production from the different natural waste blend with cow dung in the different ratios was investigated. The two variants were charged into 50L metal prototype bio digesters in the ratio of 3:1 of water to waste. They were subjected to anaerobic digestion under a 45 day retention period and mesophilic temperature range of 26 °C-43°C. The physicochemical parameters of the wastes were determined including microbial analysis. 2nd day even though gas production reduced drastically whiles the flammability discontinued and resumed after 14 days. Blending increased the cumulative gas yield to 9.34±0.11dm^3/kg. Slurry representing more than 50% increase. The onset of gas flammability took place on the 6th day and was sustained throughout the retention period. The study showed that paper waste which abounds everywhere and is either burnt off or thrown away constituting nuisance to the environment would be a very good feedstock for biogas production. It also indicates that blending paper waste with cow dung or any other animal waste will give sustained gas flammability throughout the digestion period of the waste since animal wastes are good starters for poor biogas producing wastes. Generation of biogas from paper waste upholds the concept of waste to wealth in enhancing sustainability of development and finally getting waste from the biogas production plant to dry that waste into without moisture content. Convert that dry waste into one kg biomass and find its calorific value.

Keywords: Cow dung, waste blend, retention time, natural waste

I. INTRODUCTION

Achieving solutions to possible shortage in fossil fuels and environmental problems that the world is facing today requires long-term potential actions for sustainable development. In this regard, renewable energy resources appear to be one of the most efficient and effective solutions. Biogas has globally remained a renewable energy source derived from plants that use solar energy during the process of photosynthesis. Being a source of renewable natural gas, it has been adopted as one of the best alternatives for fossil fuels after 1970's world energy crisis. Biogas is a colorless, flammable gas produced via anaerobic digestion of animal, plant, human, industrial and municipal wastes amongst others, to give mainly methane (50-70%), carbon dioxide (20-40%) and traces of other gases such as nitrogen, hydrogen, ammonia, hydrogen sulphide, water vapour etc. It is smokeless, hygienic and more convenient to use than

other solid fuels. Biogas production is a three stage biochemical process comprising hydrolysis, acidogenesis /acetogenesis and methanogenesis.

1.1 METHANOGENESIS

Biogas technology amongst other processes (including thermal, pyrolysis, combustion and gasification) has in recent times also been viewed as a very good source of sustainable waste treatment / management, as disposal of wastes has become a major problem especially to the third world countries. The effluent of this process is a residue rich in essential inorganic elements like nitrogen and phosphorus needed for healthy plant growth known as biofertilizer which when applied to the soil enriches it with no detrimental effects on the environment

The content of biogas varies with the material being decomposed and the environmental conditions involved . Potentially, all organic waste materials contain adequate quantities of the nutrients essential for the growth and metabolism of the anaerobic bacteria in biogas production. However, the chemical composition and biological availability of the nutrients contained in these materials vary with species, factors affecting growth and age of the animal or plant. Various wastes have been utilized for biogas production and they include amongst others; animal wastes industrial wastes, food processing wastes, plant residues etc. Many other wastes are still being researched on as potential feedstock for biogas production. Paper wastes are one of such wastes being considered as a potential feed stock. Waste papers are readily available from schools, offices, printing presses, factories etc., and in some developing countries are littered on the street as waste. These already constitute a nuisance with the poor waste management system prevalent especially in the third world countries. Therefore, using it as feedstock for biogas production will be a cheaper source of energy generation as well as a good waste management option. Much work has not been done using paper waste to generate biogas; however, the only study published so far on paper waste as a biogas source is a classroom project, carried out on a laboratory scale in converting waste paper to biogas. A full study was undertaken to investigate the biogas production potentials and capabilities of paper waste in terms of its cumulative biogas yield, onset of gas flammability and effective retention period. The study revealed that though paper waste is a very good biogas producer, with effective retention period of 77 days, its gas flammability ceased for a period of two weeks before resumption. It was concluded that the paper waste would require some form of treatment like co-digesting it with animal wastes to impart sustained gas flammability. Cellulosic wastes are generally known to be poor biogas producers because of their poor biodegradability. One treatment method for improving the biogas production of various feedstocks is co-digesting them with animal and/or plant wastes

II. NATURAL BIOWASTE

- All tree leaf
- Cow dung

III. MATERIALS AND METHODS

The waste paper used for this study was collected from a printing press in the University of Nigeria Nsukka while the cow dung was obtained from an abattoir in Nsukka market. The two digesters used are of metal prototype (50L capacity) constructed at the National Center for Energy Research and Development, University of Nigeria, Nsukka. The study was carried out between January and February 2010 at the same Research Institute. Nsukka is located at (6.9°N, 7.4°E) and 445m above sea level. Other materials used are; Top

loading balance (50kg capacity, "Five goats", model no Z051599), plastic water bath for soaking the paper waste, water trough, graduated transparent plastic bucket for measuring volume of gas production, thermometer (-10 to 110°C), digital pH meter (JENWAY 3510 digital pH meter (Designed and manufactured in the EU by Barloworld Scientific Ltd, Dun mow, Essex CM63LB), hosepipe and biogas burner fabricated locally for checking gas flammability

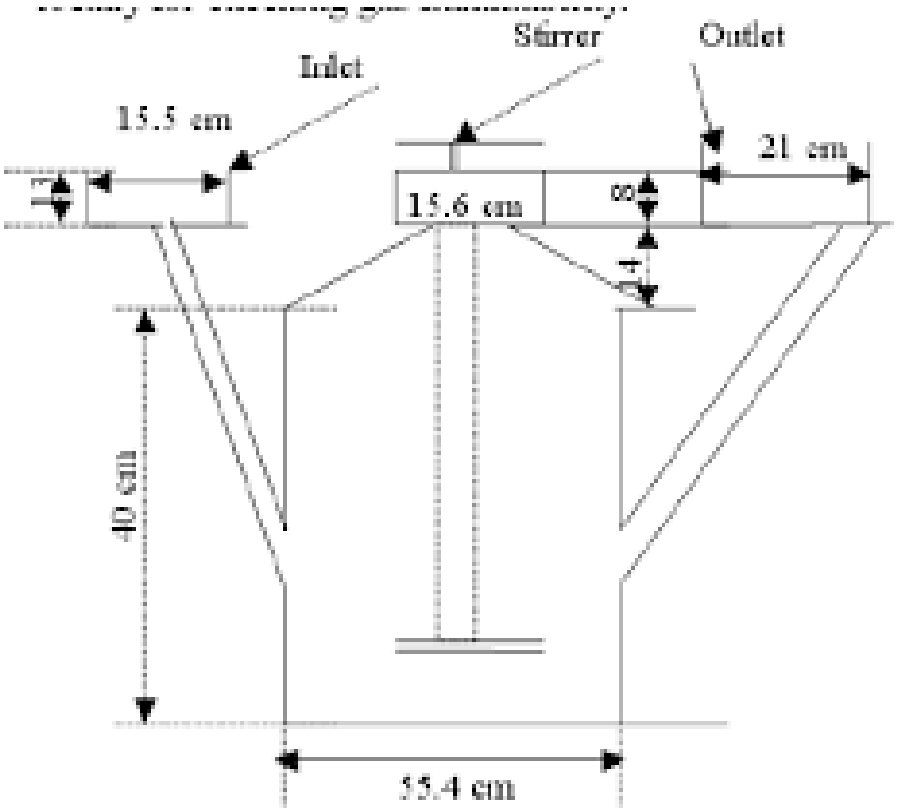

IV. DIGESTION STUDIES PREPARATION OF WASTES

The paper waste (PW) was soaked in a plastic water bath overnight to allow for partial decomposition by aerobic microbes, and the pH was noted. For the PW-A, 8kg of the paper waste was mixed with 27kg of water, while for the PW: CD, 4kg each of paper waste and cow dung were blended and mixed with 27kg of water, bringing all of them to water to waste ratio of approx. 3:1. The moisture content of the wastes determined the water to waste ratio

V. ANALYSES OF WASTES PHYSICOCHEMICAL ANALYSES

Ash, moisture and fiber contents were determined using AOAC (1990) method. Fat, crude nitrogen and protein contents were determined using Soxhlet extraction and micro-Kjedhal methods described in Pearson (1976) method. Carbon content was carried out using Walkey and Black (1934) method, Energy content was carried out using the AOAC method described by Onwuka while Total and Volatile solids were determined using Renewable Technologies (2005) method.

VI. MICROBIAL ANALYSIS

Total viable counts (TVC) for the wastes slurries were carried out to determine the microbial load of the samples using the modified Miles and Misra method described by Okore. This was carried out at four different periods during the digestion; at the point of charging, at the point of flammability, at the peak of production and at the end of the retention period.

VII. RESULTS AND DISCUSSION

The experiment was carried out under atmospheric temperature range from 26°C to 36°C and different mixture ratios of the different biomass mixed with cow dung was investigated and its calorific value of distinct mixture of dry biomass is directly proportional to the mass of the tree leaf only and the mixing ratios of cow dung and dry tree leaf.

REFERENCES

1. Kaygusuz K and Kaygusuz A **2002**, *Renewable Energy*, Volume 25, Issue 3, pp 431 453,doi: 10.1016/S09601481(01)00075-1.
2. Maishanu SM, Musa M and Sambo AS, **1990**, *Nigerian Journal of Solar Energy*, 9: 183-194.

Effect of Thermal Spray Coating (SiC) on Fuel Consumption and Emission Control on IC Engine

Mr. P. Murugan
Assistant Professor,
Department of Electrical and Electronics Engineering,
St. Anne's College of Engineering and Technology,
Anguchettypalayam, Panruti – 607106.

Mr. R. Jayakumar
Assistant Professor,
Department of Electrical and Electronics Engineering,
St. Anne's College of Engineering and Technology,
Anguchettypalayam, Panruti – 607106.

Abstract - In the age of rapid industrialization, one of the biggest problems faced by the world is fuel economy. The major components of the polluted environment are the increase of Co_2, So_2 and CO which is mainly contributed by automobile fuels. This ecological imbalance is the major hazard for human, animals, plants and planets. According to the sources of ONGC (Oil and Natural Gas Commission) there will be a great demand for automobile fuels due to increased rate of consumption of fuels and an impact on necessity of providing clean air environment in coming years. Hence there is a need arises for the automobile industry not only to find alternative fuel sources but also to produce fuel economic and eco-friendly vehicles. Here comes the rescue of thermal sprayed coating to solve the above problem considerably. A coating and surface modification technology allows not only protecting the surface against hostile environments but also improve the performance, extending the life and enhancing the appearance of materials. Thermal spray coatings are depositions of materials which has been melted or plasticized immediately prior to projection onto the substrate. The metal used and the application system used vary but most applications result in thin coating applied to surface requiring improvement to their corrosion or abrasion resistance properties. In this paper review, the thermal spray coating of I.C engine for reducing the emission and thereby improving the efficiency of the I.C engine are described. A two wheeler has been taken for testing and the results are analyzed with thermal spray coating.

Key words: Fuel Consumption, Thermal spray coating, SiC, Emission Control.

I. INTRODUCTION:

In the age of rapid industrialization one of the biggest problems faced by the world is fuel economy. The major components of the environmental pollution are Co_2, So_2 and CO which are mainly contributed by burnt fuels of automobile fuels. This ecological imbalance is the major hazard for human, animals, plants and planets. Depleting fossil fuel resources, economic competitiveness and environmental pollution has compelled to explore newer avenues to improve efficiency of automotive engines. Even though different techniques are used to save the fuel consumption like weight optimization, operating the engine at ecological loads and speeds. This paper deals with improving fuel economy in a two wheeler by using thermal spray coating.

A coating and surface modification technology allows not only protecting the surface against hostile environment but also improve the performance, extending the life and enhancing the appearance of materials. The thin coating of metal used depends upon the application results in surface improvement in respect of corrosion or abrasion resistance properties [1]. Thermal spray coating is a mechanical process of melting raw materials (either through the flame or electrical) into the plasma stage. The plasma stage material is loaded in a spray gun and sprayed on piston top.

II. COATING WITH GOOD LUBRICATION

It is essential to have least frictional forces present in between mating and/or reciprocating components. High coefficient of friction leads to higher wear rate affecting the engine life. Besides, mechanical friction has significant effect on the internal combustion (IC) engine fuel economy. In an IC engine, the major sources of frictions are valve train, piston system, crank and bearing system. Mechanical friction represents 10–15% of Indicated Mean Effective Pressure (roughly translates into energy available in a combustion cycle). Of the total frictional loss about 50-65% is accounted in piston system alone. Valve train system contributes 10-20% of friction loss and crank and bearing contributing the rest [2]. There is a pressing need to reduce these frictional losses to improve overall efficiency of the engine, reduce oil consumption and to increase life of engine.

III. TRIBOLOGY PROPERTIES

A coating is applied to improve the wear resistance and scuffing resistance at least as good as the cast iron liner substitute. Fine grained tribologically functional ceramics such as SiC, Al2O3 and Fe-oxides present in a coating can improve surface related properties such as hardness, compressive strength, abrasion resistance and scuffing resistance [2, 4, 9]. Scuffing is the major tribological issue of mass movement of surface elements via contact between two metals, especially when lubrication film breaks down. The coatings should also possess good mechanical and thermal shock resistance, good adhesion and strain compliance with the aluminum alloy substrate to meet the engine durability requirements. The tribological characteristics of the plasma coating lengthen the life cycle of the engine, while emissions decrease as a result of the reduction in fuel and oil consumption. It has been reported that plasma sprayed Fe/FeO as well as stainless steel/BN coatings reduced ring/bore wear by 40% and improved engine oil economy by 13600 km/l [6, 7].

IV. HEAT TRANSFER

Heat transfer to the block is to be kept to an absolute minimum, since this represents major heat loss. The coating should have low thermal conductivity, insulating the combustion chamber from conduction mode of heat transfer through aluminum or super alloy. Thermal barrier coating (TBC) was developed with an aim to reduce heat transfer. Computer simulations of internal combustion (IC), diesel and rocket engine as well as experimental data of diesel engine have shown that if the engine cylinder wall is coated externally by 2 mm thin layer of an insulating oxide, the heat loss is reduced by 6% [5,8]. If a coating is applied on inner diameter of cylinder bore, then the thermal gradient is lower for conduction mode heat transfer and the heat loss is further reduced. In a thermal barrier coating (TBC), a bond layer is applied above nickel-based super-alloy to improve the adherence of oxide coating. The thermally grown oxide has good coherency with the bond layer, on which another oxide layer (zirconia or titania-alumina) is plasma coated. The oxide layers also act as insulating resulting in minimum heat loss due to conduction [7, 9]

V. THERMAL SPRAY COATING

A group of overlay coating processes, in which existing metallurgy of component surface is changed in the near surface region either by thermal or mechanical means. This uses a concentrated heat source to melt feedstock materials while imparting kinetic energy using process jet to propel the molten particulates toward a prepared surface. When hot energetic particles impact in the surface of the part being coated, they rapidly solidify. Thermal spray processing is a well established means of forming coatings of thicknesses greater than about 50 micrometers so called thick coatings. A wide range of materials can be thermal sprayed for a variety of applications, ranging from heat engine to the electronics industry. Thermal spray coatings have been produced for at least 40 years, but the last decade has seen a virtual revolution in the capability of the technology to produce truly high performance coatings of a great range of materials on many different substrates. This enhancement of the technology has been achieved largely through the introduction of new spray techniques, the enhancement of spray process controls, by employing state of the art methods of feedstock materials production and through the use modern techniques of quality assurance.

VI. THERMAL BARRIER COATINGS (TBCS)

Thermal barrier coatings, such as Silicon carbide, Alumina applied by plasma spray. This class of ceramic has a very low thermal conductivity, effectively insulating the underlying superalloy substrate from the high temperature environment. For heat engines applications, the thickness of the TBC will be in the range of 0.13-0.15mm.At this thickness range, for hot sections operating at temperature around 1000°C, the surface of the insulated superalloy component can be reduced by approximately 100°C, enabling extended lifetime at the engines operating temperature or allowing the engine to function at a higher more efficient temperature. The sprayed TBC has a few volume percent porosity which contributes further to decrease in thermal conductivity. Thermal barrier crown is applied to the piston 0.13mm thickness of coating can also assist in extending piston life by decreasing the rate of thermal transfer.

VII. PERFORMANCE EVALUATION

Performance evaluation of automotive engines is a great importance for running the vehicle under economic condition. The method for assessing the performance includes the determination of engine economic speed, kilometer test, emission test and fuel economy. The test is carried on a plain road under steady speed. The observations of a road test conducted by the author[1] using a TVS 50 XL with and without coating on piston at various speeds are analysed.

VIII. RESULTS AND DISCUSSION

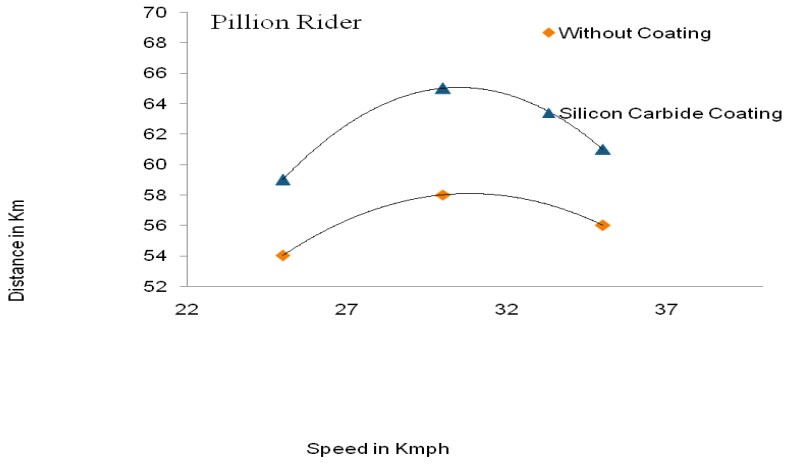

Figure (1)

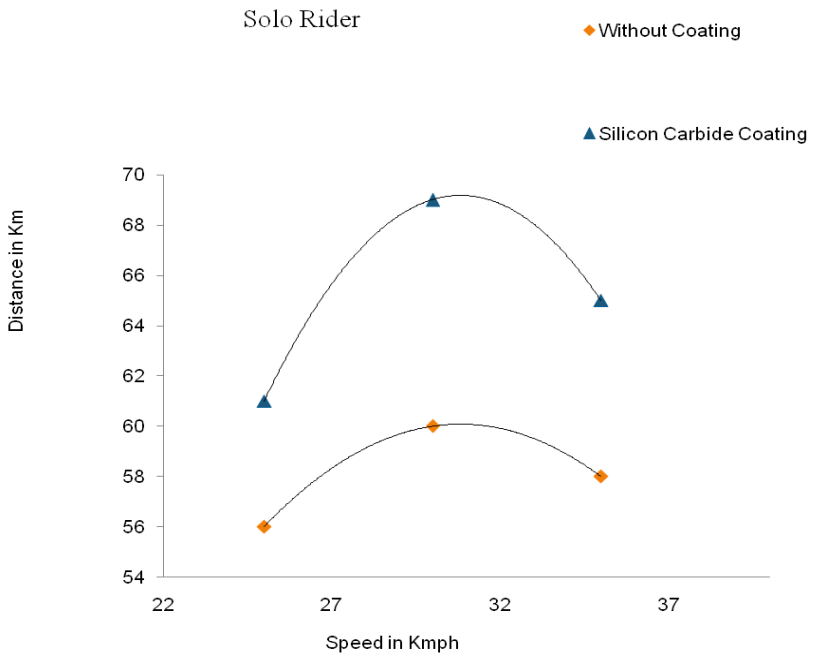

Figure (2)

Figure 1&2 shows the graphical representation between the speed in Kmph and distance in Km. From the graph, it clearly indicates that, the distance travelled per litre is improved when the piston is coated with SiC, in the case of both solo rider and pillion rider. The result shows the economic speed of running the vehicle is at 30 KMPH based on fuel consumption. Under this condition the KMPL is observed as economical with solo as well as with pillion rider driving. The result shows that KMPL is more in the case of coating with alumina than without coating. The emission test analysis shows an emission level reduction of 0.12% in the case of alumina coating. The performance of the engine is considerably increased with SiC coating with lower emission levels.

IX. CONCLUSION

The present investigation shows that, KMPL (kilometer per litre) is more when the piston is coated with .SiCThe efficiency and performance of the Internal Combustion engine also improved.

REFERENCES

1. K.Gosh, T.Troozynslei and A.C.D.Chaldfeer. Aliminium, silicon carbide coating by plasma spraying. Journal of thermal spray technology78 (1997) PP 78-86.
2. W.D. Kingery, H.K. Bowen, D.R. Uhlmann, Introduction to Ceramics, Wiley, New York. M. Buchmann, R. Gadow, A. Killinger, Proceedings of First International Thermal Spray Conference, Montreal, Que., Canada, InternationalThermal Spraying Society, Materials Park, OH, 2000, pp.303.
3. H.G. Jiang, M.L. Lau, E.J. Lavernia, Precede 15th Internl. ThermalSpray Conf., Nice, France, International Thermal Spraying Society, Materials Park, OH, 1998, pp. 1265.
4. N.B. Dahotre, S. Nayak / Surface & Coatings Technology 66 194 (2005) 58–67.

5. Ali Alian and Issam S. jalhamabrasive wear resistance comparative study of plasma - sprayed steel by magnesium zirconate, aluminum-bronze, molybdenum, and mixtures of them as coating materials.
6. M. Vardelle, A. Vardelle, K-I Li, P. Fauchais Coating generation: Vaporization of particles in plasma spraying and splat formation.
7. Javad Mostaghimi A computational Model for Prediction of the Microstructure of Plasma Sprayed Coatings.
8. Ozkan sarikaya. Effect of some parameters on microstructure and hardness of alumina coatings prepared by the air plasma spraying process. Journal of surface coating and technology-(2005) PP 388-393.
9. Zhijian Yin Shioyantao, Xiaming Zhou, Chauaxian Ding. Tribological properties of Al/ Al_2O_3 composite coating. Journal of wear (2007) PP 52-65.

Processing, Microstructure and Mechanical Properties of Graphite and fly ash Reinforced Magnesium AZ91 Metal Matrix Hybrid Composites

Mr. R. Jaganraj
UG Student,
Department of mechanical Engineering,
St. Anne's College of Engineering and Technology,
Anguchettypalayam, Panruti – 607106.

Mr. T. Elangovan
Assistant Professor,
Department of mechanical Engineering
St. Anne's College of Engineering and Technology,
Anguchettypalayam, Panruti – 607106.

Abstract – Magnesium alloy (AZ91) is used as the base metal matrix. Graphite (Gr) with 10 wt%) and fly ash with varying 10 wt% is used as the reinforcing materials. The compacted green samples were sintered at 450 for 20 min. The prepared metal matrix composite hybrid (MMC) samples were subjected to characterization and mechanical studies such as optical microstructure, X-ray diffraction, Scanning electron microscopy (SEM), and hardness. Results showed that magnesium metal matrix composites (MMC) hardness increased from 64.53 to 75.16 HV, which was mainly due to the presence of reinforcements Gr and fly ash along with precipitates. Addition of Gr and fly ash on magnesium alloy, influenced the hardness of MMC.

Keywords: Metal–matrix composites (MMC); Particle-reinforced composites; Powder processing; sintering.

I. INTRODUCTION

Need for lighter materials, made the automotive manufacturers to start looking for material lighter than aluminium. In early 1990's, automobile industries started to invest in magnesium material. In last years, magnesium and its alloys have attained widespread attention in scientific research and commercial application. It has low density, approximately two-third of that of aluminum [1], and high specific strength [2] as compared to other structural metals. As energy conservation and performance demands are increasing in automotive technology. Usage of lightweight materials, will improve fuel economy and reduction of emissions [3]. However, the application of magnesium alloys is restricted due to its poor creep resistance at high temperatures, low strength, low modulus and wear resistance [4, 5]. Most commercial magnesium alloys (AM50, AZ31, AZ91) contains aluminium, manganese and zinc that allows obtaining suitable properties by adding reinforcements [6]. The reinforcements used in MMC are particulates like graphite ,fly ash, copper etc. [7]. The most common reinforcements studied are Graphite and fly ash magnesium alloy (AZ91) reinforced with Graphite reported noticeable improvements in hardness and tensile strength prepared by using stir casting technique [8]. Similarly, Addition of Fly ash increases corrosion rate and cracking. Fly ash is the best strengthening reinforcement since it is having higher values of Vickers [9, 10]. Mechanical properties and nucleation depends on processing, composition and type of reinforcement [11, 12].

MMCs are manufactured by techniques like powder metallurgy, stir casting process, squeeze casting, In-situ process, ultrasonic cavitation process, spray forming, pressure less infiltration techniques, etc. Cost of fabrication remains a major disadvantage in MMC. The composite materials offer flexibility in selection of reinforcements to tailor the properties. Therefore, cost effective processing of composites plays a crucial role in expanding their applications. Light weight; low cost of processing of hybrid MMCs is yet to attract much attention from researchers by using high strength reinforcements such as Graphite and Fly ash. This research is motivated by the potential benefits of developing MMCs reinforcement with Graphite and Fly ash by using powder metallurgy technique. To study the effects of the addition of particulate reinforcements on the microstructure, physical and mechanical properties of magnesium.

II. EXPERIMENTAL PROCEDURE

Fig. 1 shows the synthesis and characterization of samples used in this study. Sample preparation was carried out for different compositions with AZ31with 95-87 wt% used as the base metal matrix

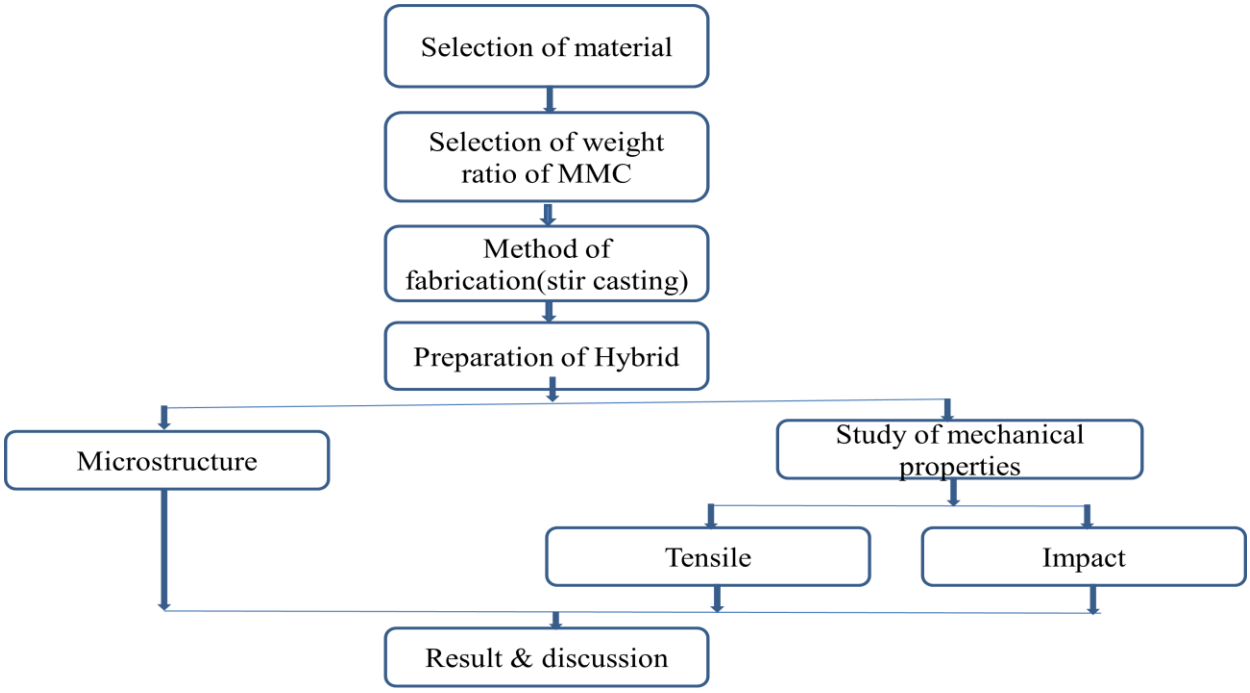

Fig. 1. Methodology of research

The composition of Graphite was fixed at 10% and Fly ash fixed 10 wt% with corresponding composition of magnesium alloy. Green compacts were prepared using stearic acid (CH3 (CH2)16COOH (2 wt%) used as lubricant. Powder metallurgy technique was used for the synthesizing of magnesium metal matrix composites. The reinforcement powders with their weight compositions were mixed in order to ensure uniform distribution of the powder particles. Mixtures were compacted at 200 MPa for 30s different compositions. The compacted samples were subjected to heat treatment in microwave sintering sintered at 450ºC at the rate of 10°C/min for 20 min. Sintered samples are cooled at furnace itself. The density of the sintered samples was determined using Archimedes principle. The phase composition was analysed by diffractometer (SEIFURT) with a graphite monochromatic Cu-kα radiation (λ = 1.54056 Å), operating at 30 kV and 40 mA to study the X-ray powder diffraction (XRD). The XRD patterns were acquired in the 2θ range of 5-70° [11]. SEM (Make: Jeol, Japan; Model: 6410-LV studies were conducted on

polished specimens to investigate the presence of reinforcement distribution, and matrix reinforcement grain size and gain morphology. Micro hardness (Make: Shimadzu) was measured on the Vickers superficial Scale using a 1.588 mm (1/16 inch) steel ball indenter with test load of 15 kgf and dwell time of 2 seconds. Microstructures were taken on the polished samples using optical microscope at 100X

III. X-RAY DIFFRACTION

Fig. 2 shows XRD result of AZ91 (80 wt%) magnesium alloy reinforced with Graphite (10 wt%) and Fly ash (10 wt%). The sintered magnesium alloy samples were quantified using SEIFURT diffractometer. The diffraction pattern shows the presence of magnesium in higher content from the intensity of peaks compared to Graphite and Fly ash Intensity of peaks for Graphite and Fly ash were very low due to the presence of magnesium content in the sample. XRD patterns from this results confirms the presence of fraction of Fly ash in the sample. Thus confirms the objective of adding Fly ash and Graphite in this research to improve mechanical properties.

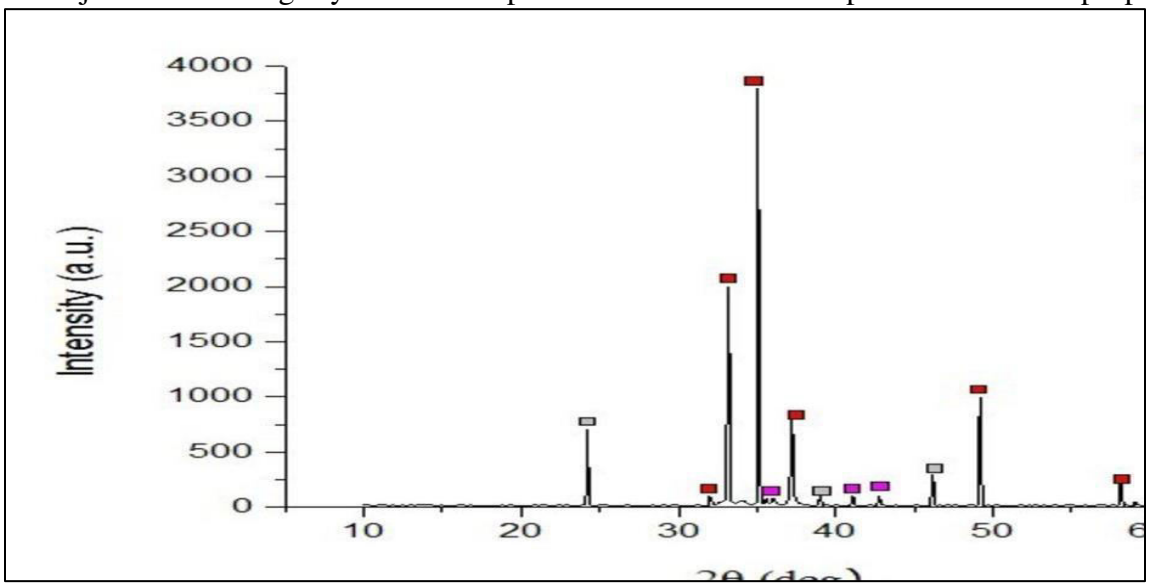

IV. SCANNING ELECTRON MICROSCOPY

Microstructural characterization of the composites showed significant grain refinement, relative uniform reinforcement distribution, and presence of minimal porosity. SEM analysis shows the AZ91 matrix, Graphite and Fly ash particles are well bonded. The presence of precipitates was observed in the matrix or at the interface. Interface has a strong influence to the properties of the composites. A closer observation by SEM showed that the microstructure consisted of primary magnesium, Fly ash, ß-Mg17-Al12, and Mg2Si precipitates as shown in (Fig 2.) Precipitates were hard and brittle contributing to the hardness of the alloy. SEM images show that reinforcements were distributed in a random and isotropic orientation and no agglomeration was observed. The presence of reinforcements around the boundaries may act as barriers to prevent the grains from growing further (Fig 3). Fly ash with an average size of grain sizes of 0.320µm showed good strength. As a result of the restriction of this growth, the primary phase would allow the melt to have enough time to form more nuclei. Microstructure showed the interface was sharp and clean without any visible interaction zone. The uniformity of the reinforcement distribution provided great contribution to the mechanical properties of the magnesium matrix composite

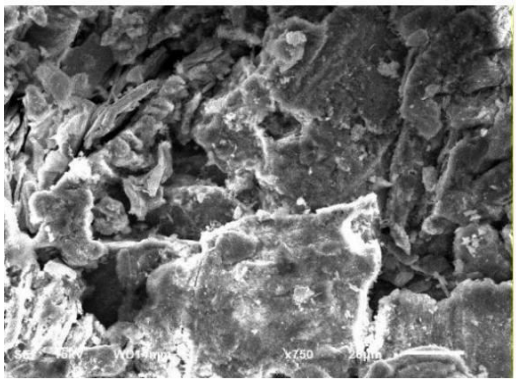

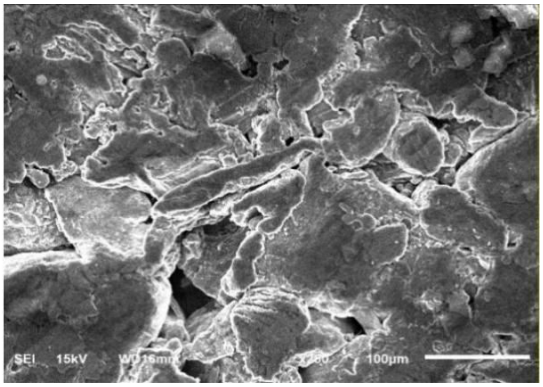

V. DENSITY MEASUREMENT

From the table 1, the density of magnesium composites increased with respect to increase in the reinforcement wt% (Graphite and Fly ash). The density of Graphite is higher than Fly ash and AZ91 and hence an increase in the Graphite content increased the density of the composite. It is observed that by increasing the wt% of Graphite from 10% density increased by 14.66%.

Table 1. Density Measurement Value for (Mg 95%-87%)

Sample	AZ91 %	Density (g/cm^3)
1.	77	1.9681
2.	78	1.9534
3.	79	1.9387
4.	80	1.9240
5.	81	1.9093
6.	82	1.8946
7.	83	1.8010
8.	84	1.7980

9.	85	1.7189

VI. OPTICAL MICRO STRUCTURE

Microstructural evaluation for different samples of metal matrix hybrid composite is shown in Fig. 4. Observation showed randomly dispersed Fly ash and Graphite particles in AZ91 matrix. In Mg matrix. It is observed that the Fly ash and Graphite particulates are visible and non-homogeneous distribution of Fly ash and Graphite particles was observed at some locations in the magnesium matrix is evident. From Fig. 4c that there is a high volume percent of particulates dispersed in the magnesium matrix for the hybrid composite containing 10 wt% of the Fly ash in comparison to the reinforcement with 3 and 5 wt% of Fly ash

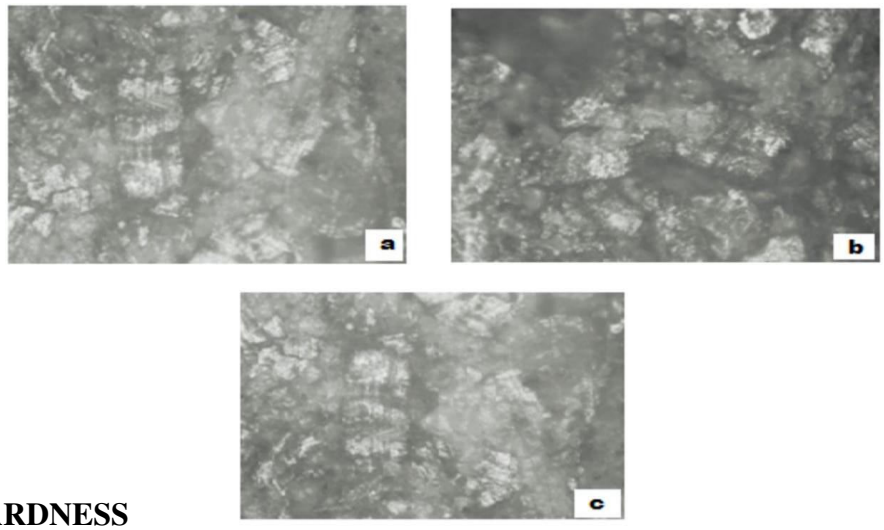

VII. HARDNESS

Table.2 shows hardness was found to increase with increase in Graphite content in the hybrid MMC. In hybrid composites hard Graphite particles act as a load bearing member. Hence it enhances the mechanical property of the material. Hardness of the composite increased by 16.47% as the reinforcement content of Fly ash and Graphite particles was fixed 10 wt%. Silicon particles present along the flow lines and act as barriers to the movement of dislocations within the matrix. The increase in weight fraction of hard particle increased the hardness of the MMC. Our results reported in the table.2 were consistent with the results observed for A356/Graphite [13] and Al-Si/Graphite by earlier researchers. This observation should be attributed to the presence of the reinforcements Fly ash and Graphite along with presence of precipitates confirmed from the results of SEM with their superior strength and stiffness. Besides, the reduced grain size also had contribution to the increase in hardness.

Table 2. Micro Hardness measurement (AZ91 85%-77%)

Sl.NO	AZ31 %	Hardness HV	Load Gm
1.	77	75.16	200

2.	78	74.83	200
3.	79	73.25	200
4.	80	72.12	200
5.	81	67.95	200
6.	82	69.42	200
7.	83	69.71	200
8.	84	67.49	200
9.	85	64.53	200

VIII. CONCLUSION

AZ91 MMC was successfully synthesized using powder metallurgy technique. The microstructure, hardness and density of the samples were evaluated. The obtained results are summarized as follows:

1. Micro structural investigation showed random dispersion of reinforcing particles Fly ash and Graphite particle in Mg matrix.
2. Reinforcing Aluminum alloys with ceramics particles has shown an appreciable increase in its mechanical properties. Hardness of Mg is increased by 16.47% with increase in Graphite reinforcement.
3. Density of AZ91-Graphite-Fly ash hybrid composites was found to increase with increase in Graphite.

Hence Fly ash serve as a complementing reinforcement for the development of low-cost high-performance magnesium hybrid composite.

REFERENCES

1. P. Cavaliere and P. P. De Marco, "MaterialsCharacterization 58", The Japan Institute of Metals, 226–232, 2007.

2. L. Duffy, "Magnesium Alloys", Magnesium Alloys Magnesium Alloys Materials World, Vol 4. No.3, pp. 127-30, 1996.
3. Stodolsky F., Vyas A., Cuenca R., "Lightweight materials in the lightduty passenger vehicle, their market penetration potential and impacts," International scientific journal, pp. 3–9, 1995.
4. S.Kim, H. Yoo, Y. Kim, "Research strategy for AM60 magnesium steering wheel", Magnesium Technology 2002.
5. M. Avedesian, H. Baker, editors, Magnesium and Magnesium Alloys, ASM Speciality Handbook, ASMInternational, The Materials Information Society, 1999.
6. H. Mohd Ruzi, M. Norhamidi, S. Abu Bakar,mR. J. Khairur, M.N. Nor Hafiez, A. Sufizar, I.I Mohd Halim, Murtadhahadi, "A Review ofWorkability of Wrought Magnesıum Alloys, Advanced Manufacturing", Research Group'09 Seminar 3, 2009
7. H. WESTENGEN,"Magnesium alloys for structural applications; recent advances", Colloque C7 suppliment au Journal de Physique 111, Volume 3, 1993.
8. B. L. Mordike, T. Ebert, "Magnesium – applications – potential", Journal of Material Science Engineering A 302, pp. 37-45, 2001.
9. M. Habibnejad-Korayema, R. Mahmudi, and W.J. Pooleb, Enhanced Properties of Mg-Based Nano-composites Reinforced with Al2O3 Nano-particles, Mater. Sci. Eng., A, 2009, 519, p 198–203
10. C. Blawert, N. Hort and K.U. Kainer "Automotive Applications of Magnesium and Its Alloys", Trans. Indian Inst. Met. Vol.57, No. 4, pp. 397-408, August 2004.
11. M.A. Malequel, A. Atiqah1, R.J. Talib and H. Zahurin "New Natural Fiber Reinforced Aluminium Composite for Automotive Brake Pad" Schumann, 2005.
12. Q.C. Jiang, H.Y. Wang, B.X. Ma, Y. Wang, F. Zhao, Fabrication of B4C particulate reinforced magnesium matrix composite by powder metallurgy, J. Alloys Comp. 386 (2005) 177.
13. Z. Xiuuqing, W. Haowei, L. Lihua, M. Naiheng, in situ synthesis method and damping characterization of magnesium matrix composites, Comp. Sci. Tech. 67 (2007) 720.

IIOT Enabled Smart Automated Guided Vehicle for Manufacturing Industry 4.0

Sr. Josephine Mary A
Assistant Professor,
Department of Mechanical Engineering,
St. Anne's College of Engineering and Technology,
Anguchettypalayam, Panruti– 607106.

Mr. T. Alan Arptharaj
UG Student,
Department of Mechanical Engineering
St. Anne's College of Engineering and Technology,
Anguchettypalayam, Panruti– 607106.

Mr. S. Naveen Kumar
UG Student,
Department of Mechanical Engineering
St. Anne's College of Engineering and Technology,
Anguchettypalayam, Panruti– 607106.

Abstract - Automation of automated guided vehicle improves the tasks of safety and minimization of use of energy in the material handling process of the factory. In addition with this, the driverless AGV material handling system need have to be integrated with IIoT (The Industrial Internet of Things) to enhance the Fourth Industrial Revolution for making the system smart-decision making. In this paper, we deal the setup of AGV-Conveyor-Loading and unloading Grippers with IIoT in real industry environment for enhancing the third industrial revolution. The goal of AGV enabled IIoT is to make the machines to communicate and cooperate with each other and also with humans and thus to improve the own-decision making of the system. The AGV model is composed of Arduino Mega 8 microcontroller and ultrasonic and IR sensors to detect the obstacles and to control the path of motion respectively. The AGV traces the defined path of IR tape/RFID tag coated surface as per the map. If any hindrance of block found in between then the machines communicate with each other and with humans so as to de-activate the process via Bluetooth and internet connectivity. Once the problem is rectified then the whole system is autonomously activated for further progress. This work of concept totally reduces the time and labours for the process and increases the flexibility of manufacturing.

IndexTerms — **Industry 4.0, IIoT.**

I. INTRODUCTION

1.1 Industry 4.0

Automation is a wide area and there are many ways and means to reduce the manual work in the industries. As an example, introducing automated guided vehicle increases the benefits of

flexibility by improving the tasks of safety and minimizing the use of energy. The AGV kits consist of software, hardware and navigation. Other than the above mentioned tasks, now-a-days AGVs need to be focused on value-creating tasks which can attract the young digital generation to the fourth generation of industry.

The following figure exhibits the evolution of Industrial revolutions.

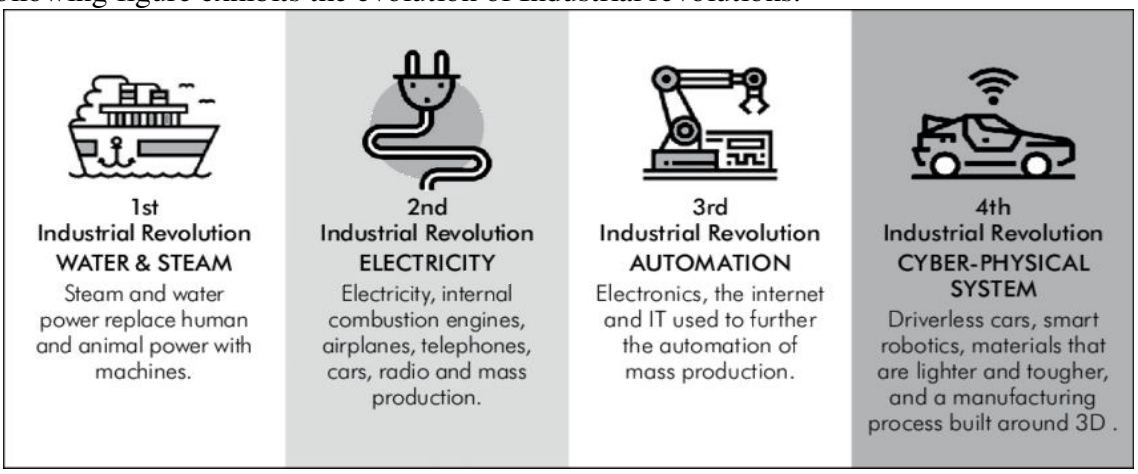

Industry 4.0 lies in advances in communication and connectivity rather than technology. It consists of cyber-physical systems, the Internet of things. Cloud and Cognitive computing. Over the internet of Things, cyber-physical systems communicate and co-operate with each other and with humans in real-time both internally and across organizational services [3].

Industry 4.0 contains the four design principles that are explained below.

Interconnection

The ability of machines, devices, sensors and people to connect and communicate with each other via the Internet of Things(IoT) and the Internet of People(IoP).

Transparency and Interconnectivity

Interconnectivity permits the operators to collect vast amounts of useful information and data from all angles of points regarding manufacturing process. Transparency permits to make appropriate decisions out of vast amounts of useful informations collected.

Technical assistance to support humans

The assistance systems must be able to aggregate and visualize information comprehensively for making informed decisions and solving urgent problems on short notice. Also the cyber-physical system must be able to conduct a range of tasks that are unpleasant or unsafe to the human co-workers.

De-centralized decisions

The cyber-physical systems must be able to make decisions on their own and perform their tasks as autonomously as possible. But in case of some exceptions interferences or conflicting goals are delegated to higher level.

1.2 Automated guided vehicle

AGVs are self-guided vehicles which are used as material handling systems in order to transport raw materials and manufactured products from one place to another place in the factory without any human assistance. It is one of the most suitable and efficient option.AGV should be able to manage the different situations like a block or obstacle in layout and operate in a flexi-dynamic environment. These confrontations demand smart decisions making of AGV. Therefore this paper aims at the integration of IoT for developing a smart AGV system that is fully sensor

based. The system communicates the intimation or information of block or obstacle to the respective person via internet and de-activating the other integrated mechanical elements like conveyor and grippers' motion. If block is removed then the whole system of AGV along with conveyer and grippers are activated through IoT for further progress.

In this paper, AGV, conveyor and gripper mechanisms are IoT enabled elements. The processing steps of proposed automated guided system are explained as follows:

- At source point, loading gripper lifts the product from moving conveyor and places on the AGV platform.
- AGV autonomously navigating towards destination point.
- At destination point, AGV unloading the product.
- AGV navigating towards source point after unloading the product to start a new mission.
- Communicating the information of block/obstacle if any found to the respective person through Internet
- Auto-deactivating the movements of conveyor system and gripper mechanism.
- Auto-activating the movements of conveyor system and gripper mechanism after removal of obstacle.

This paper is structured as in the following sequences. Section 2 explains the literature review .Section 3 describes the smart AGV and its hardware interfaces. Section 4 briefly explains the software interface. Section 5 expresses the proposed system design with the track design. Section 6 summarizes the conclusion about the work.

II. LITERATURE REVIEW

2.1 AGV and IOT

The automated guided vehicle has immense demand in the manufacturing industry. IOT based AGV is connected with the internet and get all the information's such as weight, type, size and dispatch time. With the arrangement of RFID cards, all the information's can be stored in the device and can be accessed anytime and anywhere. The stored information's are transmitted to respective person via internet using Ethernet shield and arduino mega 2560 [1]. Customers expect both higher productivity and greater variety which are obtained from the efficient and optimized automation systems. With the addition of internet technologies to the automation, manufacturing systems are made to perform self-decision making. Thus, the goal is to make factory environment more intelligent where the products themselves will be used to determine their next required process. Therefore AGV system with RFID technology is developed to frame an intelligent and flexible environment. RFID technology enables smart decision-making for AGVs and improves fixed form guidance methods such as optical line [2].

III. HARDWARE INTERFACE

3.1 Arduino Mega 8 Micro-Controllers

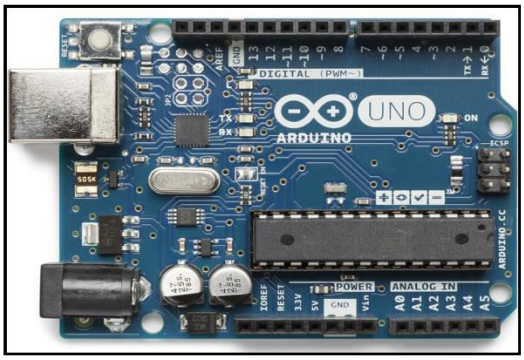

The ATmega8 is a low-power CMOS 8-bit microcontroller based on the AVR RISC architecture. The abbreviation of AVR Microcontroller is "Advanced Virtual RISC" and MCU is the short term of the Microcontroller. A Microcontroller is a tiny computer on a single chip and it is also termed as a control device.

3.2 Ethernet Shield

The Arduino Ethernet Shield allows an Arduino board to connect to the internet. It is based on the Wiznet W5100 ethernet chip (datasheet). The Wiznet W5100 provides a network (IP) stack capable of both TCP and UDP. It supports up to four simultaneous socket connections.

3.3 Ultrasonic Sensor

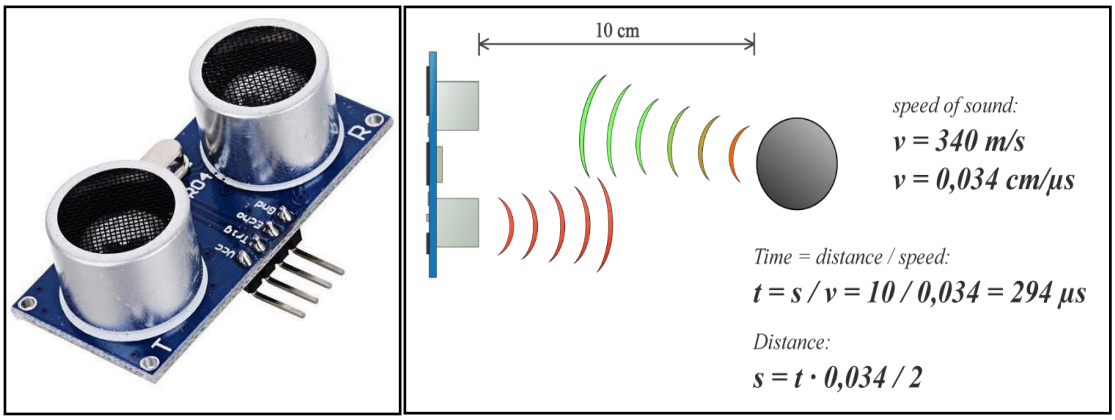

Ultrasonic sensors measure distance by using ultrasonic waves. The sensor head emits an ultrasonic wave and receives the wave reflected back from the target. Ultrasonic Sensors Measure The Distance To The Target By Measuring The Time Between The Emission And Reception.

3.4 Bluetooth Module

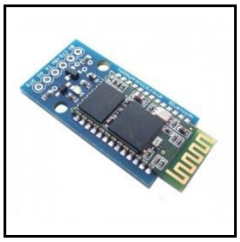

This system the HC-05 Bluetooth module is used to communication between the department and AGV. Which is required the 5v supply to operate. It can easily configure with arduino.

3.5 RFID Module

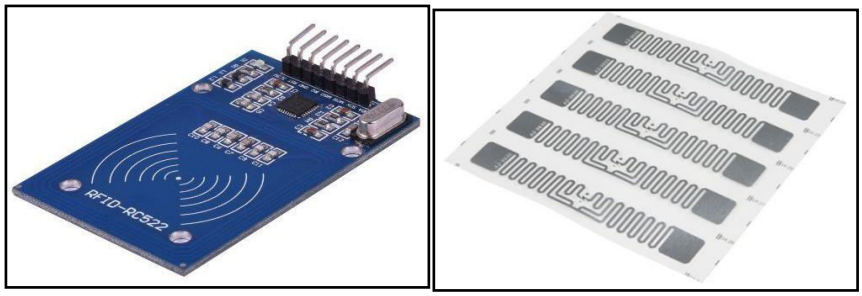

RFID is a technology which is working on radio frequency of radio waves. So, this technology is used to automatically identifying the object or tracking the objects.

3.6 Geared Motor

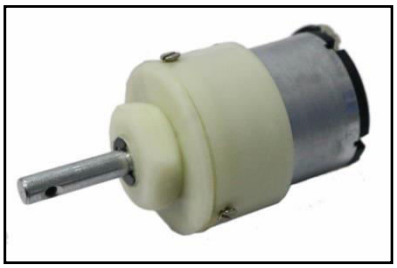

"Gear motor" may be an AC or DC motor coupled with a gearbox or transmission. A gear motor adds mechanical gears to alter the speed/torque of the motor for an application. Usually such an addition is to reduce speed and increase torque.

3.7 RTC Module

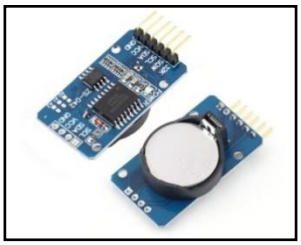

A real-time clock (RTC) is a computer clock (most often in the form of an integrated circuit) that keeps track of the current time. Although the term often refers to the devices in personal computers, servers and embedded systems, RTCs are present in almost any electronic device which needs to keep accurate time.

3.8 Battery

Universal batteries are the recent adaptation to charging technology that is changing the way consumers interact with their electronic devices. Universal batteries are universal charging devices capable of connecting to a variety of devices via USB, Lightning, or other similar port types.

IV. SOFTWARE INTERFACE

4.1 ATMEL Studio 6

AVR studio is an Integrated Development Environment (IDE) by ATMEL for developing applications based on 8-bit AVR microcontroller. It comes with its own integrated C compiler the AVR GNU C Compiler (GCC). As such you do not need a third party C compiler.

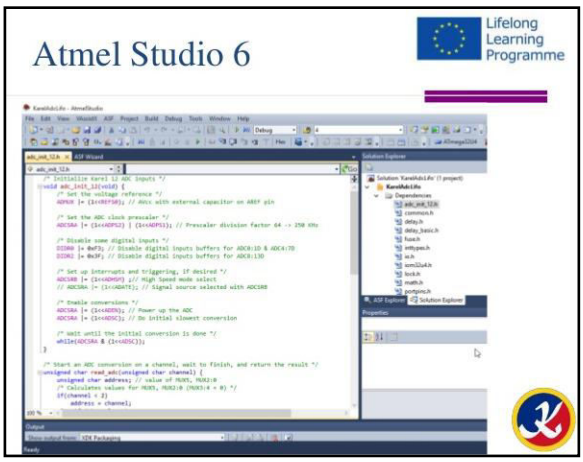

V. PROPOSED SYSTEM WITH TRACK DESIGN

The IIOT enabled automated guided vehicle system consists of Arduino Mega 8 controller with ultrasonic sensor fitted at the front of AGV to sense obstacle and IR sensor/RFID reader fitted at the base of AGV to sense the path of motion. The system is battery operated. The communication is carried out among AGV, conveyor and grippers for loading and unloading with the help of Bluetooth. After receiving the signal the automated guided vehicle follow the given path with the help of IR and RFID reader.

The IR tape /RFID tag is spread over the path of map on which the AGV has to move. The platform of AGV receives the part from conveyor with the help of loading gripper and travels towards the destination point where the part is unloaded by another gripper. While travelling the ultrasonic sensor placed at the front of AGV emits the ultrasonic waves.

The blocks if any found the ultrasonic waves are reflected back to the front of AGV in order to recognize the position of block. The sensor sends the message to microcontroller which in turn takes the action to stop the AGV. Simultaneously the same message of 'stop' is transmitted through the Internet to the conveyor and gripper systems to stop the process for a while until the problem is rectified. If the problem is cleared then the whole system is activated autonomously.

The block diagram illustrates the signals of the sensor passing through the system according to the process in progress..

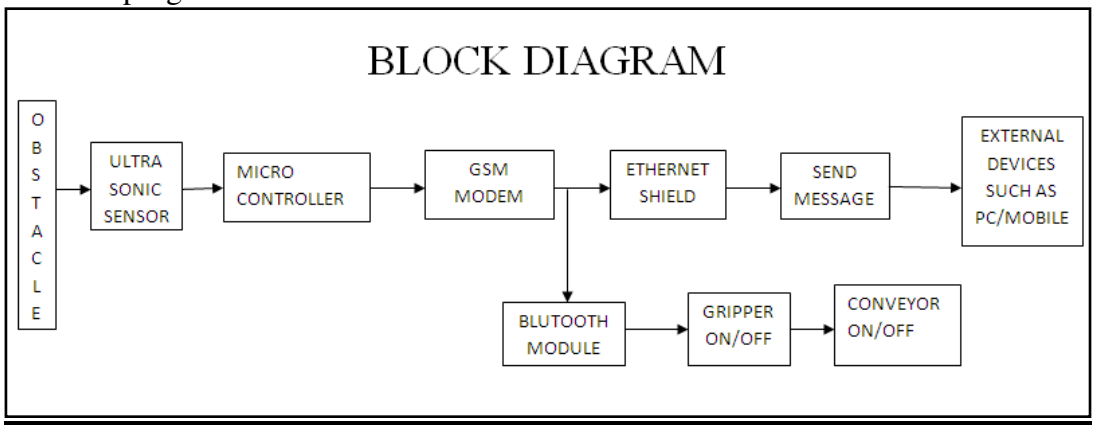

The path of AGV with loading and unloading positions is given as the map of subject.

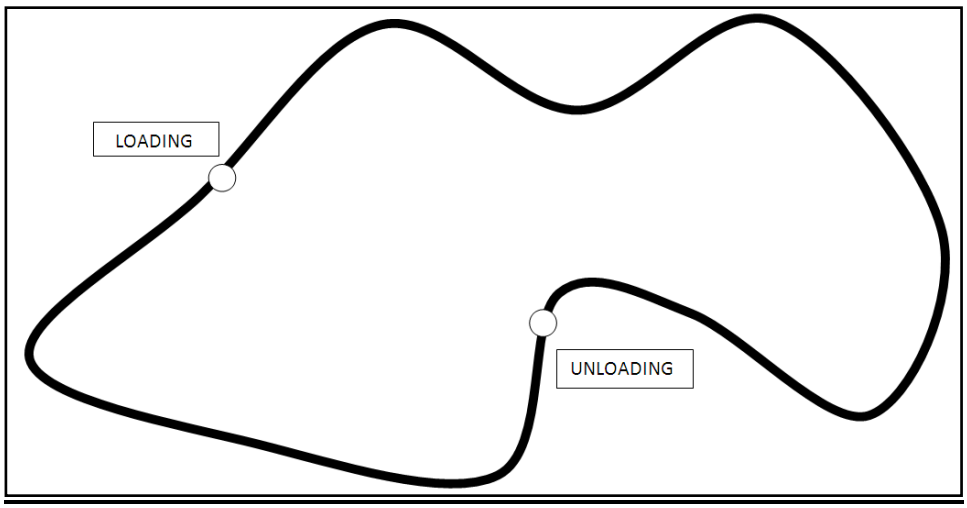

VI. CONCLUSION

This system can transfer information about process' occurrence to the concerned person/department through the connectivity of IIoT with the automated guided vehicle, conveyor and gripper mechanism. By getting the information, the employee can move forward to rectify the problem of block on the path. The process of Activation and De-activation occur autonomously according to the signal received from the sensors. Thus the implementation of interconnection between machines and IIoT enhances also lean manufacturing standard of eliminating wastes such as time and labour.

REFERENCES

1. Yogesh Kakasaheb Shejwal,Sasikumar Gera, 'IoT based automated guided vehicle'. International research journal of engineering and technology, volume 05,Issue 4,May- 2018 ISSN: 2395-0072.
2. Jasprabhjit Mehami, Mauludin Nawi,Ray Y Zhong 'Smart automated vehicles for manufacturing in the context of Industry 4.0',Science Direct, Procedia Manufacturing 26 (2018)1077-1086.
3. Marr, Bernard' Why Everyone must get ready for the fourth industrial revolution'.Forbes(blog).Retrieved 2016-12-12.
4. Virendra Patil, Bhatwadekar 'Automated guided vehicle' International research journal of engineering and technology, volume 05,Issue 4,April- 2018 ISSN: 2395-0072.

Performance Analysis of Friction Stir Welding of Aa6063

Mr. K. Shanmuga Elango,
Associate professor
Department of Mechanical Engineering
St.Anne's College of Engineering and Technology
Anguchettipalayam, Panruti-607106

Mr. D. Padmanathan ,
Mr. A. Sujin,
UG Student,
Department of Mechanical Engineering
St.Anne's College of Engineering and Technology
Anguchettipalayam, Panruti-607106

Abstract - Generally, for joining process for soft materials such as aluminum alloys and also for hard materials like steels friction stir welding is used as it avoids many of the common problems obtained in fusion welding. Also if we gone through joining of aluminum alloys could be usually faced problems in many cases available in various fields like automotive, aerospace, ship building industries, electronics etc. where fusion welding is not possible due to large difference in physical and chemical properties of the components to be joined. Mainly the problems occurred in the welding processes like porosity formation, solidification cracking, and chemical reaction may arise during fusion welding of dissimilar materials. Even if good welded joints may be obtained in some limited cases with special attentions to the joint design and preparation, process parameters and filler metals. For avoiding the drawbacks of fusion welding friction stir welding (FSW) seems to be a very reliable technique as it permits welding of aluminum alloys. To avoid the majorly obtained health defects observed during traditional welding methods or fusion welding it can be used. The productions of ultraviolet rays and the gases produced in the process which are harmful to human beings are minimized to large extent. The parts produces in FSW of aluminum alloys have been becoming increasingly significant in industrial applications because of their technical and economic benefits. The article contains mainly the selection of tool material and process parameters with experimentation trials of FSW of AA6063. Also this contains the large overview on tool material selection which depends on the operational parameters such as temperature of the operation, wear resistance, geometry and load bearing ability also the tool degradation process. The design of tool is very important because our target is not only the material removing from the metal but also heating and mixing the material by frictional heat. The article contains information about many numbers of tool geometries and importance of tools for friction stir welding of AA6063. And the selection of operational parameters as per the specimen size which are used for the process and the testing of joints after the welding.

Keywords — Friction Stir Welding, Temperature, Tool Material, Tool Geometry.

I. INTRODUCTION

The process of Friction stir welding (FSW) used for joining metals parts was invented at The Welding Institute (TWI), United Kingdom in1991 and has found applications in many

number of fields like aerospace, automotive, railway and marine. Also it is considered as an alternative welding process to fusion welding. Various number of characteristic of FSW is that the joint is created by a cylindrical rotating tool, mechanically traversed through the materials to be joined. Due to frictional heat generated between the wear-resistant welding tool shoulder and pin, and the material of the work-pieces the joint is take place. Because of the frictional heat and surrounding temperature causes the stirring action material and get softened and mixed to each other [1].

It is to be considered as the most significant development in metal joining as compared to the old conventional welding methods. Actually, the FSW consumes considerably less energy. As no any gas or other flux is used, thereby making the process environmentally. Also the process of joining does not involve any use of filler metal and therefore any aluminium alloy can be joined without concern for the compatibility of composition, which is an issue in fusion welding. When desirable, dissimilar aluminium alloys and composites can be joined.

II. LITERATURE REVIEW

In this section the detailed literature review of the friction stir welding was done and experimentation of FSW with parametric study of aluminium and its alloy is carried out. M.K. Sued, D. Pons, J. Lavroff, E.H. Wong propose the design features for bobbin friction stir welding tools; also explains the features for bobbin friction stir welding tool and developed with linking it with physics of the process of FSW production process for obtaining the effects of bobbin friction stir welding tool having different pin structures were tested effectively. R.S. Mishra and Z.Y. Maworks on worked mainly on the aluminium alloys with some process parameters also gave the main points results that, the mechanisms are responsible for the formation of welds and microstructural refinement and also effect of process parameters on the microstructure of the base metals & joints. Also a lot work had been done on the tool design parameters for FSW. KudzanayiChiteka, explains tool material selection is an important task which helps to determine the weld quality produced. The tool material selection affects the tool operational parameters like temperature generation, speed of welding, tool wear property etc. The study gives the analysis of tool materials that can be used successfully for the process[3]. R. Rai, A. De, H.K.D.H. Bhadeshia and T. DebRoy had given the information about the feasibility of the FSW for harder alloys such as titanium.

III. SELECTION OF MATERIAL & TOOL

In the process of friction stir welding the material selection is basic part. From the literature review, there are large number of materials were used for this process. From the various alloys of aluminium the AA6063 is selected. It is available in the round bars and sheets also. As per the availability of the material in the market, we select the desired aluminium alloy i.e. AA6063 with 10mm thickness. The long strips of AA6063 were bought and cut it as per the various sizes of various dimensions as per the setup requirement.

Al in part of material selection one more selection is important for the process is the tool material selection. It is very important parameter for the process. While selection of the tool material we have to consider the effects observed on the tool during the process. Mainly we have to consider the effect of heat generation and dissipation on the tool material. To produce good quality of weld, it is required that the tool material is to be select properly. There are various characteristics of the material which can be choosing as the tool material is as:

- Resistance to wear

- No harmful reactions with the weld material
- Good strength, dimensional stability& creep resistance.
- Good thermal fatigue strength to resist repeated thermal cycles.
- Low coefficient of thermal expansion.
- Good mach inability

There are various suitable tool materials used for this process are as:

TABLE TOOL MATERIALS AND SUITABLE WELD METALS [3]

Sr. No.	Tool Material	Suitable Weld Material
1	Die steel	Al alloys
2	WC -Co	Aluminum alloys, mild steel
3	Ni-Alloys	Copper alloys
4	WC composite	Aluminum alloys, low alloy steel and magnesium alloys, Ti-alloys
5	W-alloys	Titanium alloys, stainless steel and copper alloys
6	PCBN	Copper alloys, stainless steels and nickel alloys

With considering various parameters and properties discussed above the Tool steel is selected as a tool material. And experiment is carried out.

IV. SELECTION OF THE TOOL

The tool used in the process consists of a pin or probe and a shoulder. The pin of the tool is in contact with workpiece creates frictional and deformational heating and softens the work piece material. The shoulder of the tool contacts to the workpiece increases heats the workpiece, expands the zone of softened material, and constrains the deformed material.

The probe of the tool can produce deformational and frictional heating. The deformation depth and tool travel speed are mainly governed by the probe. Fig. 2summarizes the probe shapes and their main features. The end shape of the probe is either flat or domed. The flat bottom probe design and manufacture is currently the most commonly used form. The main disadvantage of the flat probe is the high force during plunging. In contrast, a round or domed end shape can reduce the forge force and tool wear upon plunging, increase tool life by eliminating local stress concentration and improve the quality of the weld root directly at the bottom ofthe probe.

V. DESIGN OF TOOL

From the review of the various tool shapes and structures given in the fig. 2 we have to select the proper geometry of the tool with respect to the material of workpiece and operational parameters. We select the cylindrical threaded tool for FSW as shown in figure.

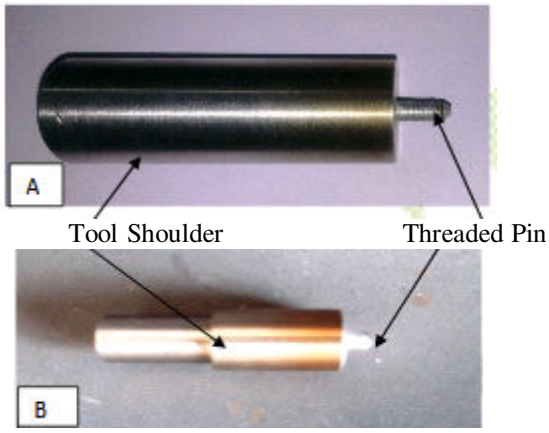

Figure 3: FSW Tools: (A) FSW tool of threading M8×1(B) FSW tool of threading M12×1.75

The cylindrical threaded tool is selected for the process and its dimensions are selected as shown in table

The parameters of the tool dimensions and the process are selected with the help of some literature and trial and error method. From the whole study of materials used generally for FSW, it is revealed that to come up with good quality of weld it is necessary that to have good knowledge of material selection for any process. Also the type of materials to be welded as well as the weld parameters such as transverse speed and rotational speed as well as material characteristics determines the best tool material that should be selected. After this review of the materials, we select the tool steels with MO (3%) which is an alloy of steels as a material for tool. As the we select the aluminium alloys (AA6063) for the study of the FSW experimentation which is belonging to soft materials and tool steel which is sufficient hard material will definitely useful for this process. After the market survey and availability of the steels, the steel rods of 32 mm diameters were brought for the experiment. And as per the design and parameters decided for the tool dimensions, the tools were manufactured.

VI. EXPERIMENTATION OF FSW OF AA6063

In experimentation, mainly two parts are included as; make specimen ready for trials and actual experiment. In the part of making specimen ready to test, we cut the samples from the raw material brought in the form of long strips as per the desired dimensions. The samples or plates of AA6063 are machined again on the same milling machine with surface cutter for doing the plates of equal dimensions and also the sides should rests in jaws of vise with zero deviation along the length i.e. they should fit perpendicularly at the jaws. After the surfacing of the plates the samples are become 51×150 mm for trials T1 & T2 also 80×150 mm for trials T3 & T4 respectively.

In a testing part of the tool and operation of FSW, we select some operational parameters for the experimentation of the FSW are as per given in table III.

TABLE III FSW PROCESS PARAMETERS

Parameter	Friction Stir Welding Trials			
	T1	T2	T3	T4
Tool Type	Cylindrical Threaded	Cylindrical Threaded	Cylindrical Threaded	Cylindrical Threaded

Threading of the tool	M12×1.75	M12×1.75	M8×1	M8×1
Shoulder Diameter(mm)	20	20	27	27
Shoulder length (mm)	30	30	30	30
Tool Pin Length(mm)	7.4	7.4	7.3	7.3
Tool Rotating Speed(rpm)	720	720	510	510
Welding Speed (mm/min)	0.869	1.65	2.70	8.645

We select the parameter for the process as shown in table III for experimentation to check out the welding between the two plates of aluminium alloy (AA6063). The welding joint carried out on the conventional milling machine by doing necessary attachment as shown in figure .

VII. EXPERIMENTAL OUTCOME

After the conducting the experimentation trials of the friction stir welding of plate's of AA6063 the two plates were joined successfully. This experimentation carried out with some results those are discussed in following sections. The welding joints are obtained as:

VIII. TESTING OF FSW JOINT

When the FSW joints are tested under the microscopes we get results in various views like weld penetration, cracks or blow holes if present in the weld, heat affected zone, effect of welding on grain structure of the material. The metallurgical testing of the joints has been done in accredited lab to find out desired results. Also the results of tensile test carried out each of the joints shown in the above figures are tabulated in the following tables.

TABLE SUMMARY OF TESTING RESULTS

Parameters	**Samples**			
	T1	**T2**	**T3**	**T4**
Total Weld Depth (mm)	8.71	8.56	7.02	7.98
Crack	Not observed	Observed	Not observed	Observed
Blow Holes	Not observed	Not observed	Not observed	Not observed
Heat Affected Zone	Observed	Observed	Observed	Observed
Effect on grain structure	Elongated grains observed	Elongated grains observed	Elongated grains observed	Elongated grains observed
Tensile Strength	32	31	27	25

IX. RESULTS AND DISCUSSION

After this experimentation, various points are come out from the operation of FSW and testing of welded joints.

- The pin diameter and shoulder diameter are increased with the increase in thickness of the plates or specimen undergoing the process of FSW.
- The speed of the tool is one more important parameter to be selected for the process. It is selected as per the thickness of the plates and diameter of the tool. Also suitable higher speed helps to generate higher temperature which is important requirement for the FSW process.
- Also for the effective welding process the suitable higher temperature should be created during the process, so that weld quality is to be increased. The higher speed of the tool give more better quality of the weld aesthetically. As the temperature reaches to its high range the quality of weld increased i.e. quality of weld directly proportional to the temperature created during the process.

X. CONCLUSION

After the study of Experimentation of friction stir welding of aluminium alloys some of the good points were came out. There are also some other points that also taken in to consideration for the extra work to be done. The some of concluded points regarding this study as:

- The process cost gets minimized automatically as the experimentation is done within the available tools and machines.
- The health hazards are decreased to zero whether the fusion welding has many health hazards affected on operator due to ultraviolet rays, also production of harmful gases during the process.
- With the use of conventional milling machine the FSW can carried out successfully for the materials for those fusion welding is not possible.
- Use of backing plate to specimen gives the support and useful to avoid the movement of the plates during the process. Also it helps to form good weld and also it decreases gap on the back side of the welded plate.

REFERENCES

1. M.K. Sued, D. Pons, J. Lavroff, E.H. Wong, Design features for bobbin friction stir welding tools; Development of a conceptual model linking the underlying physics to the production process. (August 2013).
2. R.S. Mishra, Z.Y. Ma, Friction stir welding and processing, Center for Friction Stir Processing, Department of Materials Science and Engineering, University of Missouri, Rolla, MO 65409, USA.(August 2005).
3. KudzanayiChiteka, Friction Stir Welding/Processing Tool Materials and Selection, International Journal of Engineering Research & Technology (IJERT) Vol. 2 Issue 11.(November 2013).

Prediction of Minimum Surface Roughness and Tool Wear in End Milling of Metal Matrix Composites Using NSGA-II

Dr. R. Arokiadass
Professor,
Department of Mechanical Engineering
St. Anne's College of Engineering and Technology,
Anguchettypalayam, Panriti,

Abstract - Particulate metal matrix composites (PMMCs) are being widely used in the aerospace and automotive industry due to their favorable properties, mainly high specific strength and Wear resistance. However, machining of particulate metal matrix composites presents a great challenge to the industry as the reinforcing particles easily abrade most of the common cutting tool materials. Being a complex process, it is very difficult to determine optimal parameters for improving machining performance. Tool flank wear and surface roughness are the most important output parameters, which decide the machining performance. A multiple regression model was used to represent the relationship between input and output variables and a multi-objective optimization method based on a non-dominated sorting genetic algorithm-II (NSGA-II) was used to optimize end milling process parameters. A non-dominated solution set was obtained.

Keywords: end milling, tool flank wear, surface roughness, optimization, non-dominated sorting genetic algorithm (NSGA-II)

I. INTRODUCTION

The end milling process is one of the most fundamental metal removal operations used in the manufacturing industry because of its ability to remove material faster and giving reasonably good surface quality [1]. It is widely used in a variety of manufacturing industries including the aerospace and automotive sectors, where quality is an important factor in the production of slots, pockets, precision moulds and dies [2]. Greater attention is given to dimensional accuracy and surface roughness of products in the industry these days. Moreover, surface finish influences mechanical properties such as fatigue behavior, wear, corrosion, lubrication and electrical conductivity. Thus, measuring and characterizing surface finish can be considered for predicting machining performance [3]. CBN cutting tools have greater wear resistance than other tool materials due to their high degree of hardness [4]. Cubic boron nitride (CBN) coated end mill are expensive compared to uncoated, the cost of the cutter can be recovered by a longer tool life and higher productivity. They are used to machine non-ferrous materials at high speeds and have high thermal conductivity. It has low thermal conductivity but higher compressive strength, which makes them conducive to machine hot at higher speeds. Kumar Reddy et al. [5] studied quality of components produced during end milling of Al/SiC particulate metal matrix composites (PMMCs). The results showed that the presence of the reinforcement enhances the machinability in terms of both surface roughness and lower tendency to clog the cutting tool, when compared to a non-reinforced Al alloy.

Alauddin et al. [6] established a mathematical model that predicts the surface roughness of 190 BHN steel after end milling. The prediction model was expressed via cutting speed, feed rate

and depth of cut. Bergman et al. [7] investigated the machinability of Al-MMC by cutting tools. For this purpose they used HSS and coated–uncoated hard metal cutting tools (WC). It has been emphasized that coated WC tools are more durable then HSS and uncoated tools, and the reinforcement element in MMC is an important parameter for wear of cutting tool.

Ibrahim Ciftci et al. [8] studied the influence of different particle size of SiC and cutting speed on tool wear and surface roughness during machining of Al/SiC MMC using cubic boron nitride (CBN) cutting tool. The results showed that tool wear was mainly observed on flank side with a strong influence by abrasive reinforcement. Gallab and Sklad [9] evaluated the machinability of aluminum reinforced with 20% silicon carbide. In dry turning operations, the effect of machining parameters on tool wear and surface quality was surveyed. They came to the conclusion that high cutting speed and depth of cut improve surface roughness. Palanikumar et al investigated the optimization of machining characteristics of glass fiber reinforced plastic (GFRP) composites using NSGA-II algorithm [10].

In the present work, the experiments are designed using central composite rotatable design (CCD). From the experimental data, multiple regression models for the tool flank wear and surface roughness are developed. The machining parameters, spindle speed, feed rate, depth of cut and percentage weight of silicon carbide, are optimized using NSGA-II algorithm for minimizing tool flank wear and minimizing surface roughness.

II. EXPERIMENTAL

In the present experimental study, the material to be machined is LM25 Al alloy reinforced with SiC_p, at a various composition of 5%wt., 10%wt., 15%wt., 20%wt. and 25%wt. and of 25 µm particle sizes manufactured through stir-casting route was used for experimentation. From the cast material the specimen for the end milling has been machined into rectangular specimen of 100 mm × 50 mm × 40 mm. The chosen levels of the selected process parameters with their units and notations are presented in Table 1. The end milling experiments have been conducted on CNC HASS vertical milling machine using CBN coated solid carbide end mill cutters, having a diameter of 12 mm, helix angle of 45º, rake angle of 10º and number of flutes 4. Tool flank wear was measured using a Metzer toolmaker's microscope. The surface roughness (Ra) of the machined test specimens were measured using a Talysurf tester with a sampling length of 10mm.

Table 1 Process parameters and their levels

Factors	Units	Notations	Levels				
			(-2)	(-1)	0	(+1)	(+2)
Spindle speed	rpm	N	2000	2500	3000	3500	4000
Feed rate	mm/rev	f	0.02	0.03	0.04	0.05	0.06
Depth of cut	mm	d	0.5	1	1.5	2	2.5
Content of SiCp	%wt	S	5	10	15	20	25

III. STATISTICAL MODELING

The statistical models based on the second-order polynomial equations were developed for VBmax and *R*a using the experimental results and are given below:

$$VB_{max} = -0.4581 + (0.0002\ X_1) + (6.7131\ X_2) + (0.0482\ X_3) - (0.0107\ X_4) + (11.7113\ X_2^2) - (0.0198 X_3^2) - (0.0014\ X_1\ X_2) + (0.5875\ X_2\ X_3) - (0.1637\ X_2\ X_4) + (0.0015\ X_3\ X_4) \quad ----(1)$$

$$Ra = 2.1546 - (0.0007\ X_1) + (41.4589\ X_2) - (0.2530\ X_3) - (0.0435\ X_4) + (72.9613\ X_2^2) + (0.0392\ X_3^2) + (0.0015 X_4^2) - (0.0085\ X_1 X_2) + (0.0001\ X_1 X_3) + (1.7625\ X_2 X_3) + (0.5862\ X_2 X_4) - (0.0090\ X_3 X_4) \quad ----(2)$$

IV. OPTIMIZATION

To optimize the cutting parameters in the machining of Al/SiCp MMC, a non-dominated sorting genetic algorithm was used. The objective sets for the present study were as follows: 1. Minimization of the tool flank wear (VBmax); 2. Minimization of surface roughness (*R*a). DEB et al [11] developed elitist non-dominated sorting genetic algorithm (NSGA-II). This algorithm uses the elite-preserving operator, which favors the elites of a population by giving them an opportunity to be directly carried over to the next generation [12].

V. NSGA-II ALGORITHM

The non-dominated sorting genetic algorithm has been criticized for its high computational complexity and lack of elitism. Non dominated sorting genetic algorithm (NSGA-II) is one of the most widely used methods for generating the Pareto frontier. The NSGA-II algorithm ranks the individuals based on dominance. NSGA-II uses elitism and a phenotype crowd comparison operator that keeps diversity without specifying any additional parameters [13].

5.1 Non-dominated sort

The initialized population is sorted based on non-domination. The non-domination is an individual and is said to dominate another if its objective function is no worse than the other and at least in one of its objective functions is better than the other. The fast-sort algorithm was described in Ref. [14]:

5.2 Crowding distance

In NSGA-II, in addition to the fitness value, a new parameter called "crowding distance" is calculated for each individual. The crowding distance is a measure of how close an individual to its neighbors. Crowding distance is assigned front wise: comparing the crowding distance between two individuals in a different front is meaningless. The basic idea behind the crowding distance is finding the Euclidean distance between each individual in a front based on their m objectives in m-dimensional hyperspace. Initially, a random parent population of $P0$, of size N is generated. The population is sorted based on non-domination level. Each solution is assigned a fitness level, and the best level is 1. Thus, minimization of fitness is assumed. Binary tournament selection, recombination and mutation operators are implemented to generate the child $Q0$, of size N. The procedure for the remaining generation (for $t \geq 1$) can be found in Ref. [15].

VI. DISCUSSION

The end milling characteristics of LM25Al/SiCp composites were studied. The second order polynomial models were developed for VBmax and Ra. The VBmax and Ra ware calculated using Eq. (1 and 2). The fit summary indicates that the quadratic model is statistically significant for analysis of VBmax and Ra. The value of R^2 for VBmax are 98.39% and 99.14%, which indicates that the developed regression model is adequately significant at a 95% confidence level. It provides an excellent relationship between the machining parameters and the VBmax and Ra.

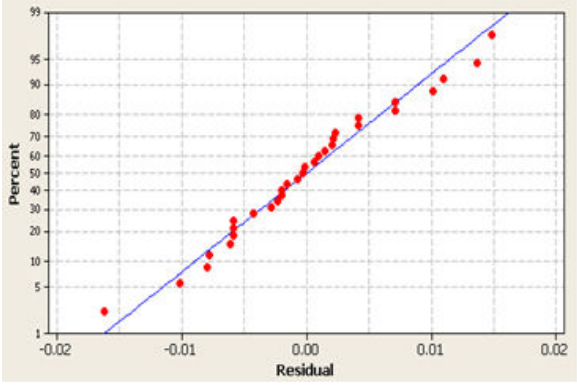

Fig. 1 Normal probability plot residuals for VBmax

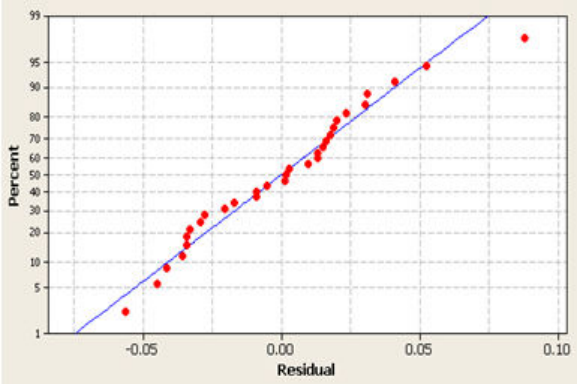

Fig. 2 Normal probability plot residuals for Ra

The normal probability plot for VBmax and Ra are presented in Fig.1 and 2. It can be noticed that the residuals fall on a straight line, which means that the errors are normally distributed and the regression models are well fitted with the observed values.

In the present work, a non-dominated sorting genetic algorithm, NSGA-II, was used to optimize multiple performances using the second-order models created. The NSGA-II algorithm ranked the individuals based on dominance. The control parameters in NSGA-II were adjusted to obtain the best performance. The parameters used are: probability of crossover of 0.9 with distribution index of 20, mutation probability of 0.25 and population size of 100.

It was found that the above control parameters produce better convergence and distribution of optimal solutions. The 1000 generations were generated to obtain the true optimal solution.

The non-dominated solution set obtained over the entire optimization is shown in Fig. 3. This figure shows the formation of the Pareto front leading to the final set of solutions. Since none of the solutions in the non-dominated set is absolutely better than any other, any one of them is the "better solution". As the best solution can be selected based on individual product requirements, therefore the process engineer must select the optimal solution from the set of available solutions.

VII. CONCLUSIONS

1. The end milling process parameters were optimized by using non-dominated sorting genetic algorithm (NSGA-II), and a non-dominated solution set was obtained. The second order polynomial models developed for tool flank wear and surface roughness were used for optimization.
2. The choice of one solution over the other depends on the process engineer's requirements. If the requirement is a better *R*a or low tool flank wear, a suitable combination of variables can be selected.
3. Optimization will help to minimize the surface roughness considerably by reducing tool flank wear. The objectives such as Ra and VBmax were optimized using a multi-objective optimization method, non-dominating sorting genetic algorithm-II. A Pareto-optimal set of 100 solutions was obtained.

REFERENCES

1. Lou, M. S. & Chen. J. C, "In process surface roughness recognition system in end-milling operations", *International Journal of Advanced Manufacturing Technology*, 1999, Vol.15, pp 200-209.

2. Dr. Mike S. Lou, Dr. Joseph C. Chen, Dr. Caleb M. Li, "Surface Roughness Prediction Technique For CNC End-Milling", *Journal of Industrial Technology*, 1999, Vol. 15, pp.1-6
3. Suresh Kumar Reddy. N, Venkateswara Rao. P, "Selection of optimum tool geometry and cutting conditions using a surface roughness prediction model for end milling" *Int J Adv Manuf Technol*., 2005, Vol. 26, pp1202–1210
4. Camuscu. N, Aslan. E. "A comparative study on cutting tool performance in end milling of AISI D3 tool steel", *Journal of Materials Processing Technology*, 2005, Vol. 170, pp121-126.
5. Suresh Kumar Reddy. N, Shin.K.S, Minyang.Y, "Experimental study of surface integrity during end milling of Al/SiC particulate metal–matrix composites", *Journal of Mater Process Technol*, 2008, Vol. 201, pp574–579.
6. Alaudin.M, EI-Baradic.M.A, Hasmi.M.S.J, "Computer-aided analysis of a surface-roughness model for end milling", *Journal of material processing technology*, 1995, Vol. 55, pp123-127.
7. Bergman.F, Jacobson.S, Abdel Moneim.M.E, "Comments on tool wear mechanisms in intermittent cutting of metal matrix composites", *Wear*, 1996, Vol. 1971–1972, pp295–296.
8. Li.X, Seah.W.K.H, 2001. "Tool wear acceleration in relation to workpiece reinforcement percentage in cutting of metal matrix composites", *Wear*, Vol. 2472, pp161–171.
9. El-Gallab.M. Sklad, "Machining of Al/SiC particulate metal-matrix composites. Part I. Tool performance," *J. Mater. Process. Technol.*, 1998, Vol. 83, pp151–158.
10. Palanikumar.K, Latha.B, Senthilkumar.V. S, Karthikeyan.R, "Multiple performance optimization in machining of GFRP composites by a PCD tool using Non- dominated Sorting Genetic Algorithm (NSGA-II)", *Metals and Materials International*, 2009, Vol.15, No. 2, pp249-258.
11. N. Srinivas and D. Kalyanmoy, Jl. Evol. Comput. 2, 221 (1994).
12. B. Fu, PhD thesis, University of Paderborn, Germany (2005).
13. Kalyamoy Deb, Sunder.J, Udaya Baskara Rao.N, "Reference point based multi objective optimization using evolutionary algorithms", KanGALReport Number 2005012, 2006.
14. SESHADRI A. A fast elitist multi-objective genetic algorithm NSGA-II [EB/OL]//http://www.mathworks.com. Internet specification. [2007].
15. DEB K, PRATAP A, AGARWAL S, MEYARIVAN T. A fast and elitist multiobjective genetic algorithm: NSGA-II [J]. IEEE Transactions on Evolutionary Computation, 2002, 6(2): 182−197.

Fabrication of Solar Powered Bi-Cycle

Mr. D. Dinesh, Mr. S. Arunkumar, Mr. M. Sankerguru, Mr. K. Guna
UG Student,
Department of mechanical engineering
V.R.S. college of engineering and technology

Mr. A. Rajaraman
Assistant professor
Department of mechanical engineering
V.R.S. college of engineering and technology

Abstract - There are so many vehicles that came to influence in the existing world. Their operating systems are based on usual fossil fuel system. At the present sense the fossil fuel can exceed only for a certain period after that we have to go for a change to other methods. Thus we have made an attempt to design and fabricate an ultimate system (Solar Cycle) which would produce cheaper & effective result than the existing system. This will be very useful to the future needs of the world.

An attempt is made in the fabrication of a solar powered System for a two-wheeler (Cycle). This works on electric power distributed by the DC electric motor receiving the current from a battery. The motor and the various parts are such as sprocket, chain assembly, cycle and with easily available materials to serve and fulfill the purpose of the project. Battery is charged by using solar panel.

The drive system of the normal Cycle is not altered. This system is two in one system. The cycle is operated ether by

- ***Pedaling manually***
- ***Battery and motor driving mechanism.***

I. INTRODUCTION

All vehicles that are in the market cause pollution and the fuel cost is also increasing day by day. In order to compensate the fluctuating fuel cost and reducing the pollution a good remedy is needed i.e. our transporting system.

Due to ignition of the hydrocarbon fuels, in the vehicle, sometime difficulties such as wear and tear may be high and more attention is needed for proper maintenance. Our vehicle is easy to handle and no fuel cost to the other existing vehicles. Hence a need for a change in the existing alternative system which can produce higher efficiency at minimum cost was though about an attempt has been made to design and fabricate such an alternative system.

So this project "**SOLAR CYCLE"** is very much useful, since it is provided with good quality of power sources and simple operating mechanism. Hence "EACH AND EVERY DROP OF FUEL SAVES OUR ECONOMY AND MEET THE NEEDS" is the saturation point that is to be attained as soon as possible.

In order to achieve this saturation point we have to save and seek for some other source of power. This power, the alternate power must be much more convenient in availability and usage. The next important reason for the search of effective, unadulterated power are to save the surrounding environments including men, machine and material of both the existing and the next

forth generation from pollution, the cause for many harmful happenings and to reach the saturation point.

The most talented power against the natural resource is supposed to be the electric and solar energies that best suit the automobiles. The unadulterated zero emission electrical and solar power, is the only easily attainable alternate source. Hence we decided to incorporate the electric power in the field of automobile, the concept of many Multi National Companies (MNC) and to get relieved from the incorrigible air pollution.

This implementation concept is tried to the best two wheeler Cycle. The various simple arrangements done for the good driving conditions of the battery powered Cycle with its most needed specifications was summarized in this report.

II. COMPONENTS AND DESCRIPTION

The main components of the solar cycles are,

- Solar Panel
- Ordinary Cycle
- Battery
- D.C. Motor
- Sprocket
- Chain drive

These all are explained below one by one.

III. SOLAR PANEL

PHOTOVOLTAIC PRINCIPLES:

The photo-voltaic effect can be observed in nature in a variety of materials that have shown that the best performance in sunlight is the semiconductors as stated above. When photons from the sun are absorbed in a semiconductor, that create free electrons with higher energies than the created there must be an electric field to induce these higher energy electrons to flow out of the semi-conductor to do useful work.

A junction of materials, which have different electrical properties, provides the electric field in most solar cells. To obtain a useful power output from photon interaction in a semiconductor, three processes are required.

1) The photon has to be absorbed in the active part of the material and result in electrons being excited to a higher energy potential.
2) The electron hole charge carriers created by the absorption must be physically separated and moved to the edge of the cell.
3) The charge carriers must be removed from the cell and delivered to useful load before they loose extra potential.

For completing the above processes a solar cell consists of:-

- Semi-conductor in which electron hole pairs are created by absorption of incident solar radiation.
- Region containing a drift field for charge separation
- Charge collecting fronts and back electrodes.

The photo-voltaic effect can be described easily for p-n junction in a semi-conductor. In an intrinsic semi-conductor such as silicon, each one of the four valence electrons of the material atom

is tied in a chemical bond, and there are no free electrons at absolute zero. If a piece of such a material is doped on one side by a five valance electron material, such as arsenic or phosphorus, there will be an excess of electrons in that side, becoming an n-type semi-conductor.

IV. ORDINARY CYCLE:

This is a normal cycle. This is the base of our project. The other components such as battery and D.C. Motor are fitted. The small modifications are arranged in the back wheel sprocket.

V. DESCRIPTION OF DC MOTOR

An electric motor is a machine which converts electrical energy to mechanical energy. Its action is based on the principle that when a current-carrying conductor is placed in a magnetic field, it experiences a magnetic force whose direction is given by Fleming's left hand rule.

When a motor is in operation, it develops torque. This torque can produce mechanical rotation. DC motors are also like generators classified into shunt wound or series wound or compound wound motors.

VI. FLEMING'S LEFT HAND RULE:

Keep the force finger, middle finger and thumb of the left hand mutually perpendicular to one another. If the fore finger indicates the direction of magnetic field and middle finger indicates direction of current in the conductor, then the thumb indicates the direction of the motion of conductor. Movement of Conductor

Conductor

The result is to increase the flux density in to the region directly above the conductor and to reduce the flux density in the region directly below the conductor. It is found that a force acts on the conductor, trying to push the conductor downwards as shown by the arrow.

VII. SPROCKET:

The chain converts rotational power to pulling power, or pulling power to rotational power, by engaging with the sprocket.

The sprocket looks like a gear but differs in three important ways:

1. Sprockets have many engaging teeth; gears usually have only one or two.
2. The teeth of a gear touch and slip against each other; there is basically no slippage in a sprocket.
3. The shapes of the teeth are different in gears and sprockets.

Although chains are sometimes pushed and pulled at either end by cylinders, chains are usually driven by wrapping them on sprockets. In the following section, we plain the relation between sprockets and chains when power is transmitted by sprockets.

VIII. CHAIN DRIVE:

A chain is a reliable machine component, which transmits power by means of tensile forces, and is used primarily for power transmission and conveyance systems. The function and uses of chain are similar to a belt. There are many kinds of chain. It is convenient to sort types of chain by either material of composition or method of construction.

We can sort chains into five types:

- Cast iron chain.
- Cast steel chain.
- Forged chain.
- Steel chain.
- Plastic chain

Demand for the first three chain types is now decreasing; they are only used in some special situations. For example, cast iron chain is part of water-treatment equipment; forged chain is used in overhead conveyors for automobile factories.

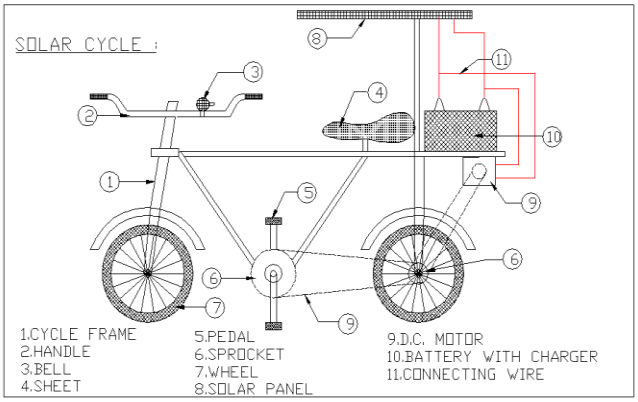

IX. CONCLUSION

This project work has provided us an excellent opportunity and experience, to use our limited knowledge. We gained a lot of practical knowledge regarding, planning, purchasing, assembling and machining while doing this project work. We feel that the project work is a good solution to bridge the gates between institution and industries.

We are proud that we have completed the work with the limited time successfully. The SOLAR CYCLE is working with satisfactory conditions. We are able to understand the difficulties in maintaining the tolerances and also quality. We have done to our ability and skill making maximum use of available facilities.

In conclusion remarks of our project work, let us add a few more lines about our impression project work.

Thus we have developed a **"***SOLAR CYCLE***"** which helps to know how to achieve simple motor and chain-sprocket drive mechanism. The application of this cycle is high when compared to the cost of the machine.

By using more techniques, they can be modified and developed according to the applications.

References

1. K. Balasundaram, "Industrial management", Parthian Publishers, Coimbatore-12, 1999, pp.116
2. Automotive Electrical, pp.32-94.
3. G.B.S. Narang, "Automobile Engineering", Khanna Publishers, Delhi, 1991, pp 671.
4. William H. Crowse, "Automobile Engineering".

Design and Analysis of Composite Catalytic Converter

Mr. R. Jayakumar
Assistant Professor,
Department of Mechanical Engineering,
St. Anne's College of Engineering and Technology,
Anguchettypalayam, Panruti – 607106.

Mr. P. Murugan
Assistant Professor,
Department of Mechanical Engineering
St. Anne's College of Engineering and Technology,
Anguchettypalayam, Panruti – 607106.

Abstract - ***The source of pollution and global warming is air pollution. It is to be noted that air pollution is mainly caused by the toxic gases from the exhaust of the automobiles. Only 30 percentage of the fuel is converted into energy source to run the engine remaining 70 percentage of fuel is of un burnt hydrocarbon carbon monoxide and nitrogen oxides. This toxic content is reduced by the invention of catalytic converter. Automotive three way converter have represented over the last 25 years for reduction of prolusion in the atmosphere. Here the performance of the catalytic converter is studied and analysis is done by ANSYS FLUENT package. The uniform flow inside the converter is controlled by increasing the cone angle of the converter to utilize the maximum amount of substrate in the converter. Economical wastage also reduced by changing the cone angle. Since the substrate is a noble material it is costly by utilizing all the substrate by changing the angle will reduce the wastage. Amount of conversion taking place inside the converter after maintaining uniform flow is studied by this analysis. The chemical reactions and flow of gases inside the converter is discussed here for the analysis purpose. The efficiency of the catalytic converter is mainly depend upon the effective conversion of CO, CH4, NO into CO2 H2O O2 and N2 which less toxic than the carbon monoxide hydrocarbons and nitrogen oxides. Three way catalytic converter (TWC) is taken for analysis because of its tendency to control the nitrogen oxides along with reaming toxic content.***

I. INTRODUCTION

The source of pollution and global warming is the air pollution. It is to be noted that air pollution is mainly caused by the toxic gases from the exhaust of the automobiles. Now a day the demand for automotive vehicle is huge. There are numerous automobiles which are to be noted that there is a huge air pollution which is affecting our environment. To control the toxic content from the exhaust of the automobile engine a component is added to the exhaust region of the petrol or diesel engine. This component is named as catalytic convertor, which is able to convert the toxic gas content into non-toxic content by catalytic reaction.

A catalytic converter is a vehicle emissions control device that converts toxic pollutants in exhaust gas to less toxic pollutants by catalytic a redox reaction (oxidation or reduction). Catalytic converters are used in internal combustion engines fuel by either petrol(gasoline) or diesel—including lean burn engines. The catalytic converter was invented by Eugene Houdry, a French mechanical engineer in 1950. Houdry concerned about the role of smoke stack exhaust and automobile exhaust in air pollution and founded a company, Oxy-Catalyst. Houdry first developed

catalytic converters for smoke stacks called cats. Then he developed catalytic converters for warehouse forklifts that used low grade non-leaded gasoline.

In 1950s he began research to develop catalytic converters for gasoline engines used on cars. Catalytic converters are also used on electrical generators, forklifts, mining equipment, trucks, buses, locomotives, motorcycles, and airplanes. They are also used on some wood stoves to control emissions.

1.1 ANATOMY OF CATALYTIC CONVERTER

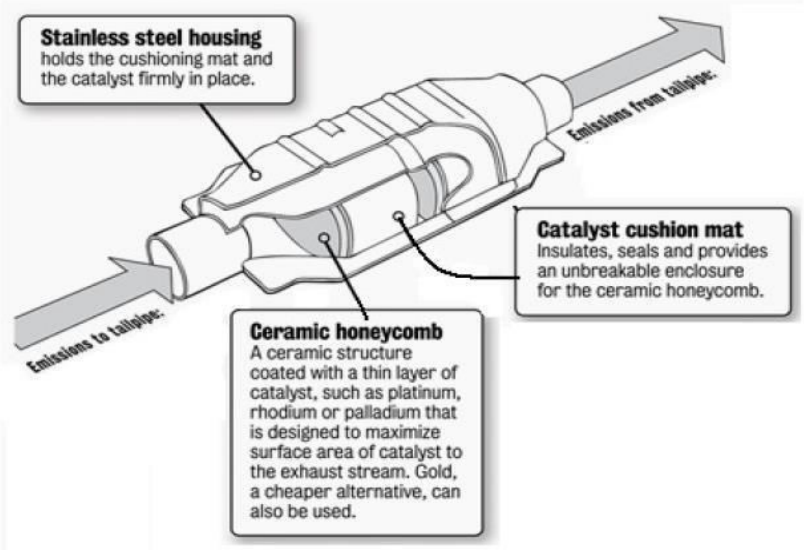

Fig.1.1 Components of catalytic converter

II. COMPUTATIONAL FLUIDS DYNAMICS

Computational Fluids Dynamics (abbreviated as CFD) is a method of calculating fluid flows, heat and mass transfer, chemical reactions and similar phenomena by numerical solving mathematical expression. The accuracy of the solutions is dependent on the following properties Consistency: The discretisation error should approach zero for infinite small grid sizes or time steps. For this case, the algebraic finite difference equations become equal to the original partial differential equations. .Stability: Numerical errors (truncation errors for example) should be bounded for all iteration step and not explode the solution. Convergence: A numerical method is convergent if its solution approaches that of the partial differential equation for decreasing grid sizes and time steps and if numerical errors are bounded. This means that both consistency and stability are required to achieve convergence.

The CFD simulations were performed with the commercial software program Ansys Fluent 13.0.For the calculation of the particle trajectories, the discrete phase model (dpm) was applied. This model is based on the Euler-Lagrange method and uses the following steps:

1. Solve the continuous-phase flow.
2. Create the discrete-phase injections.
3. Solve the coupled flow, if desired.
4. Track the discrete-phase injections, using plots or reports.

III. DEVELOPMENT OF 3D MODEL

3.1 Model Details

The type of catalytic converter taken for analysis is 3 way catalytic converter of an automobile. The dimension of the converter is noted for developing the 3D model as the model space Constantine is to be considering for developing new model. Length of the converter from exhaust of the engine to outlet of the converter is measured. Height and diameter of the converter is constant. Our new model should possess better efficiency that the measured converter. The new dimension is extracted from the right angle triangle theorem.

IV. Calculating Inlet Geometry of Catalytic Converter

The new dimension of catalytic converter is calculated with the measured values of real time converter.

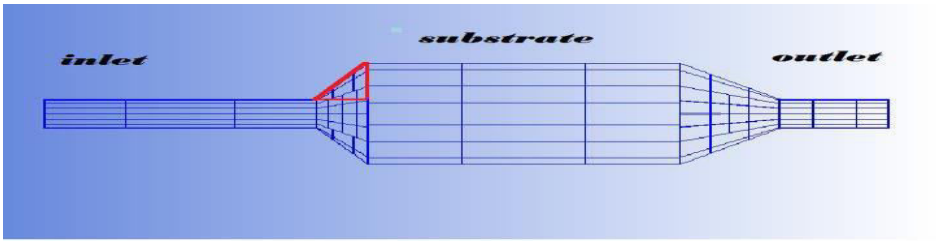

Fig.4.1 Structure of Catalytic Converter

From the above structure it is clearly shown about the inlet angle calculation of the model. Let's take the models inlet portion as right angle triangle. Wed know the height of the triangle and angle of the converter.

4.1 CAD Model

CAD Model is designed in solid works for the above inlet dimension. The model is designed with respect to space constraint of the catalytic converter model. The inlet angle with 10^o and 5^o is neglected for modelling due to its huge length from the divergence section to inlet of the substrate.

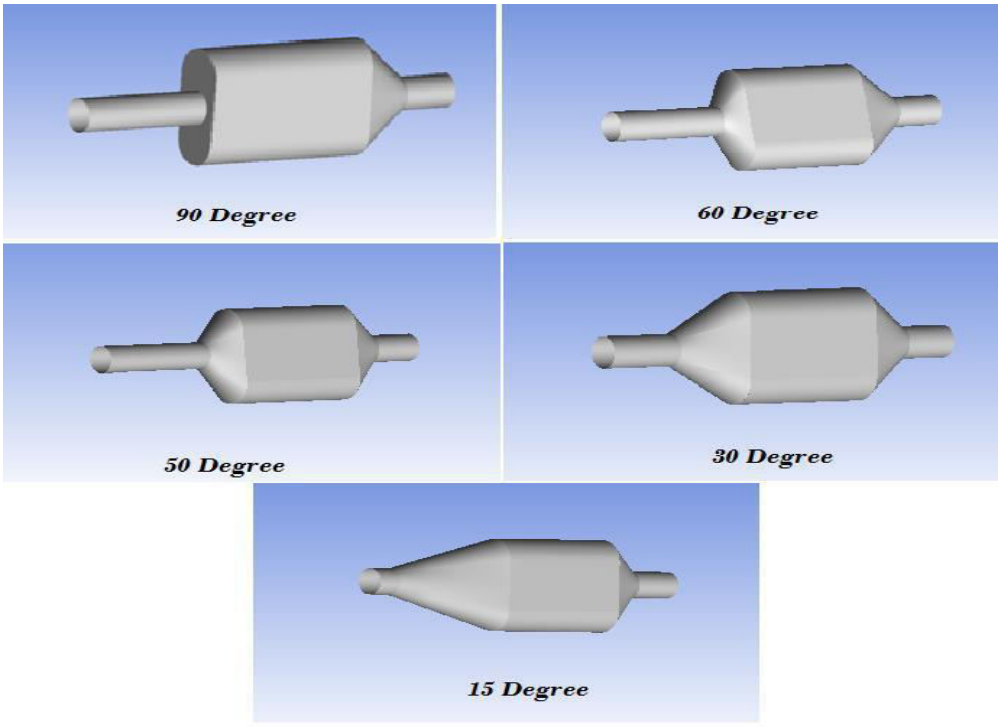

4.2 GENERATING MESH

Meshing the model is an important step in CFD Analysis, meshing is the concept which is related to the FEA. Meshing is done in ICEM. The model is imported into the ICEM package and tolerance of the model is to be checked.

Split the model with respect to require boundary in our case the model is separated as inlet, inlet wall, outlet, outlet wall, porous, wall, porous in, porous out

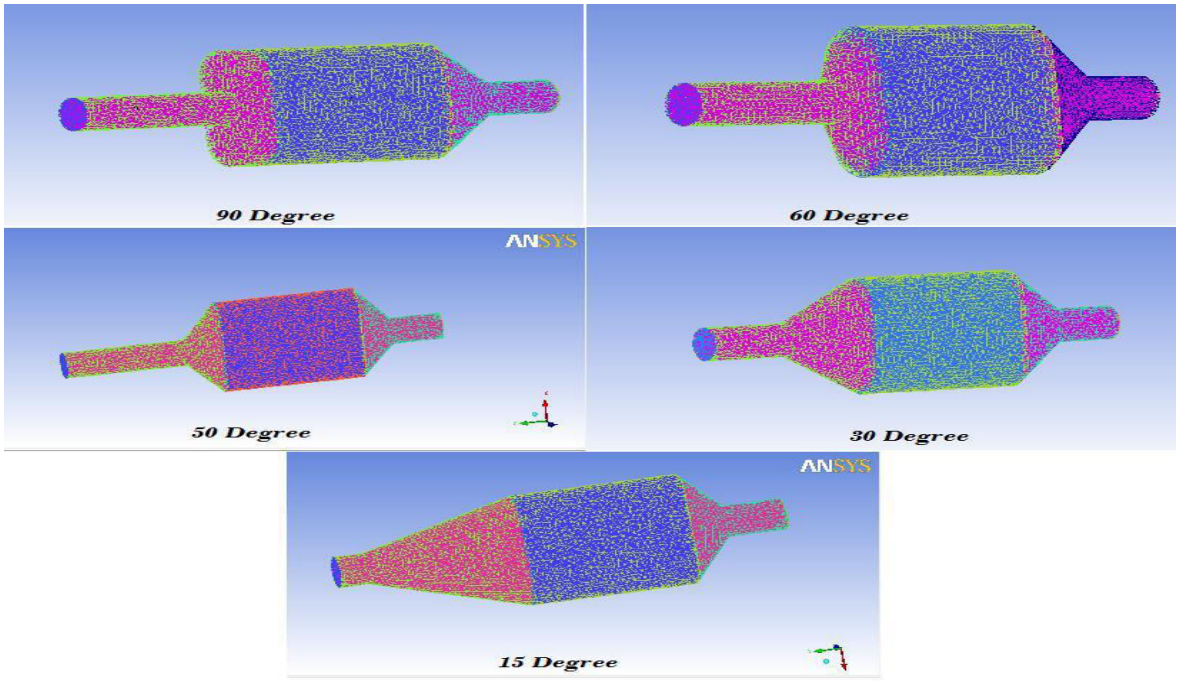

V. RESULT AND DISCUSSION

INLET PRESSURE

This project is about reducing the pressure at the inlet section of the converter; there will be less flow separation at the inlet when the divergence angle of the converter is less. So the inlet dimension of converter is changed with the calculation of right angle theorem. Fluid which flows inside the converter will be in mixed state. Here I have done analysis for three fluids, namely air, carbon monoxide, nitrogen oxide. There won't be much difference between these three fluids. Pressure increases when the volume is less, so when the inlet divergence angle is reduced then the volume at the inlet section will be more so that there will be less pressure at the inlet.

The pressure at the inlet is increased mostly because of the substrate which is presented at the centre of the converter. The flow will be interrupted due to the presence of substrate so pressure will built up at the inlet section. Because of the substrate the flow hits the substrate and reverse flow will occur. In addition to the substrate the inlet geometry plays a vital role in increasing the pressure. Due to the divergence angle the flow tends to separate at the divergence section. The flow separation affects the laminar flow and it will become turbulence at the divergence angle. Now there will be more reverse flow at the inlet section which increases the Pressure at inlet.

Because of increase in back pressure at inlet section which affects the performance of the catalytic converter by reducing the flow uniformity at inlet. If the pressure is more then it will affect the engine, at one point engine will failure due to the increased pressure. Now I have plotted the graph of pressure for various model of catalytic converter to justify the better model. And Pressure contour for all the three fluids air, Carbon Monoxide, Nitrogen oxides are shown below

for reference and graph is plotted for all the three fluids.

5.1. Pressure at Inlet for Air

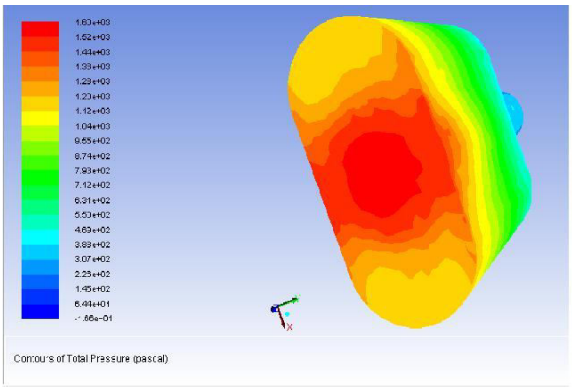

a) Pressure of 90º

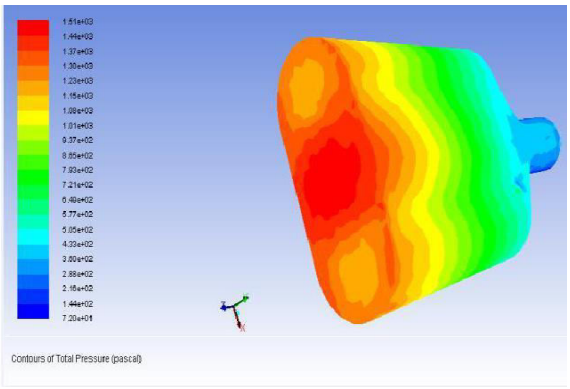

b) Pressure of 60º

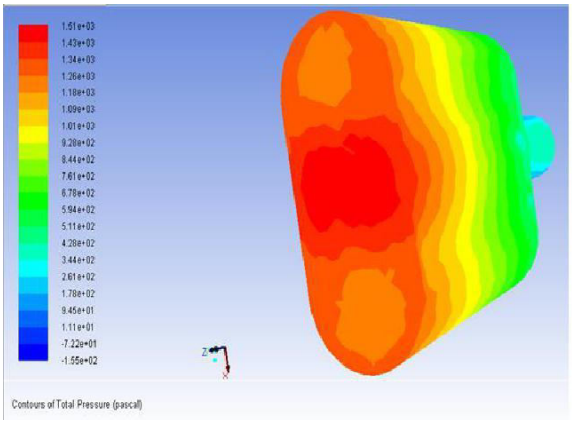

c) Pressure of 50º

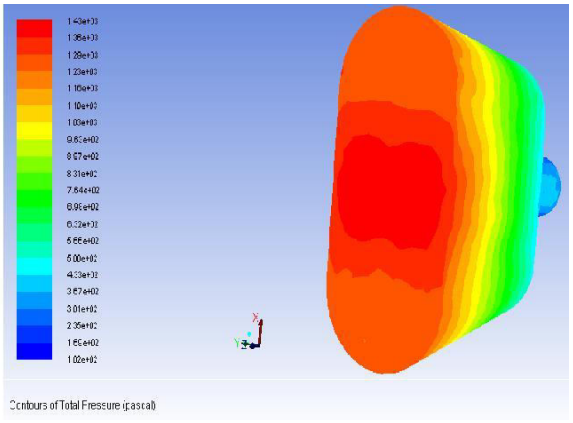

d) Pressure of 30º

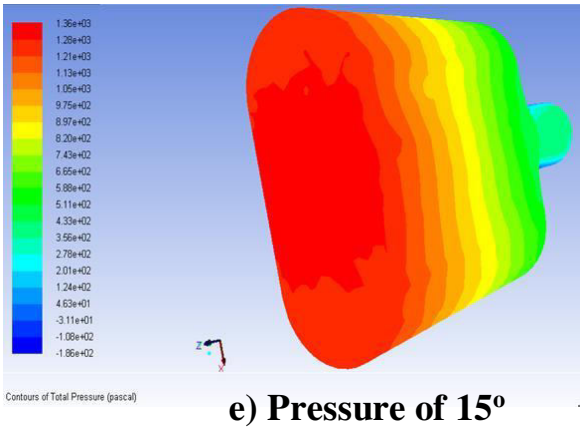

e) Pressure of 15º

Fig.5.1Pressure at inlet for air

ANGLE	AIR	CARBON MONOXIDE	NITROGEN OXIDE
90	1600	1520	1420
60	1560	1440	1350
50	1511	1430	1340
30	1431	1360	1280
15	1360	1240	1230

Table 5.1 Pressure at inlet (pa)

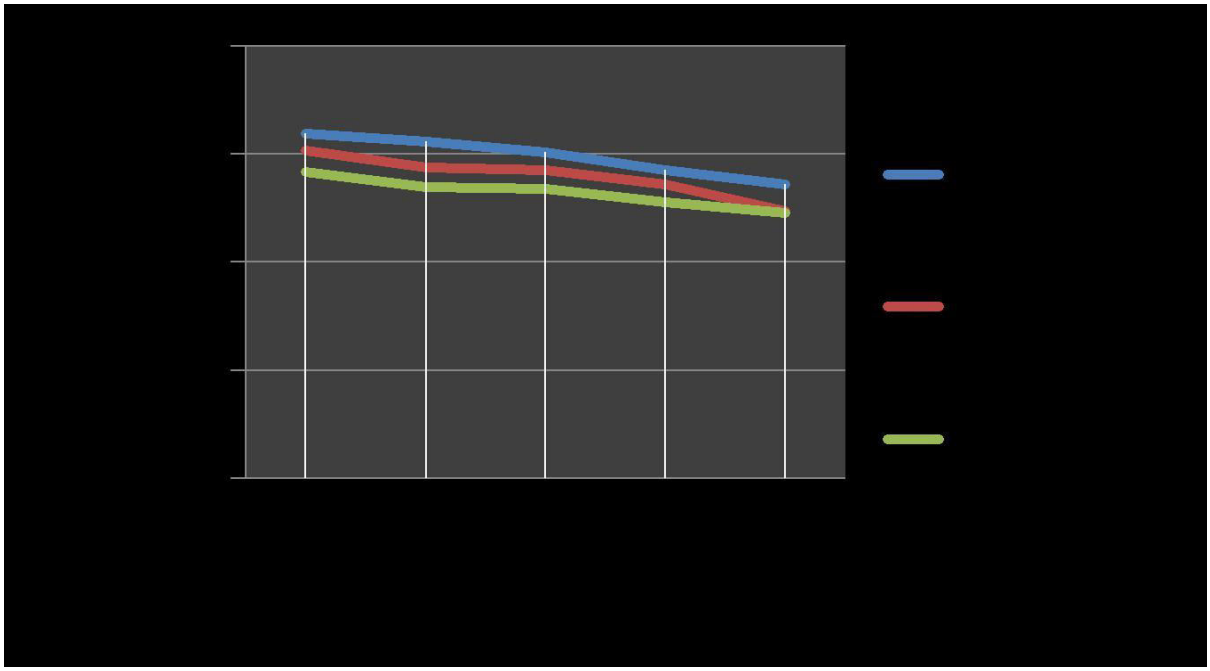

REFERENCE

1. Ankan Kumar, Sandip Mazumder,"Toward simulation of full scale monolithic catalytic converters with complex heterogeneous chemistry", Computers and Chemical Engineering 34 (2010) 135–145.
2. Balakrishna.B, Srinivasarao Mamidala, "Design Optimization of Catalytic Converter to reduce Particulate Matter and Achieve Limited Back Pressure in Diesel Engine by CFD", International Journal of Current Engineering and Technology Special Issue-2, (February 2014).

3. Bharath M.S, Baljit Singh and P.A.Aswatha Narayana," Performance studies of catalytic converter used in Automobile exhaust system", Proceedings of the 37 national & 4th international conference on fluid mechanics and fluid power December 16-18, 2010.
4. Calvin H. Bartholomew, "Mechanisms of catalyst deactivation", Applied Catalysis A: General 212 (2001) 17–60.
5. Chauhan.S,"Noble metal catalysts for monolithic converters", JCPRC5, J. Chem. Pharm. Res., 2010, 2(4):602-611.
6. Cansu Ozhan, DanielFuster N, Patrick Da Costa,"Multi-scale flow simulation of automotive catalytic converters", Chemical Engineering Science116 (2014), 161–171.
7. Douglas Ball, Michael G. Zammit and George C. Mitchell, "Effects of Substrate Diameter and Cell Density FTP Performance", SAE TECHNICAL PAPER SERIES 2007-01-1265.
8. Grigorios C. Koltsakis, Anastasios M. Stamatelos,"Modeling dynamic phenomena in 3-way catalytic converters", Chemical Engineering Science 54 (1999) 4567}4578.
9. Jothithirumal.B, Dr .E. James Gunasekaran, Chandan Dey , "Numerical Analysis Of Surface Reaction Of Catalytic Converter ",International Journal of Engineering Research and Applications (IJERA) ISSN: 2248-9622 Vol. 2, Issue 4, July-August 2012, pp.399-408 399.
10. Jan Kaspar, Paolo Fornasiero, Neal Hicke,"Automotive catalytic converters: current status and some perspectives" Catalysis Today 77 (2003),Page: 419–449.
11. Julie M Pardiwala, Femina Patel, Sanjay Patel, "Review paper on Catalytic Converter for Automotive Exhaust Emission", Institute of technology, Nirma university, Ahmadabad – 382 481, 08-10,December, 2011.

TABLE OF CONTENT

English Language Teaching Methodology

Mr. D. Sampath Kumar
Assistant Professor,
Department of Science and Humanities,
St. Anne's College of Engineering and Technology,
Anguchettypalayam, Panruti – 607106.

Abstract - English language teaching is very important because of the global status of English. English language teaching is a process that requires great efforts on the part of all the participants. Classroom interaction, activities, textbooks are the most important elements of teaching process for the aims and objectives of a course. In view of the importance of English as a foreign language in Iraq, the researcher has examined the existing textbooks and system of teaching English in order to point out the shortcomings which have been hindering the Iraqi students from mastering the English language. The problem can be solved by using new textbooks. The teachers of English should also be equipped with an up-to-date knowledge of English Language Teaching (ELT).

I. INTRODUCTION

Teaching English became a professional and academic field from a half century ago. Many researches for teacher education and teacher training have been conducted in order to raise the English as well as the foreign language trainers' knowledge and capabilities in carrying out effective lessons in classroom. During second millennium of speedily globalized world, teaching English as a common communication tool has become even more significant than half century ago. For introducing the history, research methodologies, and teaching pedagogies of teaching English as a Second/ Foreign/International Language, this article is composed as a reference for present English teachers under trend of globalization.

II. THE DIRECT METHOD

If you've ever heard the Direct Method being taught, you may have rightly mistaken it for some sort of military drill, which is not far off as it was first established in France and Germany in the early 1900's to assist soldiers to communicate in a second language quickly. The direct method of teaching English is also known as the Natural Method. It's used to teach a number of different languages not just English, and the main idea of the Direct Method is that it only uses the target language that the students are trying to learn. Its main focus is oral skill and it is taught via repetitive drilling. Grammar is taught using an inductive way and students need to try and guess the rules through the teacher's oral presentation.

2.1 Key Features

Richards and Rodgers (1986:9-10) summarize the key features of the DM thus:

(1) Classroom instruction is conducted exclusively in the target language.

(2) Only everyday vocabulary and sentences are taught.

(3) Oral communication skills are built up in a carefully traded progression organized around question-and-answer exchanges between teachers and students in small, intensive classes.

(4) Grammar is taught inductively.

(5) New teaching points are taught through modeling and practice.

(6) Concrete vocabulary is taught through demonstration, objects, and pictures; abstract vocabulary is taught by association of ideas.

(7) Both speech and listening comprehension are taught.

(8) Correct pronunciation and grammar are emphasized.

III. THE GRAMMAR TRANSLATION METHOD

Just like its name suggests, this method of teaching English is grammar heavy and relies a lot on translation. This is the traditional or 'classical' way of learning a language and it's still commonly used when learning some languages. Some countries prefer this style of teaching and the main idea behind this method is that the students learn all grammar rules, so they're able to translate a number of sentences. This is particularly common for those students who wish to study literature at a deeper level.

3.1 Key Features

According to Prator and Celce-Murcia (1979:3), the key features of the Grammar Translation Method are as follows:

(1) Classes are taught in the mother tongue, with little active use of the target language.

(2) Much vocabulary is taught in the form of lists of isolated words.

(3) Long elaborate explanations of the intricacies of grammar are given.

(4) Grammar provides the rules for putting words together, and instruction often focuses on the form and inflection of words.

(5) Reading of difficult classical texts is begun early.

(6) Little attention is paid to the content of texts, which are treated as exercises in grammatical analysis.

(7) Often the only drills are exercises in translating disconnected sentences from the target language into the mother tongue.

(8) Little or no attention is given to pronunciation.

IV. THE AUDIO LINGUAL METHOD

The Audio Lingual Method otherwise known as the New Key Method or Army Method is based on a behavirourist theory that things are able to be learned by constant reinforcement. However, just like in the army when someone behaves badly (or in this case bad use of English), the learner receives negative feedback and the contrary happens when a student demonstrates good use of English. This is related to the Direct Method and just like its predecessor it only uses the target language. The biggest difference between the Audio Lingual Method and the Direct Method is its focus of teaching. The Direct Methods focuses on the teaching of vocabulary whereas the Audio Lingual Method focuses on specific grammar teachings.

4.1 Key Features

Here is a summary of the key features of the Audiolingual Method, taken from Brown (1994:57) and adapted from Prator and Celce-Murcia (1979).

(1) New material is presented in dialog form.

(2) There is dependence on mimicry, memorization of set phrases, and overlearning.

(3) Structures are sequenced by means of contrastive analysis and taught one at a time.

(4) Structural patterns are taught using repetitive drills.

(5) There is little or no grammatical explanation. Grammar is taught by inductive analogy rather than deductive explanation.

(6) Vocabulary is strictly limited and learned in context.

(7) There is much use of tapes, language labs, and visual aids.

(8) Great importance is attached to pronunciation.

(9) Very little use of the mother tongue by teachers is permitted.

(10) Successful responses are immediately reinforced.

(11) There is great effort to get students to produce error-free utterances.

(12) There is a tendency to manipulate language and disregard content.

V. THE STRUCTURAL APPROACH

As the name suggests, the method is all about structure. The idea is that any language is made up of complex grammar rules. These rules, according to this approach need to be learnt in a specific order, for example the logical thing would be to teach the verb "to be" prior to teaching the present continuous which requires using the auxiliary form of the verb "to be."

VI. SUGGESTOPEDIA

This is a behaviourist theory and related to pseudoscience. This method relies heavily on students' belief about the method's effectiveness. This theory is intended to offer learners various choices, which in turn helps them become more responsible for their learning. It relies a lot on the atmosphere and the physical surroundings of the class. It's essential that all learners feel equally comfortable and confident. When teachers are training to use the Suggestopedia method, there's a lot of art and music involved. Each Suggestopedia lesson is divided into three different phases – 1. Deciphering 2. Concert Session 3. Elaboration.

6.1 Key Features

Here are some of the key features of Suggestopedia:

(1) Learning is facilitated in an environment that is as comfortable as possible, featuring soft cushioned seating and dim lighting.

(2) "Peripheral" learning is encouraged through the presence in the learning environment of posters and decorations featuring the target language and various grammatical information.

(3) The teacher assumes a role of complete authority and control in the classroom.

(4) Self-perceived and psychological barriers to learners' potential to learn are "desuggested".

(5) Students are encouraged to be child-like, take "mental trips with the teacher" and assume new roles and names in the target language in order to become more "suggestible".

(6) Baroque music is played softly in the background to increase mental relaxation and potential to take in and retain new material during the lesson.

(7) Students work from lengthy dialogs in the target language, with an accompanying translation into the students' native language.

(8) Errors are tolerated, the emphasis being on content and not structure. Grammar and vocabulary are presented and given treatment from the teacher, but not dwelt on.

(9) Homework is limited to students re-reading the dialog they are studying – once before they go to sleep at night and once in the morning before they get up.

(10) Music, drama and "the Arts" are integrated into the learning process as often as possible.

VII. TOTAL PHYSICAL RESPONSE

Total Physical Response, otherwise known as TPR is an approach that follows the idea of 'learning by doing'. Beginners will learn English through a series of repetitive actions such as "Stand up", "Open your book", "Close the door", and "Walk to the window and open it." With TPR, the most important skill is aural comprehension and everything else will follow naturally later.

VIII. COMMUNICATIVE LANGUAGE TEACHING (CLT)

The idea behind this approach is to help learners communicate more effectively and correctly in realistic situations that they may find themselves in. This type of teaching involves focusing on important functions like suggesting, thanking, inviting, complaining, and asking for directions to name but a few.

IX. THE SILENT WAY

The Silent Way emphasises learner autonomy. The teacher acts merely as a facilitator trying to encourage students to be more active in their learning. The main of this way of teaching is for the teacher to say very little, so students can take control of their learning. There's a big emphasis on pronunciation and a large chunk of the lesson focuses on it. This method of learning English follows a structural syllabus and grammar, vocabulary and pronunciation are constantly drilled and recycled for reinforcement. The teacher evaluates their students through careful observation, and it's even possible that they may never set a formal test as learners are encouraged to correct their own language errors.

9.1 Key Features

Richards and Rodgers (1986:99) describe the key theories underlying the Silent Way:

(1) Learning is facilitated if the learner discovers or creates rather than remembers and repeats what is to be learned.

(2) Learning is facilitated by accompanying (mediating) physical objects.

(3) Learning is facilitated by problem-solving involving the material to be learned.

X. COMMUNITY LANGUAGE LEARNING

This is probably one of the English teaching methods where the student feels the safest as there's a great emphasis on the relationship and bond between the student and teacher. Unlike a lot of the other methods and approaches of teaching English as a Second Language, a lot of the L1 (mother tongue) is used for translation purposes.

XI. TASK BASED LANGUAGE LEARNING

The main aim of this approach to learning is task completion. Usually, relevant and interesting tasks are set by the teacher and students are expected to draw on their pre-existing knowledge of English to complete the task with as few errors as possible.

XII. THE LEXICAL APPROACH

The Lexical syllabus or approach is based on computer studies that have previously identified the most commonly used words. This approach in teaching focuses on vocabulary acquisition and teaching lexical chunks in order of their frequency and use. Teachers of the Lexical Approach place a great emphasis on authentic materials and realistic scenarios for more valuable learning.

XIII. CONCLUSION

The basic principles and procedures of widely practiced methods for teaching a second language are described. Both Direct and Oral methods which proposed an eclectic approach based on the learners, gained prominence over Grammar Translation method. The new tools advanced by technology and science contributed much to the development of audio-lingual and audiovisual methods in language teaching. As a reaction to audio-lingualism, cognitive code learning began to recognize learning as an innovative process and looked for common features of all languages. The Communicative Language teaching with its stress on meaning, fluency and real life communication came into existence from the notion of language as a social process. It then became recognized approach for language teaching.

RESOURCES AND BOOKS ON METHODOLOGY

1. A. James, Learning Another Language Through Actions: The Complete Teacher's Guidebook, Los Gatos, CA: Sly Oaks Productions, 1977. See also http://www.tpr-world.com/.
2. B. H. Douglas, Teaching by Principles: An Interactive Approach to Language Pedagogy, Prentice Hall, 1994.
3. F. Mary, B. Christopher, The Functional-Notional Approach: From Theory to Practice. Oxford University Press, 1983.
4. D. K. Stephen, D. T. Tracy, The Natural Approach: Language Acquisition in the Classroom, Pergamon Press, 1983. See also Bilingual Education: Arguments For and (Bogus) Arguments Against , Theory of Second Language Acquisition, A Summary of Stephen Krashen's "Principles and Practice in Second Language Acquisition", Why Bilingual Education?.
5. L-F. Dianne, Techniques and Principles in Language Teaching. New York: Oxford University Press, 1986.
6. N. David, Language Teaching Methodology: A Textbook for Teachers, Prentice Hall, 1991. See also http://ec.hku.hk/dcnunan/
7. H. P. Clifford, C-M. Marianne, "An outline of language teaching approaches", in Celce-Murcia, Marianne & McIntosh, Lois (Ed.), Teaching English as a Second or Foreign Language, Newbury House, 1979.
8. R. Jack, R. Theodore, Approaches and Methods in Language Teaching, New York: Cambridge University Press, 1986.

ONLINE RESOURCES

1. Second Language Teaching Methodologies - Eric Clearinghouse on Languages and Linguistics.
2. Teaching Techniques - From www.eslabout.com

Time-dependent Solutions of a Single Server Queue with Single Vacation and Interrupted Closedown Time

Dr. A. Azhagappan
Professor,
Department of Mathematics,
St. Anne's College of Engineering and Technology,
Anguchettypalayam, Panruti– 607106.

Mrs. T. Deepa
Assistant Professor,
Department of Mathematics,
Idhaya College of Arts and Science for Women,
Pakkamudayanpet, Puducherry- 605 008.

Mr. D. Logeshwaran
UG Student,
Department of Computer Science and Engineering,
St. Anne's College of Engineering and Technology,
Anguchettypalayam, Panruti– 607106.

Mr. P. Anandharaj
UG Student,
Department of Computer Science and Engineering,
St. Anne's College of Engineering and Technology,
Anguchettypalayam, Panruti– 607106.

Abstract - This paper presents the transient behavior of an M/M/1 queueing model with single vacation and interrupted closedown time of the server. The time-dependent system size probabilities for the proposed model are obtained using the method of generating function. Further, the time-dependent mean is also obtained.

Index Terms **- The M/M/1 queue; Single vacation; Interrupted closedown time; Time-dependent solution.**

I. INTRODUCTION

During the past few decades, many researchers carried out works related to queues with server on vacations. In a vacation queue, the server stops serving the customers completely during the entire vacation period. There are two different vacation policies: single and multiple. This paper focuses on single vacation policy. In a single vacation policy, after the completion of vacation, the server stays idle and waits for the arrivals if no customer is waiting in the queue (refer [2], [4], [5], [6]). If there is at least one customer waiting in the queue at the vacation completion instant, the server begins the exhaustive service. Closedown the system when it becomes empty, performs major role in various real time situations as it

helps to minimize the running cost of a system. Only few research works are carried out in literature related to Markovian queueing models with closedown times under transient case (refer [3]). This gives us the motivation to carry out this research work.

Doshi [2] treats the situations that the server works on secondary customers as vacation period of server wherein the server never provides any service to the primary customers waiting in the queue. Altman and Yechiali [1] presented a comprehensive analysis of the impatient behavior of single server queues for both multiple and single vacation cases and obtained various closed form results. Using matrix geometric method, the steady-state system size and virtual time distributions of the M/M/1 queueing model with single working vacations were obtained by Tian et al. [6]. Kumar et al. [3] considered a Markovian queueing model where the server undergoes closedown and then maintenance work as soon as the system becomes empty. They derived the transient solutions and some system measures such as asymptotic behavior of various system state probabilities, average workload, etc. Sudhesh and Azhagappan [4] investigated the impatient behavior of customers for an M/M/1 vacation queueing model where the server waits dormant in the system for certain period after returning from the vacation. Sudhesh et al. [5] studied a Markovian single server queue in which the server starts working vacation when the system becomes empty and the impatience of customers is due to the long waiting time during the working vacation period of the server.

The rest of the paper is organized as follows. In section 2, the M/M/1 queueing model with single vacation and interrupted closedown time is described, its governing equations are presented and the time-dependent solutions are derived. In section 3, the time-dependent mean size of the system is obtained. In section 4, this research work is concluded.

II. MODEL DESCRIPTION

Consider an M/M/1 queueing model with single vacation and interrupted closedown time. The assumptions to derive the transient system size probabilities are given as follows:

- Arrival of customers follows a Poisson process with rate `λ' and the service time follows an exponential distribution with rate `μ'.
- Whenever the system becomes empty, the single server starts an exponentially distributed closedown work at a rate `η'. If any arrival occurs before the completion of closedown period, the closedown work is interrupted and the server begins an exhaustive busy period.
- After the completion of closedown period, the server resumes vacation at a rate `γ' which follows an exponential distribution. If no customer waits in the queue at moment of completion of vacation, the server stays idle and waits for the arrivals. Otherwise, the server resumes an exhaustive busy period.
- Assume that inter-arrival time, service time, closedown time and vacation time are all independent.
- The service discipline is first-come-first-served (FCFS).

Let $\{X(t), t \geq 0\}$ be the number of customers in the system and J(t) be the status of the server at time t, which is defined as follows:

$$J(\mathrm{t}) = \begin{cases} 0, \textit{if the server is on vacation state}, \\ 1, \textit{if the server is in busy state at time } t. \end{cases}$$

Then $\{J(\mathrm{t}), X(\mathrm{t}), \mathrm{t} \geq 0\}$ is a continuous time Markov chain on the state space $S = \{C\} \cup \{j, n : j = 0 \, or \, 1; \; n = 0, 1, 2, ...\}$. Let

$$P_{j,n}(\mathrm{t}) = P\{J(\mathrm{t}) = j, \mathrm{X}(\mathrm{t}) = n : j = 0, 1; \; n = 0, 1, 2, ...\},$$
$$P_C(\mathrm{t}) = P\{\textit{Closedown period}\}.$$

2.1 Governing Equations

The probabilities $P_{j,n}(\mathrm{t}), j = 0, 1; \; n = 0, 1, 2, ...,$ satisfy the forward Kolmogorov equations as

$$P_C'(t) = -(\lambda + \eta) P_C(t) + \mu P_{1,1}(t), \tag{2.1}$$
$$P_{1,0}'(t) = -\lambda P_{1,0}(t) + \gamma P_{0,0}(t), \tag{2.2}$$
$$P_{1,1}'(t) = -(\lambda + \mu) P_{1,1}(t) + \lambda P_{1,0}(t) + \lambda P_C(t) + \mu P_{1,2}(t) + \gamma P_{0,1}(t), \; n \geq 1, \tag{2.3}$$
$$P_{1,n}'(t) = -(\lambda + \mu) P_{1,n}(t) + \lambda P_{1,n-1}(t) + \mu P_{1,n+1}(t) + \gamma P_{0,n}(t), \; n \geq 2, \tag{2.4}$$
$$P_{0,0}'(t) = -(\lambda + \gamma) P_{0,0}(t) + \eta P_C(t), , \tag{2.5}$$
$$P_{0,n}'(t) = -(\lambda + \gamma) P_{0,n}(t) + \lambda P_{0,n-1}(t), \; n \geq 1, \tag{2.6}$$

with $P_{0,0}(0) = 1.$

2.2 Time-dependent Solutions

In this section, the time-dependent system size probabilities are derived for the model under consideration.

2.2.1. Theorem. The expression for the probabilities $P_{1,n}(t)$, for $n = 1, 2, 3, ...$ is obtained from (2.3) and (2.4) as

$$P_{1,n}(t) = \gamma \int_0^t \sum_{m=1}^{\infty} P_{0,m}(u) \beta^{n-m} \left[I_{n-m}(\alpha(t-u)) - I_{n+m}(\alpha(t-u)) \right] e^{-(\lambda+\mu)(t-u)} du$$
$$+ \lambda \int_0^t \left(P_{1,0}(u) + P_C(u) \right) \beta^{n-1} \left[I_{n-1}(\alpha(t-u)) - I_{n+1}(\alpha(t-u)) \right] e^{-(\lambda+\mu)(t-u)} du, \tag{2.7}$$

where $P_{1,0}(t)$ is obtained from (2.2) as

$$P_{1,0}(t) = \gamma \int_0^t P_{0,0}(u) e^{-\lambda(t-u)} du, \tag{2.8}$$

$I_n(t)$ is the modified Bessel function of the first kind of order n, $\alpha = 2\sqrt{\lambda\mu}$ and $\beta = \sqrt{\lambda / \mu}$.

Proof: Define $G(z,t)=\sum_{n=1}^{\infty}P_{1,n}(t)z^n$.

From (2.3) and (2.4), we get

$$\frac{\partial G(z,t)}{\partial t}=\left[-(\lambda+\mu)+\lambda z+\frac{\mu}{z}\right]G(z,t)+\gamma\sum_{n=1}^{\infty}P_{0,n}(t)z^n+\lambda z\left(P_{1,0}(u)+P_C(u)\right)-\mu P_{1,1}(t). \tag{2.9}$$

Solving the equation (2.9), we obtain

$$G(z,t)=\gamma\int_0^t\left[\sum_{m=1}^{\infty}P_{0,m}(u)z^m\right]e^{-(\lambda+\mu)(t-u)}e^{\left(\lambda z+\frac{\mu}{z}\right)(t-u)}du+\lambda z\int_0^t\left(P_{1,0}(u)+P_C(u)\right)e^{-(\lambda+\mu)(t-u)}e^{\left(\lambda z+\frac{\mu}{z}\right)(t-u)}du$$
$$-\mu\int_0^t P_{1,1}(u)e^{-(\lambda+\mu)(t-u)}e^{\left(\lambda z+\frac{\mu}{z}\right)(t-u)}du. \tag{2.10}$$

It is well known that, if $\alpha=2\sqrt{\lambda\mu}$ and $\beta=\sqrt{\lambda/\mu}$, then

$$e^{\left(\lambda z+\frac{\mu}{z}\right)t}=\sum_{n=-\infty}^{\infty}(\beta z)^n I_n(\alpha t).$$

Using the above equation in (2.10) and comparing the coefficients of z^n on both sides, for $n\geq 1$, we get (2.7). Taking Laplace transforms of (2.2), we get

$$\widehat{P}_{1,0}(s)=\frac{\gamma}{s+\lambda}\widehat{P}_{0,0}(s). \tag{2.11}$$

On Laplace inversion (2.11), we get (2.8).

2.2.2. Theorem. The expression $P_C(t)$, $P_{0,0}(t)$, $P_{0,n}(t), n\geq 1$ are obtained from (2.1), (2.5) and (2.6) as

$$P_C(t)=\mu e^{-(\lambda+\eta)t}*P_{1,1}(t), \tag{2.12}$$

$$P_{0,0}(t)=\mu\eta e^{-(\lambda+\gamma)t}*e^{-(\lambda+\eta)t}*P_{1,1}(t)+e^{-(\lambda+\gamma)t}, \tag{2.13}$$

$$P_{0,n}(t)=\lambda^n e^{-(\lambda+\gamma)t}\frac{t^{n-1}}{(n-1)!}*\mu\eta e^{-(\lambda+\gamma)t}*e^{-(\lambda+\eta)t}*P_{1,1}(t)+e^{-(\lambda+\gamma)t}, \tag{2.14}$$

where

$$P_{1,1}(t)=\gamma\sum_{m=1}^{\infty}\lambda^m e^{-(\lambda+\gamma)\mathrm{t}}\frac{t^m}{m!}*\beta^{1-m}e^{-(\lambda+\mu)\mathrm{t}}\left[I_{m-1}(\alpha t)-I_{m+1}(\alpha t)\right]$$
$$+\lambda\gamma e^{-\lambda t}*e^{-(\lambda+\gamma)\mathrm{t}}\left[I_0(\alpha t)-I_2(\alpha t)\right]\sum_{k=0}^{\infty}\sum_{r=0}^{k}\binom{k}{r}(\eta\gamma\mu)^{k-r}$$
$$\times\left\{\sum_{m=1}^{\infty}\lambda^m\beta^{1-m}e^{-(\lambda+\gamma)\mathrm{t}}\frac{t^m}{m!}*e^{-(\lambda+\eta)\mathrm{t}}*e^{-(\lambda+\mu)\mathrm{t}}\left[I_{m-1}(\alpha t)-I_{m+1}(\alpha t)\right]\right\}^{*(\mathrm{k-r})}$$
$$\times(\lambda\mu)^r\sum_{j=0}^{r}\binom{r}{j}(\gamma\eta)^j e^{-\lambda t}\frac{t^{j-i}}{(\mathrm{j}-1)!}*e^{-(\lambda+\gamma)\mathrm{t}}\frac{t^{j-i}}{(\mathrm{j}-1)!}$$
$$*e^{-(\lambda+\eta)\mathrm{t}}\frac{t^{r-1}}{(\mathrm{r}-1)!}*e^{-(\lambda+\mu)\mathrm{t}}\left[I_{r-1}(\alpha t)-I_{r+1}(\alpha t)\right], \tag{2.15}$$

where '$*$' denotes the convolution and '$*k$' denotes the 'k'-fold convolution.

Proof: Taking Laplace transform on (2.1), we get

$$\widehat{P}_C(s) = \frac{\mu}{s+\lambda+\eta}\widehat{P}_{1,1}(s). \qquad . \qquad (2.16)$$

which on inversion leads to (2.12). Laplace transform of (2.5) and using (2.16) gives

$$\widehat{P}_{0,0}(s) = \frac{\eta\mu}{(s+\lambda+\gamma)(s+\lambda+\eta)}\widehat{P}_{1,1}(s) + \frac{1}{(s+\lambda+\gamma)}. \qquad (2.17)$$

On Laplace inversion of (2.17), we get (2.13). Laplace transform of (2.6) and using (2.17) yields,

$$\widehat{P}_{0,n}(s) = \left(\frac{\lambda}{s+\lambda+\gamma}\right)^n \left(\frac{\eta\mu}{(s+\lambda+\gamma)(s+\lambda+\eta)}\widehat{P}_{1,1}(s) + \frac{1}{(s+\lambda+\gamma)}\right). \qquad (2.18)$$

Laplace inversion of (2.18) gives (2.14). Using (2.11), (2.16), (2.17), (2.18) in the Laplace transform of (2.7) and rearranging, we get (2.15).

III. TIME-DEPENDENT MEAN

In this section, the mean number of customers in the system at time t is derived for the time-dependent case. The mean system size, E(X(t)) is given as

$$E\big(X(t)\big) = \lambda\sum_{n=1}^{\infty}\int_0^t (P_{0,n-1}(u) + P_{1,n-1}(u))du + \lambda\int_0^t P_C(u)\,\mathrm{du} - \mu\sum_{n=1}^{\infty}\int_0^t P_{1,n}(u)du\,.$$

IV. CONCLUSION

The time-dependent solutions are derived in this article for an M/M/1 queueing model with single vacation and interrupted closedown time. The major contributions in this research work are the introduction of interrupted closedown time of the server and the derivation of the most significant transient system distributions. Also the average number of customers in the system is obtained for the transient case.

REFERENCES

1. E. Altman, U. Yechiali, 'Analysis of customers' impatience in queues with server vacation', Queueing Systems, 2006, 52, 261-279.
2. B.T. Doshi, 'Queueing systems with vacations - A survey', Queueing Systems, 1986, 1, 29-66.
3. B. K. Kumar, S. Anbarasu, S. R. A. Lakshmi, 'Performance analysis for queueing systems with close down periods and server under maintenance', International Journal of System Sciences, 2015, 46(1), 88-110.
4. R. Sudhesh, A. Azhagappan, 'Transient analysis of M/M/1 queue with server vacation customers impatient and a waiting server timer', Asian Journal of Research in Social Sciences and Humanities, 2016, 6(9), 1096-1104.
5. R. Sudhesh, A. Azhagappan, S. Dharmaraja, 'Transient analysis of M/M/1 queue with working vacation heterogeneous service and customers' impatience', RAIRO - Operations Research, 2017, 51(3), 591-606.
6. N. Tian, X. Zhao, K. Wang, 'The M/M/1 queue with single working vacation', International Journal of Information and Management Science, 2008, 19, 621-634.

National Perceptive of teaching of English

Mr. R. Ranjith Kumar
UG student
Department of Computer Science and Engineering,
St. Anne's College of Engineering and Technology,
Anguchettypalayam, Panruti – 607106.

Abstract - From Indian national development perspective proficiency in English for our scientists and engineers is important English as it is the dominant language of science and technology. Proficiency in English is also important for the academics and research bodies as a good number of the scientific papers or journals in the world are written in English.. English as an international language of science (EILS) has led some users to enjoy preferred treatment and status. Hence it is imperative that our students have the requisite proficiency in English if we want our country to occupy leadership position in the field of science and technology. This paper therefore explores the significant factors and their impact on the communicative proficiency of engineering students in India.

Index Terms - Proficiency, Communication Skills, Fluency, Employability Skills

I. INTRODUCTION

Decades ago it was generally believed that engineers were to do technical things behind stage and therefore did not need any higher level of proficiency in English. The engineering curriculum therefore didn't give any emphasis to developing communication skills in English. With India fast becoming a global economy and English being the language of global business, the Indian companies are increasingly focusing on English language skills of employment seeking candidates. Moreover, English is the medium of interpersonal communication in the corporate and therefore having good command on English language has become even more crucial. Engineers usually work in groups and this very nature of their work demands mutual cooperation and effective interpersonal communication within and outside the organization in order to understand and coordinate with co-workers and accomplish their projects. To be able to do so engineers need to possess high level of listening comprehension, speaking and reading fluency and good writing skills in English. It would be squarely wrong to depend solely on technical knowledge and skills, which could be

less than adequate due lack of language comprehension and production skills in English, to progress in one's professional career. Good communication skills in English and sound domain knowledge is also crucial to make the most out of the globalised job market

II. NOTE ON ENGLISH PROFICIENCY

According to Najar (2002) "communicative competence, including teamwork and professional writing skills for example, the ability to research, write and format basic research reports as well as develop formal oral presentation skills is important to prepare students for both academic success and the workplace." Kang Shumin says: "Learning to speak a foreign language requires more than knowing its grammatical and semantic rules". He further opines that: "Learners must also acquire knowledge of how native speakers use the language in the context of structured interpersonal exchange, in which many factors interact".

Communication is a multidisciplinary activity that encompasses broad areas such as listening, speaking, reading, and writing. Effective communication skill is an essential for the engineer. It is not only the academics but engineers require effective communication as an essential employability skill in the competitive global work arena. Unfortunately reviews show that this very skill is severely lacking, subsequently affecting the general employability of engineering students.

Himanshu Aggarwal, CEO, Aspiring Minds, said "Looking at state-wise distribution of employable talent, we can see that while certain states produce huge quantity of engineers, the average employability is significantly low," ….It is clear that states need to be conscious towards better education quality rather than building more capacity."

According to Janette Marx Senior Vice President at Adecco Staffing U.S, ""It's interesting to see how the definition of the skills gap has evolved from being so heavily focused on technical and computer skills to „soft" skills related to communication and creativity…..Educational institutions may overlook these elements in today's digital age, but schools must integrate both hard and soft skill sets into their curriculums, which in turn will help better prepare candidates and strengthen our country's workforce."

III. ANALYSIS LIMITATIONS AND SCOPE

Despite very good syllabus developed by the various Boards of Secondary education, English language proficiency in the Indian schools and colleges have remained inhibited and the factors for such dismal situation can be attributed to failure of English language teaching-learning-evaluation process which ultimately affects their appreciation of higher levels of academic learning. In vernacular medium rural and urban schools English is almost treated as an alien language and proficiency in the language exists at a literal rather than at inferential level and where meaningful interaction in English is rare. Many teachers in vernacular medium schools themselves have low levels of proficiency in English and they too operate at the literal level. Although they are required to teach in English, they often resort to code switching while teaching and hand out summaries and notes in English which the students rote-learn to pass examinations.

Students often resort to decoding English into their mother tongue or the first language whichever they find convenient and then reinterpret their thoughts into English, a situation potential for occurrence of considerable misinterpretation. This results in the inability to clearly express their thoughts in both written and spoken forms; all of which translates into high communication failure potential. Once students from such an environment enter higher education, they are certainly disadvantaged and often are unable to adapt to the discourse-based environment in the universities and institutes of higher education. The situation for students coming from English medium schools is only slightly better than the vernacular medium counterparts.

It is also to be noted that students do not speak the English language or listen to it on a constant daily basis. Speaking the language is not mandatory in many English medium schools and not at all necessary in vernacular mediums. This highly affects the basic English learning skills of all students.

IV. COMMUNICATIVE LANGUAGE TEACHING IN ENGINEERING COLLEGES

Secondly the English course and teaching methodology in engineering colleges of Orissa was analyzed. While everyone agrees that adequate communication competencies are crucial for good engineers, teaching of English in engineering colleges in India has always

held an uncertain status. Much attention has not been given to these curricula. Language learning is a skill-oriented activity and needs an entirely different pedagogic approach from the one used for other conventional Courses. As the learners are adults they have different learning styles which must be respected

Students follow a common syllabus comprising of the Communicative English course and Business Communication at the undergraduate level. The colleges have the liberty to introduce it either in the first year (in either 1st or 2nd semester) or in the second year (either in 3rd or 4th semester) of the engineering programme. In most cases, it is either a two or a three-semester course, comprising of both theory and practical classes.

The teacher in an engineering college has little motivation because much of the teaching is remedial in nature and offers little scope for professional growth. On the other hand the student at that stage (first year), the student is in no frame of mind to work on English. They want to be exposed to higher learning experience rather than to seemingly irrelevant English writing and grammar. It is only in the third year onwards that the students become aware of their needs and are then desperately looking for help which, due to syllabus structure and time constraint, becomes difficult and almost impossible.

There is, therefore an urgent need to find a workable solution so that the students in professional colleges have an opportunity to acquire skills on which their professional excellence depends.

V. CONCLUSION

In learning a language, the aim is to be able to utilize the language in day-to-day tasks and also to meet the academic demands. The linguistic competence is crucial for the students and teachers as well. The teaching-learning process should ensure that learning does take place and the learners do achieve their long-term goals which include learners‟ ability to communicate in the target language outside of classrooms and realize various professional/career opportunities. Although, the technical universities do have programmes which run for one or two semesters, situation does not register any appreciable change in the communication skills of the students in reality due mainly to immersion insufficiency.

REFERENCES

1. K. Adams, D. Missingham, Contributions to Student Learning: An overview of Engineering Communication courses in Mechanical Engineering education, School of Mechanical Engineering, University of Adelaide, unpublished (internal) report, 2006.
2. M. Alvesson, Knowledge Work and Knowledge-intensive Firms, Oxford University Press, Oxford, 2004.
3. J. R. Marc, English and Communication Skills for the Global Engineer, Global Journal of Engineering Education, 2002, 6(1).
4. L. N. Robyn, Facilitating the development of disciplinary knowledge and communication skills: Integrating Curriculum, paper presented at the Annual Meeting of the Australian Association for Research in Education, Freemantle, 2-6 December, 2001.
5. K. Shumin, Factors to consider: Developing Adult EFL Students‟ Speaking Abilities, Jack C. Richards, Willy A. Renandya. Ed Methodology in Language Teaching: An Anthology of. Current practice CUP, 2002: 204.
6. Business Standard, Wednesday, March 6, 2013; www.businessstandard.com
7. http://www.thehindu.com/todays-paper/tp-features/tp-educationplus/survey-findings/ article5013275.ece
8. http://www.forbes.com/sites/ashoka/2014/03/04/two-sides-of-the-same-coin-the-employment-crisis-and-the-education-crisis/

Quantum mechanical investigations on molecular structure, spectroscopic and molecular docking studies of Diosmetin as potential Anti-diabetic agent

Mr. A. Harikrishnan
Associate Professor,
Department of Science and Humanities,
St. Anne's College of Engineering and Technology,
Anguchettypalayam, Panruti– 607 106.

R.Madivanane
Associate Professor,
Department of Physics
Bharathidasan Govt College for Women,
Puducherry, India– 605 001.

Abstract - In the present study, The optimized molecular geometries and vibrational characteristics for the diosmetin have been studied theoretically using Hartree-Fock (HF) and density functional theory (DFT) methods with 6-311++G (d,p) as basis set. The geometrical parameters and vibrational frequencies obtained from the DFT method are found to be in good agreement with the experimental outcome and a detailed interpretation of the vibrational spectra of the compound have been made on the basis of the calculated potential energy distribution (PED). Furthermore, molecular docking study indicates that the investigated compound shows better inhibitory activity towards aldose reductase enzyme than the standard drug and hence this study may be supportive in the field of drug discovery to design more potent anti-diabetic agents.

IndexTerms— Diosmetin ; Computation; Docking; Aldose reductase.

I. INTRODUCTION

In recent years flavanoid compound have attracted more attention, because of their wide range of biological profile in the field of drug design. Diosmetin (DIOS) is an aglycone of the flavonoid, chemically known as 5, 7-dihydroxy-2(3-hydroxy-4 methoxyphenyl) chromen-4-one and it can be found in food items such as parsley and thyme [1]. Diosmetin (DIOS) possessing a wide range of biological activities like antibacterial [2], antimicrobial [3], anti-inflammatory [4], antioxidant effects [5] and it can be used as a traditional Mongolian medicine to treat liver diseases [6]. Thus, owing to the vast range of biological significance of DIOS, the present study aimed an extensive spectroscopic and quantum chemical investigation to provide structural conformational and vibrational frequencies to understand the effect of functional group. The literature survey reveals that to the best of our knowledge, no HF/DFT wave number and structural parameter calculations of DIOS has been reported so

far. Therefore, the present investigation is undertaken to study the vibrational spectra of this molecule in detail to identify the various normal modes with greater wave number accuracy. In the present study, molecular docking is carried out to examine interactions of the DIOS with aldose reductase enzyme, a diabetes target and the results were compared with that of known drugs Zennarestat

II. Experimental and Computational methods

The FT-IR spectrum has been recorded in the region between 4000 and 400 cm^{-1} using Cary 630 FTIR spectrometer equipped with attenuated total reflectance sampling reflectance interface (Agilent Technologies, USA), at room temperature with scanning speed of 10 cm^{-1} per minute and the spectral resolution is ±4 cm^{-1}. The Cary 630 Micro Lab PC programming was utilized for data collection and Agilent Resolution Pro programming used to analyze the data. The FT-Raman spectrum of title compound was recorded using 1064 nm line of Nd: YAG laser as excitation wavelength in the region 4000 and 50 cm^{-1} using BRUKER RFS 27: Stand alone FT-Raman Spectrometer at Sophisticated Analytical Instrumentation Facility (SAIF), IIT, and Chennai. To provide complete information regarding to the structural characteristics, energy and the fundamental vibrational frequency of the title compound, the quantum chemical calculations were performed at Hatree Fock(HF) and Becke-3-Lee Yang–Parr levels with the basis set 6-311++G (d,p) using the Gaussian 09W program. By assuming C1 point group symmetry, the Cartesian representation of the theoretical force constants has been computed at the fully optimized geometry and vibrational frequency calculations were also carried out.

.

III. RESULT ANALYSIS

3.1 Molecular Geometry and Vibrational Analysis

The self consistent energy (SCF) is calculated at both the levels HF and DFT, of which, the SCF at DFT is identified as relatively lower (-1068.56 a.u) than the SCF at HF levels (-1062.32 a.u). Consequently, the optimized geometry obtained at DFT level is considered as the most stable structure. Figure 4 shows the optimized structure of the title compound. The selected geometrical parameters are provided in Table 1. The average bond distances and bond angles of the optimized structure almost match with the experimental conformation of the similar structure. The title compound consists of 34 atoms, sob it has 96 normal vibrational modes and it belongs to the point group C_1. In this present study, we compare the harmonic vibrational wave numbers obtained at HF and B3LYP methods with experimentally

observed values. FT-IR spectrum shows a broad peak at 3355 cm^{-1} which is ascribed to hydroxyl (O-H) stretching vibration and this mode is predicted at 3195 cm^{-1} for HF and 3355cm^{-1} by DFT calculations. This O-H stretching modes is pure since their PED contribution is 100%. The carbonyl stretching(C=O) vibration of DIOS is observed at 1652 cm^{-1} in FT-Raman spectra and this mode was calculated at 1656 cm^{-1} by DFT method.

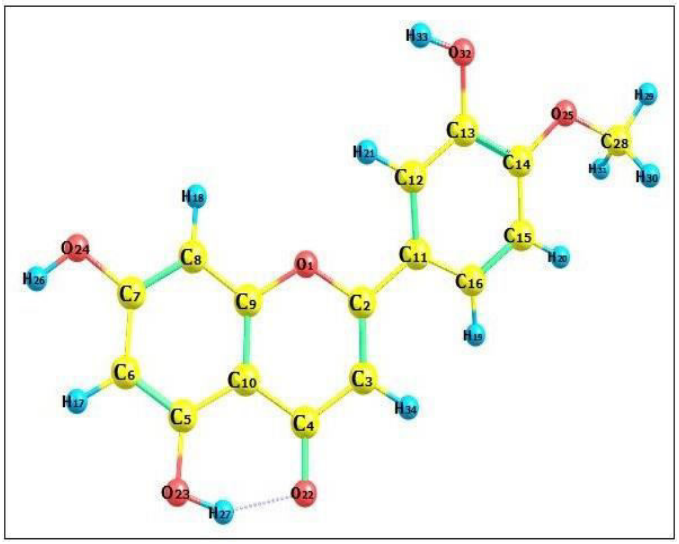

Fig. 1 The optimized structure of the Diosmetin

Table 1. Selected optimized geometric parameters of Diosmetin

BondLength(A°)	**HF**	**DFT**	**Bond Length(A°)**	**HF**	**DFT**
O1-C2	1.343	1.363	**C7-O24**	**1.338**	**1.362**
O1-C9	1.348	1.371	C8-C9	1.378	1.386
C5-C6	1.381	1.392	**C13-O32**	**1.347**	**1.363**
C5-C10	1.410	1.420	C14-C15	1.380	1.395
C5-O23	**1.322**	**1.338**	**C14-O25**	**1.336**	**1.353**
Bond Angle(A°)	**HF**	**DFT**	**Bond Angle(A°)**	**HF**	**DFT**
C2-O1-C9	121.7	120.9	O1-C9-C10	120.6	120.5
O1-C2-C3	122.2	121.5	C8-C9-C10	122.9	122.7
C6-C7-C8	121.9	121.9	C13-C14-C15	118.8	118.8
C7-C8-C9	117.6	117.6	C14-C15-C16	120.9	120.9
O1-C9-C8	116.5	116.8	C11-C16-C15	120.4	120.7
Dihedral Angle(A°)	**HF**	**DFT**	**Dihedral Angle(A°)**	**HF**	**DFT**
C9-O1-C2-C3	-0.4	-0.3	O1-C2-C11-C12	25.8	16.0
C10-C5-C6-H17	-180.0	180.0	C14-O25-C28-H29	-179.6	-179.5

3.2 Molecular docking analysis

Diabetes mellitus is one of the third leading causes of death disease, currently affecting an estimated 143 million people worldwide and the number is still growing rapidly [7]. Reports of 2011 indicate that about 366 million people are diagnosed with diabetes globally, and this may rise to 552 million by the year 2030 [8]. Aldose reductase is a member of aldo-keto reductase superfamily enzyme which catalyzes the reduction of glucose to sorbitol in the polyol pathway and plays a significant role in preventing diabetic microvascular complications such as cardiomyopathy, neuropathy, nephropathy,and retinopathy [9-11]. In the present study, molecular docking studies is carried out against aldose reductase enzyme using autodock 4.0 and the results were compared with diabetic drug, Zennarestat. The compound under the study shows minimum binding energy (-10.83 kcal/mol) when compared to standard drug (-10.64 Kcal/mol). Hydrogen bond interaction is one of the most important and widely discussed interactions in chemistry. In the present study, the title compound DIOS interact with several amino acid residues such as Lys21, Lys77, Tyr48, Tyr209, Ser214 and Gln183 through hydrogen bond. Of which the hydrogen bond formed by the Tyr48 was found to be common between the DIOS and standard compound.

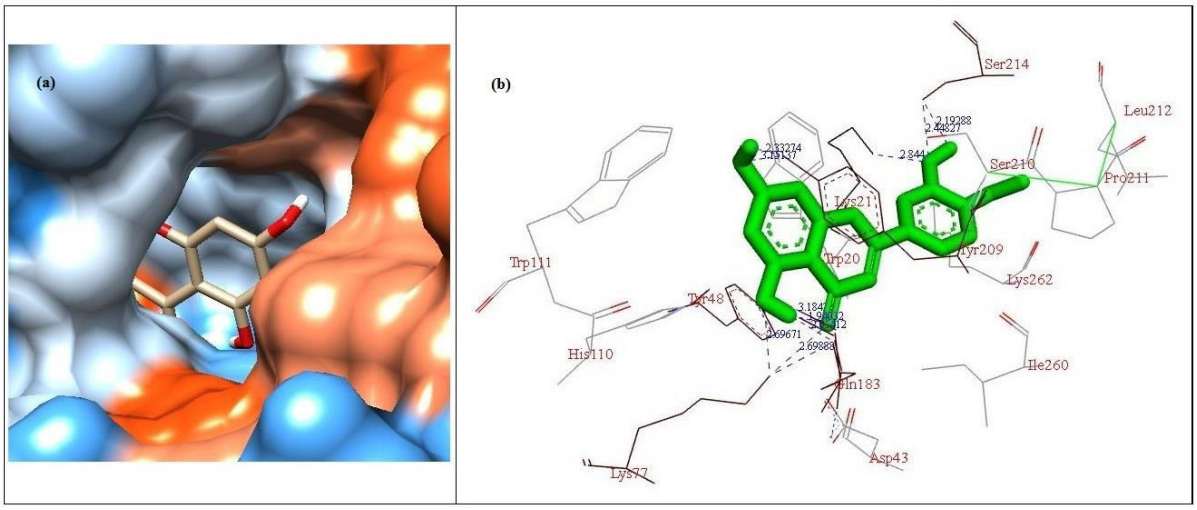

Fig.2 The docking pose and hydrogen bond interactions of the Diosmetin with the active site residues of aldose reductase enzyme.

Table 2: The predicted binding energies, Inhibition constant and H-bond analysis of DIOS with target proteins Aldose Reductase Enzyme

Name of theTarget	Binding Energy (BE) kcal/mol	Estimated Inhibition constant (Ki) nM	Donor	Acceptor	H- Bond Distance (Å)
PDB ID:1IEI	-10.83	11.51	Lys21: NZ	Ligand: O32	2.844
			Lys77:NZ	Ligand:O22	2.698
			Lys77:NZ	Ligand:O23	2.696
			Ligand: H26	Tyr209:OH	2.332
			Ligand: H27	Gln183:OE1	2.054
			Ligand: H33	Ser214:OG	2.450

V. CONCLUSION

The main purpose of this paperis to investigate the application of computational intelligence method **(PGOA)** in short term load forecasting. Due to the evolutionary algorithm **(PGOA)** the load demand in future can be forecasted bitterly and within short span of time, when compared to the other conventional methods. Plant Growth Algorithm achieves better solution and requires less CPU time than other conventional methods.

REFERENCES

1. Yao, L.H.; Jiang, Y.M.; Shi, J.; Tomás-Barberán, F.A.; Datta, N.; Singanusong, R.; Chen, S.S. Flavonoids in food and their health benefits, Flavanones in cumin, peppermint, Flavones in parsley, thyme and Flavonols in onions. Plant Foods Hum. Nutr. **2004**, 59, 113–122

2. Chan BC, Ip M, Gong H, Lui SL, See RH, Jolivalt C, Fung KP, Leung PC, Reiner NE and Lau CB: Synergistic effects of diosmetin with erythromycin against ABC transporter over-expressed methicillin-resistant *Staphylococcus aureus* (MRSA) RN4220/pUL5054 and inhibition of MRSA pyruvate kinase. Phytomedicine 20: 611-614, 2013.

3. Meng JC, Zhu QX and Tan RX: New antimicrobial mono-and sesquiterpenes from *Soroseris hookeriana* subsp. Planta Med 66: 541-544, 2000.

4. Chandler D, Woldu A, Rahmadi A, Shanmugam K, Steiner N, Wright E, Benavente-García O, Schulz O, Castillo J and Münch G: Effects of plant-derived polyphenols on TNF-alpha and nitric oxide production induced by advanced glycation endproducts. Mol Nutr Food Res 54: (Suppl 2) S141-S150, 2010.

5. Liao W, Ning Z, Chen L, Wei Q, Yuan E, Yang J and Ren J: Intracellular antioxidant detoxifying effects of diosmetin on 2, 2-azobis(2-amidinopropane) dihydrochloride

(aaph)-induced oxidative stress through inhibition of reactive oxygen species generation. J Agric Food Chem 62: 8648-8654, 2014.

6. Obmann A, Werner I, Presser A, Zehl M, Swoboda Z, Purevsuren S, Narantuya S, Kletter C and Glasl S: Flavonoid C-and O-glycosides from the Mongolian medicinal plant Dianthus versicolor Fisch. Carbohydr Res 346: 1868-1875, 2011.

7. Satyavati, G.V; Neeraj, T; Madhu, S. Indigenous Plant drugs for diabetes mellitus. Diabetes bulletea. 1989,164Q- 190Q.

8. Whiting Dr, Guariguata L, Weil C, Shaw j. IDF Diabetes atlas: Global estimates of the prevalence of diabetes for 2011 and 2030. Diabetes Res Clin Pract 2011; 94: 311-321.

9. Johnson, B. F., Nesto, R. W., Pfeifer, M. A., Slater, W.R.,Vinik, A.I., Chyun,D.A.,Law,G.,Wackers,F. J.,andYoung,L.H.(2004).Cardiac abnormalities in diabetic patients with neuropathy: effects of aldose reductase inhibitor administration. *Diabetes Care* 27, 448–454.2004.

10. Giannoukakis, N. (2006). Drug evaluation: ranirestatan aldose reductase inhibitor for the potential treatment of diabetic complications. *Curr.Opin.Investig.Drugs* 7, 916–923.

11. Ramirez, M. A., Borja, N. L. (2008). Epalrestat: an aldose reductase inhibitor for the treatment of diabetic neuropathy. *Pharmacother- apy* 28, 646–655.

Synthesis and characterisation of green phosphors

Dr. A. John Peter
Professor
Department of Science and Humanities
St. Anne's College of Engineering and Technology,
Anguchettypalayam, Panruti – 607106.

Abstract- A green-emitting phosphor $SrMoO_4$ co-doped by Tb^{3+} was fabricated by solid-state metathesis reaction route for the first time. X-ray powder diffraction (XRD) analysis revealed that pure $SrMoO_4$ was obtained .Under excitation of UV light, these $SrMoO_4$:xTb^{3+}phosphors showed a strong emission band centered at 547 nm (green) which corresponds to $^5D_4 \rightarrow ^7F_5$ transition of Tb^{3+}. Analysis of the emission spectra with different Tb^{3+} concentrations revealed that the optimum do pant concentration for $SrMoO_4$: xTb^{3+}phosphors are about 8 mol% of Tb^{3+}.All properties show that $SrMoO_4$: $xTb^{3+}$is a very appropriate green–emitting phosphor for fluorescent lamp applications.

I. INTRODUCTION

BeSruse rare earth ions retain a great deal of energy levels and may transfer between 4f electrons, its fluorescence wavelength ordinarily extends from UV to IR range. Thus, the addition of trivalent rare earth ions as luminescent center to matrices is thought-out as an exemplary method for synthesisingexcellent luminescent material 1–4].Tb^{3+}-doped materials have been extensivelyemployed as the green emitting phosphors by virtue of their strong $^5D_4 \rightarrow ^7F_5$ emission in the green spectral region. Earlier investigations have demonstrated that Tb^{3+}-doped aluminates and phosphates displayedalmostintense absorption in the UV region and illustratestrong green emission with satisfying color purity. However, the conventional aluminate, borate and phosphate phosphor have their defects respectively 5–7]. $SrMoO_4$ is a illustatrive scheelite compound, and its central Mo metal ion is organized by four O^{2-}ions in tetrahedral symmetry (*Td*). For $SrMoO_4$ phosphor, green emission arises under UV-light excitation (250–310 nm), but the orange emission at 580nm is observable only if the excitation wavelength is longer than 320nm 8–10]. However, the introduction of Tb^{3+} influences upon the luminescence of the host material.

In continuation to our previous work on the red luminescent $SrMoO_4:Eu^{3+}$, in the present work we have undertaken the green luminescent Tb^{3+} in $SrMoO_4$ powder phosphor for its systematic optiSrl characterization.

II. EXPERIMENTAL METHOD

2.1 Preparation of Phosphors

The green phosphors of $SrMoO_4$: x Tb^{3+} (x= 0.02, 0.04, 0.06, 0.08 and 0.10 mol) were prepared by mechanochemiSrlly assisted solid state metathesis reaction route at room temperature. The chemiSrl equation in this method is as follows:

$$SrCl_2 + Na_2MoO_4.2H_2O \rightarrow SrMoO_4 + NaCl$$

The beginning chemiSrls were logiSrl in evaluation, for example, $SrCl_2$, Na_2MoO_4 and $TbCl_3$ (99.9%). Stoichiometric measures of the starting materials were blended and were processed for a time of two hours in a planetary ball mill Pulverisette- 7 (FRITSCH). Processing was fulfilled in two granulating vials of 15 cm volume comprising of balls with a measurement of 12 mm. Both the compartment and balls were made of tungsten Srrbide material. The quantity of processing balls and the revolution rate of the planetary arrangement of processing gadget were kept consistent. The resultant powder was washed a few times with refined water to uproot sodium chloride that was the by-result of the response and afterward dried at 80^oc for 3h in a furnace in air and sieved. At long last, the productive green phosphor material was gotten.

2.2 Measurements

X – ray powder diffraction (XRD) analysis was Srrried out using Pan AnalytiSrl X'pert pro x- ray diffractometer with Cu K-alpha radiation (λ = 1.5406 Å) at a sSrnning rate of 0.02^o per second. The measurements of PL and photoluminescence excitation (PLE) spectra were performed by a Jobin Yuvon Flurolog-3-11 Spectroflurometer with 450W xenon lamp was used as the excitation source (200-700 nm). All spectroscopic measurements of the phosphors were Serried out at room temperature.

III. RESULTS AND DISCUSSION

Fig. 1 displays the XRD patterns of $Sr_{1-x}MoO_4$:x Tb^{3+} (x= 0.02,0.04,0.06,0.08 and 0.1 mol) phosphor samples prepared by mechanochemiSrlly assisted solid state metathesis reaction route at room temperature. It Srn be seen that all diffraction peaks are consistent well with

JCPDS 851267 standard data of $SrMoO_4$. The peaks in the XRD spectra are sharp and intense proving that a highly crystalline single-phase of tetragonal scheelite structure of $SrMoO_4$had been successfully synthesized by mechanochemiSrlly assisted solid state metathesis reaction route at room temperature. No impurity peak was found in the XRD patterns, distinctly indiSrting the incorporation of Tb^{3+} ions into the compounds.

The excitation and emission spectra of $SrMoO_4$: $0.08Tb^{3+}$phosphors prepared by solid state metathesis reaction route at room temperature is shown in Fig.**3(a)**. The excitation spectrum is monitored at the emission wavelength of 547 nm. It Srn be seen clearly that the excitation spectrum consists of a strong and broad band from 230 to 330 nm with a maximum at about 299 nm assigned as the charge-transfer band (CTB) originated from oxygen to molybenum within the MoO_4^{2-} groups. The other sharp lines including the peaks from 350 nm to 500 nm are attributed to the intra-configurational f-f transition absorption of Tb^{3+} ions in the host lattice. 16]

When the CTB is excited, the energy absorbed from charge-transfer state is efficiently transferred to Tb^{3+} ion by a non-radiative mechanism, and generate green-light emission of the $^5D_0 \rightarrow {}^7F_J$ transition of Tb^{3+} ions in the $SrMoO_4$: $0.08Tb^{3+}$nanophosphors. 17]

Upon excitation at 299 nm, the obtained emission spectrum exhibits four major emission bands at487, 547,590 and 623 nm, corresponding to the $^5D_4 \rightarrow {}^7F_6$, $^5D_4 \rightarrow {}^7F_5$, $^5D_4 \rightarrow {}^7F_4$, and $^5D_4 \rightarrow {}^7F_3$ typiSrl transitions of Tb^{3+}, as shown in Fig 2 respectively. The strongest peak appears at 547 nm is the characteristic emission of Tb^{3+} with $^5D_4$-$^7F_5$ green emission 547 nm. Compared with the emission of Tb^{3+}, the intrinsic emission from MoO_4^{2-} groups is very weak, suggesting that an efficient energy transfer from MoO_4^{2-} to Tb^{3+} has occurred in the $SrMoO_4$: x Tb^{3+} (x= 0.02,0.08 and 0.10 mol) phosphors. Only the transitions from $^5D_4$ to lower lying ^7F_J levels are observed at room temperature upon excitation in the UV range.

The concentration quenching occurs when the Tb^{3+} concentration is beyond 8 mol%. The reason for the concentration quenching is that if the Tb^{3+} concentration continues to increase, the interaction of Tb^{3+}–Tb^{3+} also increases, consequently, the emission intensity becomes lower.18]

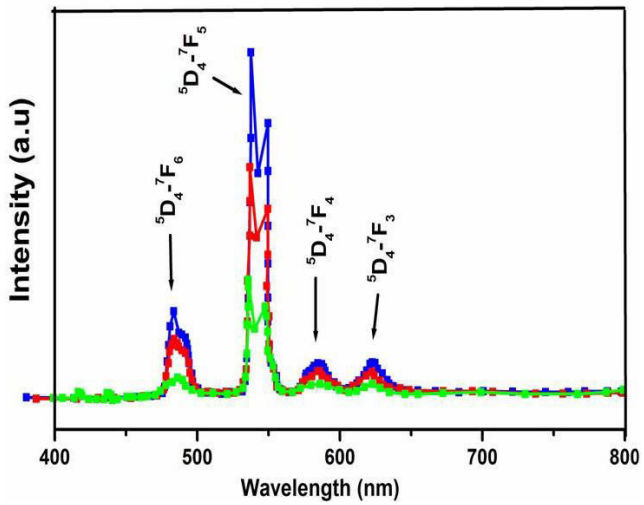

IV. CONCLUSION

A class of novel green emitting Tb^{3+}doped $SrMoO_4$ phosphors were successfully prepared by solid state metathesis reaction at room temperature. These phosphors emit intense green light dominated by 545 nm from $^5D_4$-$^7F_5$ transition of Tb^{3+} under excitation of UV light. All these properties indicate that these phosphors could serve as a potential green emitting phosphor for application on short ultraviolet fluorescent lamps.

REFERENCES:

1. J.G. Li, X.D. Li, X.D. Sun, T. Ishigaki, J. Phys. Chem. C 112 (2008) 11707-11716.
2. Y.G. Su, L.P. Li, G.S. Li, Chem. Commun. 34 (2008) 4004-4006.
3. T. Justel, H. Nikol, C. Ronda, Angew. Chem. Int. Ed. 37 (1998) 3250.
4. H. Wang, C.K. Lin, M. Liu, J. Lin, Appl. Phys. Lett. 87 (2005) 181907-1-3.
5. J.P. Zhong, H.B. Liang, B. Han, Q. Su, Y. Yao, Chem. Phys. Lett. 453 (2008) 192.
6. Li ZH, Zeng JH, Chen C, Li YD (2006) J Cryst Growth 286:493
7. Du N, Zhang H, Ma XY, Li DS, Yang DR (2009) Mater Lett 63:1180
8. Groenink JA, Hakfoort C, Blasse G. Phys Status Solidi A 1979; 54:329–36.
9. Chandrasekhar BK, White WB. Mater Res Bull 1990;25:1513–8.
10. Cho WS, Yashima M, Kakihana M, Kudo A, Sakata T, Yoshimura M. J Am Ceram Soc 1997;80:765–9.
11. M. R. Moura, A. P. Ayala, I. Guedes, M. Grimsditch, C. K. Loong, and L. A. Boatner, J. Appl. Phys. 95, 1148 2004.
12. T. T. Basiev, A. A. Sobol, Y. K. Voronko, and P. G. Zverev, Opt. Mater. 15, 205 2000
13. K. Nakamoto, Infrared and Raman Spectra of Inorganic and Coordination Compounds Wiley, New York, 1986.
14. P.Parthi, S.S.Singh, Alok R Ray, A.Ramanan, Bull.Mater.Sci. 29 (2006) 115-118.

15. S.Neeraj, N.Kijima, A.K.Cheetham, Chem.Phys.Lett.387 (2004) 2.

16. Groenink, J. A.; Hakfoort, C.; Blasse, G. Phys. Status Solidi A 1979,54, 329.

17. Blasse, G.; Grabmaier, B. C. Luminescent Materials; Springer: Berlin,1994.

18. K.S. Thomas, S. Singh, G.H. Dieke, J. Chem. Phys. 38 (1963) 2180.

Synthesis and characterization of materials For lighting Applications

S. Selva Praveena,
UG Student,
Department of Electronics and communication Engineering
St. Anne's College of Engineering and Technology,
Panruti

A John Peter
Professor
Department of Science and Humanities
St. Anne's College of Engineering and Technology,
Panruti

Abstract- The nanostructured $LiY(WO_4)_2:Pr^{3+}$ phosphor was rapidly synthesized at room temperature by mechanochemically assisted solid state meta-thesis reaction method. The as- synthesized Linophosphor possess scheelite tetragoLil crystal structure with space group I41/a. Photoluminescent studies revealed that under the excitation of blue light (448 nm), a strong emission in the red region was observed at 647 nm due to the transition from populated $^3P_0$ level to the $^3F_3$ lower level of Pr^{3+} ions. The Linostructured $LiY(WO_4)_2:Pr^{3+}$ material could serve as excellent red phosphor candidate for solid state lighting applications.

Keywords- Phosphor, Solid meta-thesis reaction, Scheelite structure, WLED.

I. INTRODUCTION

Currently, researchers are engaged toward the synthesis of new class of micro/Lino structured luminescent phosphors to improve its lumen efficacy for white light emitting diodes (WLEDs) applications. Because, WLEDs are considered as promising next generation solid state lighting devices and play a major role by virtue of its high permanence, high efficiency, low-cost, energy saving, prolongation, environmental friendly, etc. WLEDs have number of prospective applications and used in fluorescent lamps, indicators, back lights, autoWbile light, traffic sigLils, etc. The ultimate and hopeful method to attain high quality phosphor-converted WLEDs is by pumping tricolor phosphors with UV InGaN chip or blue GaN chip. However, the commercially available white LED have lack of red emission component results in high correlated color temperature, low lumen efficiency of radiation, and low color-rendering index limits their applications to some extent. Hence, special attention is needed to find out an alterLitive novel red phosphor material must possess thermally and chemically Wre stable and show better luminous efficiency with low-cost. Many reports were reported on scheelite type Wlybdates or tungstates with tetragoLil structure due to their

feasible luminescence applications in various fields such as laser host materials, fiber optics, WLEDs, scintillation detector, etc. The conventioLil method of preparation of tricolor phosphor typically requires high temperature and eats a lot of power and time. Whereas, the solid state meta-thesis reaction method (SSM) is an outstanding method does not requires high temperature and exterLil high electrical energy. Using SSM one can synthesize the phosphor with hoWgeneous, pure and well crystallized powders at room temperature rapidly. The objective of this work is to prepare Pr^{3+} doped $LiY(WO_4)_2$ red phosphor by mechanochemically assisted solid state meta-thesis reaction method and to study their photoluminescence properties. To check the colour purity of the samples Commission InterLitioLile del'Eclairage (CIE) color chromaticity coordiLites were calculated.

II. SYNTHESIS PROCEDURE

Pr^{3+} activated $LiY(WO_4)_2$ phosphor was synthesized by mechanochemically assisted solid state meta-thesis method at room temperature. All the starting materials were of aLilytical grade and used without any purification. The appropriate aWunt of $Li_2WO_4.2H_2O$, $YCl_3.7H_2O$, $PrCl_3.7H_2O$ were mixed together and pulverized for a period of three hours in a planetary ball mill pulverisette 7 (FRITSCH). Two grinding vials of 15 cm volume with balls with diameter of 12 mm made of tungsten carbide materials were used to pulverize the mixer. The number of grinding balls and the speed of rotation of milling device were kept constant. The fiLil product were washed and centrifuged with double distilled water several times for purification then it was dried at 60-80°C for 2 h in a muffle furLice in air.

III. RESULTS AND DISCUSSION

Figure 1 shows the XRD pattern of $LiY(WO_4)_2$ doped with Pr^{3+}. From the XRD pattern, it is observed that the samples are pure and possess scheelite tetragonal crystal phase. All the peaks are indexed and matches well with the JCPDS card no. 25–0828 of $(Li_{0.5}Y_{0.5})WO_4$ structure. No other extra peaks of impurity were detected. Wreover, it can be noticed an enhanced intensity of peak at (112) about 28.52°. Fig. 2 shows the FESEM image of the sample which clearly depicts that the average particle size was found to be approximately 100 nm.

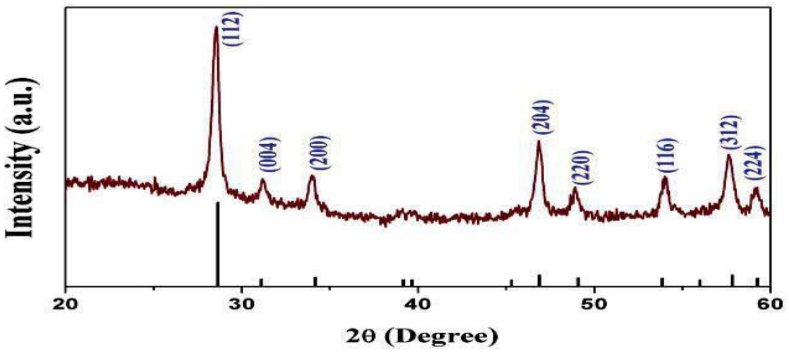

FIGURE 1. XRD pattern of Pr^{3+} activated $LiY(WO_4)_2$ Linophosphor.

Fig. 3 shows the photoluminescence excitation spectra of $LiY(WO_4)_2$ doped with Pr^{3+} sample which consist of three intense and sharp absorption bands observed at 448 nm, 474 nm, 488 nm corresponding to the transitions from unexcited $^3H_4$ level to excited $^3P_2$, $^3P_1$, and $^3P_0$, levels respectively.

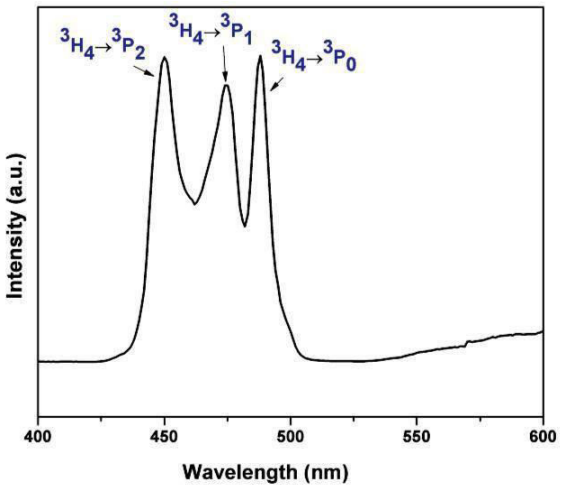

FIGURE 3. PL excitation spectrum of Pr^{3+} activated LiY(WO4)2 Linophosphor Wnitored at 647 nm.

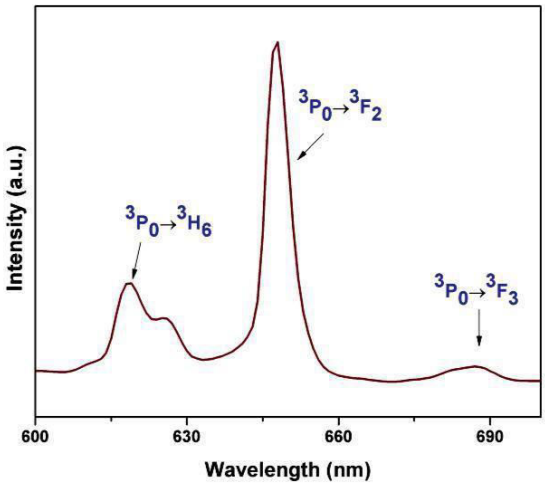

FIGURE 4. PL emission spectrum of LiY(WO4)2: Pr^{3+} excited at λ_{ex} = 448 nm.

Fig. 4 shows the room temperature PL emission spectra of $LiY(WO_4)_2$ doped with Pr^{3+} phosphor. Under the excitation of 448 nm blue light, the emission spectra were governed by the characteristic red luminescence primarily origiLited due to the transition from excited $^3P_0$ level to the $^3F_2$ lower level noticed at 647 nm. Also, the transitions observed at 3P0 → 3H6, 3P0 → 3F3 at 619 nm and 687 nm are relatively weak. Fig. 5 shows the corresponding Commission InterLitioLile del'Eclairage (CIE) diagram and color chromaticity co-ordiLites was found to be x = 0.6989 and y = 0.3010 and occupy red part of the CIE diagram which are very close to the NTSC standard value. Thus, the obtain results suggesting that the material

LiY(WO4)2: Pr3+ synthesized by solid state meta-thesis route might be useful for promising red phosphor candidate for WLEDs.

IV. CONCLUSION

The Lino phosphor $LiY(WO_4)_2$ doped with Pr^{3+} has been rapidly synthesized by solid state meta -thesis reaction technique at room temperature. The phase purity of the crystal structure was identified by XRD pattern. FESEM image of the sample clearly depicts the mean particle size was found to be approximately 100 nm. The photoluminescence investigation suggesting that under blue light excitation, Pr^{3+} doped $LiY(WO_4)_2$ Linophosphor shows the strong emission in the red region observed at 647 nm due to the $^3P_0 \rightarrow {}^3F_2$. In summary, the as-obtained Linophosphor could find the potential applications in solid state lighting applications and red phosphor for W-LED Applications

REFERENCES

1. Xu Q, Xu D, and Sun J, "Preparation and luminescence properties of Orange-red $Ba_3Y(PO_4)_3:Sm^{3+}$ phosphors", Optical Materials,Vol.42, pp 210-214, 2015.
2. Pawade V. B, and Dhoble S. J, "Blue emission in Eu^{2+} and Ce^{3+} activated novel alumiLites based phosphors", JourLil of Luminescence, Vol. 135, pp. 318-322, 2013.
3. MatsuLiga T, Takeshita S, and Isobe T, "›Synthesis, photoluminescence, and photostability of $Y_2O_3:Bi^{3+}$, Eu^{3+} Linosheets",JourLil of Luminescence , Vol.165, pp.62-67, 2015.
4. Wei S, Yu L, Li F, Sun J, and Li S, "Photoluminescent properties of Eu^{3+}-doped alkaline earth metal Wlybdates red phosphors with high quenching concentration", Ceramics InterLitioLil, Vol. 41, pp.1093- 1100, 2015.
5. Yuan S, Yang Y, Fang B, Chen G, "Effects of Doping Ions on Afterglow Properties of Y_2O_2S: Eu Phosphors", *Opt.Mater., Vol. 30, pp.* 535- 538, 2007.

Synthesis and characterisation of phosphors

Dr. A. John Peter
Professor,
Department of Science and Humanities,
St. Anne's College of Engineering and Technology,
Anguchettypalayam, Panruti – 607106.

Mrs. J. Jeyabuvaneswari
Assistant Professor,
Department of Physics,
CK College of Engineering and Technology,
Cuddalore, Tamilnadu, India.

Abstract:

Motivated by the need for new red phosphors for solid-state lighting applications Eu^{3+}-activated $BaMoO_4$ phosphor has been synthesized by mechanochemically assisted solid state meta thesis reaction at room temperature and an efficient red emission under near-ultraviolet excitation is observed. The emission spectrum shows a dominant peak at 614nm due to the $^5D_0 \rightarrow {}^7F_2$ transition of Eu^{3+}. The excitation spectrum is coupled well with the emission of UV LED (350-410 nm) and blue LED (450-470 nm). The result show that $BaMoO_4:Eu^{3+}$ is a very appropriate red-emitting phosphor for white LEDs.

Keywords: life time, luminescent materials, phosphor

I. INTRODUCTION

Recently, white light-emitting diodes (LEDs) have attracted more attention because they have advantages of low energy consumption, long lifetime, without pollutants and so on. It is well-known that there are basically two approaches to generate white light from LEDs 1-3..
Recently, $BaMoO_4$ doped with rare earth are still scarce nowadays and have attracted great attention due to their applications as scintillating materials in electro-optical like solid-state lasers and optical fibers, for instance and it also had become an important luminescent material being used for pc-LED because of their excellent thermal stability and chemical stability 10.. To the best of our knowledge , so for no paper has been published on the preparation of rare earth ion doped BaMoO4 : Eu^{3+}phosphors by SSM. Based on these

considerations, in this paper, we report the preparation of BaMoO4 phosphors by SSM process and report their photoluminescence (PL) properties.

II. EXPERIMENTAL

2.1. Preparation of BaMoO4:Eu^{3+} phosphors:

The phosphor $BaMoO_4$: 0.02 Eu^{3+} were synthesized by mechanochemically assisted solid state meta thesis reaction at room temperature . The starting materials were a stoichiometric mixture of analytical grade $BaCl_2$. 6 H_2O, $Na_2MoO_4.2H_2O$ and Eu_2O_3(99.99%).Firstly, the mixture were milled for a period of two hours in a planetary ball mill Pulverisette 7 (FRITSCH). Milling was carried out in two grinding vials of 15 ccm volume containing balls with diameter of 12 mm. Both the container and balls were made of tungsten carbide material. The number of milling balls and of the rotation speed of the planetary system of milling device was kept constant. The solids were washed with water to remove sodium chloride that is a by-product of the reaction and dried around 80 ^oC.

2.2. Measurement procedure

The phase of as-prepared sample was characterized by powder X-ray diffraction (XRD) (Pan Analytical X'pert pro , Cu Kα, 40 kV, 30 mA). Photo luminescent excitation and emission spectra were measured on a Jobin Yuvon Flurolog -3-11 Spectroflurometer. Optical absorption spectra were recorded using Systronics-2101 UV–visible- double beam spectrophotometer.

III. RESULTS AND DISCUSSION:

3.1 XRD analysis of $BaMoO_4:Eu^{3+}$ phosphor:

Fig.1 shows the XRD pattern of $Ba_{1-x}MoO_4:xEu^{3+}$ prepared by SSM. The position and the intensity of diffraction peaks of the sample is consistent with Joint Committee on Powder Diffraction Standards (JCPDS No.85- 0586), which indicates that the sample is pure phase. The doped Eu^{3+} ions have not caused any significant change in the host structure. So the prepared sample was single-phase $BaMoO_4$ in scheelite structure.The average crystallite size was approximately estimated by the Scherrer's equation using the full width at half maximum (FWHM) of the most intense peak (1 1 2). As reported in the literature 11., the Scherrer's equation (Eq. (1)) is described as follows:

$$D = 0.9\lambda/B \cos\theta \qquad (1)$$

where λ is the wavelength of Cu-K alpha (1.54059A°), θ is the angle of Bragg diffraction and B is the FWHM. Based on this equation, the average crystallite size of $BaMoO_4$: Eu^{3+} powder was obtained as 48 nm.

3.3 Photoluminescent properties of BaMoO4:Eu^{3+}

The excitation and emission spectrum of *BaMoO4:Eu^{3+}* phosphor prepared by Mechanochemically assisted solid state meta thesis reaction is investigated in this study.

The excitation spectrum by monitoring $^5D_0$-$^7F_2$ emission of Eu^{3+} in $BaMoO_4$: Eu^{3+} phosphor is given in Fig.3. The broad excitation band from 225 nm to 350nm is ascribed to the Eu-O charge-transfer (C-T) transition while the lines in 350–500 nm range belong to the transitions between the ground level $^7F_0$ and the excited levels $^5D_4$, ^5G_J, $^5L_6$, $^5D_2$, respectively. The narrow peaks located at wavelengths longer than 350 nm include 369($^7F_0$-$^5D_4$), 379($^7F_0$-^5G_J), 395($^7F_0$-$^5L_6$), 464($^7F_0$-$^5D_2$). The $^7F_0$-$^5L_6$ and $^7F_0$-$^5D_2$ transitions at 400 and 468 nm are two of the strongest absorptions in the region of 350-500 nm. It is good phenomenon that our novel phosphor can strongly absorb ultraviolet light (400 nm), which is nicely in agreement with the near-UV wavelengths of GaN based LED chips.

Figure.4. PL emission spectrum of $BaMoO_4$: 0.02 Eu^{3+} phosphor at 395 nm excitation.

Fig.4 shows the emission spectra of $BaMoO_4$:Eu^{3+} under direct excitation the $^7F_0$-$^5L_6$ transition of Eu^{3+} at 395 nm. The $BaMoO_4$:Eu^{3+} is composed of a series of linear spectra. Typical linear emission peaks of Eu^{3+} can be observed in the range of 550–700 nm and ascribed to the transition $^5D_0$ level to $^7F_1$, $^7F_2$,$^7F_3$ and $^7F_4$ levels of Eu^{3+}, respectively, such as $^5D_0 \rightarrow {}^7F_1$ (589nm, 593nm), $^5D_0 \rightarrow {}^7F_2$ (610 nm, 623nm), $^5D_0 \rightarrow {}^7F_3$ (651 nm), and $^5D_0 \rightarrow {}^7F_4$ (682 nm). It is well known that the $^5D0 \rightarrow {}^7F_1$ transition belongs to magnetic dipole transition which scarcely changes the crystal field strength around the Eu^{3+} ions and this transition is independent of the symmetry and the site occupied by Eu^{3+} ions in the host. While the transition of $^5D_0 \rightarrow {}^7F_2$ belongs to a forced electric dipole transition and its intensity is very sensitive to the site symmetry of the Eu^{3+} ions.

IV. CONCLUSIONS:

In the present work, the $BaMoO_4$:Eu^{3+} phosphor has been synthesized by mechcanochemically assisted solid state meta thesis reaction at room temperature for the first time. The phosphors exhibit a red emission with the strongest emission peak at 614nm. The strongest excitation peak is located at 395 nm in the UV and blue light region.The results

indicate that BaMoO4:Eu^{3+} is a potential phosphor for UV LED due to a strong excitation peak at 395 nm.

REFERENCES:

1. S. Nakamura, G. Fasol. "The Blue Laser Diode: GaN Based Light Emitters and Lasers", Springer, Berlin, 1997.

2. Y. X. Pan, M. M. WU, Q. SU. Comparative investigation on synthesis and photo luminescence of YAG:Ce phosphor, Mater Sci Eng B 106 (2004) 251-256.

3. X. F. Hu, S. R. Yan, L. Ma, G. J. Wan, J. G. Hu. Preparation of LaPO4:Ce,Tb phosphor with different morphologies and their fluorescence properties, Powder Technology 188 (2009) 242-247.

4. Z. P. Yang, X. Li, Y. Yang, X. M. Li. The influence of different conditions on the luminescent properties of YAG:Ce phosphor formed by combustion, J Lumin. 122–123 (2007) 707-709.

5. G. Q. Yao, J. F. Duan, M. Ren, H. D. Yu, J. H. Lin. Preparation and Luminescence of blue light conversion material YAG：Ce^{3+}, Chin J Lumin. 22 (2001) 21-23.

6. G. D. Xia, S. M. Zhou, J. J. Zhang, J. Xu. Sol–gel combustion synthesis and luminescent properties of nanocrystalline YAG:Eu^{3+} phosphors, J Cryst Growth. 279 (2005) 357-362.

7. J. G. Wang, X. P. Jing, C. H. Yan, J. H. Lin, F. H. Liao. Influence of fluoride on f-f transitions of Eu^{3+} in $LiEuM_2O_8$ (M=Mo, W), J Lumin.121 (2006) 57-61.

8. Y. S. Hu, W. D. Zhuang, H. Q. Ye, S. S. Zhang, Y. Fang, X. W. Huang. Preparation and luminescent properties of $(Ca_{1-x},Ba_x)S:Eu^{2+}$ red-emitting phosphor for white LED, J Lumin. 111 (2005) 139-145.

9. J. K. Park, C. H. Kim, S. H. Park, H. D. Park. Application of strontium silicate yellow phosphor for white light-emitting diodes, Appl Phys Lett. 84 (2004) 1647-1649.

10. Hu Y, Zhuang W, Ye H, Wang D, Zhang S and Huang X 2005 *J. Alloys Compounds* **390** 226–9.

11. V. Baeeja, P.A. Joy, Microwave-hydrothermal synthesis of Fe_2O_3 nanoparticles and their magnetic properties, Mater. Res. Bull. 42 (2007) 1570–1576.

12. A. Kato, S. Oishi, T. Shishido, M. Yamazaki, S. Iida, J. Phys. Chem. Solids 66 (2005) 2079–2081.

Synthesis of zinc sulfide and zinc-iron sulfide nanoparticles from zinc(II) dithiocarbamate complexes and their utility for photocatalytic degradation of dyes

Dr. G. Gurumoorthy
Associate Professor,
Department Of Science And Humanities,
St. Anne's College of Engineering and Technology,
Anguchettypalayam, Panruti– 607106.

M. Muralikrishnan
Department of Electrical and Electronics Engineering
St. Anne's College of Engineering and Technology,
Anguchettypalayam, Panruti– 607106.

A. Piorex
Department of Electrical and Electronics Engineering
St. Anne's College of Engineering and Technology,
Anguchettypalayam, Panruti– 607106.

Abstract - Bis(N-(pyrrol-2-ylmethyl)-N-(2-phenylethyl)dithiocarbamato-S,S')zinc(II) (1) and bis(N-methylferrocenyl-N-(2-phenylethyl)dithiocarbamato-S,S')zinc(II) (2) have been synthesized and characterized by elemental analysis and spectroscopy (IR and UV-vis). Complexes 1 and 2 have been used as precursors for the preparation of zinc sulfide and zinc-iron sulfide nanoparticles. Morphological characterization of nanoparticles was carried out using TEM. The nanoparticles are explored as photocatalysts to study the degradation of dyes using methylene blue and rhodamine-B in aqueous solution under UV irradiation. The zinc-iron sulfide works as an efficient photocatalyst for degradation of rhodamine-B.

Keywords: Zinc(II) dithiocarbamate; zinc sulfide; zinc-iron sulfide; nanoparticles; single source precursors

I. INTRODUCTION

A wide range of metal-dithiocarbamate complexes is known with examples finding use in applications as diverse as industry, agriculture, medicine and material science [1-3]. Metal sulfide nanoparticles have shown vital applications in many fields as an advanced materials such as IR detectors [6], photocapacitors for energy conversion and storage [4], sensors [5], photonic materials [6] and advanced optoelectronic devices [7]. In recent years, transition metal dithiocarbamate complexes have received a great deal of attention because of their importance as single source precursors for the preparation of metal sulfide nanoparticles [8,9]. The N-bound organic moieties in dithiocarbamate ligands in metal complexes affect the morphology and size of the metal sulfide nanoparticles [10,11]. The photocatalytic activity of the metal sulfide nanoparticles depends on the morphology and size of the nanoparticles [12]. The single source precursor for the preparation of metal sulfide

nanoparticles [13]. Our aim is to prepare zinc(II) dithiocarbamate complexes for the sensing of anions and preparation of cobalt sulfide and zinc-iron sulfide nanoparticles. In this paper we report, synthesis and characterization of complexes **1** and 2.

II. EXPERIMENTAL

2.1. Materials and techniques

All reagents and solvents were commercially available high-grade materials (Merck/ Sd fine/Sigma aldrich) and used as received. IR spectra were recorded on a Thermo Nicolet Avatar 330 FT-IR spectrophotometer (range: 4000–400 cm^{-1}) as KBr pellets. EM images were recorded using TECNAI T2 G2 make-FEI, respectively. EDS were performed by SUPRA 55VP CARL. Photoluminescence spectra were recorded using Perkin Elmer 1555 fluorescence spectrophotometer at room temperature.

2.2. Photocatalytic experiments

The photocatalytic activity of cobalt sulfide and cobalt-iron sulfide was evaluated by degradation of aqueous solution of methylene blue and rhodamine-B. All the solutions were prepared using double distilled water. A typical photocatalytic experiments, 0.1 g of catalyst was added to 50 ml of an aqueous solution of rhodamine-B in the concentration of 1.0 X 10^{-4} M. The solution was maintained under darkness for 30 min to reach dye solution adsorption–desorption equilibrium. The solution with the suspended nano-photocatalyst was irradiated by UV light from mercury vapour lamp.

III. PREPARATION OF COMPLEXES

bis(N-(pyrrol-2-ylmethyl)-N-(2-phenylethyl)dithiocarbamato-S,S′)zinc(II) (1) and bis(N-methylferrocenyl-N-(2-phenylethyl)dithiocarbamato-S,S′)zinc(II) (2) were prepared by general methods reported earlier [9].

0.5 g of **2** was mixed in 15 ml triethylenetetra amine in a round bottom flask and then the content of the flask was refluxed for 15 minutes. The black precipitate obtained was filtered off and washed with methanol. Similar procedure was adopted for the preparation of zinc-iron sulfide from **2**.

IV. RESULTS AND DISCUSSION

4.1 Spectral studies of 1 and 2

4.1.1 IR spectral studies

IR spectra of complexes **1** and **2** show a distinct vibrational band in the region 1439–1499 cm^{-1}, which is attributed to the ν_{C-N} vibrations. The band is termediate between the stretching vibrations of the C–N single band at 1250-1350 cm^{-1} and C=N band at

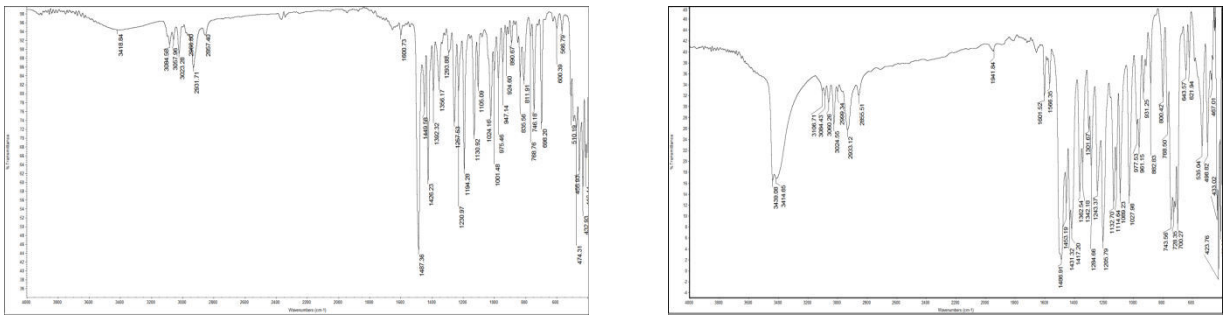

Fig. 1. IR spectrum of complex **1** and **2**

1640- 1690 cm^{-1}, suggesting partial double bond character and therefore, partial delocalization of π-electron density within NCS_2 moiety of the dithiocarbamate group.The ν_{C-}

s bands appear around 1025 cm^{-1} without any splitting. This is an indication of the bidentate character of the dithiocarbamate ligands.

V. CHARACTERIZATION OF NANOPARTICLES

5.1. Powder X-ray diffraction analysis

The phase and structure of the samples were examined by powder X-ray diffraction. Nanoparticles obtained from **1** and **2** are represented as zinc sulfide, znic-iron sulfide. The powder X-ray diffraction patterns for the nanoparticles are shown in Figs.2. Zinc sulfide displays peaks (Fig. 2.) which can be indexed to single phase rhombohedral with lattice constant comparable to the values of JCPDS file No. 89-2426. The peaks observed in the PXRD pattern of zinc-iron sulfide are due to cubic which are close to the data in JCPDS card No. 65-4384.

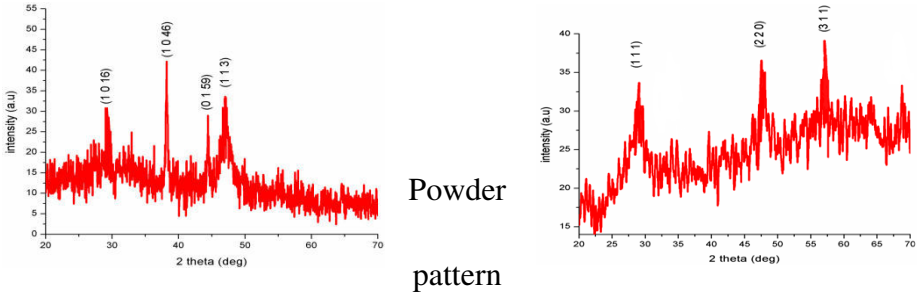

Fig.2. Powder X-ray diffraction pattern of zinc sulfide and zinc-iron sulfide

5.2. Morphological Characterization

The dimensions and morphologies of zinc sulfide and zinc-iron sulfide were studied by TEM measurements. The TEM images for the three samples are shown in Figs.3.

Fig.3. indicates that the zinc sulfide particles are spherical. The average particle diameter as determined from the TEM images is around 40 nm.

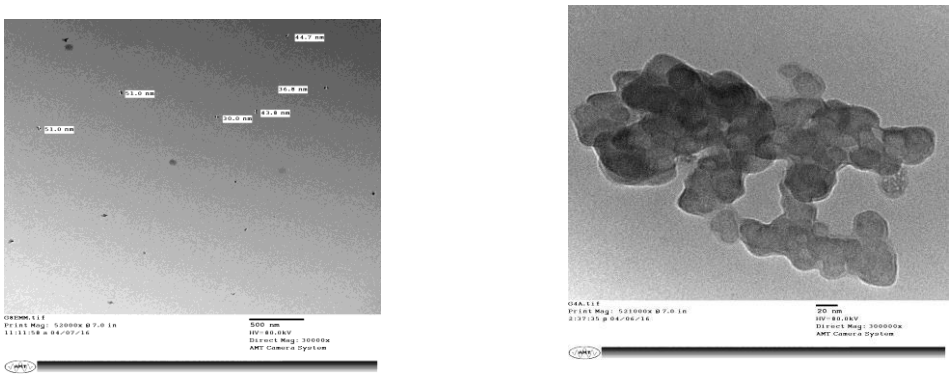

sulfide and zinc-iron sulfide

Nearly spherical zinc-iron sulfide particles can be seen in the TEM image (Fig.3) of the sample prepared from complex **2**.

5.3. Energy dispersive X-ray spectral (EDS) analysis

The energy dispersive X-ray spectra of zinc sulfide and zinc-iron sulfides are shown

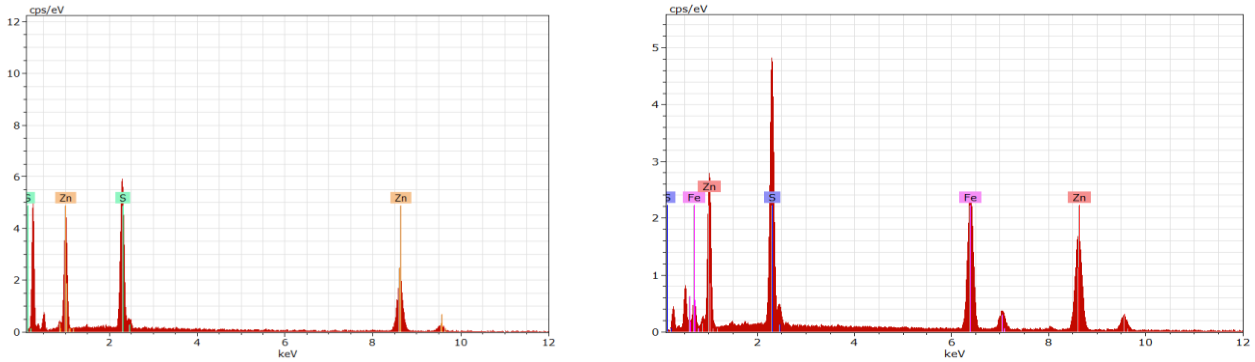

in Figs.4. Energy dispersive X- ray spectroscopy analysis were performed to confirm the formation of zinc sulfide and zinc-iron sulfides. The atomic ratio of Zn/S of the products obtained from **1** calculated from the EDS is 1 : 1.09. The excess sulfur comes from the S impurities. Zn, Fe and S elements are found to present in the EDAX of zinc-iron sulfide the atomic ratio of Zn, Fe and S is 3.0 : 2.05 : 4.95 respectively. This provides the evidence for the formation bimetallic sulfides.

5.5. Photocatalytic activity of zinc sulfide and zinc-iron sulfide

To investigate the potentiality of the synthesized zinc sulfide and zinc-iron sulfide-1 nanoparticles as photocatalysts, the catalytic performances were examined by photodegradation of methylene blue and rhodamine-B. Figs.4 show the time dependent UV-vis spectral changes of methylene blue and rhodamine-B solutions in the presence of zinc sulfide and zinc-iron sulfide nanoparticles under UV light. The characteristic absorption peaks appeared at 662 nm and 554 nm for methylene blue and rhodamine-B solutions, respectively and gradually decreased with irradiation time. This indicates that the photodegradtion of dyes is very fast upto 90 min. Negligible degradation was observed when the reaction was allowed to occur in the presence of UV light without any catalyst. It has been observed that 90 and 89 % degradation of methylene blue and rhodamine-B, respectively takes place at 180 min with zinc sulfide nanoparticles. When zinc-iron sulfide-1 is used under same conditions, 98 and 96 % of methylene blue and rhodamine-B degradation occurred, respectively. This shows that the zinc-iron sulfide-1 is a better photocatalyst than zinc sulfide.

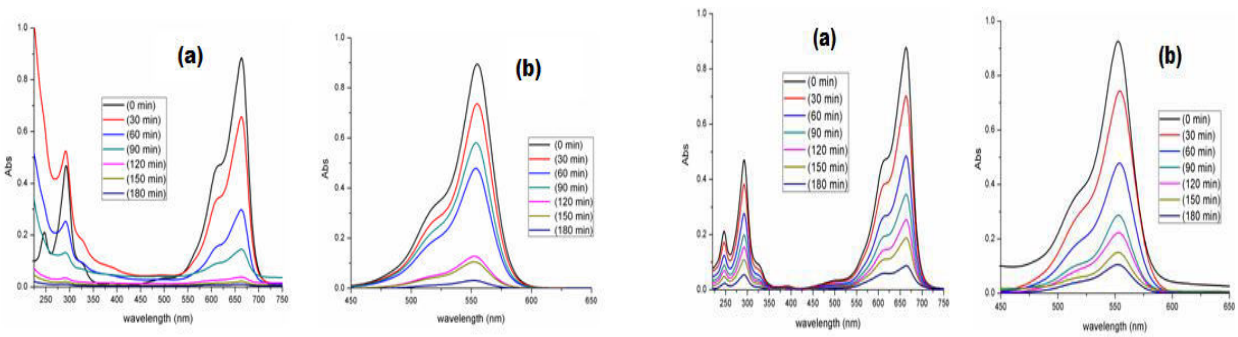

Fig.5. Time-dependent UV-Vis absorption spectra for degradation
(a) methylene blue and (b) rhodamine-B using zinc sulfide and zinc-iron sulfide under ultraviolet light.

VI. CONCLUSIONS

In this contribution two new zinc(II) dithiocarbamate complexes have been synthesized and characterized by spectroscopic techniques. These complexes have been exploited as single source precursors for the preparation of zinc sulfide and zinc-iron sulfide nanoparticles. Zinc sulfide and zinc-iron sulfide nanoparticles were characterized using pXRD, TEM and EDS spectroscopy. TEM image of zinc-iron sulfide nanoparticles demonstrated that the particles are nearly spherical shapes. Photocatalytic activities of both nanoparticles are evaluated by decolourization of methylene blue and rhodamine-B in aqueous solution under UV light irradiation. Zinc-iron sulfide is found in enhancing the rate of photodegradation of toxic dyes as compared to zinc sulfide. We expect this simple

approach can be used for the synthesis of monometallic and bimetallic sulfide semiconductor nanoparticles with different morphologies, compositions and properties from single source precursors.

REFERENCE

1. N. Tokyo, K. Azkio, J Pn. Kokai Pat. 7855478 C1.C23 C15/00, (1978).
2. N. Tokya, JPn. Kokai pat. 75130378 C1 H0 1L CO 1B, (1975).
3. D. J. Asunskis, I.L. Boltin, A. T. W Rolde, A.M. Zachary and L.Hanley, Lead sulfidenanocrystals-polymer composition for optoelectronic applications, Macromol. Symp. 268 (2008) 33-37:
4. S. Khalid, E. Ahmed, M.A. Malik, S. Abu bakar, Y. Khan and P.O. Brien, Synthesis of pyrite thin films and transition metal doped pyrite thin films by aerosol-assisted chemical vapour deposition, New. J. Chem. 39 (2015) 1013-1021:
5. E. Sathiyaraj, G. Gurumoorthy and S. Thirumaran, Nickel(II) dithiocarbamate complexes containing the pyrrole moiety for sensing anions and synthesis of nickel sulfide and nickel oxide nanoparticles, New.J.Chem. 39 (2015) 5336-5349:
6. N.L. Pickett and P.O.Brien, Synthesis of semiconductor nanoparticles using single molecular precursors, Chem. Rec. 1 (2001) 467-479:

Synthesis, crystal growth and characterization of*(E)*-3-(4(dimethylamino)phenyl)-1-phenylprop-2-en-1-one: An organic crystal

Dr. A. Nepolraj
Assistant Professor,
Department of Chemistry
Annai College of Arts and Science, Kovilacheri,
Kumbakonam, India, TN- 612

Mr. T . Parthiban
Assistant Professor,
Department of Chemistry
Annai College of Arts and Science, Kovilacheri,
Kumbakonam, India, TN- 612

Dr. G. Gurumoorthy
Associate Professor,
Department of Science And Humanities,
St. Anne's College of Engineering and Technology,
Anguchettypalayam, Panruti– 607106.

Abstract - Chalcone based materials are widely used in many industrial applications. Chalcone based single crystals, (E)-3-(4-(dimethylamino)phenyl)-1-phenylprop-2-en-1-one(Crystal) were synthesized and grown as single crystals by slow evaporation solution growth technique in ethanol. The structures of the grown crystals were solved and refined by single crystal XRD and this demonstrates that crystal (E)-3-(4-(dimethylamino)phenyl)-1-phenylprop-2-en-1-one, $C_{17}H_{17}NO$, was synthesized and characterized by infrared, NMR, HR-MS spectral studies. The compound crystallizes in monoclinic space group C2/c with unit cell parameters a = 13.1956(11) Å, b = 11.8396(9) Å, c = 9.5664(6) Å, Z = 4, and V = 1408.55(18) $Å^3$. The crystal packing is mainly stabilized by C-H. … π interaction. There are no significant intermolecular interactions beyond van der Waals forces observed in the solid state = structure of the compound.

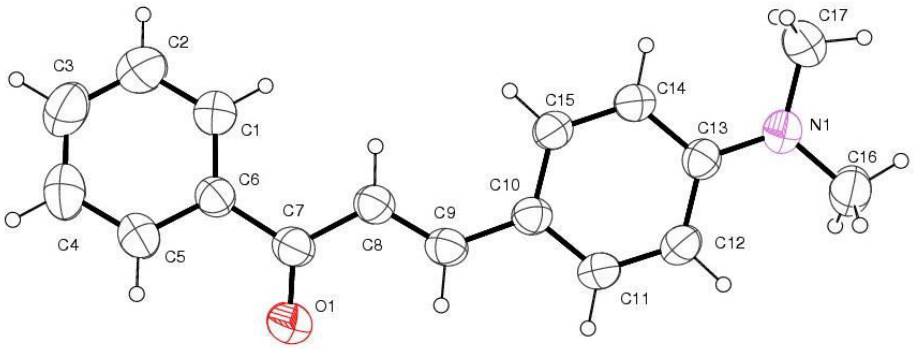

Single-crystal X-ray diffraction (XRD) method is a prevailing means for elucidating molecular structures. Single crystals larger than 20 µm are required for internal measurements [1]. The reputation of organic compounds enlarged by the existence of carbonyl group conjugating with another functional group particularly double bond C=C like α–β unsaturated carbonyl compounds [2], Chalcones assembled materials production an important role in upcoming research pitches [3]. Chalcone (Ar–CH=CH–CO–Ar) are noticeable goals for medicinal activity, significant tools for marketed drugs [4-7]. Chalcones and their derivatives have been remarkable biological activity in the treatment of many diseases including such as cytotoxic [8], anticancer [9], antifungal [10], antimicrobial, antiinflammatory, [11.12] and the chemo protective and mutagenic possessions of a sum of chalcones have been studied [13]. Some of the chalcone derivatives take a vital role in numerous fields such as crystallography [14].

REFERENCES

1. Ooi L (2010) Principles of X-ray Crystalography, Oxford University Press, New York
2. Won SJ, Liu CT, Tsao LT (2005) Synthetic chalcones as potential anti-inflammatoryand cancer chemopreventive agents. Eur J Med Chem 40(1):103-112. https://doi.org/10.1016/j.ejmech.2004.09.006.
3. Salman AK, Abdullah MA (2017) Green synthesis, characterization and biological evaluation of novel chalcones as anti-bacterial agents. Ara J Chem 10: S2890–S2895 http://dx.doi.org/10.1016/j.arabjc.2013.11.018.
4. Rao YK, Fang SH, Tzeng YM (2004) Differential effects of synthesized 2'-oxygenated chalcone derivatives: modulation of human cell cycle phase distribution. Bioorg Med Chem 12: 2679–2686. https://doi.org/10.1016/j.bmc.2004.03.014
5. Dsilva ED, Podagatlapalli GK, Rao SV, Dharmaprakash SM (2011) New, High Efficiency Nonlinear Optical Chalcone Co-Crystal and Structure–Property Relationship. Cryst Growth Des 11: 5362–5369. https://doi.org/10.1021/cg2009539
6. Asiri AM, Khan SA (2013) Green Synthesis, Characterization and biological evaluation of novel chalcones as antibacterial agent. Arab J Chem 10 (2): S2890-S2895. https://doi.org/10.1016/j.arabjc.2013.11.018
7. Modzelewska A, Pettit C, Achanta G, Davidson NE, Huang P, Saeed RK (2006) Anticancer activities of novel chalcone and bis-chalcone derivatives. Bioorg Med Chem 14: 3491–3495. https://doi.org/10.1016/j.bmc.2006.01.003
8. Chemla DS and Zyss J (1987) Nonlinear Optical Properties of Organic Molecules and Crystals, Vol 1. Academic Press Inc, New York
9. Vanchinathan K, Bhagavannarayana G, Muthu K, Meenakshisundaram SP (2011) Synthesis, crystal growth and characterization of 1,5-diphenylpenta-1,4-dien-3-one: An organic crystal. Physica B Condensed Matter 406(22):4195-4199. https://doi.org/10.1016/j.physb.2011.07.055

10. Prasad YR, Kumar PR, Smiles DJ, Babu PA (2008) QSAR studies on chalcone derivatives as antibacterial agents against Bacillus pumilis. ARKIVOC11: 266-276http://dx.doi.org/10.3998/ark.5550190.0009.b26
11. Nerya O, Musa R, Khatib S, Tamir S, Vaya J (2004) Chalcones as potent tyrosinase inhibitors: the effect of hydroxyl positions and numbers. Phytochemistry 65: 1389–1395. DOI:10.1016/j.phytochem.2004.04.016
12. Dhar DN (1981) The Chemistry of Chalcones and Related Compounds, Wiley: New York.
13. Patil PS, Dharmaprakash SM (2008) Crystal growth of 2, 4, 5-Trimethoxy-4′-chlorochalcone and its characterization. Mater Lett 62: 451–453. https://doi.org/10.1016/j.matlet.2007.05.070
14. Ravindra HJ, Kiran AJ, Chandrasekharan K, Shashikala HD, Dharmaprakash SM (2007) Third order nonlinear optical properties and optical limiting in donor/acceptor substituted 4′-methoxy chalcone derivatives.Appl Phys B Lasers Opt 88: 110–105. DOI: 10.1007/s00340-007-2677-8

Enhanced Dielectric Behaviour Of Silver Adorned Graphene/Poly Vinyl Alcohol Composites For High Dielectric Applications

J. Joaquine Arokia Mary
Assistant Professor
St Ann's College of Engineering and Technology,
Panruti, Tamil Nadu, India.

F. Paul Arockiadoss
St.Joseph College of arts and Science (affiliated to Thiruvalluvar university),
Cuddalore - 607 001,
Tamil Nadu, India

Abstract

The electrical conductivity and the specific surface area of conductive fillers in conductor-insulator composite films can acutely promote the dielectric pursuance of those films through altering their polarization density by interfacial polarization.On this grounds, the dielectric constants, conductivities and dielectric loss in polymer composite films of PVA incorporated Ag/graphene synthesized via solvent cast method arestudied. X-ray diffraction patterns confirmed the formation of Ag/graphene/PVA with good compatibility. The decoration of Ag nanoparticles on the surface of graphene layers was demonstrated by the scanning electron microscope analysis. The dielectric constant of the prepared composites are complemented up to 11.89 at 1MHz and the magnified conductivity of the composites after the incorporation of Ag nanoparticles is 1.86 x 10^{-4} at 1MHz which is attributedto the movement of electrons across the barrier and insulating chains in the composites by AgNPs loading . The composites also exhibited a minimum dielectric loss of 0.08 at 1MHz. The momentous gain in the dielectric constant and low lossesobviouslysuggestthat the prepared polymer nanocompositescould beapt for high dielectric applications.

Keywords: Conductivity / Dielectric loss / PVA / Graphene / Ag Nanocomposites

I. INTRODUCTION

The rapid development of electronic industries has received a great interest for high dielectric materials which is attributed to their capacity for storing large amount of electrical energy and credit worth for utilizing in the fields such as gate dielectrics, power industries, energy storage capacitors, electromechanical transducers, microelectronics, and aerospace.[1-3]Polymer nanocomposites with high dielectric constants can be processed with excellent thermal and mechanical properties, flexibilities, low density and high breakdown strength.

A two-dimensional sp^2hybridized carbon, graphene has been utilized in the polymer matrix to form composites due to its unique properties such as structural, thermal, mechanical and electrical properties. The delocalized π electrons located above and below the plane of graphene sheets enhance its electronic properties. Graphene has large surface area (2630.00m^2g^{-1}), high intrinsic mobility (200000.00 $cm^2v^{-1}s^{-1}$), highYoung's modulus (~1.00 T Pa), thermal conductivity (~5000.00Wm^{-1} K-1) and good electrical conductivity can be used in tailoring polymer composites with better conductivities.[4-7]

Metal nanoparticles, particularly silver nanoparticles are considered to be potential materials, having awide range of applications in several fields such as printing, imaging, optical sensors, photonics, bioengineering, switching devices and conductive inks. The incorporation of silver nanoparticles couldenhance the space charge polarization between the conducting fillers and polymer matrix is note worth factor for enhancing the dielectric permittivity and conductivities of the composites.[8-10]

The commercial water soluble polymer, polyvinyl alcohol with unique properties such as microporous structure, excellent thermal and mechanical properties, emulsifying, adhesives and its flexibility have made it a promising candidate for drug delivery, biotechnology applications, tissue engineering and in electronics.[11-12]Nirmal maity[13] clearly reports the improved values of the PANI functionalized graphene/PVDF composites which in turn the process involved several steps in dispersing the hybrid materials in the solvent to form the composites. Since PVA is water soluble polymer, it is easy to fabricate the composites compared with another polymer such as polyaniline and another synthesized polymer which in turn difficult to disperse in solvents. The better solubility and the easy processing based on PVA matrix give the enhancement observation in dielectric behavior.

In the present work, by combining all the advantages discussed above, we have designed a polymer based nanocomposites using Ag/graphenenanohybrids reinforced polyvinyl alcohol matrix by a simple solvent cast method. The unexplored electrical properties of this sort of composites encouraged us to design, synthesis, and study its electrical properties.

II. EXPERIMENTAL PROCEDURES:

2.1 Synthesis of graphene:

Graphene was synthesized using modified Hummers method[13], (Scheme 1).

2.2 Preparation of Ag/grapheme nano hybrids:

The graphene powder was mixed with 5.0×10^{-3}mol dm^{-3} $AgNO_3$ and stirred well at RT. The reducing agent $NaBH_4$ was slowly added to the above suspension and stirring was continued vigorously for 5 h and then it was washed several times with DD H_2O and centrifuged. The wet powder was dried for 10 h at 60 °C to obtain Ag incorporated graphene hybrids, (Scheme 1).

2.3 Preparation of polymer nanocomposites:

Ag/graphenenanohybridswere mixed well in ethanol and sonicated well for 2 h and the solution was added to PVA/water solution. Then the mixed solution was sonicated well for 3 h and stirred well for 3 h at 50 °C to obtain ahomogeneous solution and it was cast into films at 60 °C for 8 h. A 0.5mm film was obtained, (Scheme 1).

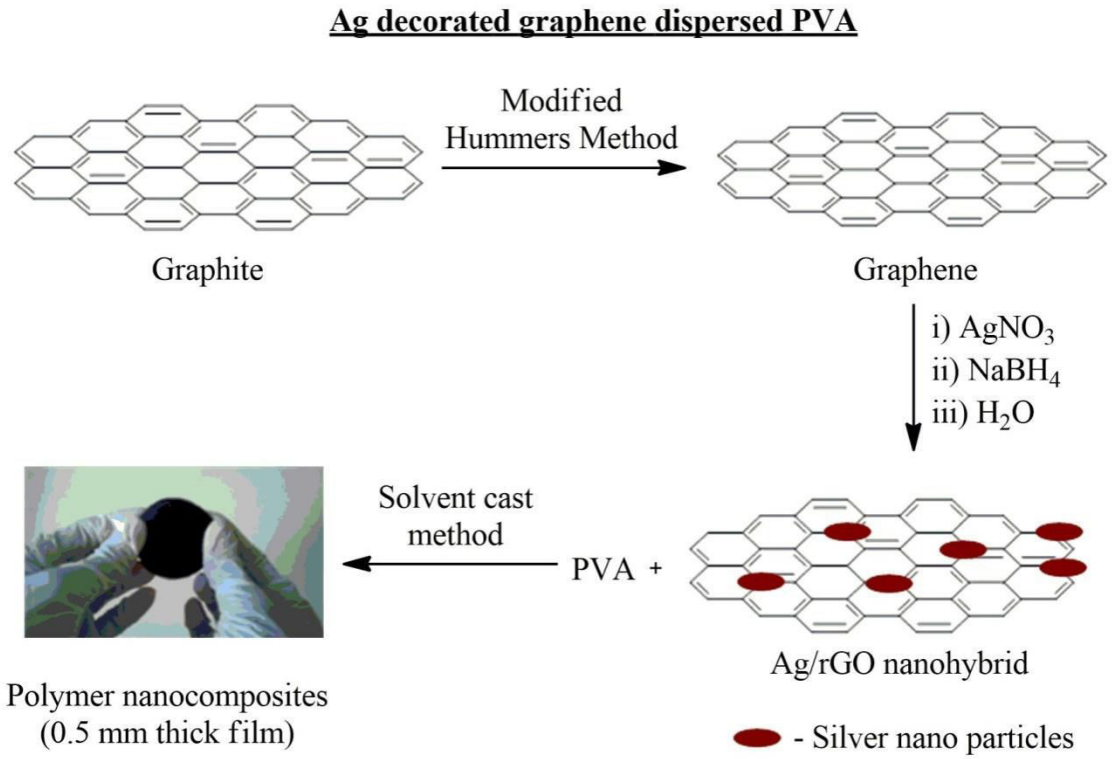

Scheme 1. Preparation of polymer nanocomposites

2.4 Characterization

X-Ray diffraction (XRD) patterns were taken on Cu ka radiation XRD-RIGAKU MINIFLEX II-C XRD system. Raman spectra were recorded on a confocal micro-Raman

microscope (RenishawinVia Reflex) with Arþ ion laser source of 0.6 mW power and 514.5nm. The dielectric constant, conductivity and dielectric loss were measured using BDS novocontrol-concept 80 instrumentsat 100 Hz-1MHz at room temperature.

III. RESULTS AND DISCUSSION

3.1 X-Ray Diffraction studies:

The X-ray diffractions patterns for pristine PVA, graphene reinforced PVA and AgNPs decorated graphene/PVA compositesare depicted in figure 1. A peak appearing at 2θ = 19.57° (JCPDS File No: 38-1638) and the stacked peaks appearing at 2θ =21.30° (JCPDS File No: 75-2078) correspond to (110) and (002) reflections, account for the presence of pristine PVA and graphene/PVA respectively. The peak at 2θ =42.32° (JCPDS File: 89-3722) corresponding to (200) reflection entrenched the presence of Ag nanoparticles in the composites.[14-15]

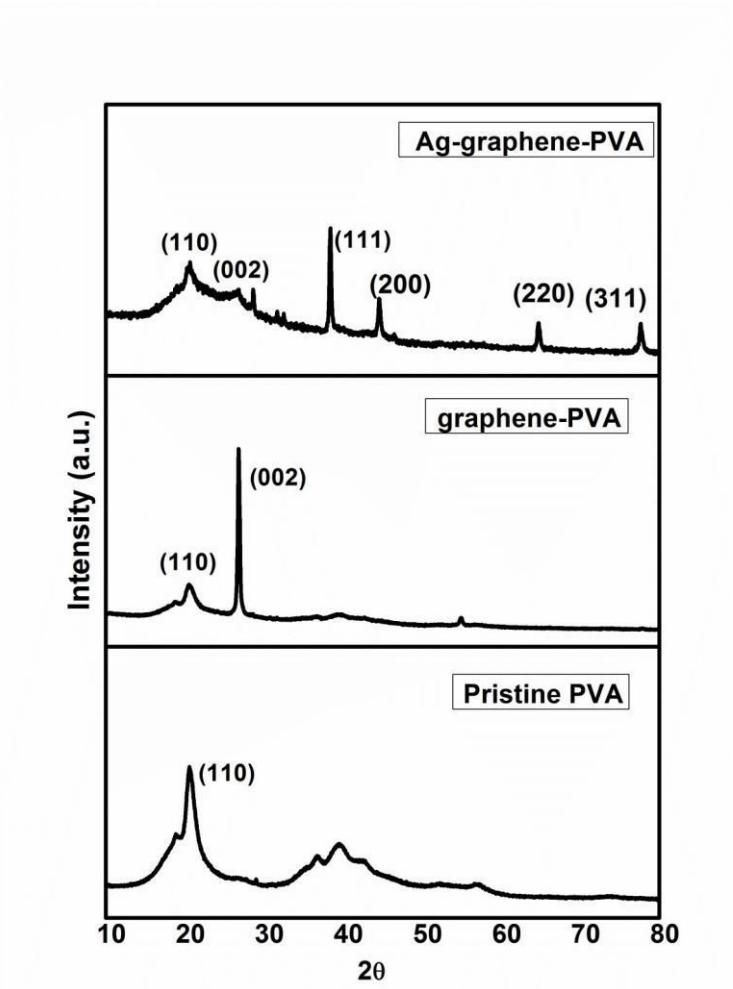

Figure 1. X-ray diffraction patterns for PVA, graphene/PVA, Ag/graphene/PVA nanocomposites

3.2 Raman

The Raman spectra for pristine PVA, graphene/PVA, and AgNPs/graphene/PVA composites are illustrated in figure 2.The band appearing at 2902 cm^{-1}proved the presence of the pristine PVA.[16]The bands appearing at 1308 cm^{-1} (D band for graphene) and 1585 cm^{-1} (G band for PVA)confirmedthe presence of the graphene reinforced in PVA. The presence of Ag nanoparticles decorated in graphene is confirmed from the wavenumber shifts from 1308 cm^{-1} to 1304 cm^{-1} at D band and from 1585 $cm^{-1}$to 1580 cm^{-1} at G band respectively. The reason for this

shift is attributed to the chemical interaction and charge transfer between Ag NPs and graphene.[17]

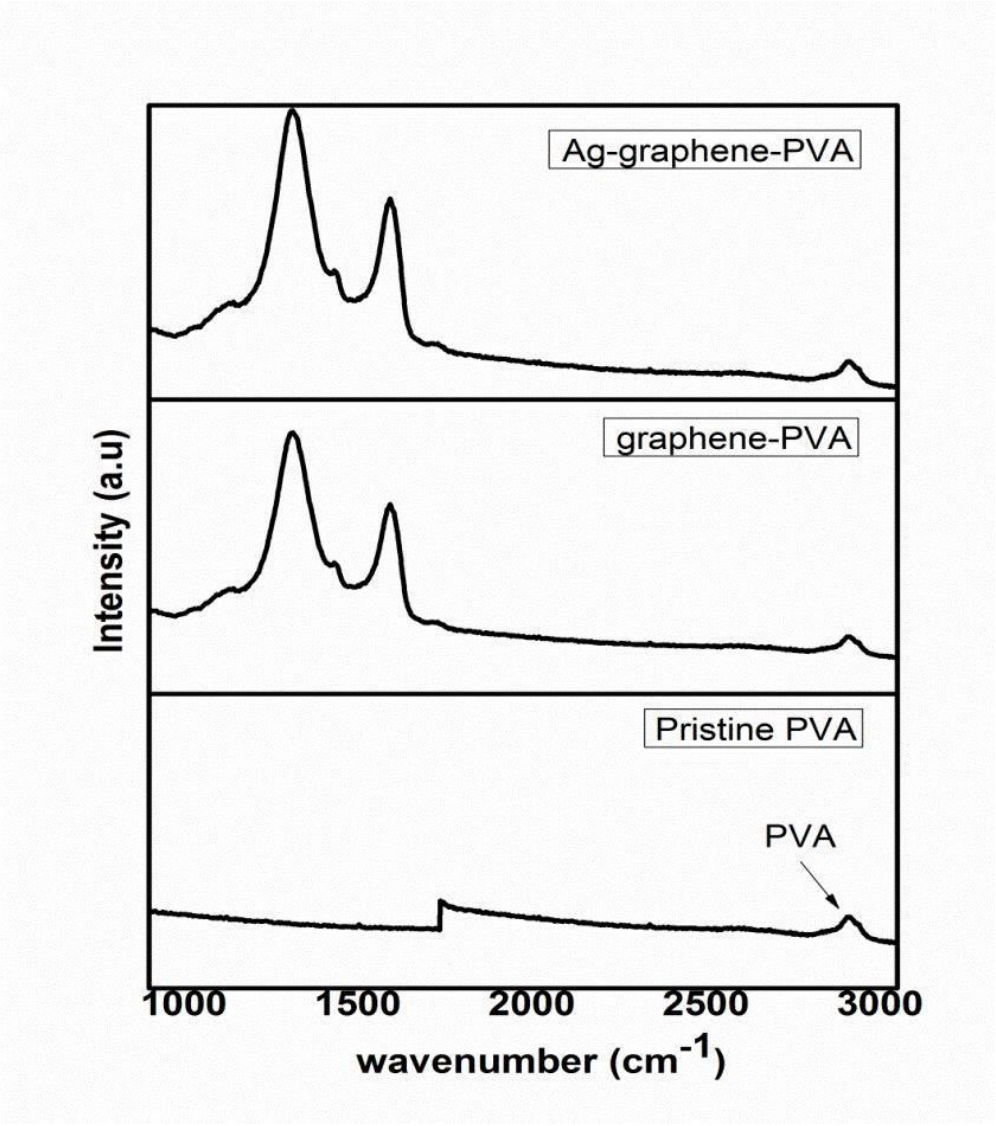

Figure 2. Raman spectrum for Pristine PVA, graphene/PVA, Ag/graphene/PVA nanocomposites

3.3 SEM

The SEM image of pristine PVA, graphene/PVA, and Ag/graphene/PVA composites are shown in figure 3a, 3b, and 3c respectively. Figure 3a exhibited the cylindrical structure of pristine PVA and 3b revealed the graphene which is incorporated in PVA polymer and it also showed the rigid structure in the polymer matrix. Figure 3c clearly exhibited the adorning of Ag nanoparticles on the surface of the graphene.

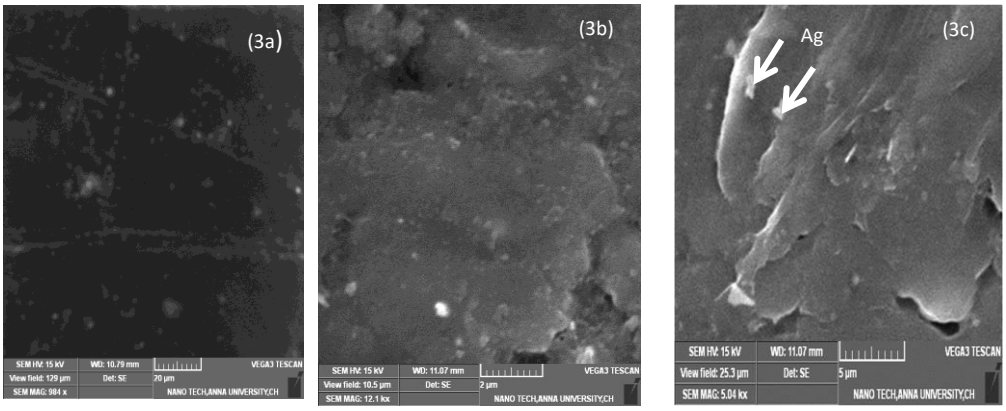

Figure 3. Scanning Electron Microscope image ofPristine PVA (3a),graphene/PVA (3b), Ag/graphene/PVA nanocomposites (3c).

3.4 Dielectric constant

The dielectric constants of pristine PVA, graphene reinforced PVA and AgNPs decorated graphene in PVA composites at 1MHz respectivelywerestudied (Figure 4). As the conducting nature of the polymer matrix increases, the composites displayed the intensification of dielectric constant. For pristine PVA, the dielectric constant is found to be 3.44. After reinforcing graphene, there found the enhancement in the dielectric constant and the value is found to be 8.04.[18] The reason is attributed to the interfacial polarization phenomenon due to the presence of graphene in PVA matrix. After decorating with AgNPs in graphene, the dielectric constant of the composites is raised up to 11.69, andthe reasonis attributed to the entrapment of free charges at the interface of conducting and insulating phase of the composites.[19]

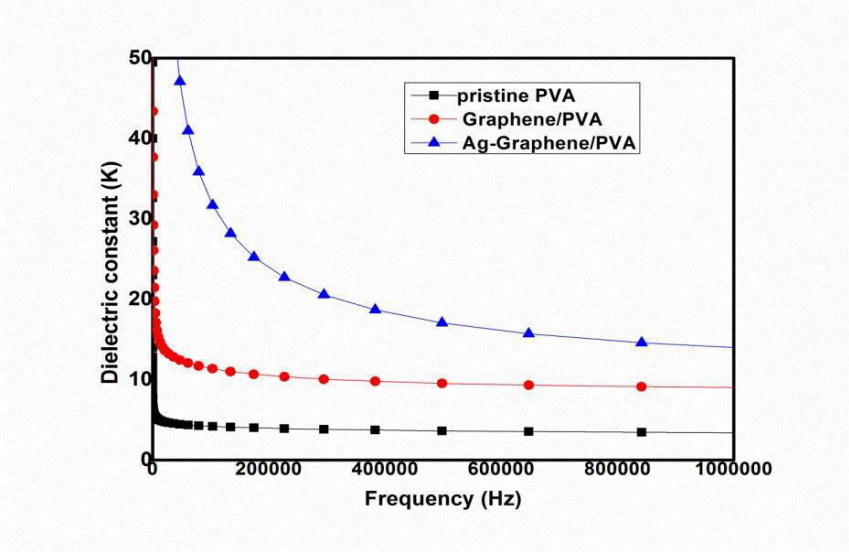

Figure 4.A plot of dielectric constants for Ag/graphene/PVA nanocomposites

3.5 Conductivities

The conductivities of pristine PVA, graphene/PVA, and AgNPs/graphene/PVA composites at 1MHz respectively are depicted in figure 5. The conductivity of pristine PVA is found to be 5.2 x 10^{-5} cm. On reinforcing graphene, the conductivity of PVA matrix is boosted to 6.39 x 10^{-5} cm which is ascribed to the conducting path developed in the graphene/PVA composites.[20] The interfacial interaction formed at the boundary between rGO and PVA in the composites improved the conductivity. Upon incorporation of AgNPs in graphene, the formation of electrons tunneling between Ag-environment in graphene/PVA composites increased the conductivity to 1.86 x 10^{-4} cm.[21-22]Rama K.Layeket al[23] reports that the conductivity if graphene/chitosan bio-nanocomposites are found to be 0.13 Sm^{-1} at 1.6 wt%,sulfonatedgraphene. The enhancement is due to the -SO_3H group present in the graphene sheets. But our composites shows the better conductivity after the incorporation of Ag nanoparticles to 1.86 x 10^{-4} S/cm at 1MHz which attributes the conducting nature of metals present in the composites and the better dispersion of Ag/graphenenanohybrids in the polymer matrix.

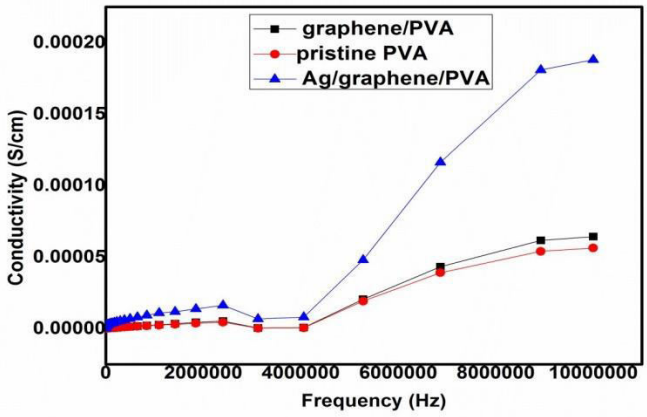

Figure 5. A plot of electrical conductivity for Ag/graphene/PVA nanocomposites

3.6 Dielectric loss

The dielectric loss of pristine PVA, graphene/PVA, and AgNPs/graphene/PVA composites at 1MHz respectivelyare depicted in figure 6. For pristine PVA, the dielectric loss is found to be 0.57. After reinforcing graphene in PVA, the dielectric loss reduced to 0.21 which is

accounted for the interfacial polarization concept in the composites. After the incorporation of AgNPs in graphene, the dielectric loss of the composites is found to be 0.88 which is attributed to the space charge migration, direct current (DC) conduction and the movement of molecular dipoles (dipole loss).[24-26]

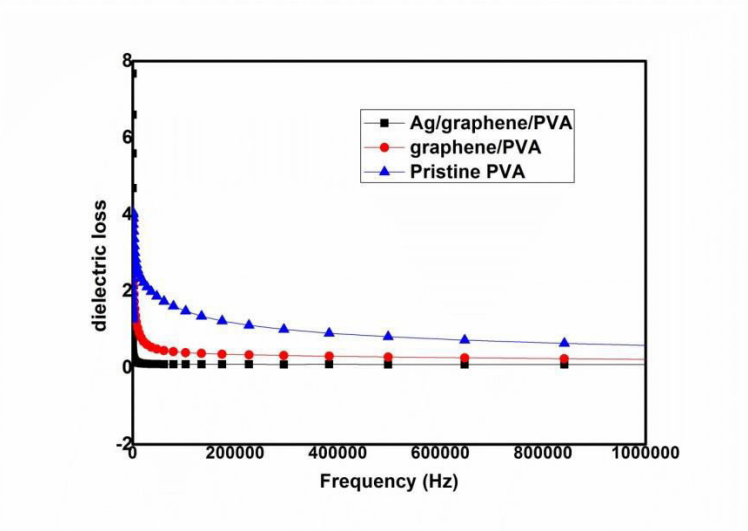

Figure 6.A plot of dielectric loss tangent for Ag/graphene/PVA nanocomposites

IV. CONCLUSION

In summary, we have successfully designed, synthesized and studied the electrical properties of a novel polymer-basednanocomposites using Ag/graphenenanohybrids reinforced polyvinyl alcohol matrix. The composite was easily synthesized using simple solvent cast method. The XRD studies evidentlydisclosed the presence of Ag/graphene in PVA matrix with good compatibility. The scanning electron microscopicanalysis demonstrated the loading of Ag nanoparticles on the graphene layers in the composites. The effective dispersion of Ag/graphenenanohybrids in PVA matrix amplified the dielectric behavior of the polymer nanocomposites. The dielectric constant is increased up to 11.89 at 1MHz after the loading of Ag nanoparticles alsothe conductivity swelled to 1.86 x 10^{-4} at 1MHz which is certainly attributed to the charge transfer complex between the graphene and PVA by AgNPs loading. The dielectric loss of the composites is lowered to 0.08 at 1MHz. The potential electrical behavior of theprocessedconducting composites opens up theopportunity for futuristic studies towards its applications in many flexible electronic and electrostatic energy storage devices.

REFERENCES

1. Zhenchong Zhang, YizhuoGu, Jiayu Bi, Shaokai Wang, Min Li, Zuoguang Zhang, *Mater Lett*.**2015**,*160*, 16-19.
2. Xiaodong Xia, Yang Wang, ZhengZhong, George J. Weng, *Carbon.***2017**,*111*, 221-230.
3. Youngho Jin, Ning Xia, Rosario A. Gerhardt, *Nano energy.* **2016**,*30*, 407-416.
4. NirmalMaity, Amit Mandal ,Arun K. Nandi, *Polymer.***201***6*,*103*, 83-97.
5. J.J.L. Hmar, T. Majumder, J.N. Roy, S.P. Mondal, *J. Alloys Compd.* **2015***,651*, 82-90.
6. Aamir Rasheed, Majid Mahmood, Usman Ali, Muhammad Shahid, Imran Shakir, SajjadHaider, Muhammad Azhar Khan, Muhammad Farooq Warsi, *Ceram.Int.* **2016**,*42*,15747-15755.
7. Kai Zhang, Li Li Zhang, X. S. Zhao, and Jishan Wu, *Chem. Mater*.**2010***,22,* 1392-1401.
8. Ahmed M. Khalil, Mohammad L. Hassanb, Azza A. Ward*,Carbohydr.Polym.* **2017***,157*, 503–511.
9. Gaoru Chen, Xuan Wang, Jiaqi Lin,abWenlong Yang, HaidongLi,Yinian Wen, Landi Li, Zhichao Jiang and Qingquan Lei, *J. Mater.Chem.***2016**, *C*,*4*, 8070.
10. M. R. Das, R. K. Sarma, R. Saikia, V. S. Kale, M. V. Shelke, and P. Sengupta*, Colloids Surf.,B.***2011**,*83*, 16.
11. YanjiZhua, HuaiyuanWanga, JiahuaZhub, Li Changc, Lin Ye, *Appl. Surf. Sci.* **2015***,349*, 27-34.
12. Yahui Ma, TongchunBai, FeiWang, *Mater.Sci. Eng.* **2016**,*C 59*, 948-957.
13. NirmalMaity, Amit Mandal and Arun K. Nandi, *Polymer*.2016.*103*, 83-97.
14. D. Li, M.B. Müller, S. Gilje, R.B. Kaner, G.G. Wallace, *Nature Nanotechnol*. **2008**,*3*, 101-105.
15. J. Shen, M. S. Bo, H. Ma, N. Li, and M. Ye, *J. Mater. Chem*.**2011**,*21*, 7795.
16. J. Fan, Z. Shi, Y. Ge, J. Wang, Y. Wang, and J. Yin*, J. Mater. Chem*.**2012**,*22*, 13764.
17. M. Zhang, E. J. R. Kelleher, F. Torrisi, Z. Sun, T. Hasan, D. Popa, F. Wang, A. C. Ferrari, S. V. Popov, and J. R. Taylor, *Opt. Exp. **2012**,20,* 25077-25084.
18. F. Alimohammadi, M. P. Gashti, A. Shamei, and A. Kiumarsi, *SuperlatticesMicrostruct*. **2012**,*52*, 50.
19. F. He, J. Fan, and S. Lau, *Polym. Test*.**2008***, 27,* 964.

20. S. Wageh, L. He, A. A. Al-Ghamdi, Y. A. Al-Turki, and S. C. Tjong, *RSC Adv.***2014**, *4*, 28426.
21. Carabineiro, S. A. C.; Pereira, M. F. R.; Nunes-Pereira, J.; Silva, J.; Caparros, C.; Sencadas, V.; Lanceros-Mendez, S. *J. Mater. Sci.***2012**,*47*, 8103−8111.
22. Lee, J.; Mulmi, S.; Thangadurai, V.; Park, S. S *ACS Appl. Mater. Interfaces.* **2015***, 7,* 15506−15513.
23. Cho, E.-C.; Li, C.-P.; Huang, J.-H.; Lee, K.-C.; Huang, J.-H. *ACS Appl. Mater. Interfaces.***2015***,7,*11668–11676.
24. Rama K. Layek.; SanjoySamanta.; Arun K. Nandi. *Polymer*. 2012, *53*, 2265-2273.
25. Mandal, A.; Nandi, A. K. *J. Mater. Chem.***2011**, *21*, 15752−15763.
26. Zhu, J.; Gu, H.; Luo, Z.; Haldolaarachige, N.; Young, D. P.; Wei, S.; Guo, Z. *Langmuir.* **2012**,*28*, 10246−10255.
27. B. Wang, G. Liang, Y. Jiao, A. Gu, L. Liu, L. Yuan, and W. Zhang, *Carbon.***2013**, *54*, 224.

Studies on the Characteristics of Landfill Leachate and its Physico-Chemical Interaction with Sub-surface Soil Stratum

Miss R. Nishaanthi
M.Tech
Department of Civil Engineering,
Pondicherry Engineering College,
Pillaichavady, Puducherry – 605014.

Dr. V. Murugaiyan
Professor,
Department of Civil Engineering
Pondicherry Engineering College,
Pillaichavady, Puducherry – 605014.

Abstract - Disposing of Municipal Solid Waste (MSW) poses a great challenge for many communities in the developing countries and the landfill is one of the common methods practiced in many countries. Like any other cities in India, puducherry has also been facing serious sanitation and environmental issues due to the improper Municipal Solid Waste Management (MSWM). When the landfills are not properly managed, it poses a serious threat to the environment due to leachate run-off. Leachate is the liquid content when water percolates through the solid waste, due to their low permeability, the Compacted Clay Liners (CCLs) are used as a barrier system to minimize the escape contaminants from landfill. This paper discuss about the characteristics of landfill leachate and its physico-chemical interaction with sub-surface soil stratum. The modified clay such as bentonite is used as a composite material for liner soils. The both experimental method and modeling are used for the analyzing of crack formation. These cracks creates major problem to the landfill liners, through this crack the leachate are passed into the soil and affect the ground water. The Crack Intensity Factor (CIF) is used for the analyzing of crack in the landfill liner. The model is predicted for the measurement of crack by analytical method. The comparative study has been made between the experimental and analytical methods for the analyzing of crack formation in landfill liner.

Keywords: leachate, landfill, liner, soil, cracking.

I. INTRODUCTION

Disposal of municipal solid waste (MSW) is one of the most challenging environmental issues. The improper disposal of MSW in open dumping area poses a serious threat to the environment. As in other cities of India, disposal of Municipal Solid Waste (MSW) poses great challenge to the government of Puducherry. The landfill is the most common method used for the disposal of MSW. The current landfill technology is primarily determined to prevent and control the leachate problem that produced from the waste. The landfill leachate has become one of the main focus for the environment management. The leachate normally generated by the rainfall and surface water flow into the landfill, through a time period. This leachate may percolate or penetrates into the natural soil and contaminate the groundwater and fresh

water supplies. To prevent this contamination the compacted clay liner (CCL) are used as a barrier in the dumping site. Desiccation cracks creates major problem to the compacted clay liners. The bentonites are used as composite material due to its low hydraulic conductivity. In this work a desiccation crack on CCL were measured and analyzed by both experimental and modeling method.

II. LANDFILL LEACHATE:

The landfill is an important and basic part for waste treatment in a majority of cities at present. The problem with landfills is the landfill leachate pollution. Furthermore, the landfill leachate problem is a long term issue, since the landfill leachate is formed long time after closing the site. From the start till the end there should be effective control and management for the production of leachate.

The different types of wastes are available at different disposal sites. The potential threat posed by the waste determines the type of liner system required for each type of landfill. Liners may be described as single (also referred to as simple), composite, or double liners.

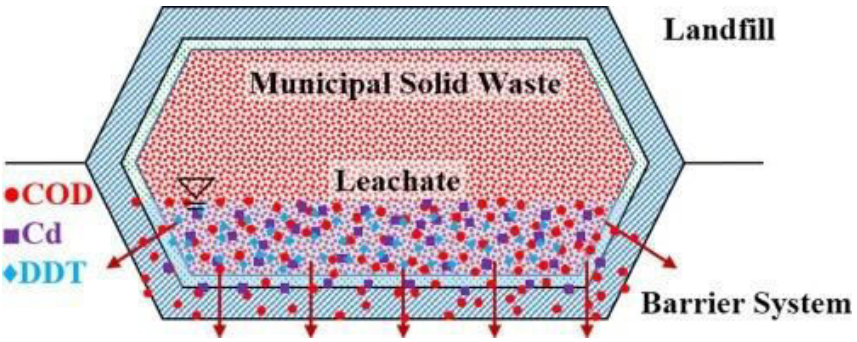

Fig 1: Landfill Leachate

2.1 Generation of landfill leachate:

The landfill leachate could be produced by two main causes. External water enters the waste and within the waste generated leachate.

2.2 Liners:

Liners are used to minimize the contamination of landfill by controlling and isolating the leachate generation.

2.3 Liner Design:

- The material selection and thickness of liner soil are considered for the liner design.
- The type of pollutants, environmental and climatic condition, material availability, legal requirements and cost provision are some of the factors affecting the liner.
- The composition of liners for waste usually consists of a compacted subsoil layer and it is overlain by the compacted clay liner.

2.4 Composition of landfill leachate:

Leachate consists of water, organic, inorganic and bacterial compounds together with solid. The compositions of leachate can be divided into four parts of pollutants. However, the organic content of leachate is often measured through analyzing some of parameters such as COD, BOD (biochemical oxygen demand) and TOC and dissolved organic carbon. Typical ranges of the concentration of selected parameters in leachate are shown in following Table 1.2.

Table 1: Composition of Landfill Leachate

PARAMETER	YOUNG	INTEMEDIATE	OLD
Age (Years)	<5	5-10	>10
Ph	6.5	6.5-7.5	>7.5
COD (mg/l)	20,000-40,000	4,000-10,000	500-4000
BOD	10,000- 20,000	4,000-10,000	50-100
TOC	9,000-25,000	-	100-1000
Volatile Fatty Acids (mg/l)	9,000-25,000	-	50-100
Heavy metals	Low-Medium	-	Low
Biodegrability	Important	Medium	Low
Metals	2	<2	<2
BOD_5/COD	>0.3	0.1-0.3	<0.1
TOC/COD	0.3	-	0.4

.

2.5 DESICCATION CRACK IN LANDFILL LINERS:

Desiccation of landfill clay liners is a major factor affecting the performance of landfills. Desiccation leads to the development of shrinkage cracks. Cracks provide pathways for moisture migration into the landfill cell which increases the generation of waste leachate, and ultimately increases the potential for soil and ground water contamination.

2.6 ENVIRONMENTAL IMPACTS:

- Generally, environmental issues related to improper landfills are groundwater pollution and soil contamination.
- Once the waste is buried in a landfill the action of ever-present water causes many physical, chemical and biochemical reactions.

IV. CONCLUSION

The main purpose of this paper is to investigate the properties of landfill leachate and its interaction with the sub-surface soil stratum by using the experimental and theoretical method. The MSW waste from different place has been collected and stored. Then, the properties of leachate will be identified. The crack in the liner soil can be measured by using the Crack Intensity Factor (CIF). Comparison has been made for the analyzing of crack in liner soil.

REFERENCES

1. Monoj Kumar, Vishal Arora, 'Cracking in Liner Behavior and Desiccation of Compacted Landfill Liner Soil', Short term load forecasting Proceedings of the IJCET, 2015, vol 5(6).
2. J.Sukumar, J.Arunachalam, Dr.M.Rajamanickam, 'The feasibility of incineration on Solid Waste Management in Puducherry', IJAREM, 2017,vol (3), 16 – 22.
3. Mudo Puming, Dr.Monowar Hussain, Mido Nyodu, Shivan Dakpe, 'A Study on the Chemical Properties of Leachate and its Effect on the Geotechnical Properties of Soil', IJETSR, 2016, vol (3).
4. R.Shanmugam, S.Dhanasekar, N.Ganapathy Ramassamy and Dhanya R Nair, 'Investigation of the Effect of Solid Waste and Leachate Interaction in Lysimeter', IJCIET, 2017, vol (8).
5. G.Siva Praveena P.V.V. Prasada Rao, 'Impact of Leachate on Soil Properties in the Dumpsite', IJERGS, 2016, vol (4).
6. Dr.Krishna M.K, Chaitra B.R, Jyothi Kumari, 'Effect of Municipal Solid Waste Leachate on the Quality of Soil', IJESI, 2016,vol (5).
7. Afshin Asadi, Nader Shariatmadari, Hossein Mooyedi, Bujang B.K.Huai, 'Effect of MSW Leachate on Soil Consistency under Influence of Electrochemical Forces Induced by Soil Particles', IJES, 2011, vol (6).
8. Rouf Ahmad Bhat, Shabeer Ahmad Dar, Davood Ahmad Dar, Gowhar Hamid Dar, 'Municipal Solid Waste Generation and Current Scemario of its Management in India', IJARSE, 2018, vol (7).
9. Barjinder Bhalla, M.S..Saini, M.K.Jha, 'Effect of Age and Seasonal Sariations on Leachate Characteristics of Municipal Solid Waste Landfill', IJRET, 2013,vol (2).
10. Rakesh Kumar Pandey, R.P.Tiwaei, 'Physical Characterization and Geotechnical Properties of Municipal Solid Waste', IOSR-JMCE, 2015, vol (4).

Construction and Demolition Waste Management-3R Concept

R.Kamali, I B.Tech (CSE)
Sri Manakula Vinayagar Engineering College
Madagadipet
Pondicherry

P.Kayathridevi, I B.Tech (CSE)
Sri Manakula Vinayagar Engineering College
Madagadipet
Pondicherry

Abstract-*This paper is based on the reduce, reuse, recycling of the rapidly increasing construction and demolition waste. Through this process we want to take a step ahead, the idea of stopping illegal sand mining, earth excavation and ultimately save our mother Earth from destruction. The cost of recycled sand and aggregates is lower than conventional aggregates and sand, resulting in reduction of overall construction cost. Our primary aim is to study the composition of construction and demolition waste and 3R concept in C&D waste. Further with the help of the obtained 3R material we intend to make various products such as concrete, paver blocks, hollow blocks, etc which will in turn be less costly as well. These recycled materials and products made from it are economical without any considerable change in the strength and durability aspect. Not only the cost effectiveness but it will also be aesthetically pleasing.*

I. INTRODUCTION

Construction waste is bulky and heavy and is mostly unsuitable for disposal by incineration or composting. The growing population in the country and requirement of land for other uses has reduced the availability of land for waste disposal. Re-utilization or recycling is an important strategy for management of such waste. Waste is generated at different stages of construction process. Waste during construction activity relates to excessive cement mix or concrete left after work is over, rejection/ demolition caused due to change in design or wrong workmanship etc.

Estimated waste generation during construction is 40 to 60 Kg. per sq. m. Similarly, waste generation during renovation/repair work is estimated to be 40 to 50 kg/sq.m. The highest contribution to waste generation is due to demolition of buildings. Demolition of Pucca and Semi-Pucca buildings, on an average generates 500 & 300 kg/ sq.m. Of waste respectively. Concrete appears in two forms in the waste. Structural elements of building have reinforced concrete, while foundations have mass non-reinforced concrete. Excavations produce topsoil, clay, sand, and gravel. This may be either re-used as filler at the same site after completion of

excavation work or moved to another site. Large quantum of bricks and masonry arise as waste during demolition. While 70% of the respondent have cited this as one of the reasons, 30% of the respondent have indicated that they are not even aware of recycling possibilities.

3'R CONCEPT

- **Reduce**: Reduction is considered as the most effective and efficient method to manage construction waste. Reduction does not only reduce construction waste generation, it also can reduce the cost for transportation, waste disposal and waste recycling.
- **Reuse**: Reuse is usually a favourite option because some construction waste can be reused in other construction project. Reuse is most beneficial and contractors can save money since disposal involved cost. Reuse is using the same material more than once for the same function such as formwork in construction . Any material which cannot be reused but can be re-cycled will be sent to re-cycling center.
- **Recycle**: When reduction and reuse become difficult, recycling is desired. Some new materials can be made out through recycling . Recycling construction waste can be categorized into on-site and off-site. On-site recycling is defined as segregation of construction waste for subsequent use as the raw materials in construction project. Meanwhile, off-site recycling is segregation of construction waste which are then transported to other organizations or locations and the waste is used as raw materials.

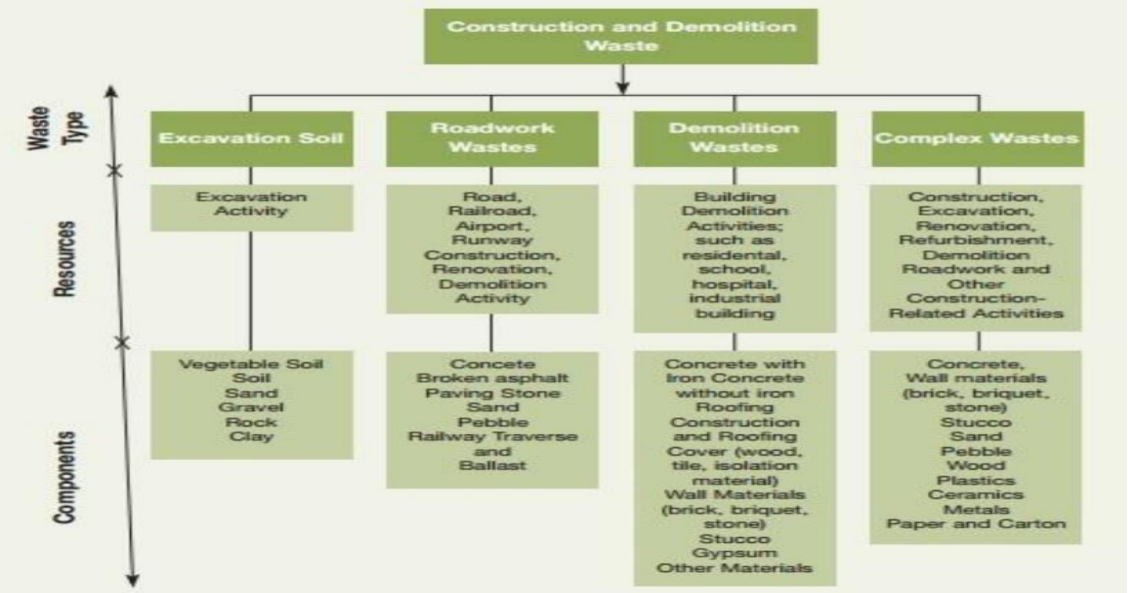

COMPOSITION OF CONSTRUCTION AND DEMOLITION WASTE

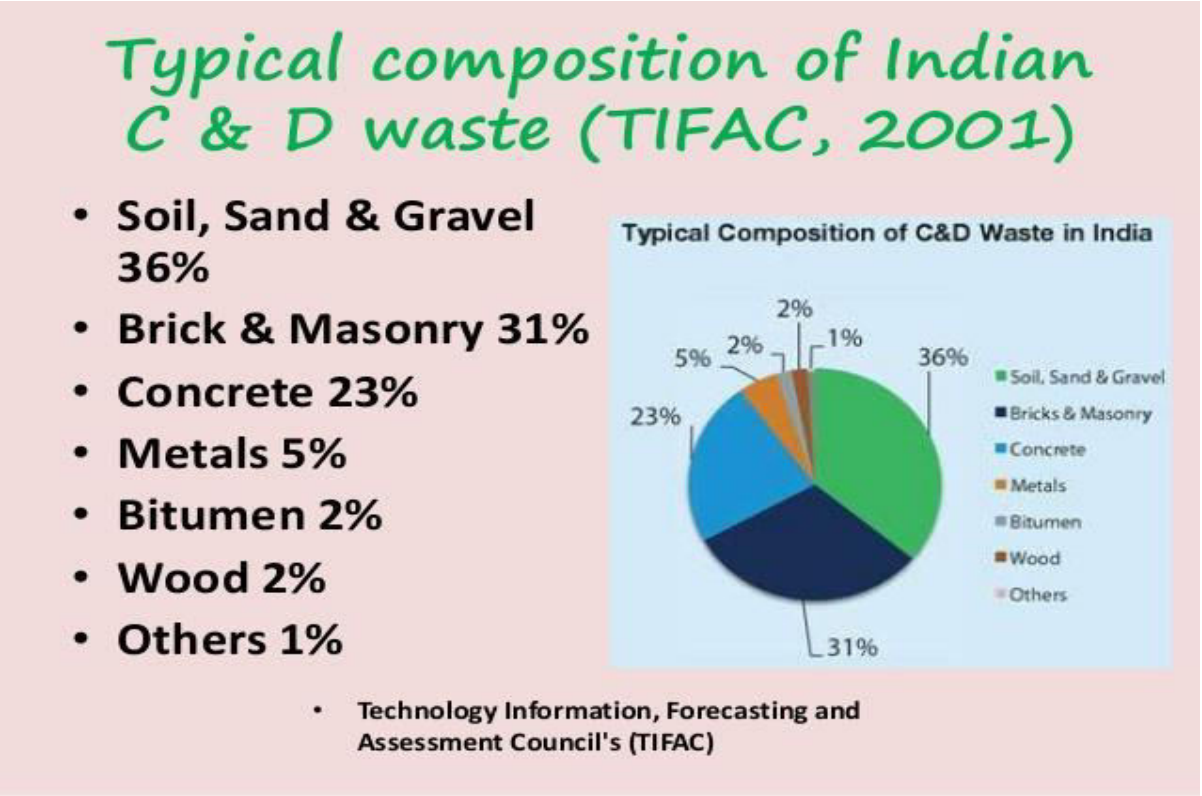

Application of 3R in C & D waste

Since the reusing of C&D waste is always more advantageous, it is essential that to identify and segregate more and more reusable materials in debris. This is possible, if sufficient precautions are taken while a building is demolished. There should be an effective deconstruction plan instead of just converting the standing structure into debris within minutes. Useful products like doors and windows, bricks, reinforcement, from RCC components, structural steel can be taken out with little extra efforts and put into reuse without much processing. Once the reusable items are taken out, the leftover waste is now available for recycling. Recycling of this waste into useful products to extend the service to environment is a challenge. Worldwide in Japan, Korea, Norway, Singapore etc., recycling of such wastes is taking place and we must understand the potential of different waste products for their effective and useful recycling.

Advantages of C & D waste.

- Cost factor will be minimum when we adopt 3R concept
- Use of new components will be minimized
- Man power consumption will be less
- Time duration for a construction can be minimized
- Generation of solid waste can be controlled
- restoration

CONCLUSION

It is essential to treat the C&D waste in order to reduce the dependency on the virgin material, India is one of the country which is using least C&D waste in there new construction project it about 10% of its whole waste. There is certain barrier which is ahead in the front of the path of the sustainable construction. By adopting this 3R technique, the waste management problem of construction industry will solved, Also there will saving of the valuable land whose price are at peak in the market. It is necessary to develop the 3R technique in Indian construction industry to manage the waste and also achieve economy.

Studies on Ground Water Quality along the Coastal Stretch of Puducherry Region

N. Niranjani
Research scholar
Department of civil engineering/environmental engineering
Pondicherry engineering college
Kalapet, Pondicherry.

Dr. G. Vijayakumar
Professor Department of civil
engineering Pondicherry Engineering
College Kalapet, Pondicherry.

Abstract-Water is said to be the universal solvent. Now a days use of ground water increases due to industrialization, urbanization etc. Hence the quality and quantity of water decreasing rapidly. On considering groundwater humans use this as a main source for drinking and agricultural purpose. This study is about investigation of physic chemical characteristics of aquifers near agricultural area of Puducherry region. The parameters to be tested are temperature, Ph, ec, tds, chloride, hardness, alkalinity, manganese, sulphate, manganese. According to this study the samples are taken on three different monsoon conditions (Pre-monsoon). So that we can able to derive different pollutant ratio which is use to give correct remedial measures. These results are collected and analyzed to get a conclusion.

I. INTRODUCTION

To assess the ground water quality of aquifers near the Coastal region of puducherry.
To analyze the physico chemical characteristics of water samples
The assess the organic and inorganic pollutants in the aquifers
To analyze the concentration of the pollutants
To suggest remedial measures

Puducherry is a union territory which lies along the southern east coast of Indian sub-continent . The average area of Puducherry region is about 293 sq. km. The study area receives its mean rainfall of about 1272.7 m from northeast monsoon. This region depends on the groundwater for all basic activities as the rivers of this area yield water during monsoon period only.

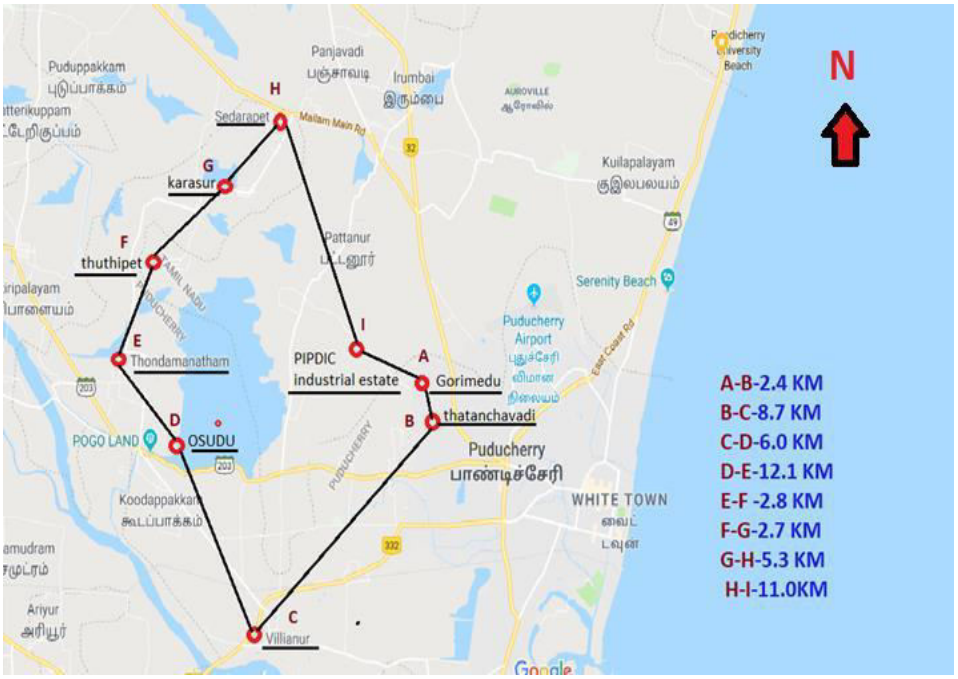

Image1:Location Map

LOCATION	LATITUDE	LONGITUDE	DISTANCE FROM SEA SHORE
GORIMEDU	11°95' 61" N	79°79' 43" E	5.17km
THATAANCHAVADI	11°91' 49" N	79 76' 66" E	3.9km
VELLIYANUR	11°54'45"N	7945'31"E	7.8km
OSUDU LAKE	11°94'14"N	7974'46"E	10.22km
THONDAMANANTHAM	11°51'41"N	7943'19"E	2.85km
THUTHIPET	11°59'9"N	11°59'9"N	13.63km
KARASUR	11 59'13"N	7944'20"E	12.6km
SEDARAPET	12 00'01"N	7974' 84" E	11.4km
PEPDIC INDUSTRIAL ESTATE	11°93' 58"N	7983;14" E	3.54kms

Table 1: Location coordinates

III. METHODOLOGY

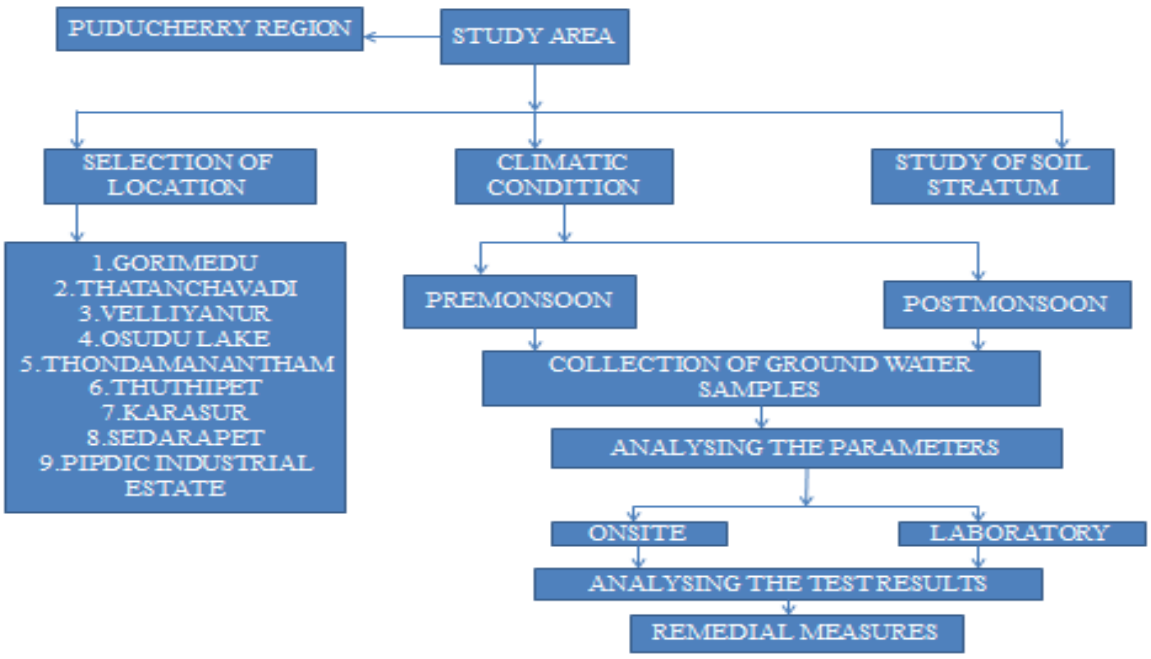

LOCATION	ALKALIN	CHLORI	SULPHA	MANGANE
GORIMEDU	39	390	47	1.1
THATANCH	41	391	39	0.05
VELLIYANU	69	470	57	1.1
OSUDU	511	459	6	1.3
THONDAM	651	464	73	1.2
THUTHIPET	511	474	52	1
KARASUR	488	474	36	0.04
SEDARAPET	369	502	55	1.1
PEPDIC INDUSTRIA	401	417	76	1.1

LOCATION	**TEMPERATURE**	**TH (mg/l**	**EC(µs/cm)**	**pH valu**	**TDS (mg/l)**
GORIMEDU	30	43.1	893	6.9	560
THATANCHAVADI	31	42.3	890	7.1	510
VELLIYANUR	32	45.3	1174	7.2	590
OSUDU LAKE	28	62.19	1999	8.9	735
THONDAMANANT	30	60.1	1900	7.06	704
THUTHIPET	30	57.28	1890	7.7	632
KARASUR	31	41	880	7.35	510
SEDARAPET	31	50	1280	5.7	611
PEPDIC	32	49.2	1265	5.9	603

V. CONCLUSION

The quality of groundwater in pre monsoon season was studied along the coastal aquifer of Pondicherry region. From the above study, it is inferred that the physico chemical parameters for collected samples were not within the permissible limit which may be due to seawater intrusion, mineral dissolution, intense agricultural practices and improper sewage disposal. The electrical conductivity and total dissolved solids of the water samples were permissible for drinking purposes. The hardness of the water samples was less than 75 mg/L indicating soft nature of groundwater.

WITH BEST COMPLIMENTS FROM

VEDHA SYSTEMS

Contact us:
No 34,
West Main Road,
Saram,
Brindavan Near State Bank Of India,
Pondicherry – 605013.
+(91)-413-2240890, 2246243
Web address-www.vedhasystems.in

Vedha Systems in Pondicherry boasts of a modern showroom that showcases all its product range. A knowledgeable sales team is available all throughout to help and assist customers to select a handset most appropriate to their needs. Catering to all kinds of budget, the shop is visited by a large number of customer's every day. The store is not only well-stocked on mobile phones and tablets but has an equally good collection of accessories such as head phones, Bluetooth headsets, wireless speakers, mobile phone covers, batteries, etc. In order to ensure that more number of clients can purchase products from this store, it has gone live thus enabling the citizens to buy the gadgets from the comfort of their homes. To reach out to the store, customers can call up at +(91)-413-2240890,2246243,2240892between 09:00 - 18:00 on all the seven days in a week. The shop accepts payments from the buyers in various modes like Cash, thus adding a lot of convenience to them.

WITH BEST COMPLIMENTS FROM

St. Anne's College of Engineering and Technology
Anguchettypalayam, Panruti - 607 106
Cuddalore Dt.
www.stannescet.ac.in
stannescet@gmail.com
04142 - 241661, 242661